12-2010

Modulated Properties of Fully Absorbable Bicomponent Meshes

Shawn Peniston
Clemson University, shawnjp@charter.net

MODULATED PROPERTIES OF FULLY ABSORBABLE BIOCOMPONENT MESHES

A Dissertation
Presented to
the Graduate School of
Clemson University

In Partial Fulfillment
of the Requirements for the Degree
Doctor of Philosophy
Bioengineering

---

by
Shawn J. Peniston
December 2010

Accepted by:
Dr. Karen J. L. Burg, Committee Chair
Dr. Shalaby W. Shalaby, Co-Advisor
Dr. Jiro Nagatomi
Dr. Ken Webb

ABSTRACT

Current meshes used for soft-tissue repair are mostly composed of single component, nonabsorbable yarn constructions, limiting the ability to modulate their properties. This situation has left the majority of soft tissue repair load-bearing applications to suffer distinctly from undesirable features associated, in part, with mesh inability to (1) possess short-term stiffness to facilitate tissue stability during the development of wound strength; (2) gradually transfer the perceived mechanical load as the wound builds mechanical integrity; and (3) provide compliance with load transfer to the remodeling and maturing mesh/tissue complex. The likelihood of long-term complications is reduced for fully absorbable systems with degradation and absorption at the conclusion of their intended functional performance.

The primary goal of this dissertation was to develop and characterize a fully absorbable bicomponent mesh (ABM) for hernia repair which can modulate biomechanical and physical properties to work with the expected needs of the wound healing process. The first study reviewed the current state of hernioplasty and proposed the subject device. The second study investigated different knitting technologies to establish a mesh construction which temporally modulated properties. To this end, a novel construction using warp knitting was developed where two degradable copolyester yarns with different degradation profiles were coknit into an initially interdependent knit construction. The developed knit construction provided an initial high level of structural stiffness; however, upon degradation of the fast-degrading yarn the mesh comprised of the slow-degrading yarn was liberated and affords high compliance. In the third study,

the segmented, triaxial, high-glycolide copolyester used as the fast-degrading yarn was optimized to retain strength for greater than 18 days. As such, the ABM physical and biomechanical transition was designed to temporally coincide with the expected commencement of wound strength.

The fourth study investigated the *in vivo* tissue response and integration of the developed degradable copolyester yarns in a novel construct to simulate the ABM. Results indicated a strong initial inflammatory response which resolved quickly and an integration process that produced a dense, compacted, and oriented collagen capsule around the implant during the transition phase. For the final study, the clinically-relevant biomechanical properties of two different ABM constructions were compared against traditional hernia meshes. Using a novel synthetic in vitro simulated mesh/tissue complex, the ABM were found to provide significantly greater early stability, subsequent biomechanics that approximated that of the abdominal wall, and evidence of restoring endogenous tension to the surrounding tissue. These results were in marked contrast to traditional hernia meshes which showed stress shielding and significantly greater stiffness than the abdominal wall.

DEDICATION

I dedicate this work to my wife, Kristin, who has brought me so much love, happiness, and understanding through this process. I could not have done it without her. To my parents, Marsha and Jim, who have supported my dreams, whatever they might be and wherever they might have taken me. To my late Grandmother, Francis, who on many occasions told me to "Stick to the books, they'll pay off." She was right. Finally, to the rest of my loving family who have provided me with the encouragement to achieve this milestone.

ACKNOWLEDGMENTS

I am indebted to my advisor, Dr. Karen J. L. Burg, for her positive comments, detailed guidance, and hard work in the preparation of this dissertation. I am forever grateful to the late Dr. Shalaby and his family. Dr. Shalaby's life long journey of acquiring knowledge, tremendous work ethic, and his passion for science provided me with this opportunity. My life is forever changed for knowing him.

I would also like to thank Dr. Jiro Nagatomi and Dr. Ken Webb for their time, support, and constructive comments. Thank you to Dr. Gerrard for his assistance with the statistical analysis and Linda Jenkins for her help in the histology lab. Thank you to Dr. Joel Corbett who performed the animal surgical procedures and the Godley-Snell research center staff at Clemson University for providing the animal care. A special thanks to all of my Poly-Med friends who have encouraged me, taught me, and assisted me over the past six years. Of course, thank you to all of my past professors who have taken the time to share their knowledge. In that spirit, I will take the time to share what I have learned with others as well.

TABLE OF CONTENTS

Page

Table of Contents (Continued)

Page

Table of Contents (Continued)

Page

LIST OF TABLES

LIST OF FIGURES

List of Figures (Continued)

Figure Page

List of Figures (Continued)

Figure Page

List of Figures (Continued)

Figure Page

PREFACE

Over one million surgical procedures for hernia repair using a mesh are completed every year worldwide. Despite the frequency of this procedure, the efficacy of hernia repair remains a challenge with high recurrence rates and a substantial percentage of patients that experience long-term complications which impact quality of life. Scientific literature is replete with animal and clinical studies which demonstrate the unmet need for a hernia mesh with improved biocompatibility.

This dissertation describes a bioengineering approach that was used to develop and evaluate a novel hernia mesh which considers the temporal needs of the wound healing process, as well as the device functional needs to improve biocompatibility. Specifically, a bicomponent fully-absorbable warp knit mesh was proposed which temporally modulates its physicomechanical properties and will (1) possess short-term structural stiffness to facilitate tissue stability during the development of wound strength; (2) gradually transfer the perceived mechanical loads as the wound is building mechanical integrity; (3) provide force-extension properties similar to the abdominal wall resulting in load transfer to the remodeling and maturing mesh/tissue complex; and (4) minimize the likelihood of long-term complications with complete degradation and absorption at the conclusion of the meshes intended function.

This dissertation consists of five chapters which cover the unmet clinical needs, conceptual evaluation, and the design and development history for the subject absorbable bicomponent mesh (ABM). The first chapter provides a detailed review of the wound healing process, anatomy and biomechanics of the abdominal wall, hernia development

and surgical intervention using meshes, etiology and pathology of hernia development, knitting technologies for meshes, meshes as biomaterials, mesh biocompatibility, and new opportunities based on currently unmet needs. In summary, Chapter 1 details the background including the current challenges associated with traditional hernia repair meshes and a proposed novel concept which evolved further in subsequent chapters.

Chapters 2 through 5 represent individual studies written in the format found in most scientific journals. Each chapter details a step in the development process for the ABM. In Chapter 2, two different mesh constructions were knit to determine the effect of knit construction on the temporal modulation of physicomechanical properties during the *in vitro* conditioned degradation of the fast-degrading yarn. The outcome resulted in the adoption of a novel warp knit construction whereby two initially interdependent knit constructions provide a high level of structural stiffness. However, the substantial degradation of the fast-degrading yarn yields an autonomous, structurally stable and compliant slow-degrading mesh. The study in Chapter 3 focuses on the development and optimization of a segmented, triaxial, high-glycolide copolyester for use as the fast-degrading yarn which retained strength for greater than 18 days to temporally coincide the biomechanical transition with the expected commencement of wound strength.

The second and third chapters detail the work completed to establish the necessary absorbable copolyesters and knit technology required to meet the initially proposed design concept described in Chapter 1. In Chapter 4, an ABM mesh was prototyped using a simplified knit construct to complete a preliminary *in vivo* study. In this study the tissue response to the simulated ABM was investigated with specific

emphasis placed on the integration of the mesh into the host tissue using evaluation time periods which bracket the critical biomechanical transition from structural stiffness to high extensibility. In Chapter 5, a mesh biomechanical study investigated the effect of two different ABM knit constructions on physicomechanical properties with comparison to two traditional hernia meshes. As part of this investigation, a novel simulated mesh tissue/complex using a synthetic material was developed to demonstrate the change in mesh biomechanics following infiltration with the extracellular matrix *in vivo*. Additionally, the strength retention of the slow-degrading yarn was determined to be load-bearing for greater than 9 months, which is the expected time period for the sufficient maturation of the infiltrated collagen.

The completed work described in this dissertation is an initial effort to develop a novel ABM with expected improved mechanical biocompatibility. The intellectual property associated with this dissertation is the subject of patent applications in several countries worldwide, a limited 40 patient clinical study in Sweden initiated in early 2009, and 510K approval from the Food and Drug Administration for clinical use in the United States in early 2010. Additionally, the contents of Chapter 1 were used to develop a chapter in the book "Mechanobiology Handbook" edited by Dr. Jiro Nagatomi which is currently in press. Results from Chapter 2 were presented at the 2008 Clemson University Annual Conference on Opportunities and Markets for Medical Materials and Technologies.

CHAPTER ONE

LITERATURE REVIEW

The Wound Healing Process

Wound healing is characterized by several overlapping, predictable stages that are strongly interlinked and contribute to the common goals of the elimination of foreign microorganisms, wound debridement, cell proliferation, matrix deposition, contraction, and maturation resulting in mechanical integrity.

Stages of Wound Healing

The major stages of wound healing include inflammation (generally 2-5 days post insult), proliferation (generally 2 days to 3 weeks post insult), and remodeling/maturation (generally 3 weeks to 2 years post insult). The timeframes are approximated because of the complex and often case specific nature of wound healing. Many factors affect the timing of the wound healing process, including the location and extent of injury, level of wound contamination and infection, rate of fluid perfusion, level of local pH, presence of foreign bodies, host comorbidities, and the regenerative capacity of proximal cells.[1,2] The wound healing process is sequentially similar throughout the body with differences specific to the length of each stage and cell autocrine and paracrine signaling often resulting in anatomical site specific cell responses such as atrophy, hypertrophy, hyperplasia, metaplasia, and/or phenotype changes. The end result of orderly and timely wound healing is ideally tissue with minimal fibrosis yet structural integrity, minimal to

no wound contraction, and pre-injury function. Often with the implantation of medical devices the measure of their biocompatibility is graded on the local resolution of the wound healing process in a timely manner. To better understand this process a brief review of the typical, wound healing process is helpful.

Injury to vascularized tissue triggers coagulation and the initiation of the inflammation process of wound healing. The inflammation process rapidly increases to a maximum at 2-3 days and then gradually resolves over the next couple of weeks. Overall, the inflammatory process can be divided into two stages of (1) vasomotor-vasopermiability and (2) leukocyte signaling and infiltration.[3] The initial vascular response to injury is a short lived vasoconstriction intended to minimize blood loss followed by a period of local vasodilation. Vasodilation increases the pressure and flow of blood to the area and causes the release of serum fluid through permeable vascular walls resulting in tissue oedema. Within the newly formed interstitial space created by the exudate, proteins such as fibronectin are deposited which will create the initial scaffolding for subsequent cellular migration and locomotion into and within the wound.[3] Within the wound site, the formation of a blood clot via the coagulation cascade blocks the continued loss of blood and provides additional scaffolding for cellular activity during the remodeling phase. The blood clot is constructed from fibrin, an insoluable, crosslinked product of fibrinogen, and activated platelets. During the formation of the blood clot, activated platelets release a myriad of cytokines including platelet derived growth factors (PDGF)[4] and transforming growth factor (TGF-β)[5] which result in the chemotaxis of leukocytes and fibroblasts. The first cell type to aggregate at the wound

site is the neutrophil. The primary role of the neutrophil is to clean the wound by removing bacteria and initiating debridement.[3,6] Neutrophils accomplish this goal through the release of free oxygen radicals and lysosomal enzymes from within their many intracellular granules. Neutrophils are short lived within wounds, especially when bacterial infiltration is minimal, and quickly (generally by day 3) become secondary in number to monocytes differentiating to macrophages. Macrophages continue to phagocytize tissue and bacterial debris taking over where the neutrophils left off; however, macrophages have the added responsibility of being crucial to cellular proliferation and recruitment. Once the wound is clear of bacteria and debris the rebuilding process can begin with the repopulation of cells.

The proliferation and remodeling phase is characterized by the increase in fibroblasts followed by the deposition of extra cellular matrix (ECM) in the wound. Proliferation is driven by macrophages that secrete growth factors such as PDGF, TGF-β, interleukins (IL), and tumor necrosis factor (TNF) which play key roles in the migration and activation of local fibroblasts.[3] Fibroblasts, which originate from mesenchymal cells located in loose tissue around blood vessels and fat, differentiate and migrate in response to these cytokines.[7] Theses newly formed fibroblasts use the fibrin/fibronectin network previously established for locomotion within the wound. In addition to collagen, fibroblasts produce glycoaminoglycans (GAGs) and proteoglycans which form the tissue "ground substance". Initially fibroblasts are primarily focused on replication and recruitment with minimal collagen synthesis. Within the first 4-6 days following insult, fibroblasts become the primary cell type and the deposition of collagen increases rapidly

for the next three weeks.[6] Concurrently during the three week time period of collagen deposition, angiogenesis progresses to provide the wound with nourishment and oxygen while removing metabolic and waste products. Macrophages and fibroblasts provide the stimulus for the progression of capillaries, arterioles, and venules toward the wound space. The generation of fibroblast growth factor (FGF) and vascular endothelial growth factor (VEGF) from macrophages are the primary, and most studied, cytokines responsible for angiogenesis.[8] Over time capillaries slowly regress as collagen fills the wound space and mature, avascular scar tissue is formed.

Wound remodeling and maturation is characterized by a gradual strengthening and reorganization of the collagen matrix over a period as short as 3 weeks or as long as 2 years. During this time, Type III collagen, so called immature collagen because of its smaller fiber diameter, greater elasticity, and lower strength, is replaced by Type I collagen. Prior to the deposition of Type I collagen the wound has essentially no mechanical integrity. During the wound maturation/remodeling process no net gain in collagen content is achieved; instead, the production of collagen is matched by the degradation of collagen by matrix metalloproteinase's (MMPs). With the turnover of Type III collagen to Type I collagen the wound site develops mechanical strength and the cells attempt to replicate the preinjury tissue characteristics by contributing to the developing structure and orientation along the lines of tension. However, typically the wound site never fully obtains the original tissue structure, while values of approximately 80% of preinjury mechanical strength are reported.[5]

The Role of Fibroblasts and Collagen in Soft Tissue Wound Healing

Collagen is the most widespread protein present in humans and consists of fibrils embedded in an amorphous gel-like matrix composed of proteoglycans and water. Fiber forming collagen, such as Types I and III, function to transmit and dissipate loads and store elastic strain energy applied to the joints of the body.[9] The mechanical characteristics of collagen lie in its unique and somewhat complex structure.

The development of collagen, the structural component to soft tissue, is paramount to effective and efficient resolution in wound healing. Collagen is synthesized by fibroblasts in a multiple step process that starts with intracellular assimilation of peptide chains and is completed with extracellular collagen fiber and fiber bundle formation into macroscopic structures such as tendons or fascia.

Within wounds, collagenous tissue function is highly dependent on its structure. Collagen fibrils are highly oriented and thus strong but they can be considered essentially inextensible.[10] The conformation of collagen fibrils is essential to determining tissue function. For example, highly oriented structures such as tendons transmit force quickly and efficiently while randomly oriented fibers in the dermis allow considerable extension before resistance is achieved. Therefore, the aggregation of fibrils into fibers and their resultant diameter as wells as the construction of the aggregate fibers gives soft tissue its mechanical properties and anatomically specific characteristics. The stress-strain curve for collagen tissue is non-linear and can be divided into three distinct regions, each of which can be attributed to a different structural element. In tendon and ligament the curve has been characterized by a low strain non-linear toe region, a curved mid-region,

and then a linear yield and failure region.[11] In the toe region, low stress is required to remove macroscopic crimp in the form of gradual straightening of collagen fibers that have varying degrees of undulations.[12] The second region is characterized by collagen fibers that begin to line-up in the direction of the load and provide increasing resistance. In addition, disordered molecules in the lateral gap region between fibrils reorganize.[13] In the third region, stretching of the triple-helices and crosslinks between helices produce side-by-side gliding of neighboring collagen molecules leading to structural changes at the level of the collagen fibrils.[14] Under typical conditions, physiologic levels are within the toe region of the stress-strain curve, resulting in a shock absorbing system, where low levels of stress are required to achieve deformations in the absence of significant molecular stretching of the fibers.[10]

Like synthetic polymers, biopolymers such as collagen are viscoelastic. The hierarchical structure of collagen, from triple-helix to tissue, provides structural components that have elastic and viscous characteristics. For example, ligament viscoelasticity under uniaxial tensile loading is attributed to the inherent viscoelasticity of the collagen fibrils (bond rotation and stretching), the local extracellular matrix, interfibrillar crosslinking, and the movement of fluid within and in/out of the tissue.[15] The degree of crosslinking between fibrils has been linked to viscoelastic properties, with low levels dominating viscous behavior and high levels dominating elastic behavior through the stretching of nonhelical ends, crosslinks, and the triple helix.[9] Furthermore, it has been determined that the overall strain in a tendon is always larger than the strain of

individual fibrils, indicating that some of the viscoelastic deformation takes place in the proteoglycan-rich interfibrillar matrix.[14]

Influence of Mechanical Stimulation in the Soft Tissue Wound Healing Process

Mechanical forces are fundamental in maintaining and regulating the structure and function of tissue. The importance of the mechanical loading of bone has been realized for many years; more recently, the importance of mechanical stimulation on other tissues such as ligament, tendon, skeletal muscle, intervertabral disc, and meniscus is being realized.[16] The influence of mechanotransduction in cellular signaling is still not fully understood. However, the influence of mechanical stimulation on fibroblasts has been investigated and determined to affect cell proliferation[17,18], collagen deposition[19,20], phenotype[21], apoptosis[22], cell spreading[23], orientation[24], and the release of matrix metalloproteinases[25]. From a biochemical aspect, observed changes in animal tendons and ligaments from joint immobilization studies include increases in the rate of collagen turnover, reduced levels of crosslinking, slight mass loss, a reduced amount of proteoglycans and hyaluronic acid, and decreased water content.[26] Biomechanically, the result of these changes is a reduction in tangent modulus, cross-sectional area, and ultimate strength.[26] Hannafin and coworkers compared static and mechanically cycled canine flexor digitorum profundus tendons *in vitro* and demonstrated that cells in static samples had altered morphology and decreased number; furthermore, cell and collagen alignment was modified, resulting in decreases in tensile modulus over an eight week period.[27] Fibroblast-matrix interactions control cell shape and orientation and also

directly regulate cellular functions, primarily through integrin receptors that cells use to adhere to and receive mechanical energy from the extracellular matrix.[28] In addition, it has been shown that elongated tendon fibroblasts, as they appear in a homeostatic, mechanically stressed extracellular matrix, produce greater amounts of collagen Type I as compared to less elongated cells.[29]

Mechanical stimulation also has a role in wound contraction. A cell subpopulation will differentiate into myofibroblasts as fibroblasts increase in number within the wound site. Myofibroblasts express different sets of cytoskeletal proteins, such as α-smooth muscle actin (α-SMA), that play an important role in contraction. Myofibroblasts are stimulated to differentiate by a combination of TGF-β1 and ED-A fibronectin (ED-A FN), both of which are critical to the induction of α-SMA expression but are not sufficient to maintain myofibroblast differentiation in the absence of mechanical stimulation.[30] It has been suggested that, for normally strained tissues such as tendons, wound contraction is an attempt to restore the physiologic condition of tension.[31] However, excessive contraction can distort and disrupt tissue structure, resulting in undesirable consequences. The contractility of rat tissue occurs in a three stage process.[30] Slow contractility occurs from 1-6 days post-wounding, is characterized by an increase in the expression of ED-A FN, and is said to be independent of myofibroblast influence.[32] Next, a steep increase is realized, with the increased expression of α-SMA. This phase lasts during a period from 3-10 days, initiating at earlier timepoints and persisting longer when the wound site is mechanically stressed. After approximately 10 days, a reduction in the α-SMA expression occurs, followed by

contraction. Contractility correlates with the level of α-SMA expression, being higher when granulation tissue is subjected to greater levels of tension.[30] Tension within the wound site is said to prevent apoptosis of myofibroblasts[33], but once stress forces are relieved apoptosis of myofibroblasts will occur even if growth factors are added to the wound.[34] Overall, mechanical stimulation is crucial to the biomechanical quality of collagen and myofibroblast modulation of the wound contraction process.

Anatomy and Biomechanics of the Abdominal Wall

Relevant Anatomical Features of the Abdominal Wall

The abdominal cavity is approximated by the spine and back muscles posteriorly, the pelvic cavity inferiorly, and the thoracic cavity superiorly. The ventral side of the abdominal wall, from superficial to deep, is comprised of (1) skin, (2) subcutaneous tissues, (3) superficial fascia (Scarpa fascia), (4) anterior rectus fascia, (5) rectus abdominis muscle, (6) posterior rectus fascia, (7) extraperitoneal adipose tissue, and (8) peritoneum with the linea alba constructing the anterior midline. Moving laterally, the lower abdominal wall in the inguinal region is comprised of the (1) skin, (2) subcutaneous tissues, (3) superficial fascia (Scarpa fascia), (4) innominate fascia, (5) intercrural fibers, (6) external oblique muscle, (7) internal oblique muscle, (8) transversus abdominis muscle/fascia, (9) transversalis fascia, and (10) peritoneum. Theoretically these structures provide the necessary support to resist herniation of the anatomic hole located in the inguinal region. This anatomic hole, as described by Fagan and Awad[35], is known as the myopectineal orifice. The myopectineal orifice is quadrangular in shape

and is divided superiorly and inferiorly by the inguinal ligament which runs from the anterior-superior iliac spine to the pubic tubercle (Figure 1.1).

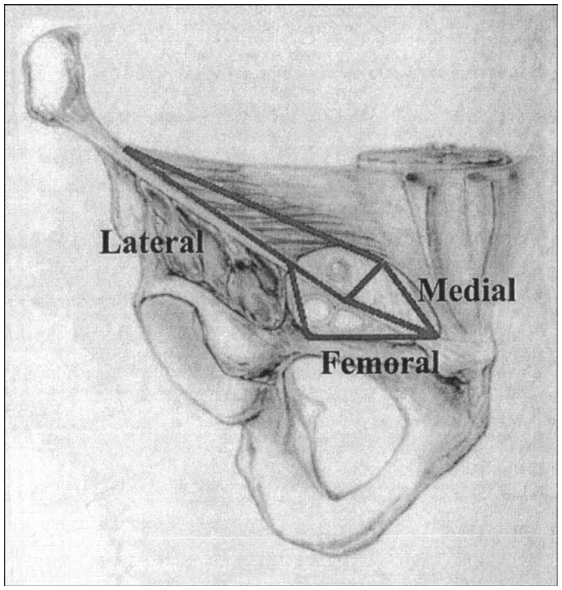

Figure 1.1

The myopectineal orifice depicting the medial, lateral, and femoral triangles.[35]

The myopectineal orifice is perforated in the medial-lateral triangle by the spermatic cord and in the femoral triangle by the femoral artery and vein. The inguinal canal is created from the passage of the spermatic cord, including the vas deferens exiting the abdominal cavity, and transcending to the testes in the scrotum. The location where the spermatic cord initially enters the abdominal wall is called the deep inguinal ring.

The pelvis is constructed of the iliac bones, pubic bones, ischial bones, and the sacrum, forming a complete circle and providing a conduit between the torso and lower extemeties.[35] The pelvis provides an anchor for the aponeurosis of the abdominal wall.

In addition, the inguinal ligament, an important anatomical landmark and structural component for the spermatic cord, travels from the anterior-superior iliac spine to the pubic tubercle.

When examining the abdominal wall from superficial to deep, the first structural component is the Scarpa fascia. The Scarpa fascia is a membranous sheet of areolar tissue that forms a discrete structure separating the superficial and deep subcutaneous fat. Next, the innominate fascia covers the external oblique muscle and spermatic cord.[35] However, neither the Scarpa nor innominate fascia are considered primary load bearing structures within the abdominal wall; this function is primarily attributed to the abdominal musculature and matrix tissues.

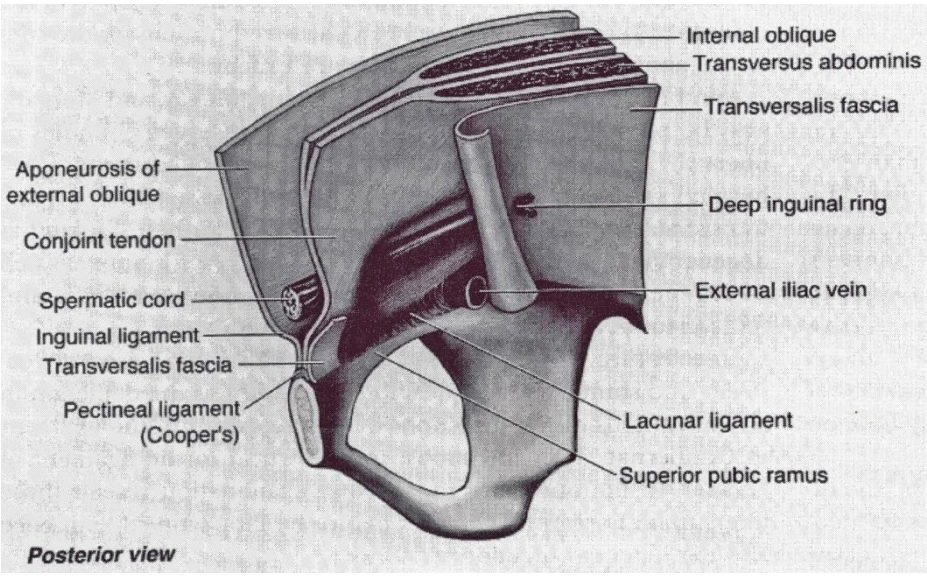

Figure 1.2

Posterior view of the inguinal region demonstrating a weak medial area caused by arching fibers of the internal oblique and transversalis fascia.[35]

The rectus abdominus is comprised of two ventrally located vertical pillars segmented on the midline by the linea alba. Attached to the rectus abdominis is a triple layer of flat muscles extending laterally and creating a cylindrical abdominal cavity that withstands internal pressure as well as external insults.[36] From superficial to deep these muscles include the external oblique, internal oblique, and transversus abdominus. The transversus abdominus is the main muscle used to retain the abdominal contents.[36]

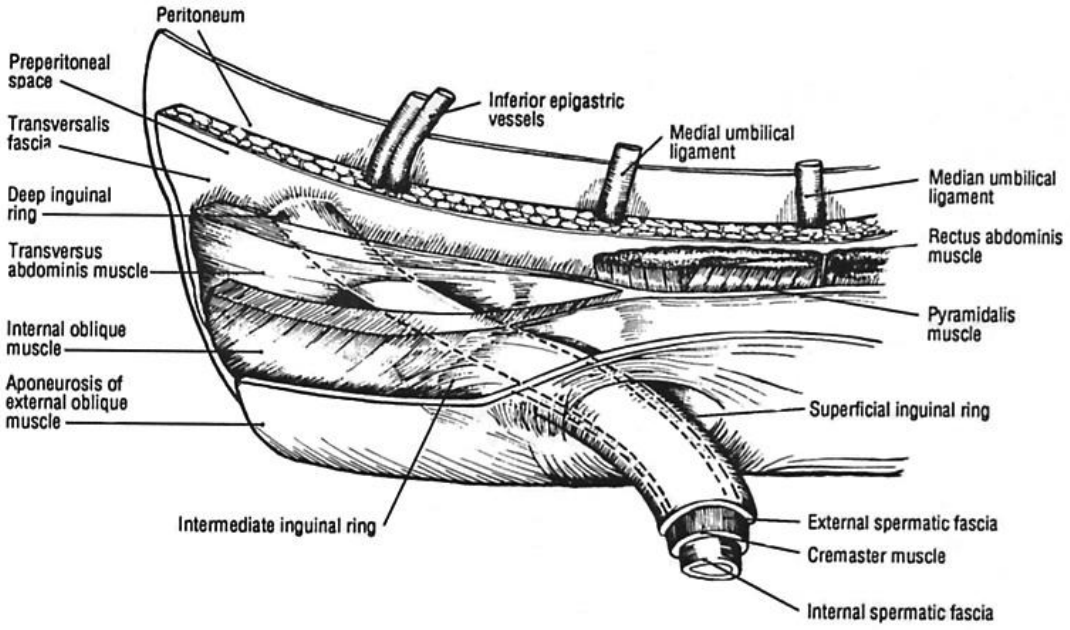

Figure 1.3

Anterior view of the inguinal region.[37]

The rectus sheath is divided by the posterior and anterior layer relative to the rectus abdominis muscle and is comprised of the aponeurosis from each layer of the triple flat abdominal muscles. The anterior layer of the rectus sheath is made up of primarily

aponeurosis fiber from the external and internal oblique muscles and the posterior layer is comprised of aponeurosis fibers from the internal oblique and transversus muscles above the level of arcuate line. The arcuate line is generally located midway between the umbilicus and pubis and represents the transition zone in which the aponeurosis of the external oblique, the internal oblique, and the transversus abdominis muscles all pass anterior to the rectus muscle.[38] Below the arcuate line the posterior sheath of the rectus abdominis lacks strength as it is comprised of only transversalis fascia, areolar tissue, and peritoneum.[38] It should be noted that aponeurosis are like tendons or ligaments, with the major difference being that they originate from large flat muscles and thus take on the form of large, flat, thin sheets. Fascial layers on the other hand are considerably more extensible and primarily function to separate layers of tissue rather than provide load bearing structural support. For this reason the myopectineal orifice is susceptible to herniation.

Biomechanics of the Abdominal Wall

The abdominal wall mechanics traditionally have been characterized by (1) the physiologic maximum force generated within the wall and (2) the extension or strain associated with that maximum physiologic force. Peiper and coworkers determined that loading of the inguinal region of the abdominal wall is predominately related to increases in intra-abdominal pressure and not muscular contraction.[39] If one assumes that intra-abdominal pressure only governs the resistive strength required in the abdominal wall, then the required strength can be derived by *Laplace's* law as suggested by Klinge and

coworkers.[40] Human abdominal pressures range from 0.2 kPa (resting) to 20 kPa maximum. According to *Laplace's* law, a thin-walled sphere where the total vessel wall tension [(pressure x vessel radius)/2) is independent of the layer thickness (wall thickness/vessel radius << 1) can be described by, F = p x d/4 (N/cm) where d = diameter, p = pressure, and F = wall tension/cm of circumference. If the longitudinal diameter of the human abdominal wall is 32 cm, a tensile force of 16 N/cm is produced at the maximum pressure. To define the physiologic strain associated with a 16 N/cm load, Junge and coworkers, analyzed the abdominal wall of 14 fresh corpses and determined that longitudinally the average extension was 25% ± 7%.[41] However, Cobb and coworkers directly measured the intra-abdominal pressure of 10 healthy male and 10 healthy female subjects performing various activities, including coughing and jumping, two known activities that produce maximum intra-abdominal pressures. These measurements indicated that the maximum tensile force ranged from 11 to 27 N/cm.[42] Wolloscheck and colleagues investigated the tissue burst force of individual layers of the lower abdominal wall. Their findings include burst force values for the transversalis fascia, peritoneum including the pre-and sub-peritoneal tissue, the aponeurosis of the internal oblique, and the aponeurosis of the external oblique measured as 10.5N, 46.6N, 51.7N and 92.6N, respectively.[43] This suggests that the transversalis fascia is the weakest of the load bearing tissues; further evidence of the minimal support provided by the transversalis fascia covering the myopectineal orifice.

Hernia Development and Surgical Intervention Using Meshes

Surgical hernia intervention is the most common elective procedure in general surgery with inguinal hernioplasty performed at the annual rate of 800,000 in the United States, 200,000 in Germany, 100,000 in France, 80,000 in the United Kingdom, and 12,000 in Finland.[44-46] The most important modern advancement in hernia surgery has been the development of so-called tension-free repair using meshes.[47]

Anatomical Classification of Hernias

Hernias of the abdominal wall form at areas susceptible to a loss of mechanical integrity through acquired or congenital pathologies. The weak points of the abdominal wall are the inguinal, umbilical, and femoral canal regions. From epidemiology data, it is known that the prevalence rates for abdominal wall hernias are approximately 73% inguinal, 9.5% umbilical, 6.2% incisional, 2.7% femoral, and 8.6% other types such as spigelian, hiatal, or epigastric.[48] Inguinal hernias are classified as direct or indirect.

Indirect inguinal hernias occur when a visceral sac leaves the abdominal cavity, enters the deep inguinal ring, and transcends the spermatic cord. The hernial sac contains peritoneum and viscera such as adipose tissue, intestinal loops, or omentum and is surrounded by all three fascial coverings of the spermatic cord. The hernia can traverse the entire inguinal canal and exit through the superficial inguinal ring. In severe cases the hernial sac enters the scrotum. Indirect inguinal hernias can occur in women, but they are twenty times more likely in males.

Direct inguinal hernias occur when the peritoneum with subperitoneum tissues and/or abdominal viscera herniate through a weak point in the abdominal wall. The typical location of direct inguinal hernias is within the confines of the medial triangle of the myopectineal orifice.[35] The hernial sac is formed by distention of the transversalis fascia lateral to the rectus abdominus muscle and it emerges to reach the superficial inguinal ring, gaining an outer covering of external spermatic fascia inside or parallel to that on the cord. It rarely enters into the scrotum. Direct hernias are most common in elderly men.

Femoral hernias occur within the femoral triangle of the myopectineal orifice and result from the distension or the rupture of the transversalis fascia.[49] It is generally accepted that they are the result of elevated intra-abdominal pressure and/or an enlarged femoral ring which facilitates the peritoneum and preperitoneal adipose tissue to protrude through the femoral ring.[50] Subsequently, the hernial sac may travel along the femoral vessels and settle in the anterior thigh.[51] Femoral hernias are more frequent in women than men (4:1).[52]

Umbilical hernia prevalence in adults has a female to male ratio of 3:1 with particular frequency in obese, multiparous women.[53] The etiology of umbilical hernias in adults is believed to initiate during embryonic development through defects in the closure of the embryo's abdominal orifice from which the umbilical cord emerges after the obliteration of the celomic sac. Over time this weakness manifests itself at the superior aspect of the umbilicus, becoming susceptible to increased intrabdominal pressure which

may drive forward gobbets of preperitoneal fat or an incipient sac. This condition stretches the fascia before it into a funnel and eventually progresses into a hernia.[54]

An incisional hernia is one that appears at the site of an incision from a previous abdominal operation. An incisional hernia can appear within months or take many years to become evident to the patient. Incisional hernias are sometimes referred to as ventral hernias, due to their typical position between the rectus abdominal muscles and through the linea alba, the preferred midline incision used by surgeons for visceral access during laparotomy.

The Surgical Repair of Hernias

Early attempts at primary intention tissue repairs of groin hernias resulted in unacceptably high recurrence rates due to dehiscence. The endogenous tissue tension of the abdominal wall accounted for the poor results in primary repairs. Primary intention repair is still performed for small defects but is outside of the scope of this review. For the last three decades, surgical repair with meshes has been considered the gold standard for any sizable hernia defect.[36] Hernia surgical repairs can be divided into two classifications; (1) open repairs and (2) laparoscopic repairs.

Two commonly used open repairs for inguinal hernioplasty are the Lichtenstein repair and the giant prosthetic reinforcement of the visceral sac repair. Lichtenstein repair is the most frequently performed hernia repair worldwide due to its short learning curve and ease with which general surgeons can obtain acceptable results.[44] The Lichtenstein procedure uses an anterior approach with, most commonly, a polypropylene

mesh. The mesh is placed in an onlay position[55] and to accommodate the spermatic cord, a slit is placed in the mesh with the two tails overlapping behind the spermatic cord to avoid recurrence lateral to the superficial inguinal ring.

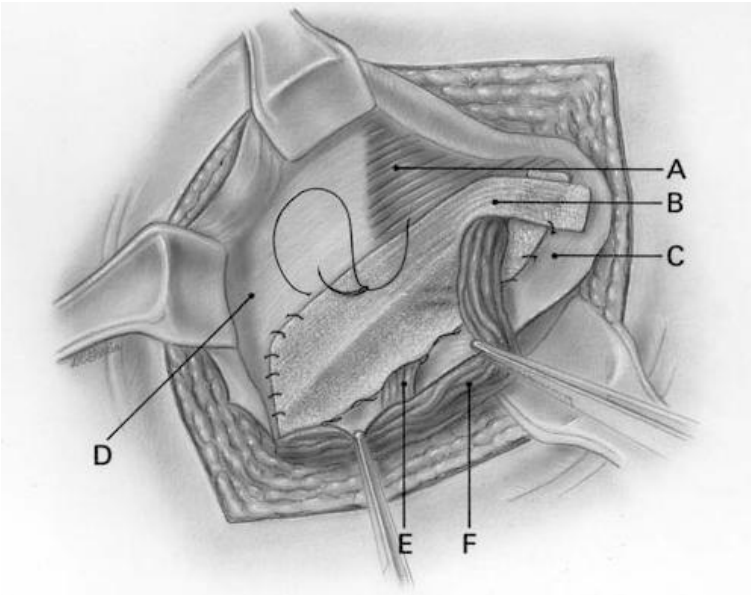

Figure 1.4

Mesh placement for the Lichtenstein procedure. A - internal oblique muscle, B - polypropylene mesh, C - inguinal ligament, D - internal oblique aponeurosis, E - lesser cord containing the genital nerve, F - spermatic cord[55]

The giant prosthetic reinforcement of the visceral sac (GPRVS) procedure[56,57] was developed to repair bilateral and complex recurrent inguinal hernias due to its use of a large mesh that covers both inguinal regions. The GPRVS's alternate approach to the Lichtenstein procedure eliminated the need to operate through distorted anatomy and scar tissue from the previous surgical site.[58] The procedure obtains preperitoneal access through a midline subumbilical incision allowing access to the preperitoneal space for blunt dissection. Short term fixation is assured by dissection pocket size, friction, and

hydrostatic pressure, all combining to achieve long-term security from tissue ingrowth.[59] The result is bilateral mesh coverage within the preperitoneal space of sufficient size to span all of the potential hernia defects of the myopectineal orifice: indirect, direct, and femoral.[60,61] The effectiveness of the GPRVS procedure was noticed by minimally invasive surgeons and the concept became the basis for laparoscopic procedures.

Currently, there are two types of laparoscopic hernia repair; the transabdominal preperitoneal (TAPP) repair and the totally extraperitoneal (TEP) repair,[62] with the TAPP repair being more common.[63] The advantage of laparoscopic techniques are decreased postoperative pain, faster recovery, quicker return to daily activities, coverage of all potential hernia defects, and minimal fixation required due to assisted stabilization from intra-abdominal pressure.[64] Critics of the process cite increased cost, the use of general anesthesia, the need for advanced skills that require a long learning curve to master, and rare but disastrous potential complications.[64,65] For the TAPP procedure, the peritoneal cavity is accessed with an incision with the subsequent creation of a pneumoperitoneum. Next, a peritoneal incision is made above the hernia defect to enter the preperitoneal space. Dissection is completed when a pocket of adequate size to cover the myopectineal orifice is achieved. The mesh is inserted and fixed, typically with staples.[66]

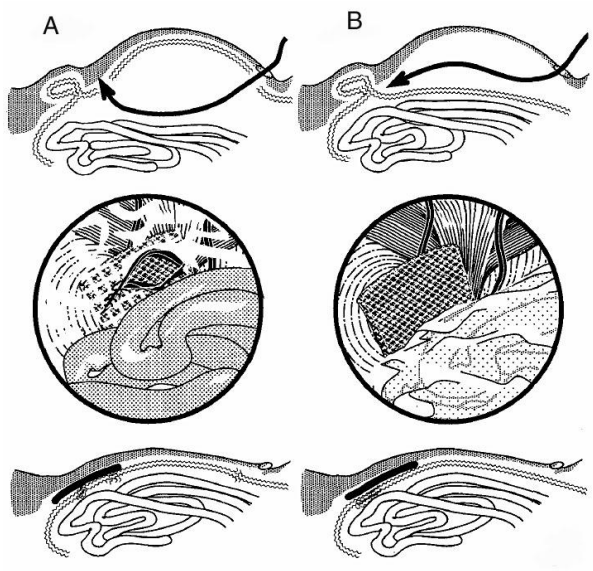

Figure 1.5

The laparoscopic techniques for hernia repair. (A) The transabdominal preperitoneal (TAPP) technique using preperitoneal mesh placement through a peritoneal incision and (B) the totally extraperitoneal technique (TEP) using a mesh placement procedure that does not enter the peritoneal cavity.[66]

The TEP procedure uses the same preperitoneal mesh placement with the exception that access to the hernia is created through the preperitoneal space using dissection to produce a pneumo-preperitoneum.[66] The TEP approach is technically more difficult but it avoids the potential risk of damaging intra-abdominal organs and no additional incisions are made into the peritoneum.

Complications Associated with Surgical Hernia Repair Using a Mesh

The introduction of non-absorbable mesh for hernia repair has reduced the incidence of recurrence, but its presence as a permanent biomaterial has produced several short-term and long-term complications, all of which have inherent interdependency.

Short-term complications include hematoma[67], morbidity from infection[68,69], seroma[70-72], primary mesh migration[73], wound dehiscence[74], or dislocation and protrusion[75,76] through the defect site. Long-term complications are of great interest due to their significant impact on patient quality of life and include neuralgia (chronic pain and paraesthesia), chronic inflammation, mesh shrinkage, stiffness or reduced abdominal wall mobility, secondary mesh migration, fistula or mesh adhesion, and recurrence.

Chronic postoperative pain caused by neuralgia is one of the main long-term complications following inguinal hernia repair and regarded to be the most common failure of groin hernia surgery.[77,78] Recent literature reviews, comparing trials with follow-ups greater than 3 months, have reported that chronic pain after inguinal hernia operation may occur in 10-62% of patients, with considerable impact on a patient's daily quality of life.[45,79,80] Suggested etiological factors for neuralgia include irritation or damage to inguinal nerves by incisions or dissections, severance by sutures or tacks, a chronic inflammatory reaction to the mesh, or entrapment/compression of nerves from scar tissue development.[45,78,81,82] Data suggests that intraoperative nerve damage may be the most important mechanism for developing chronic pain; however, a nerve lesion is not the only factor leading to neuralgia, as many more patients have paraesthesia or sensory abnormalities, rather than pain, after inguinal hernia repair.[83] As many as fifty percent of patients with a large mesh prosthesis complain of paresthesia at the palpable stiff edges of the mesh.[84] These more prevalent sensory abnormalities may originate from the chronic inflammatory response and subsequent fibrosis and/or shrinkage of the mesh. Historically, it was believed that mesh repairs reduced chronic pain compared to

primary repair but recent long-term investigations suggest that there is no statistical difference between patient complaints about mesh and primary repair.[85]

The characteristic chronic inflammatory response to non-absorbable meshes is at least in part responsible for several additional complications. Mesh shrinkage has been explored extensively following observations during revision surgeries that significant folding and shrinking of the mesh was apparent. Mesh size reduction resulting from myofibroblast activity reduces the pore size and causes buckling and folding of the prosthesis. Pore size and overall mesh length has been observed to reduce by 20% in meshes explanted from patients.[68] Furthermore, a study conducted by Klinge and coworkers, using polypropylene mesh on the posterior sheath of the rectus fascia within the preperitoneal space of dogs, produced an overall reduction in area of 46% within 4 weeks of implantation.[86] The extent of mesh shrinkage has been shown to be directly proportional to the degree of inflammatory response.[87]

In addition to shrinkage, the inflammatory response to typical mesh biomaterials results in significant fibrosis that increases the rigidity and stiffness of the abdominal wall.[88] As reviewed by Welty and coworkers, 50% of patients report some form of physical restriction of the abdominal wall.[89] Chronic inflammation is also responsible for slow and gradual secondary migration of mesh through trans-anatomical planes due to foreign-body reaction induced erosion of local tissue.[68,73] In addition, from a mechanical point of view, irritation and inflammation from a hard material in contact with soft tissue can induce erosion in the latter.[90] This is especially true in the case of stiff and rigid

monofilament polypropylene mesh. Consequently, mesh can enter the abdominal cavity causing visceral adhesions and/or fistula formation.[91]

Etiology and Pathology of Hernia Development

Is the development of abdominal wall hernias the result of an anatomical defect or collagen disease? Historically, hernia genesis was attributed to a mechanical disparity between visceral pressure and resistance of the structures within the myopectineal orifice. Which of these factors are significant contributors? Increasingly, hernia etiopathology is described as a multifactorial process linking an evolutionary anatomical weakness, predisposed defects, and dynamic factors such as increased abdominal pressure. The influence of each of these factors in the primary formation and recurrence of hernias is an area of significant debate.

Mechanisms in the Development of Primary Hernias

Evolution has clearly left human beings with a section of the abdominal wall that is weaker in comparison to the rest of the abdominal wall: the majority of hernias occur in the myopectineal orifice of the inguinal region. The thin and weak transversalis fascia of the groin coupled with the lack of fascial sheath below the arcuate line together form the argument for an intrinsic defect in the human abdominal wall.[92] Many surgeons believe the transversalis fascia does not even resemble fascia or any tendinous-like structure; the transversalis fascia is a thin, fibro-membranous peritoneum with markedly reduced strength as compared with typical fascia.[92] The myopectineal orifice is sealed by

the transversalis fascia; thus all groin hernias are the result of the displacement of this fascia by a peritoneal sac.

Hernia development can be congenital in the case of indirect hernias. In this case a visceral sac leaves the abdominal cavity and transcends the spermatic cord. Congenital predisposition in males originates during the descent of the fetal testes into the scrotum. Interruptions in the closure of the deep inguinal ring can develop into a potential defect later in life.[51] Indirect hernias are more common on the right side than left. The right testicle descends from its position near the kidney into the scrotum after the left testicle has already completed its descent. The delay in the closure of the deep inguinal ring on the right side is believed to be responsible for its side-specific hernia predominance.[92]

Increased intra-abdominal pressure is believed to be a contributing factor in the pathogenesis of herniation.[93] Risk factors include obesity and chronic constipation. Often hernias are thought to be the result of a single event (e.g. lifting a heavy object) but in fact repetitive mechanical strain is likely the damaging factor.[94] It is possible that chronic mechanical strain, not prior biologic defects, may induce secondary changes in structural tissue cellular and molecular function.[95] However, increased intra-abdominal pressure is speculative in nature with no clinical study to confirm its contribution to hernia formation.[93] Furthermore, no adequate animal model exists that can simulate hernia formation or replicate the increased intra-abdominal pressure from erect posture gravitational forces on the floor of the abdominal wall.[92]

The Role of Biochemical Mediators and Collagen in Hernia Formation

Collagen is an active living tissue that is in a constant balanced state of production and degradation. Because collagen has a long half-life and is the primary biomechanical strength component in connective tissue, collagen has become the critical component for investigation in the search for hernia genesis. So-called collagen disease is thought have two pathologies, (1) a metabolic defect and/or (2) structural abnormalities in any of the steps related to collagen fiber formation.

Imbalances in the connective tissue metabolic pathways are being investigated to explain whether the quality of collagen is caused by the presence of destructive enzymes or by the lack of inhibitors to those destructive enzymes. Collagens are mainly degraded by matrix metalloproteinases (MMPs) and under normal conditions, are required for the proper progression and maturation of wound healing.[96] MMP-1 and MMP-13 are the primary collagenases responsible for type I and type III collagen turnover.[97] Klinge and coworkers found that skin of patients with groin hernias had significantly different upregulated levels of MMP-1 and MMP-13 compared to controls.[98] In another study by Klinge and coworkers, the expression level of MMP-1 in excised hernial sacs of patients with either direct or indirect hernias was not different compared to that of peritoneum control samples.[99] In addition, MMP-13 was absent from either the hernial sac or control tissue. Rosch and coworkers analyzed MMP-1 and MMP-13 in cultured fibroblasts from the skin of patients and concluded that neither was involved in primary inguinal hernia.[100] Overall, the implications of MMP-1 and MMP-13 in hernia formation are mixed and inconclusive.

MMP-2 and MMP-9 have been identified as enzymes that break down collagen Types IV and V as well as gelatin, elastin, fibronectin, and other matrix components. Both are derived from neutrophils and have been found local to direct hernias but not indirect hernias.[101] In addition, MMP-2 overexpression in fibroblasts from the transversalis fascia has been observed in young patients with direct hernias but not in indirect hernia patients.[102,103] The increased levels of MMP-2 and MMP-9 have also been related to diminished levels of tissue inhibitors of matrix metalloproteinases, e.g. TIMP-1 and TIMP-2 are generally linked to elderly patients[104] as well as indirect and direct hernia patients.[105] Evidence suggests that MMP-2 and MMP-9 may have a link to direct hernia formation, especially in elderly patients.

Connective tissue quality is significantly influenced by the quantity and ratio of Type I/III collagen synthesis and deposition.[106] Altered collagen composition with increased levels of Type III has profound effects on tissue elasticity and resistance to applied stresses. The genetic expression of Type I or Type III procollagen mRNA affects the Type I/III ratio. The different genetic expression pathways are poorly understood, emphasizing that genetic influences on hernia formation are still not clear. In an attempt to determine whether metabolic or gene transcriptional defects are the primary factors for an altered Type I/III collagen ratio, studies have been conducted using the skin of incisional and inguinal hernia patients.[98,100,107-109] Each of these studies concluded that a statistically significant downward shift in the Type I/III ratio was evident in hernia patients as compared to controls or non-hernia patients, strengthening the position that a systemic collagen disorder may predispose patients to hernia disease. However, it should

be noted that these studies are better characterized as observations of small numbers of patients and more extensive, prospective studies are required to completely understand if aberrations within the collagen gene expression profile supports a transcriptional dysregulation relevant to hernia disease.[110]

The collagen fibril formation process is critical to collagen quality as fibrils are the principle source of structural integrity.[110] The extent of hydroxylation of lysine and glycosylation of hydroxylysine provides the intermolecular and intramolecular covalent bonds responsible for the bulk strength of mature collagen.[111] During remodeling and maturation, collagen fibers increase in diameter reflecting the change in the ratio of Types I and III collagen.[107] Differences in the rectus sheath ultrastructure of hernia patients compared to non-hernia patients have been the target of several studies.[112,113] Results indicated that for hernia patients, the ultrastructure of the rectus sheath had irregularly arranged fibers that exhibited disturbed collagen hydroxylation, fibers with caliber differences, and fewer collagen fibers that were replaced with ground substance. Unfortunately, not enough is known about the structural and molecular-cell basis of collagen fibrillogenesis to confidently define it as the etiology of hernia disease.[110]

Causes of Recurrent Hernias

In approximately 60% of all excised meshes, recurrence is the reason for extraction.[114] The recurrence of hernia repairs has frustrated surgeons for many years, especially incisional hernia recurrence with rates of 11-15% within the first year and a doubling of the high initial rates within the first nine years.[115] The stated causes of

recurrence include stress applied to the wound prior to the development of mechanical integrity, shear stresses at the margins of the mesh during collagen maturation, collagen metabolism disorders, infection, and surgical technical errors. Immediate gross failure in most cases is attributed to surgeon technical failure or infection, while longer term (> 3 months) failure stems primarily from abnormal wound healing such as varied collagen metabolism and the progress of acute wound disruptions into symptomatic failures.

There is evidence that hernia recurrence of mesh-repaired laparotomies is the result of external stresses applied to the wound site prior to the development of tissue integration and wound strength (first 2-3 weeks post insult). As reviewed by Franz, one prospective study of primary repaired incisional hernias found that the total rate of acute wound disruption was about 11% at post-operative day 30 with the majority (94%) later developing into incisional hernias.[95] Primary repaired incisional hernias fail by wound dehiscence from sutures pulling through the wound edges. Similarly, mesh acute wound failures also occur from stressed suture lines at the margins of the mesh creating mesh-fascial dehiscence. The result of the failure is a loss in tension applied across the wound. The loss of mechanical load signaling may impair fibroblast biology which promotes subsequent collagen abnormalities leading to the high rate of recurrent incisional hernia formation.[95]

Recurrent hernias develop 99% of the time at the margins of the implanted mesh.[87,114,116-118] Owing to the significant strength of most meshes, central mesh ruptures are a documented but extremely rare occurrence.[119,120] The nonphysiologically low stretching capability of the mesh/tissue complex contrasts with the highly elastic

abdominal wall resulting in shear forces at the margins of the mesh. These forces overstress developing and maturing collagen resulting in recurrence at the margins of the mesh.[84]

Incisional hernias are also being investigated as an abnormal wound healing response with an inability to produce abundant, quality, strong collagen. As with primary hernias, metabolic factors are being investigated; however, more evidence supports collagenase as a central agent involved with the development of incisional hernias when compared to primary hernia formation.[97] Though this may be, it is hard to accept metabolic factors as the primary pathway to recurrent hernia when the majority of patients do not have a history of wound healing defects and do not express any defects in organs local to the surgical site or the vascular system.

Knitting Technologies and Their Relevance to the Properties of Surgical Meshes

Knit textile structures come in two general forms; (1) weft knit and (2) warp knit. Mesh construction can be dramatically different between the two structures, but the concept of using intermeshing loops of yarn is the same for both. The properties of a knitted structure are largely dependent on the interaction of each stitch with its neighboring stitches in the course and wale directions. The course is the cross direction to the fabric production, while the wale is the parallel direction to the fabric production.

Weft Knit Mesh

The simple weft knit structure is formed by loops created by needles knitting fiber across the width of the fabric with each loop being created by pulling it through the previous loop in the same direction (Figure 1.6a). Needle movements are simply up and down and are controlled by a cam. When the needles are in the up position, each weft fiber is fed at an angle to the direction of fabric formation, single or multiple ends of fiber can be fed into the mesh at one time but each end knits the same pattern with no overlap or variation.

Looking at a cross-sectional view of the structure, all the loops are bent into the third dimension due to the manner in which loops are pulled through each other. This configuration results in an unbalanced structure which causes the mesh to curl at the edges in an attempt to release some of the strains within the loops.[121] The simplicity of the weft knit structure with minimal cross-over points between courses and wales makes it strong in burst strength, extremely porous, highly drapable, and highly elastic. However, the greatest obstacle for the weft knit construction in use for medical applications is that they easily run from their edges, especially when cut.

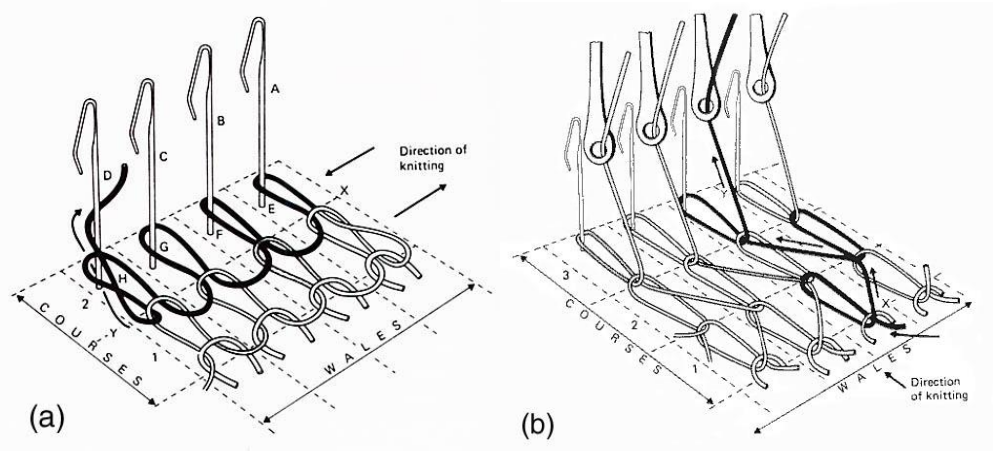

Figure 1.6

Knitted fabric from (a) a simple weft and (b) a single guide bar, half-tricot warp knit construction.[122]

Warp Knit Mesh

Warp knitting differs from weft knitting in that loops are formed by every needle in the needle bar during the same knitting cycle from series of warp fibers that are fed parallel to the direction of mesh formation (Figure 1.6b). The so-called warp, is a sheet of fiber with ends wrapped concentrically in parallel on a cylindrical beam prepared in a creel prior to being mounted on the knitting machine. The warp fibers lap the needle bar simultaneously by a series of guide bars that move through and then laterally to the needle bar. Lateral movements include underlaps which are produced on the mesh production side of the needle bar and overlap on the alternate side. The number of guide bars is pattern-specific but generally varies between one and four.

Warp knit meshes provide versatile pattern selection, control of elasticity, unraveling resistance, good drapability, control of porosity, good dimensional stability,

and high strength. Medical meshes used in hernia applications are constructed in such configurations as the queenscord, tricot lapping, atlas lapping, and the sand-fly net.[123]

Mesh Properties as Determined from Knitting Type and Construction

The elasticity and strength of a weft knit mesh is controlled by the number of needles per inch, i.e. gauge, and the stitch length, which controls the number of courses per inch. The gauge is typically set by the machine configuration leaving the stitch length as the only adjustable variable. Although elasticity and strength can be somewhat adjusted, there is no structural variability to further modify the weft knit properties.

The variability available with warp knitting allows extensive modulation of the physical and mechanical properties. To produce elastic or stretchable structures, the mesh must be designed with either (1) short underlaps or (2) an open mesh construction.[124] The most basic example of short underlaps is a single guide bar, one needle underlap and one needle overlap, commonly referred to as a half-tricot stitch. Increases in the underlap movement reduce extensibility and increase stability. The half tricot pattern produces a dimensionally stretchable mesh with relatively small pores. To produce larger openings in the mesh, loops can be formed continuously on the same needle such that there are no connections by adjacent wales (underlaps) followed by a lateral interlace after a specific number of courses.[125] Different size and shape openings can be produced with symmetrical pores when knit using partial threading of two guide bars that are lapping in opposition. Another significantly less extensible open work mesh that can be created is a lay-in mesh, i.e. a marquisette construction. Lay-in constructions,

at the most basic level, consist of a chain stitch, or series of stitches from one needle in the course direction, joined together by laying-in yarn between the loops. The lay-in yarn does not form a stitch because it does not have lateral movement during the overlap, only during the underlap. As such, the fiber does not enter the hook of the needle but rather is captured within the loops of the chain stitch.

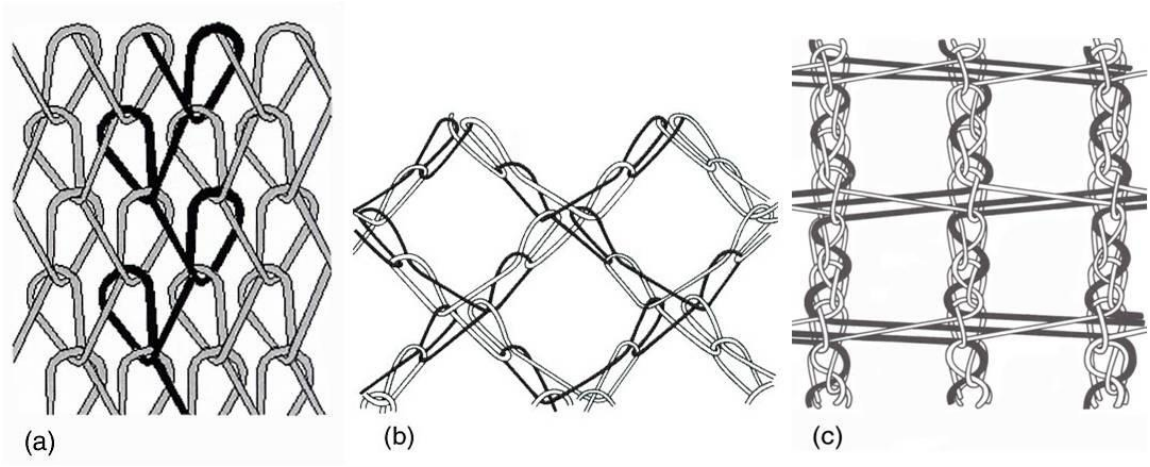

Figure 1.7

Examples of (a) a short underlap mesh (half-tricot), (b) an open work mesh (sand-fly net), and (c) a lay-in mesh (3-guide bar marquisette).[122,125]

Stabilization of Mesh Constructions using Heat Setting

Mesh dimensional stability and refinement of the fiber microstructure morphology are accomplished using a heat setting process. The effect of heat setting is affected by the temperature, time, and tension applied during the process with the most significant factor being temperature.[126] Fiber morphology is altered by relieving induced stress from orientation and increasing the fibers entropy. As a result, stresses in the

construction of the mesh are relaxed improving dimensional stability, heat stability from entropy driven shrinkage, handling characteristics, and in many cases the softness of the mesh.

Meshes as Biomaterials

An ideal mesh material should be strong, compliant, non-allergenic, sterilizable, chemically inert to the biologic environment, resistant to infection, dimensionally and chemically stable *in vivo*, non-carcinogenic, cost effective, and should stimulate fibroblastic activity for optimum incorporation into the tissue with no long-term reaction.

Clinically Relevant Mesh Materials

Each material used for the construction of hernia meshes has its advantages; however, all of them reveal some disadvantages. Currently there is no ideal mesh material, but polypropylene is most common regardless of certain drawbacks.

Polypropylene (PP)

Polypropylene is a linear aliphatic hydrocarbon with a methyl group attached to alternate carbon atoms on the chain backbone ($-C_3H_6-$). As a result it is nonpolar and highly hydrophobic. The addition of the methyl group has many physico-mechanical, structural, and chemical implications. Physico-mechanically the methyl group stiffens the chain by reduced molecular mobility from this relatively bulky side group. Polypropylene derives its mechanical properties from chain entanglement and

intermolecular secondary bond forces (van der Waals-London forces) from induced dipole hydrogen bonds between chains.[127] Structurally the methyl group produces tacticity with medical grade PP being highly isotactic with approximately 95% crystallinity. All of the methyl groups are configured to one side of the carbon backbone in the isotactic form, thereby creating a regular structure and facilitating crystallinity. Steric hindrance from the methyl group forms crystals in helical conformations, unlike the planar zigzag form of polyethylene. The presence of the methyl group also affects its chemical nature, providing a tertiary carbon atom that is susceptible to oxidation and chain scission.[128] However, overall PP is considered to be an inert, stable material that provides an adequate service life *in vivo* as a mesh material.

Polyethylene Terephthalate (PET)

Polyethylene terephthalate was introduced as a mesh material for hernia repair more than 30 years ago and continues to be used today, although its use is limited in most countries, with the exception of France.[129] PET is a heterochain linear aromatic polymer with repeat units comprised of ester groups on either side of its ring and two ethylene moieties added to one side ($-C_{10}H_8O_4-$). As such, the polymer is slightly polar, more hydrophilic, and hygroscopic than homochain hydrocarbon polymers. The characteristic feature of PET is its two ester linkages in the backbone of the polymer chain. Chemically the ester groups create chemically liable sites that are susceptible to hydrolysis and thus chain scission. However, the local hydrophobic moieties slow this reaction considerably. Physico-mechanically the stronger dipole-dipole type van der Waals-London forces

between adjacent carbonyl groups contribute to its high strength characteristics.[127] Structurally PET is a semicrystalline polymer with crystallization kinetics such that the level of crystallinity can be controlled through thermal history and strain-induced crystallization. The second most important characteristic is its aromatic ring which adds stiffness to the backbone of the chain enhancing its physical and mechanical properties. Accordingly, PET is typically processed into fine multifilaments rather than monofilament fibers in surgical meshes.

Expanded Polytetrafluoroethylene (ePTFE)

Expanded polytetrafluoroethylene is not a widely used material for hernia meshes. Its application is generally limited to surgical situations where visceral adhesion is of major concern. Polytetrafluoroethylene (PTFE) is a linear homochain polymer constructed of a carbon backbone saturated with fluorine atoms ($-CF_2-$). The characteristic feature of PTFE is its inert nature, due to the extreme stability of the carbon-fluorine bond. PTFE is highly crystalline; however, although the structure is similar to polyethylene, crystallites are not formed in the planar zigzag form. Instead, a modified form of a twisted zigzag is created due to steric hindrance from the increased size of the fluorine atom compared to hydrogen.[130] The intermolecular attraction between PTFE molecules is very small and thus its bulk properties do not possess the high rigidity and tensile strength associated with other hernia mesh materials. Also, the physical form of PTFE is the exception to the typical fiber form of hernia mesh materials. The morphological difference is due to the high crystalline melting point of PTFE being

very close to its degradation temperature leaving no melt processing window. Accordingly, ePTFE is manufactured by stretching and sintering a solid melt-extruded sheet while at the same time producing a node-fibril structure that results in micropores. This process gives rise to the "expanded" precursor designation.

Partially Absorbable Mesh Constructions

The intent of partially absorbable mesh constructions is to reduce the amount of biomaterial, e.g. polypropylene, in an attempt to reduce the foreign body response. Meshes constructed from a combination of a 10/90 copolymer of poly(L-lactide-co-glycolide) and polypropylene have become the most common form of partially absorbable mesh and are the most investigated. Theoretically the reduced level of resident mass results in less fibrosis, structural changes that result in larger pores, and less chronic inflammation.[131] Partially absorbable meshes are constructed by plying the different filaments together and then knitting the plied yarn to produce a mesh with approximately 50% absorbable polymer.[84] The high polyglycolide copolymer is a linear, aliphatic polyester comprised of a single ester and ethylene group ($-CH_2COO-$). The ester group in the chain backbone is readily hydrolyzed due to its somewhat hydrophilic nature and a lack of any side chain structures that provide steric hindrance. Polyglycolide produces relatively high levels of crystallinity from planar zigzag crystallites which give the material excellent stiffness. Mechanical properties are typically reduced about 50% in 2-3 weeks with complete absorption within 90 days.

Mesh Characteristics Pertinent to Biocompatibility

The design characteristics of meshes include construction, fiber form, fiber surface, and bulk chemistry. Collectively these characteristics significantly influence the biocompatibility of a mesh and its mechanical suitability for a particular application. However, although the design characteristics of meshes have produced significant debate with regard to their respective influences, no study has been completed which isolates each characteristic. For example, an *in vivo* study that compares the same construction and yarn form and differing chemistry does not exist. To date, studies have been conducted using commercially available meshes, and each has a different construction, fiber form, and fiber chemistry making it difficult to isolate the influence of individual mesh design variables. However, observations about mesh design variables have provided insight into their general influence on biocompatibility.

Mesh Construction

Mesh construction can be extensively varied and has implications on pore size, area weight, drape, extensibility, and strength, all which clinically translate into surgical handling characteristics, anatomical conformability, foreign body reaction, and the mechanical, cellular, and extra cellular matrix characteristics of the mesh/tissue complex.

The porosity of a mesh is best described as the amount of open space in a unit area of mesh. However, this description does not provide a complete picture as the dimensions/area of individual pores, the distance between pores, and the size and quantity of interstitial pores, are also contributing factors to *in vivo* performance. Porosity is a

rarely measured characteristic. Recently, a study using digital imaging was conducted in order to better characterize the overall porosity and the distribution of different pore sizes for clinically relevant meshes.[132] The porosity of meshes is a primary determinant for tissue response, with pore size implicated in affecting long-term abdominal wall mobility. It has been suggested that pores smaller than 1mm lead to extensive inflammation and fibrosis, resulting in a bridging of collagen between adjacent pores.[84,114,133] Ultimately this occurrence produces a dense, continuous outer fibrotic capsule covering the whole mesh. Several investigations using a rat[134-136] and a porcine[137] animal model have concluded that larger pores result in increased abdominal wall mobility due to reduced fibrotic bridging. In addition, the absence of a complete capsule covering the mesh facilitates improved fluid transport through the mesh, as well as improved vascularization and organization of connective tissue.[138] Based on increasing evidence, porosity is a key factor in the incorporation of the mesh into the surrounding tissue, and thus an important prerequisite to its biocompatibility.

Area weight, measured as the mass per area (g/m^2), is a determination of the total amount of biomaterial implanted for a given area. Theoretically, lower area weights induce a milder foreign body reaction, improved abdominal wall compliance, less contraction or shrinkage, and allow better tissue incorporation; as a result, the use of lighter weight or partially absorbable meshes has been investigated to improve hernia repair outcomes. However, the available data is contradictory and controversial. The outcomes from partially absorbable meshes are mixed. Early investigations in a rat animal model indicated long-term decreased inflammation as a result of the long-term

decreased polypropylene content.[136,139] However, Weyhe and coworkers have investigated the changes in foreign body reaction in both a rat animal model[140] and *in vitro*[141,142] and determined that simple reduction of the mesh mass was not the main determinant of biocompatibility; rather, pore size and material composition were better indicators. Clinical trials have produced conflicting outcomes as well. Several studies have found no significant differences between typical polypropylene meshes and partially absorbable meshes in multicenter studies using Lichtenstein hernioplasty.[143,144] Conze and coworkers found similar outcomes when comparing partially absorbable and standard polypropylene meshes; however, partially absorbable mesh had a trend toward increased hernia recurrence.[145] Other authors have reported improvements in some aspects of pain and discomfort using partially absorbable meshes,[146] but in addition to less chronic pain, an increase in recurrence has also been reported.[147] In a recent review of current randomized controlled trials and retrospective studies, partially absorbable meshes seem to have some advantage with respect to post-operative pain and foreign body sensations, but their use is associated with increased recurrence rates.[148] The movement toward the use of lower weight meshes has shown researchers and clinicians that long-term, lower area weight meshes appear to reduce some complications but at the cost of an apparent increase in recurrence.

The mesh construction *in vivo* can influence the mechanical properties of the mesh/tissue complex. When a mesh is stressed, the mesh filaments show minimal if any elasticity, while the mesh itself produces extensive elongation from geometric deformation within the pores perpendicular to the applied stress. Thus, the elastic

characteristics of a mesh and the ability to match those of the natural abdominal wall are predominately influenced by construction. In a study conducted by Greca and coworkers a polypropylene light weight, macroporous mesh (19 g/m^2) was compared to a typical so called 'heavy weight' mesh (85 g/m^2) in the repair a full-thickness abdominal wall defect in a dog animal model. Although the heavy weight mesh had 3.6 times the initial burst strength of the light weight mesh, after 90 days *in vivo* the mesh/tissue complex for the light weight mesh produced marginally greater average burst strengths than the heavy weight mesh.[149] The authors attributed the increased strength to a higher concentration of mature type I collagen developed around the light weight mesh. The mechanical characteristics of the mesh construction are important factors, as the maturation of the mesh/tissue complex is a critical indicator of biocompatibility.

The strength of a mesh is not only characterized by yarn diameter or denier, number of yarns, and tenacity of the yarn, but construction also affects the burst strength. The nature and extent of yarn looping within the mesh construction affects the burst strength due to stress concentrations. For a given mesh construction, stronger mesh yarn does not always translate linearly to increased mesh burst strength. Construction can play a limiting role in the strength of the construct.

Type of Yarn

Monofilament-based meshes have marked stiffness, whereas multifilament meshes have improved softness, less surface texture, and better drape characteristics for adaptation to anatomical curvatures. Multifilaments physically have a pronounced

increase in surface area, which influences their biocompatibility. *In vivo* testing in a rat animal model has suggested a more intense acute inflammatory response and increased fibrosis to multifilament yarn than monofilament yarn.[150-152] The authors attributed the upregulated response to the increased tissue/biomaterial surface contact area. Patients implanted with either multifilament or monofilament polypropylene meshes for inguinal hernioplasty were investigated for inflammatory response differences. Blood samples were collected before surgery and up to 168 hours post-surgery, and were analyzed for pro-inflammatory mediators. Results indicated a more intense acute inflammatory response to the multifilament mesh.[153] The increased response may be in part the result of the increased adsorption of host proteins to the implant, which in turn triggers the increased activation of inflammatory cells. Long-term, multifilaments have not been identified as triggering an increased level of chronic inflammation as compared with monofilaments, in fact, more leukocytes and larger multinucleated giant cells have been observed to be associated with monofilament meshes.[154]

Multifilament based mesh constructions have been implicated as producing a higher incidence of infection. Amid suggested that the infiltration and proliferation of bacteria within multifilament meshes is due to interstices or pores that are less than 10 microns.[68] The result is the development of infection by the housing of bacteria which have sizes averaging 1 micron and the exclusion of macrophages and neutrophils of 10-15 microns in size. In fact, infection associated with multifilament meshes often necessitates the removal of the mesh to alleviate the problem, while infection associated with many monofilament meshes can be treated with antibiotics and drainage of the

sepsis.[155] However, a rat study to investigate Amid's claim determined that pore size alone does not predict infection and suggested that collagen fibers and macrophages penetrated and surrounded multifilament fibers at two weeks.[154] Pore size alone is not the only variable in infection prevention. The ability of a mesh to resist infection is also a function of the surface area available for bacterial attachment, biomaterial composition and hydrophobicity, and the interaction with the local host tissue defenses.[156,157] Infection always starts with bacterial adhesion, which is influenced by the surface roughness, hydrophobicity, and the material's inherent ability to generate electro-static forces or an electric charge that transfers between the polymer surface and the bacterial wall, resulting in attraction.[158,159] Klinge and coworkers determined that the surface area of multifilament meshes was increased by a factor of at least 1.57 in comparison to monofilament, thus providing significantly more area for bacterial adhesion. The authors indicated that the increased surface area associated with multifilaments was the primary reason for the persistence of bacteria in the implant bed.[160] In the same study, rats were implanted with monofilament and multifilament meshes which were inoculated with *Staphylococcus aureus* prior to implantation. No increased infection rates were observed between the two fiber forms as compared to controls. Overall, it should be noted that both monofilament and multifilament yarn forms have produced good clinical biocompatibility with long-term experiences.

Yarn Surface and Bulk Chemistry

The surface and bulk properties of a yarn can be dramatically different. Surfaces are physically unique environments with varied mechanical, morphological, barrier, and electrical properties. The surface of a biomaterial is the interfacial transition between bulk chemistry and the *in vivo* environment. The surface provides the only direct chemical or biophysical interaction with the biologic environment. Surface properties are influenced by unsaturated secondary bonds of atoms comprising the surface and their interaction with opposing surfaces or molecules.[161] For the polymers used in meshes, their hydrophobic or hydrophilic nature is derived from unassociated polar and nonpolar groups at the surface. Bulk properties, on the other hand, arise from composition and morphology of everything below a few atoms deep of the surface, determining such properties as elastic modulus, toughness, yield strength, and hardness.

Chemical degradation that results in reduced physical and mechanical properties is the primary obstacle to long-term mesh stability. Due to the foreign body reaction, the mesh material is continuously exposed to super oxides. As previously discussed, polypropylene is susceptible to oxidative degradation. Continuous exposure of polypropylene to these oxidants can lead to chain scission, production of radicals, and degradation to the surface and bulk chemical structure. In one study, 85% of explanted polypropylene meshes exhibited cracks, surface roughness, and peeling of the surface from oxidation.[162] Surface oxidative degradation of polypropylene has been shown to result in bulk property changes such as a loss of mass, a lowering the glass transition and melt temperatures, diminished molecular mobility, and a reduction in yield stress and

elongation at break.[163-166] Moreover, both polypropylene and polyethylene terephthalate have been shown to absorb squalene, palmitic acid, and, in some cases cholesterol.[127] These small organic molecules may act as plasticizers and further decrease yield stress. The bulk degradation and fracture of polyethylene terephthalate yarn from hydrolysis has been realized for vascular grafts and meshes.[167-169] In the future, it is possible that eventual bulk degradation will be realized in polypropylene, which will limit its service life, especially in young patients for whom the mesh is expected to hold for several decades. Remarkably these finding are in contradiction to the widely accepted belief that non-absorbable mesh materials, particularly polypropylene, are stable and inert.

Biocompatibility – Meshes and the Biologic Environment

The word biocompatibility is used extensively, yet a great deal of uncertainty exists about what it actually means and about the mechanisms that collectively control the concept. Several definitions have been proposed, with none gaining widespread acceptance. Historically, the biocompatibility of long-term implanted devices has been graded on their ability to be chemically and biologically inert and do no harm to the surrounding host tissue. As knowledge of the biologic environment has grown, more emphasis is placed on functionally stimulating or avoiding specific cellular or tissue responses. A recent re-definition of biocompatibility has been suggested by Williams: "Biocompatibility refers to the ability of a biomaterial to perform its desired function with respect to a medical therapy, without eliciting any undesirable local or systemic effects in the recipient or beneficiary of that therapy, but generating the most appropriate

beneficial cellular or tissue response in that specific situation, and optimizing the clinically relevant performance of that therapy".[170] The following sections explore the current status of mesh biocompatibility.

Early Phases of Wound Healing and Mesh Integration

The early phases of normal wound healing include hemostasis and acute inflammation characterized by fibrin clot formation, bacterial clearing, and wound debridement followed by proliferation, which includes the formation of granulation tissue and wound contraction. Granulation tissue is made up of a cellular, randomly ordered extracellular matrix containing new blood vessels from angiogenesis. When the acute inflammation phase does not resolve in a timely manner it is said to enter a state of chronic inflammation.

Acute and Chronic Inflammation – Responses to Meshes

Tissue disruption and bleeding during mesh implantation results in fibrin clot formation and a burst of inflammatory cytokines that attract monocytes/macrophages, polymorphonuclear cells, and lymphocytes. From the instant that the mesh is placed *in situ*, surface protein adsorption is initiated followed by a reorganization of the protein layer as described by the Vroman effect. Resident tissue cells such as mast cells and macrophages become activated and respond to the biomaterial. It is believed that these phagocytes attach and interact with the adsorbed proteins rather than with the material itself.[114] Phagocytes attempt but are unable to remove the mesh due to its size and

relatively inert nature. As a result, the healing response moves into the chronic inflammation phase due to the continued presence of the mesh. Consequently, the proliferation phase initiates, but with the continued presence of inflammatory cells.[171]

Within the first few hours, neutrophil activity is initiated with bloodborne neutrophils entering the local tissue by diapedesis. For the ensuing weeks the presence of the mesh stimulates neutrophil activity beyond the time of its normal resolution. Blood samples from mesh and primary repaired hernia patients, up to 168 hours postoperative, suggest the presence of a mesh significantly increases the neutrophil count.[153] Neutrophil activity is detrimental to the healing wound site because of the excessive generation of matrix metalloproteinases favoring the degradation of local and newly formed tissue.[172] Neutrophil activity investigated in a rat animal model using a simulated mesh hernia repair peaked in activity at 3 days and steadily decreased in numbers until 14 days.[173] An investigation by Rosch and coworkers using a rat animal model determined that, in the early phases, the wound area contains predominately macrophages with persistent T-cell activity that lasts through 90 days.[174] In addition, within the first week, mast cell activity is elevated. The mast cell's role in inflammation is mostly credited to the recruitment of inflammatory cells from the release of their granular products including histamine. Furthermore, mast cell release of histamine facilitates increased blood flow and cell infiltration through dilation of arterials and increased permeability of venules.[175] The continuous cytokine generation, which is said to peak between 7 and 14 days, progresses the wound healing response into the proliferation phase as the host tissue attempts to isolate the mesh through encapsulation.

Proliferation – Tissue Integration and Collagen Development

The proliferation phase is primarily characterized by the increased presence of fibroblasts that produce significant amounts of extracellular matrix with maximum deposition at 2-3 weeks. Consequently, the bulk of the collagen is deposited in the proliferation stage; however, even under normal wound healing conditions, high quality collagen is not formed until later in the maturation phase. Wound mechanical integrity begins to develop as the level of crosslinking increases. Unfortunately, the overlap of the acute wound healing trajectory may further delay the recovery of wound tensile strength.[176] Wound inflammation is primarily a protective response; studies suggest that the mechanisms used to destroy bacteria and remove debris delay tissue repair.[177] Fascial tissues within the abdominal wall have been shown to develop strength faster than dermal wounds. Fibroblasts extracted from rat fascial wounds show enhanced cell proliferation and increased wound collagen deposition compared to dermal fibroblasts.[178] Mechanisms for accelerated fascial healing include earlier activation of fascial fibroblasts and earlier induction of collagen synthesis compared to dermal wounds.[179] Macrophages play a fundamental role in the process of extracellular matrix development through direct or indirect fibroblast signaling. Results from animal studies have suggested that the absence of macrophages results in defective scar formation.[180] On the other hand, increases in the time and intensity of inflammation are associated with increased levels of scarring[181]; however, the amount of collagen present at the wound site is not a good indicator of mechanical integrity. The bulk of extracellular matrix production occurs during the proliferation stage, but this does not represent the time at which the

extracellular matrix is complete. Significant changes in orientation and conformation of fiber bundles have yet to occur during the remodeling and maturation stage in order to develop quality collagen.

Development of Vascular Structures – Angiogenesis

Wound repair and normal healing depends on an adequate arterial circulation supplying the newly forming tissue with oxygen. Angiogenesis begins during the proliferation phase. Vasculature in the wound periphery develop small buds or sprouts that grow into the fibrin/fibronectin-rich wound clot and, within a few days, organize into a microvascular network within the granulation tissue. Several factors including vascular endothelial growth factor (VEGF), basic fibroblast growth factor (bFGF), platelet-derived growth factor (PDGF), and transforming growth factor (TGF-β) induce angiogenesis,[182] which is then directed to the wound area by low oxygen tension gradients and elevated lactic acid levels.[183] The development of new blood vessels is critical since healing will not proceed unless new, functioning blood vessels supply oxygen and nutrients to the developing tissue and remove metabolic waste. However, the distribution of oxygen by neovascularization goes beyond nutritional support. There are several posttranslational steps in collagen synthesis that are oxygen dependent and responsible for the development of tensile strength in healed wounds.[184,185] At the end of the proliferative phase, cellular activity is decreasing and there is less need for a rich vascular supply. Consequently, some capillaries aggregate into larger vessels but most of the recently formed blood vessels quickly involute through apoptosis of endothelial cells. Overall,

wound angiogenesis represents a response to coagulation, inflammation, and the temporary increased metabolic need of the wound area that is well beyond the capacity of the vessels that once fed the site.[186]

Laschke and coworkers[187] developed a novel, quantitative method of investigating angiogenesis for mesh implantation in a rat animal model and found that by day 3 of implantation the protrusion of capillary buds and sprouts had originated from the host microvasculature. Until day 10, the sprouts interconnected to form loops and a new microvascular network. By day 14, the vascular ingrowth was complete with venular diameters and volumetric blood flow comparable to those in the host tissue, distant from the mesh. In a study to investigate the effect of yarn diameter on tissue response, fibrotic capsule thickness around individual yarns was reduced when vascular structures were observed close to the filament.[188] The finding is consistent with the expectation that tissue response is more favorable if nutrients are available locally. Additionally, vascular constructs in close proximity to the mesh improve the cellular response to infection. For other implanted, mesh-like constructions such as vascular grafts, investigations have found that the potent cytokines secreted by chronically active macrophages are inhibitors to angiogenesis.[189] This suggests that intense acute inflammation may inhibit angiogenesis. In conclusion, the extensive vascularization of an implanted mesh is imperative to the optimal integration and resultant mechanical properties of the mesh/tissue complex.

Contraction of the Mesh/Tissue Complex

Collagen deposition is accompanied by wound contraction as a natural phenomenon that decreases the area of the wound defect. For mesh hernia repair, it is an undesired consequence that initiates during the second week and is associated with recurrence, migration, and pain.[190,191] The etiology is largely unknown but it has been suggested that during proliferative scars the impaired activity of myofibroblasts renders them unable to control normal fibrillar arrangement; in addition, excessive production of TGF-β during chronic inflammation increases contraction.[192] Early and complete integration of the mesh into the surrounding tissue may decrease mesh shrinkage. In a swine study to investigate the association between tissue ingrowth and mesh contraction, suture detachment from fixation points was observed, indicating that shrinkage occurred before the mesh had time to integrate into the tissue.[190] On the other hand, meshes that exhibited strong integration into the surrounding tissue exhibited the least amount of contraction. As reviewed by Garcia-Urena, in a study comparing mesh shrinkage with or without fixation after 90 days, the meshes in the fixation group shrank less and retained their original shape indicating the importance of mesh stability to shrinkage.[191] As previously indicated, the extent of mesh shrinkage has been shown to be directly proportional to the degree of inflammatory response.[87] It is also known that extensive inflammation delays the proliferative phase of tissue deposition, which may reduce the integration of the mesh into the surrounding tissue. Together, the physical consequences of delayed tissue ingrowth due to inflammation and inadequate mesh stability have potential contributing roles in mesh shrinkage.

Meshes and the Immune Response

The immune system protects the body from potentially harmful substances by recognizing and responding to antigens or non-self molecules. For meshes, the immune response is a rarely investigated topic because synthetic materials are not considered immunogenic. However, fluids from the *in vivo* environment can facilitate mesh yarn swelling which results in the leaching of low molecular weight particles such as impurities, antioxidants, plasticizers, and unreacted monomer. These particles themselves are not immunogenic, but if they covalently bond to a secretory protein or protein on a cell surface they become haptens and the complex is then recognized as an antigen by the immune system. Another potential pathway is from activated macrophages, at or near the surface of the polymer, which release highly reactive radicals that damage the polymer surface and create degradation products that can act as haptens to adsorbed proteins.[193,194] Depending on the physicochemical properties of the implant surface and type of absorbed proteins, the rate of degradation and thus the immune response will be variable.[114] The immunologic response triggers the activation of macrophages, which respond by releasing pro-inflammatory chemokines that attract additional immune cells. Furthermore, immune cells under typical wound healing conditions have a role in wound resolution. It has been demonstrated that T lymphocytes have an active role in cytokine production at the wound site and are essential to a successful healing process.[195] T-lymphocytes have been shown to have a nonspecific reaction against biomaterials with influences in macrophage recruitment, formation of giant cells, and the phagocytosing activity of macrophages and giant cells.[174] On the

other hand, there is no evidence that B lymphocytes play a significant role in wound healing.[196] In all, the adaptive immune response to synthetic meshes is thought to be minimal, and only a small part of the overall acute inflammatory response. A more significant nonspecific or innate role is played by T-lymphocytes, with influences over macrophage activity.

Mesh/Tissue Complex Stability and Applied Tension

The surgical repair of hernias with mesh results in a lower level of tension applied to the wound. Unlike primary repair, the edges of the hernia are not completely approximated; instead, the mesh is sutured in place with the defect forming what is known as a hernia ring that is spanned on all sides by the mesh. The mesh then becomes the scaffold, allowing extracellular matrix to develop within and around the hernia ring. The reduced wound tension of mesh repairs compared to primary repair has increased the clinical use of meshes for incisional hernia repair from 35% in 1987 to 66% in 1999.[197] This shift is due to an observed reduction in recurrence, which has been attributed to lower levels of wound tension. The most common cause of wound failure in primary repair is dehiscence, from the tearing of suture through the fascia. Although less common, the mechanism exists for meshes because of the endogenous tension of the tissue being repaired. However, early biomechanical wound disruption for meshes occurs almost exclusively at the suture line located at the margins of the mesh. For example, during the first few weeks after hernia repair, minimal extracellular matrix integrity has developed, and applied loads are concentrated at the points of suture

attachment.[198] Concurrently, recovering surgical patients return to physical activity, placing increased loads across the acute wound during its weakest phase.[39,199] Therefore, suture integrity at the margins of the mesh must exclusively resist the applied stresses. Failure to resist the applied stress results in mesh-fascial dehiscence.

The general clinical consensus is that wound tension should be minimized during early post-operative periods.[200] Burger and coworkers, using computed tomography scans in a retrospective study, determined that, although incisional hernias in some cases are not realized until several months or years after surgery, the hernia process starts during the first postoperative month with observable separation of the rectus abdominal muscles.[201] These defects may initiate small and asymptomatic, but can steadily increase in size, eventually allowing the protrusion of abdominal contents and visible bulging. DuBay and coworkers designed a rat surgical model that produces acute fascial separation following the rapid dissolution of cat gut suture.[202] The ensuing incisional hernias have a well defined hernia ring, protruding hernia sac, and visceral adhesions, providing all of the characteristics that clinically develop in humans. Following mesh repair of the induced hernia, animals were evaluated on post operative days 7, 14, 28, and 60 for the development of recurrent incisional hernias. It was determined that 16% of the total 21% recurrences occurred by post operative day 7.[202] The authors concluded that recurrent incisional hernia formation is an early postoperative occurrence.

In addition to recurrence, wound biomechanical disruptions can affect angiogenesis. During the early stages of angiogenesis, capillary sprouts lack full thickness which renders them delicate and easily disrupted. Budding vessels are so

fragile that collagen fibers must surround them to prevent rupturing when blood pressure is imposed by arterial inflow.[182] Immobilization of the granulation tissue is essential through the proliferation phase to permit vascular regrowth and prevent microhemorrhages.[7] The prevention of these microhemorrhages facilitates the progression of the wound healing process without the release of additional pro-inflammatory cytokines. Wound stability during the early postoperative period is critical to preventing wound disruptions at the suture line that can evolve into recurrences and is critical for optimal wound site vascularization.

Advanced Phases of Wound Healing and Maturation

The so-called maturation phase of wound healing is characterized by a decrease in cell density and metabolic activity followed by balanced collagen degradation and deposition process whereby the wound site is remodeled through collagen fiber bundle organization based on chemical and mechanical stimulation.

The Long-Term Foreign Body Response to Meshes

All meshes demonstrate a chronic, persistent foreign body reaction. The long-term tissue reaction at the interface to the mesh is independent of implantation time and characterized by many macrophages, granulomas, and foreign body giant cells.[203] Aggregated, activated, and frustrated macrophages lead to macrophage fusion and the formation of foreign body giant cells on the surface of implanted biomaterials.[193] Foreign body giant cells are the predominant cell type of the long-term foreign body reaction,

with their numbers more than doubling from 2 months to 6 months around polypropylene filaments in a swine animal study.[204] This process initiates early and persists for years, being observed in explanted meshes 15 years after patient implantation.[205] Patients with polyethylene terephthalate mesh hernia repairs were biopsied during later operations to study the tissue response.[206] At 16 months, a layer of foreign body giant cells developed around the yarns, macrophages collected in an intermediate layer of mature granuloma with fine fibrillar collagen, and a denser outer border of collagen bundles aligned along stress lines and was populated by fibroblasts. The partial volume of cells and physical nature of the foreign body response has been reported to be affected by the type of mesh material. Polyethylene terephthalate induced tissue reactions show comparatively little inflammation but have heavily macrophage populated granulomas, whereas polypropylene shows an increased amount of inflammation and connective tissue.[203] It should be noted that the yarn form, construction, pore sizes, and so on, are different between typical polyethylene terephthalate and polypropylene meshes; other factors beyond material type likely influence long-term foreign body reaction. Altogether, non-absorbable mesh causes a persistent, long-term inflammatory reaction at the interface between polymer yarn and host tissue; the reaction is comprised mostly of foreign body giant cells and macrophages within granulation tissue, which is surrounded by a collagen capsule.

Wound Maturation – Collagen Reorganization and Crosslinking

The wound site extracellular matrix surrounding the mesh progresses from a blood-based provisional matrix of fibrin clot and serum protein deposition (inflammation phase), to a loose, disorganized, weak collagen network that, after several weeks begins to crosslink and develop strength (proliferation), to finally a complete replacement and reorganization of the collagen fibers and fiber bundles and established integrity of the local tissue. During remodeling, collagen turnover allows the randomly deposited scar tissue to be rearranged and restore some level of functionality. To achieve this goal, quality collagen is produced by adequate synthesis, degradation, crosslinking, and remodeling of collagen fibrils in response to mechanical stimulation.

The goal of hernioplasty should be to restore the morphology and functions of the abdominal wall such that the prosthesis provides a substitute with characteristics closest to the tissue's normal function, with a low elastic modulus more relevant to performance than the relative strength of the mesh.[207] Increasingly, it is being recognized that the growth and remodeling of fibrotic tissue that supports mechanical loads is governed by the same principles as Wolffs' Law for bone.[171] A lack of stress produces atrophy while excessive stress results in necrosis. Ideally, low forces produce extracellular matrix distention, providing endogenous stress that fibroblasts maintain under tensional homeostasis.[208] Meshes begin to significantly decrease the mobility of the abdominal wall 2-3 weeks after implantation from the induction of the scar plate.[208] In the uniaxial direction, typical meshes have low initial elastic modulus due to deformations within the pores. However, biaxially, with fixation on all sides, current meshes have a high elastic

modulus with very low elongation even at maximum physiologic conditions. Consequently, the mesh absorbs most of the mechanical load and the stress-deprived extracellular matrix will not efficiently remodel or mature. Matching of the implant load/extensional characteristics to the tissue should create a fibrotic capsule that is substantial and strong, with elastic properties that more closely match those of the surrounding tissue. Furthermore, when two contacting materials have marked differences in their elastic moduli, the result is high shear stress concentrations at the interface.[171] This difference is evidenced in reports of collagen fibers, which orientate along stress lines, aligning parallel to individual filaments of yarn and around the outer fibrotic capsule around the mesh[203,205], but with little or no orientation reported within the pores. Relative motion at the mechanical interface may also be responsible in part for the foreign body response to meshes. Increased shear stresses and a lack of mechanical stability at the interface may cause load mediated cell necrosis and general irritation to the tissue stimulating inflammation.[171]

A mesh/tissue complex that has firm attachment and close matching of the mesh and tissue elastic moduli is critical to the long-term mesh/tissue complex mechanical properties and the level of foreign body response to the mesh. Mechanical stimulation significantly influences the remodeling of the mesh/tissue complex and the development of proper physiology.

New Opportunities Based On Currently Unmet Needs

Since the development of absorbable sutures over three decades ago, there has been interest in using absorbable multifilament yarn for constructing absorbable meshes. However, this interest has been limited by unsuccessful attempts to repair load bearing soft tissues such as abdominal wall hernia repairs. Meshes constructed of only fast absorbing polyglycolide or 90/10 poly(glycolide-co-lactide) provide inadequate strength beyond three to four weeks of breaking strength retention. In addition, development of meshes constructed from relatively slow degrading high-lactide yarn has generated little to no interest. This situation has left the majority of soft tissue repair load bearing applications to be filled by non-absorbable materials, which suffer distinctly from undesirable features associated, in part, with their inability to (1) possess short-term stiffness to facilitate tissue stability during the development of wound strength; (2) gradually transfer the perceived mechanical loads as the wound is building mechanical integrity; (3) provide compliance with load transfer to the remodeling and maturing mesh/tissue complex; and (4) minimize the likelihood of long-term complications with their degradation and absorption at the conclusion of their intended functional performance. Wound healing is a dynamic process that results in different criteria at different phases for the optimal development of the mesh/tissue complex. Current non-absorbable or partially absorbable meshes may not provide adequate early stability and then a sufficient level of long-term mechanical stimulation to the remodeling and maturing collagen.

Absorbable medical meshes in the form of multicomponent systems possessing different degradation rates can produce modulated mechanical, chemical, and physical properties which individually or collectively may improve the wound healing process. Figure 1.8 illustrates the characteristics of a multicomponent mesh that has two different strength profiles compared to the wound strength profile and typical phases of wound healing. Each characteristic or phase is indicated with anticipated time intervals.

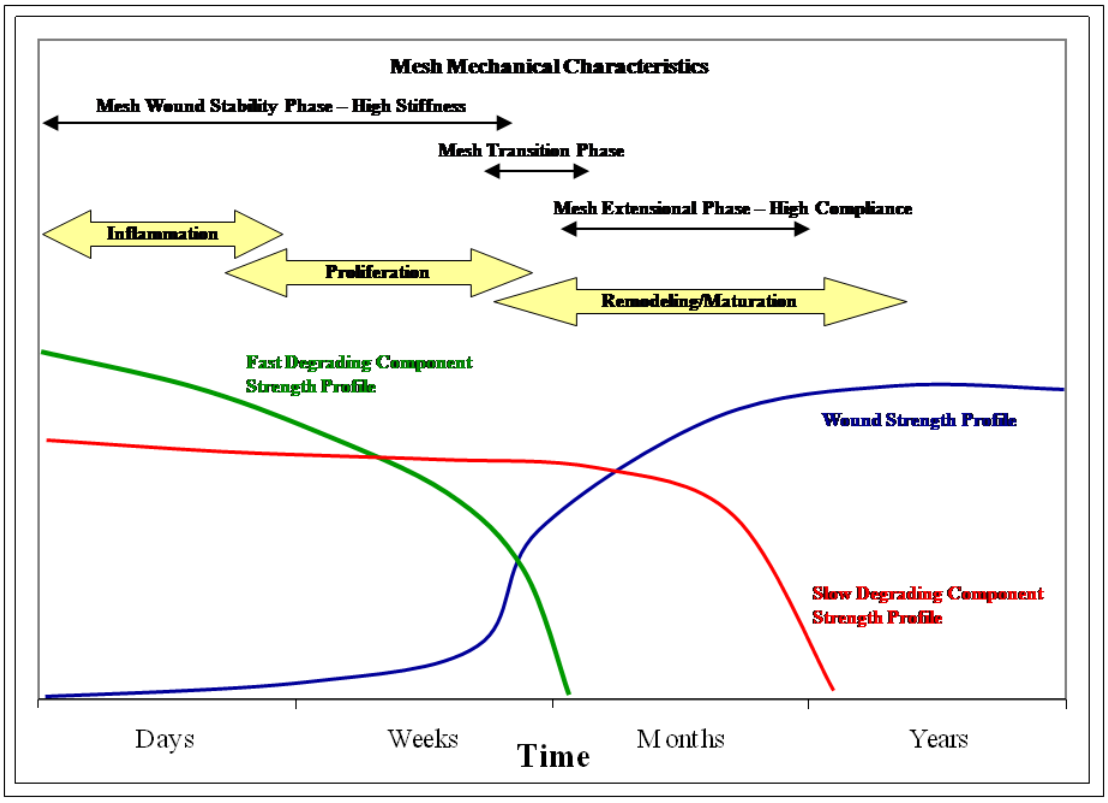

Figure 1.8

The modulated mechanical characteristics of a multicomponent mesh superimposed with the wound healing response.

The mesh wound stability phase continues through the inflammation and proliferation phases. Early stiffness of the mesh may facilitate uninterrupted tissue integration and angiogenesis, while reducing the risk of recurrence from applied wound stresses prior to the development of wound strength. In addition, the added stiffness and stability may resist and/or minimize the wound contraction process. As the wound develops load bearing capability, stress is slowly transferred as the fast degrading component loses strength. Once the fast degrading component of the mesh is removed, the long lasting component is well encapsulated in the extracellular matrix. The mesh is positioned in a relaxed configuration such that the newly deposited collagen becomes load bearing and tensional homeostasis is returned to the abdominal wall. Over the ensuing months the remodeling/maturing process of collagen degradation and synthesis adapts the tissue to the loading conditions. Finally, the slow degrading component loses its mechanical integrity by hydrolysis and is metabolized, leaving the wound site without the continuous foreign body response. Ultimately, the abdominal wall is left with a functional, sustainable layer of tissue that seals the defect area preventing future hernia formation.

References

1. Dee KC, Puleo DA. An introduction to tissue-biomaterials interactions. Hoboken, NJ: Wiley-Liss; 2002.

2. Mulder GD, Brazinsky BA, Harding KG, Agren MS. Factors influencing wound healing. In: Leaper DJ, Harding KG, editors. Wound biology and management. Oxford, England: Oxford University Press; 1998. p 52-69.

3. Stadelmann WK, Digenis AG, Tobin GR. Physiology and healing dynamics of chronic cutaneous wounds. Am J Surg 1998;176(2A Suppl):26S-38S.

4. Paul M. Wound healing - aiming for perfect skin regeneration. Science 1997;276:75-81.

5. Witte MB, Barbul A. General principles of wound healing. Surg Clin North Am 1997;77(3):509-28.

6. Lorenz HP, Longaker MT. Wounds: biology, pathology, and management. In: Norton JA, Bollinger RR, Chang AE, Lowry SF, Mulvihill SJ, Pass HI, Thompson RW, editors. Surgery: Basic science and clinical evidence. New York, NY: Springer-Verlag; 2003. p 77-88.

7. Hardy MA. The biology of scar formation. Phys Ther 1989;69(12):1014-24.

8. Yang GP, Lim IJ, Phan TT, Lorenz HP, Longaker MT. From scarless fetal wounds to keloids: molecular studies in wound healing. Wound Repair Regen 2003;11(6):411-8.

9. Silver FH, Christiansen DL, Snowhill PB, Chen Y. Transition from viscous to elastic-based dependency of mechanical properties of self-assembled type I collagen fibers. J Appl Polym Sci 2000;79:134-42.

10. Bailey AJ, Paul RG, Knott L. Mechanisms of maturation and ageing of collagen. Mech Ageing Dev 1998;106(1-2):1-56.

11. Fratzl P, Misof K, Zizak I, Rapp G, Amenitsch H, Bernstorff S. Fibrillar structure and mechanical properties of collagen. J Struct Biol 1998;122(1-2):119-22.

12. Silver FH, Ebrahimi A, Snowhill PB. Viscoelastic properties of self-assembled type I collagen fibers: molecular basis of elastic and viscous behaviors. Connect Tissue Res 2002;43(4):569-80.

13. Misof K, Rapp G, Fratzl P. A new molecular model for collagen elasticity based on synchrotron X-ray scattering evidence. Biophys J 1997;72(3):1376-81.

14. Puxkandl R, Zizak I, Paris O, Keckes J, Tesch W, Bernstorff S, Purslow P, Fratzl P. Viscoelastic properties of collagen: synchrotron radiation investigations and structural model. Philos Trans R Soc Lond B Biol Sci 2002;357(1418):191-7.

15. Bonifasi-Lista C, Lake SP, Small MS, Weiss JA. Viscoelastic properties of the human medial collateral ligament under longitudinal, transverse and shear loading. J Orthop Res 2005;23(1):67-76.

16. Benjamin M, Hillen B. Mechanical influences on cells, tissues and organs - 'Mechanical Morphogenesis'. Eur J Morphol 2003;41(1):3-7.

17. Screen HR, Shelton JC, Bader DL, Lee DA. Cyclic tensile strain upregulates collagen synthesis in isolated tendon fascicles. Biochem Biophys Res Commun 2005;336(2):424-9.

18. Webb K, Hitchcock RW, Smeal RM, Li W, Gray SD, Tresco PA. Cyclic strain increases fibroblast proliferation, matrix accumulation, and elastic modulus of fibroblast-seeded polyurethane constructs. J Biomech 2006;39(6):1136-44.

19. Yang G, Crawford RC, Wang JH. Proliferation and collagen production of human patellar tendon fibroblasts in response to cyclic uniaxial stretching in serum-free conditions. J Biomech 2004;37(10):1543-50.

20. Park SA, Kim IA, Lee YJ, Shin JW, Kim CR, Kim JK, Yang YI. Biological responses of ligament fibroblasts and gene expression profiling on micropatterned silicone substrates subjected to mechanical stimuli. J Biosci Bioeng 2006;102(5):402-12.

21. Eckes B, Zweers MC, Zhang ZG, Hallinger R, Mauch C, Aumailley M, Krieg T. Mechanical tension and integrin alpha 2 beta 1 regulate fibroblast functions. J Investig Dermatol Symp Proc 2006;11(1):66-72.

22. Bride J, Viennet C, Lucarz-Bietry A, Humbert P. Indication of fibroblast apoptosis during the maturation of disc-shaped mechanically stressed collagen lattices. Arch Dermatol Res 2004;295(8-9):312-7.

23. Puk CK, Miller DJ, Gamradt S, Wu BM, McAllister DR. The effects of short-term stimulation on fibroblast spreading in an in vitro 3D system. J Biomed Mater Res A 2006;76(4):665-73.

24. Eastwood M, Mudera VC, McGrouther DA, Brown RA. Effect of precise mechanical loading on fibroblast populated collagen lattices: morphological changes. Cell Motil Cytoskeleton 1998;40(1):13-21.

25. Prajapati RT, Chavally-Mis B, Herbage D, Eastwood M, Brown RA. Mechanical loading regulates protease production by fibroblasts in three-dimensional collagen substrates. Wound Repair Regen 2000;8(3):226-37.

26. Yasuda K, Hayashi K. Changes in biomechanical properties of tendons and ligaments from joint disuse. Osteoarthritis Cartilage 1999;7(1):122-9.

27. Hannafin JA, Arnoczky SP, Hoonjan A, Torzilli PA. Effect of stress deprivation and cyclic tensile loading on the material and morphologic properties of canine flexor digitorum profundus tendon: an in vitro study. J Orthop Res 1995;13(6):907-14.

28. Eckes B, Kessler D, Aumailley M, Krieg T. Interactions of fibroblasts with the extracellular matrix: implications for the understanding of fibrosis. Springer Semin Immunopathol 1999;21(4):415-29.

29. Li F, Li B, Wang QM, Wang JH. Cell shape regulates collagen type I expression in human tendon fibroblasts. Cell Motil Cytoskeleton 2008;65(4):332-41.

30. Hinz B, Mastrangelo D, Iselin CE, Chaponnier C, Gabbiani G. Mechanical tension controls granulation tissue contractile activity and myofibroblast differentiation. Am J Pathol 2001;159(3):1009-20.

31. Faryniarz DA, Chaponnier C, Gabbiani G, Yannas IV, Spector M. Myofibroblasts in the healing lapine medial collateral ligament: possible mechanisms of contraction. J Orthop Res 1996;14(2):228-37.

32. Mirastschijski U, Haaksma CJ, Tomasek JJ, Agren MS. Matrix metalloproteinase inhibitor GM 6001 attenuates keratinocyte migration, contraction and myofibroblast formation in skin wounds. Exp Cell Res 2004;299(2):465-75.

33. Grinnell F, Zhu M, Carlson MA, Abrams JM. Release of mechanical tension triggers apoptosis of human fibroblasts in a model of regressing granulation tissue. Exp Cell Res 1999;248(2):608-19.

34. Burgess LP, Morin GV, Rand M, Vossoughi J, Hollinger JO. Wound healing. Relationship of wound closing tension to scar width in rats. Arch Otolaryngol Head Neck Surg 1990;116(7):798-802.

35. Fagan SP, Awad SS. Abdominal wall anatomy: the key to a successful inguinal hernia repair. Am J Surg 2004;188(6A Suppl):3S-8S.

36. Park AE, Roth JS, Kavic SM. Abdominal wall hernia. Curr Probl Surg 2006;43(5):326-75.

37. Annibali R, Fitzgibbons RJ, Quinn T. Surgical anatomy of the inguinal region from a laparoscopic perspective. In: Bendavid R, Abrahamson J, Arregui M, Flament J, Phillips E, editors. Abdominal Wall Hernias: Priciples and Management. New York, NY: Springer-Verlag; 2001.

38. Flament J, Avisse C, Delattre J. Anatomy of the abdominal wall. In: Bendavid R, Abrahamson J, Arregui M, Flament J, Phillips E, editors. Abdominal Wall Hernias: Principles and Management. New York, NY: Springer-Verlag; 2001. p 39-63.

39. Peiper C, Junge K, Prescher A, Stumpf M, Schumpelick V. Abdominal musculature and the transversalis fascia: an anatomical viewpoint. Hernia 2004;8(4):376-80.

40. Klinge U, Klosterhalfen B, Conze J, Limberg W, Obolenski B, Ottinger AP, Schumpelick V. Modified mesh for hernia repair that is adapted to the physiology of the abdominal wall. Eur J Surg 1998;164(12):951-60.

41. Junge K, Klinge U, Prescher A, Giboni P, Niewiera M, Schumpelick V. Elasticity of the anterior abdominal wall and impact for reparation of incisional hernias using mesh implants. Hernia 2001;5(3):113-8.

42. Cobb WS, Burns JM, Kercher KW, Matthews BD, James Norton H, Todd Heniford B. Normal intraabdominal pressure in healthy adults. J Surg Res 2005;129(2):231-5.

43. Wolloscheck T, Gaumann A, Terzic A, Heintz A, Junginger T, Konerding MA. Inguinal hernia: measurement of the biomechanics of the lower abdominal wall and the inguinal canal. Hernia 2004;8(3):233-41.

44. Bhattacharjee P. Surgical options in inguinal hernia: Which is the best. Ind J Surg 2006;68(4):191-200.

45. Paajanen H. A single-surgeon randomized trial comparing three composite meshes on chronic pain after Lichtenstein hernia repair in local anesthesia. Hernia 2007;11(4):335-9.

46. Schwab R, Klinge U. Principle actions for re-currences. In: Schumpelick V, Fitzgibbons RJ, editors. Recurrent Hernia. Berlin, Germany: Springer-Verlag; 2007.

47. Awad SS, Fagan SP. Current approaches to inguinal hernia repair. Am J Surg 2004;188(6A Suppl):9S-16S.

48. Weber A, Garteiz D, Valencia S. Epidemiology of inguinal hernia: a useful aid for adequate surgical decisions. In: Bendavid R, Abrahamson J, Arregui M, Flament J, Phillips E, editors. Abdominal Wall Hernias: Principles and Management. New York, NY: Springer-Verlag; 2001.

49. Palot J, Avisse C. Open techniques of femoral hernia repair. In: Bendavid R, Abrahamson J, Arregui M, Flament J, Phillips E, editors. Abdominal Wall Hernias: Priniciples and Management. New York, NY: Springer-Verlag; 2001.

50. Temiz A, Akcora B, Temiz M, Canbolant E. A rare and frequently unrecognised pathology in children: femoral hernia. Hernia 2008;12(5):553-56.

51. Bax T, Sheppard BC, Crass RA. Surgical options in the management of groin hernias. Am Fam Physician 1999;59(1):143-56.

52. Rodrigues AJ, Rodrigues C, Plopper C, Terra RM. Do the dimensions of the femoral canal play a role in the genesis of femoral hernia? Hernia 2000;4:45-51.

53. Velasco M, Garcia-Urena MA, Hidalgo M, Vega V, Carnero FJ. Current concepts on adult umbilical hernia. Hernia 1999;4:233-39.

54. Deysine M. Umbilical hernias. In: Bendavid R, Abrahamson J, Arregui M, Flament J, Phillips E, editors. Abdominal Wall Hernias: Principles and Management. New York, NY: Springer-Verlag; 2001.

55. Amid PK. Lichtenstein tension-free hernioplasty: its inception, evolution, and principles. Hernia 2004;8(1):1-7.

56. Wantz GE, Fischer E. Unilateral giant prosthetic reinforcement of the visceral sac: preperitoneal hernioplasties with Dacron. In: Bendavid R, Abrahamson J, Arregui M, Flament J, Phillips E, editors. Abdominal Wall Hernias: Principles and Management. New York, NY: Springer-Verlag; 2001.

57. Lowham AS, Filipi CJ, Fitzgibbons RJ, Jr., Stoppa R, Wantz GE, Felix EL, Crafton WB. Mechanisms of hernia recurrence after preperitoneal mesh repair. Traditional and laparoscopic. Ann Surg 1997;225(4):422-31.

58. Kurzer M, Belsham PA, Kark AE. Prospective study of open preperitoneal mesh repair for recurrent inguinal hernia. Br J Surg 2002;89(1):90-3.

59. Kugel RD. Minimally invasive, nonlaparoscopic, preperitoneal, and sutureless, inguinal herniorrhaphy. Am J Surg 1999;178(4):298-302.

60. Muldoon RL, Marchant K, Johnson DD, Yoder GG, Read RC, Hauer-Jensen M. Lichtenstein vs anterior preperitoneal prosthetic mesh placement in open inguinal hernia repair: a prospective, randomized trial. Hernia 2004;8(2):98-103.

61. Sinha R, Sharma N, Dhobal D, Joshi M. Laparoscopic total extraperitoneal repair versus anterior prepertitoneal repair for inguinal hernia. Hernia 2006;10:187-91.

62. Ridings P, Evans DS. The transabdominal pre-peritoneal (TAPP) inguinal hernia repair: a trip along the learning curve. J R Coll Surg Edinb 2000;45(1):29-32.

63. Horgan LF, Shelton JC, O'Riordan DC, Moore DP, Winslet MC, Davidson BR. Strengths and weaknesses of laparoscopic and open mesh inguinal hernia repair: a randomized controlled experimental study. Br J Surg 1996;83(10):1463-7.

64. Fenoglio ME, Bermas HR, Haun WE, Moore JT. Inguinal hernia repair: results using an open preperitoneal approach. Hernia 2005;9(2):160-1.

65. Nyhus LM. Herniology 1948-1998: Evolution toward excellence. Hernia 1998;2:1-5.

66. Liem MS, van Vroonhoven TJ. Laparoscopic inguinal hernia repair. Br J Surg 1996;83(9):1197-1204.

67. Beltran MA, Cruces KS. Outcomes of Lichtenstein hernioplasty for primary and recurrent inguinal hernia. World J Surg 2006;30(12):2281-7; discussion 2288-9.

68. Amid PK. Classification of biomaterials and their related complications in abdominal wall hernia surgery. Hernia 1997;1:15-21.

69. Mann DV, Prout J, Havranek E, Gould S, Darzi A. Late-onset deep prosthetic infection following mesh repair of inguinal hernia. Am J Surg 1998;176(1):12-4.

70. Susmallian S, Gewurtz G, Ezri T, Charuzi I. Seroma after laparoscopic repair of hernia with PTFE patch: is it really a complication? Hernia 2001;5(3):139-41.

71. Tsereteli Z, Ramshaw B, Ramaswamy A. Chronic posterior seroma with neoperitoneum following laparoscopic ventral hernia repair: treatment algorithm. Hernia 2008;12(4):363-66.

72. Mayagoitia JC, Almaraz A, Diaz C. Two cases of cystic seroma following mesh incisional hernia repair. Hernia 2006;10(1):83-6.

73. Agrawal A, Avill R. Mesh migration following repair of inguinal hernia: a case report and review of literature. Hernia 2006;10(1):79-82.

74. van't Riet M, de Vos van Steenwijk PJ, Bonjer HJ, Steyerberg EW, Jeekel J. Mesh repair for postoperative wound dehiscence in the presence of infection: is absorbable mesh safer than non-absorbable mesh? Hernia 2007;11(5):409-13.

75. Binnebosel M, Rosch R, Junge K, Flanagan TC, Schwab R, Schumpelick V, Klinge U. Biomechanical analyses of overlap and mesh dislocation in an incisional hernia model in vitro. Surgery 2007;142(3):365-71.

76. Kes E, Lange J, Bonjer J, Stoeckart R, Mulder P, Snijders C, Kleinrensink G. Protrusion of prosthetic meshes in repair of inguinal hernias. Surgery 2004;135(2):163-70.

77. Staal E, Nienhuijs SW, Keemers-Gels ME, Rosman C, Strobbe LJ. The impact of pain on daily activities following open mesh inguinal hernia repair. Hernia 2008;12(2):153-7.

78. Palumbo P, Minicucci A, Nasti AG, Simonelli I, Vietri F, Angelici AM. Treatment for persistent chronic neuralgia after inguinal hernioplasty. Hernia 2007;11(6):527-31.

79. Nienhuijs S, Staal E, Strobbe L, Rosman C, Groenewoud H, Bleichrodt R. Chronic pain after mesh repair of inguinal hernia: a systematic review. Am J Surg 2007;194(3):394-400.

80. Hompes R, Vansteenkiste F, Pottel H, Devriendt D, Van Rooy F. Chronic pain after Kugel inguinal hernia repair. Hernia 2008;12(2):127-32.

81. Aasvang E, Kehlet H. Surgical management of chronic pain after inguinal hernia repair. Br J Surg 2005;92(7):795-801.

82. Ndiaye A, Diop M, Ndoye JM, Konate I, Ndiaye AI, Mane L, Nazarian S, Dia A. Anatomical basis of neuropathies and damage to the ilioinguinal nerve during repairs of groin hernias. (about 100 dissections). Surg Radiol Anat 2007;29(8):675-81.

83. Aasvang E, Kehlet H. Chronic postoperative pain: the case of inguinal herniorrhaphy. Br J Anaesth 2005;95(1):69-76.

84. Doctor H. Evaluation of various prosthetic materials and newer meshes for hernia repairs. J Min Access Surg 2006;2(3):110-16.

85. Poobalan AS, Bruce J, King PM, Chambers WA, Krukowski ZH, Smith WC. Chronic pain and quality of life following open inguinal hernia repair. Br J Surg 2001;88(8):1122-6.

86. Klinge U, Klosterhalfen B, Muller M, Ottinger AP, Schumpelick V. Shrinking of polypropylene mesh in vivo: an experimental study in dogs. Eur J Surg 1998;164(12):965-9.

87. Kockerling C, Schug-Pass C. Recurrence and mesh material. In: Schumpelick V, Fitzgibbons RJ, editors. Recurrent Hernia. Berlin, Germany: Springer-Verlag; 2007.

88. Champault G, Bernard C, Rizk N, Polliand C. Inguinal hernia repair: the choice of prosthesis outweighs that of technique. Hernia 2007;11(2):125-8.

89. Welty G, Klinge U, Klosterhalfen B, Kasperk R, Schumpelick V. Functional impairment and complaints following incisional hernia repair with different polypropylene meshes. Hernia 2001;5(3):142-7.

90. Klinge U, Krones CJ. Can we be sure that the meshes do improve the recurrence rates? Hernia 2005;9:1-2.

91. Felemovicius I, Bonsack ME, Hagerman G, Delaney JP. Prevention of adhesions to polypropylene mesh. J Am Coll Surg 2004;198(4):543-8.

92. McArdle G. Is inguinal hernia a defect in human evolution and would this insight improve concepts for methods of surgical repair? Clin Anat 1997;10(1):47-55.

93. Rosch R, Junge K, Lynen P, Mertens P, R., Klinge U, Schumpelick V. Hernia - A collagen disease? Eur Surg 2003;35:11-15.

94. Kang SK, Burnett CA, Freund E, Sestito J. Hernia: is it a work-related condition? Am J Ind Med 1999;36(6):638-44.

95. Franz MG. The biology of hernias and the abdominal wall. Hernia 2006;10(6):462-71.

96. Rosch R, Junge K, Binnebosel M, Bertram P, Klinge U, Schumpelick V. Laparoscopy and collagen metabolism. Hernia 2006;10(6):507-10.

97. Donahue TR, Hiatt JR, Busuttil RW. Collagenase and surgical disease. Hernia 2006;10(6):478-85.

98. Klinge U, Zheng H, Si Z, Schumpelick V, Bhardwaj RS, Muys L, Klosterhalfen B. Expression of the extracellular matrix proteins collagen I, collagen III and fibronectin and matrix metalloproteinase-1 and -13 in the skin of patients with inguinal hernia. Eur Surg Res 1999;31(6):480-90.

99. Klinge U, Zheng H, Si ZY, Schumpelick V, Bhardwaj R, Klosterhalfen B. Synthesis of type I and III collagen, expression of fibronectin and matrix metalloproteinases-1 and -13 in hernial sac of patients with inguinal hernia. Int J Surg Investig 1999;1(3):219-27.

100. Rosch R, Klinge U, Si Z, Junge K, Klosterhalfen B, Schumpelick V. A role for the collagen I/III and MMP-1/-13 genes in primary inguinal hernia? BMC Med Genet 2002;3:2.

101. Bendavid R. The unified theory of hernia formation. Hernia 2004;8(3):171-6.

102. Bellon JM, Bujan J, Honduvilla NG, Jurado F, Gimeno MJ, Turnay J, Olmo N, Lizarbe MA. Study of biochemical substrate and role of metalloproteinases in fascia transversalis from hernial processes. Eur J Clin Invest 1997;27(6):510-6.

103. Bellon JM, Bajo A, Ga-Honduvilla N, Gimeno MJ, Pascual G, Guerrero A, Bujan J. Fibroblasts from the transversalis fascia of young patients with direct inguinal hernias show constitutive MMP-2 overexpression. Ann Surg 2001;233(2):287-91.

104. Ashcroft GS, Herrick SE, Tarnuzzer RW, Horan MA, Schultz GS, Ferguson MW. Human ageing impairs injury-induced in vivo expression of tissue inhibitor of matrix metalloproteinases (TIMP)-1 and -2 proteins and mRNA. J Pathol 1997;183(2):169-76.

105. Abci I, Bilgi S, Altan A. Role of TIMP-2 in fascia transversalis on development of inguinal hernias. J Invest Surg 2005;18(3):123-8.

106. Junge K, Klinge U, Rosch R, Mertens PR, Kirch J, Klosterhalfen B, Lynen P, Schumpelick V. Decreased collagen type I/III ratio in patients with recurring hernia after implantation of alloplastic prostheses. Langenbecks Arch Surg 2004;389(1):17-22.

107. Si Z, Bhardwaj R, Rosch R, Mertens PR, Klosterhalfen B, Klinge U. Impaired balance of type I and type III procollagen mRNA in cultured fibroblasts of patients with incisional hernia. Surgery 2002;131(3):324-31.

108. Friedman DW, Boyd CD, Norton P, Greco RS, Boyarsky AH, Mackenzie JW, Deak SB. Increases in type III collagen gene expression and protein synthesis in patients with inguinal hernias. Ann Surg 1993;218(6):754-60.

109. Zheng H, Si Z, Kasperk R, Bhardwaj RS, Schumpelick V, Klinge U, Klosterhalfen B. Recurrent inguinal hernia: disease of the collagen matrix? World J Surg 2002;26(4):401-8.

110. Lynen Jansen P, Klinge U, Mertens PR. Hernia disease and collagen gene regulation: are there clues for intervention? Hernia 2006;10(6):486-91.

111. El Sherif A, Yano F, Mittal S, Filipi CJ. Collagen metabolism and recurrent hiatal hernia: cause and effect? Hernia 2006;10(6):511-20.

112. Jansen PL, Mertens Pr P, Klinge U, Schumpelick V. The biology of hernia formation. Surgery 2004;136(1):1-4.

113. Szczesny W, Cerkaska K, Tretyn A, Dabrowiecki S. Etiology of inguinal hernia: ultrastructure of rectus sheath revisited. Hernia 2006;10(3):266-71.

114. Klosterhalfen B, Junge K, Klinge U. The lightweight and large porous mesh concept for hernia repair. Expert Rev Med Devices 2005;2(1):103-17.

115. Hollinsky C, Sandberg S. Measurement of the tensile strength of the ventral abdominal wall in comparison with scar tissue. Clin Biomech (Bristol, Avon) 2007;22(1):88-92.

116. Junge K, Klinge U, Klosterhalfen B, Rosch R, Stumpf M, Schumpelick V. Review of wound healing with reference to an unrepairable abdominal hernia. Eur J Surg 2002;168(2):67-73.

117. Schumpelick V, Klinge U, Rosch R, Junge K. Light weight meshes in incisional hernia repair. J Min Access Surg 2006;2(3):pNA.

118. Klinge U, Marcel B, Rosch R, Peter M. Hernia recurrence as a problem of biology and collagen. J Min Access Surg 2006;2(3):151-54.

119. Schippers E. Central mesh rupture - myth or real concern? In: Schumpelick V, Fitzgibbons RJ, editors. Recurrent Hernia. Berlin, Germany: Springer-Verlag; 2007.

120. Langer C, Neufang T, Kley C, Liersch T, Becker H. Central mesh recurrence after incisional hernia repair with Marlex--are the meshes strong enough? Hernia 2001;5(3):164-7.

121. Matic-Leigh SR. Dimensional stability, aesthetic and mechanical properties of micro-fiber blended knitted fabrics. Nat Tex Cent Quart Rep 1993;April-June:13-5.

122. Spencer D. Weft and warp knitting. In Knitting Technology: A comprehensive handbook and practical guide, 3rd Edition. Cambridge, England: Woodhead Publishing Limited; 2001.

123. Soares BM, King MW, Marois Y, Guidoin RG, Laroche G, Charara J, Girard JF. In vitro characterization of a fluoropassivated gelatin-impregnated polyester mesh for hernia repair. J Biomed Mater Res 1996;32(2):259-70.

124. Raz S. The karl mayer guide to technical textiles: Karl Mayer Textilmaschinenfabrik, GmbH; 1998.

125. NoAuthor. Open work fabrics. American LIBA literature:48-58.

126. Gaoming J, Xuhong M, Dajun L. Process of warp knitting mesh for hernia repair and its mechanical properties. Fibres Text East Eur 2005;13(3(51)):44-6.

127. Bracco P, Brunella V, Trossarelli L, Coda A, Botto-Micca F. Comparison of polypropylene and polyethylene terephthalate (Dacron) meshes for abdominal wall hernia repair: a chemical and morphological study. Hernia 2005;9(1):51-5.

128. Brydson J. Aliphatic polyolefins other than polyethylene, and diene rubbers. In Plastic Materials, 7th Edition. Oxford, England: Butterworth-Heinemann; 1999.

129. Fernandez-Lobato R, Tartas-Ruiz A, Jimenez-Miramon FJ, Marin-Lucas FJ, de Adana-Belbel JC, Esteban ML. Stoppa procedure in bilateral inguinal hernia. Hernia 2006;10(2):179-83.

130. Brydson J. Fluorine-contraining polymers. In Plastic Materials, 7th Edition. Oxford, England: Butterworth-Heinemann; 1999.

131. Bellon JM, Rodriguez M, Garcia-Honduvilla N, Pascual G, Bujan J. Partially absorbable meshes for hernia repair offer advantages over nonabsorbable meshes. Am J Surg 2007;194(1):68-74.

132. Muhl T, Binnebosel M, Klinge U, Goedderz T. New objective measurement to characterize the porosity of textile implants. J Biomed Mater Res B Appl Biomater 2008;84(1):176-83.

133. Schumpelick V, Klinge U. Prosthetic implants for hernia repair. Br J Surg 2003;90(12):1457-8.

134. Klinge U, Junge K, Stumpf M, Ap AP, Klosterhalfen B. Functional and morphological evaluation of a low-weight, monofilament polypropylene mesh for hernia repair. J Biomed Mater Res 2002;63(2):129-36.

135. Junge K, Klinge U, Klosterhalfen B, Mertens PR, Rosch R, Schachtrupp A, Ulmer F, Schumpelick V. Influence of mesh materials on collagen deposition in a rat model. J Invest Surg 2002;15(6):319-28.

136. Klinge U, Klosterhalfen B, Muller M, Anurov M, Ottinger A, Schumpelick V. Influence of polyglactin-coating on functional and morphological parameters of polypropylene-mesh modifications for abdominal wall repair. Biomaterials 1999;20(7):613-23.

137. Cobb WS, Burns JM, Peindl RD, Carbonell AM, Matthews BD, Kercher KW, Heniford BT. Textile analysis of heavy weight, mid-weight, and light weight polypropylene mesh in a porcine ventral hernia model. J Surg Res 2006;136(1):1-7.

138. Klinge U, Klosterhalfen B, Birkenhauer V, Junge K, Conze J, Schumpelick V. Impact of polymer pore size on the interface scar formation in a rat model. J Surg Res 2002;103(2):208-14.

139. Rosch R, Junge K, Quester R, Klinge U, Klosterhalfen B, Schumpelick V. Vypro II mesh in hernia repair: impact of polyglactin on long-term incorporation in rats. Eur Surg Res 2003;35(5):445-50.

140. Weyhe D, Schmitz I, Belyaev O, Grabs R, Muller KM, Uhl W, Zumtobel V. Experimental comparison of monofile light and heavy polypropylene meshes: less weight does not mean less biological response. World J Surg 2006;30(8):1586-91.

141. Weyhe D, Hoffmann P, Belyaev O, Mros K, Muller C, Uhl W, Schmitz F. The role of TGF-beta1 as a determinant of foreign body reaction to alloplastic materials in rat fibroblast cultures: comparison of different commercially available polypropylene meshes for hernia repair. Regul Pept 2007;138(1):10-4.

142. Weyhe D, Belyaev O, Buettner G, Mros K, Mueller C, Meurer K, Papapostolou G, Uhl W. In vitro comparison of three different mesh constructions. ANZ J Surg 2008;78(1-2):55-60.

143. Bringman S, Wollert S, Osterberg J, Smedberg S, Granlund H, Fellander G, Heikkinen T. One year results of a randomised controlled multi-centre study comparing Prolene and Vypro II-mesh in Lichtenstein hernioplasty. Hernia 2005;9(3):223-7.

144. Smietanski M. Randomized clinical trial comparing a polypropylene with a poliglecaprone and polypropylene composite mesh for inguinal hernioplasty. Br J Surg 2008;95(12):1462-8.

145. Conze J, Kingsnorth AN, Flament JB, Simmermacher R, Arlt G, Langer C, Schippers E, Hartley M, Schumpelick V. Randomized clinical trial comparing lightweight composite mesh with polyester or polypropylene mesh for incisional hernia repair. Br J Surg 2005;92(12):1488-93.

146. Bringman S, Wollert S, Osterberg J, Smedberg S, Granlund H, Heikkinen TJ. Three-year results of a randomized clinical trial of lightweight or standard polypropylene mesh in Lichtenstein repair of primary inguinal hernia. Br J Surg 2006;93(9):1056-9.

147. O'Dwyer PJ, Kingsnorth AN, Molloy RG, Small PK, Lammers B, Horeyseck G. Randomized clinical trial assessing impact of a lightweight or heavyweight mesh on chronic pain after inguinal hernia repair. Br J Surg 2005;92(2):166-70.

148. Weyhe D, Belyaev O, Muller C, Meurer K, Bauer KH, Papapostolou G, Uhl W. Improving outcomes in hernia repair by the use of light meshes--a comparison of different implant constructions based on a critical appraisal of the literature. World J Surg 2007;31(1):234-44.

149. Greca FH, Souza-Filho ZA, Giovanini A, Rubin MR, Kuenzer RF, Reese FB, Araujo LM. The influence of porosity on the integration histology of two polypropylene meshes for the treatment of abdominal wall defects in dogs. Hernia 2008;12(1):45-9.

150. Krause HG, Galloway SJ, Khoo SK, Lourie R, Goh JT. Biocompatible properties of surgical mesh using an animal model. Aust N Z J Obstet Gynaecol 2006;46(1):42-5.

151. Klosterhalfen B, Klinge U, Schumpelick V. Functional and morphological evaluation of different polypropylene-mesh modifications for abdominal wall repair. Biomaterials 1998;19(24):2235-46.

152. Conze J, Rosch R, Klinge U, Weiss C, Anurov M, Titkowa S, Oettinger A, Schumpelick V. Polypropylene in the intra-abdominal position: influence of pore size and surface area. Hernia 2004;8(4):365-72.

153. Di Vita G, Patti R, Sparacello M, Balistreri CR, Candore G, Caruso C. Impact of different texture of polypropylene mesh on the inflammatory response. Int J Immunopathol Pharmacol 2008;21(1):207-14.

154. Papadimitriou J, Petros P. Histological studies of monofilament and multifilament polypropylene mesh implants demonstrate equivalent penetration of macrophages between fibrils. Hernia 2005;9(1):75-8.

155. Amid P. Polypropylene prosthesis. In: Bendavid R, Abrahamson J, Arregui M, Flament J, Phillips E, editors. Abdominal Wall Hernias: Principles and Management. New York, NY: Springer-Verlag; 2001.

156. Carbonell AM, Kercher KW, Sing RF, Heniford BT. Susceptibility of prosthetic biomaterials to infection. Surg Endosc 2005;19(12):1670.

157. Engelsman AF, van der Mei HC, Busscher HJ, Ploeg RJ. Morphological aspects of surgical meshes as a risk factor for bacterial colonization. Br J Surg 2008;95(8):1051-9.

158. Speranza G, Gottardi G, Pederzolli C, Lunelli L, Canteri R, Pasquardini L, Carli E, Lui A, Maniglio D, Brugnara M and others. Role of chemical interactions in bacterial adhesion to polymer surfaces. Biomaterials 2004;25(11):2029-37.

159. Aggarwal P, Phaneuf MD, Bide MJ, Sousa KA, Logerfo FW. Development of an infection-resistant bifunctionalized Dacron biomaterial. J Biomed Mater Res A 2005;75(1):224-31.

160. Klinge U, Junge K, Spellerberg B, Piroth C, Klosterhalfen B, Schumpelick V. Do multifilament alloplastic meshes increase the infection rate? Analysis of the polymeric surface, the bacteria adherence, and the in vivo consequences in a rat model. J Biomed Mater Res 2002;63(6):765-71.

161. Kossovsky N, Frieman C, Howarth D. Biomaterials Pathology. In: Bendavid R, Abrahamson J, Arregui M, Flament J, Phillips E, editors. Abdominal Wall Hernias: Principles and Management. New York, NY: Springer-Verlag; 2001.

162. Costello CR, Bachman SL, Ramshaw BJ, Grant SA. Materials characterization of explanted polypropylene hernia meshes. J Biomed Mater Res B Appl Biomater 2007;83(1):44-9.

163. Larena A, Ochoa S, Dominguez F. Dynamic-mechanical analysis of the photo-degradation of long glass fibre reinforced polypropylene: Mechanical properties' changes. Polym Degrad Stab 2006;91:940-46.

164. Yakimets I, Lai D, Guigon M. Effect of photo-oxidation cracks on behaviour of thick polypropylene samples. Polym Degrad Stab 2004;86:59-67.

165. Fayolle B, Audouin L, Verdu J. Initial steps and embrittlement in the thermal oxidation of stabilised polypropylene films. Poly Degr Stab 2002;75:123-29.

166. Fayolle B, Audouin L, Verdu J. Oxidation induced embrittlement in polypropylene - a tensile testing study. Poly Degr Stab 2000;70:333-40.

167. Vinard E, Eloy R, Descotes J, Brudon JR, Guidicelli H, Magne JL, Patra P, Berruet R, Huc A, Chauchard J. Stability of performances of vascular prostheses retrospective study of 22 cases of human implanted prostheses. J Biomed Mater Res 1988;22(7):633-48.

168. Riepe G, Loos J, Imig H, Schroder A, Schneider E, Petermann J, Rogge A, Ludwig M, Schenke A, Nassutt R and others. Long-term in vivo alterations of polyester vascular grafts in humans. Eur J Vasc Endovasc Surg 1997;13(6):540-8.

169. Klinge U, Klosterhalfen B, Ottinger AP, Junge K, Schumpelick V. PVDF as a new polymer for the construction of surgical meshes. Biomaterials 2002;23(16):3487-93.

170. Williams DF. On the mechanisms of biocompatibility. Biomaterials 2008;29(20):2941-53.

171. Hilborn J, Bjursten LM. A new and evolving paradigm for biocompatibility. J Tissue Eng Regen Med 2007;1(2):110-9.

172. Menke NB, Ward KR, Witten TM, Bonchev DG, Diegelmann RF. Impaired wound healing. Clin Dermatol 2007;25(1):19-25.

173. Dubova EA, Shchyogolev AI, Chekmaryova IA, Filatkina NV, Chizhov DV, Yegiev VN. Tissue reaction to implantation of light polypropylene meshes. Bull Exp Biol Med 2006;142(6):729-33.

174. Rosch R, Junge K, Schachtrupp A, Klinge U, Klosterhalfen B, Schumpelick V. Mesh implants in hernia repair. Inflammatory cell response in a rat model. Eur Surg Res 2003;35(3):161-6.

175. Li J, Chen J, Kirsner R. Pathophysiology of acute wound healing. Clin Dermatol 2007;25(1):9-18.

176. Franz MG, Kuhn MA, Wright TE, Wachtel TL, Robson MC. Use of the wound healing trajectory as an outcome determinant for acute wound healing. Wound Repair Regen 2000;8(6):511-6.

177. Szpaderska AM, DiPietro LA. Inflammation in surgical wound healing: friend or foe? Surgery 2005;137(5):571-3.

178. Dubay DA, Wang X, Kirk S, Adamson B, Robson MC, Franz MG. Fascial fibroblast kinetic activity is increased during abdominal wall repair compared to dermal fibroblasts. Wound Repair Regen 2004;12(5):539-45.

179. Franz MG, Smith PD, Wachtel TL, Wright TE, Kuhn MA, Ko F, Robson MC. Fascial incisions heal faster than skin: a new model of abdominal wall repair. Surgery 2001;129(2):203-8.

180. Bellon JM, Bujan J, Contreras L, Hernando A. Integration of biomaterials implanted into abdominal wall: process of scar formation and macrophage response. Biomaterials 1995;16(5):381-7.

181. Franz MG, Steed DL, Robson MC. Optimizing healing of the acute wound by minimizing complications. Curr Probl Surg 2007;44(11):691-763.

182. Hopf HW, Gibson JJ, Angeles AP, Constant JS, Feng JJ, Rollins MD, Zamirul Hussain M, Hunt TK. Hyperoxia and angiogenesis. Wound Repair Regen 2005;13(6):558-64.

183. Singer AJ, Clark RA. Cutaneous wound healing. N Engl J Med 1999;341(10):738-46.

184. Gordillo GM, Sen CK. Revisiting the essential role of oxygen in wound healing. Am J Surg 2003;186(3):259-63.

185. Strodtbeck F. Physiology of wound healing. NBIN 2001;1(1):43-52.

186. Schugart R, Friedman A, Zhao R, Sen CK. Wound angiogenesis as function of tissue oxygen tension: A mathmatical model. PNAS 2007;105(7):2628-33.

187. Laschke MW, Haufel JM, Thorlacius H, Menger MD. New experimental approach to study host tissue response to surgical mesh materials in vivo. J Biomed Mater Res A 2005;74(4):696-704.

188. Sanders JE, Stiles CE, Hayes CL. Tissue response to single-polymer fibers of varying diameters: evaluation of fibrous encapsulation and macrophage density. J Biomed Mater Res 2000;52(1):231-7.

189. Salzmann DL, Kleinert LB, Berman SS, Williams SK. Inflammation and neovascularization associated with clinically used vascular prosthetic materials. Cardiovasc Pathol 1999;8(2):63-71.

190. Gonzalez R, Fugate K, McClusky D, 3rd, Ritter EM, Lederman A, Dillehay D, Smith CD, Ramshaw BJ. Relationship between tissue ingrowth and mesh contraction. World J Surg 2005;29(8):1038-43.

191. Garcia-Urena MA, Vega Ruiz V, Diaz Godoy A, Baez Perea JM, Marin Gomez LM, Carnero Hernandez FJ, Velasco Garcia MA. Differences in polypropylene shrinkage depending on mesh position in an experimental study. Am J Surg 2007;193(4):538-42.

192. Robson MC, Steed DL, Franz MG. Wound healing: biologic features and approaches to maximize healing trajectories. Curr Probl Surg 2001;38(2):72-140.

193. Anderson JM, Miller KM. Biomaterial biocompatibility and the macrophage. Biomaterials 1984;5(1):5-10.

194. Klosterhalfen B, Hermanns B, Rosch R, Junge K. Biological response to mesh. Eur Surg 2003;35:16-20.

195. Regan M, Barbul A. The role of the immune system in the regulation of wound repair. Clin Mat 1991;8:197-201.

196. Schaffer M, Barbul A. Lymphocyte function in wound healing and following injury. Br J Surg 1998;85(4):444-60.

197. Flum DR, Horvath K, Koepsell T. Have outcomes of incisional hernia repair improved with time? A population-based analysis. Ann Surg 2003;237(1):129-35.

198. Franz MG. The biological treatment of the hernia disease. In: Schumpelick V, Fitzgibbons RJ, editors. Recurrent Hernia. Berlin, Germany: Springer-Verlag; 2007.

199. Robson MC, Dubay DA, Wang X, Franz MG. Effect of cytokine growth factors on the prevention of acute wound failure. Wound Repair Regen 2004;12(1):38-43.

200. Carlson MA. Acute wound failure. Surg Clin North Am 1997;77(3):607-36.

201. Burger JW, Lange JF, Halm JA, Kleinrensink GJ, Jeekel H. Incisional hernia: early complication of abdominal surgery. World J Surg 2005;29(12):1608-13.

202. DuBay DA, Wang X, Adamson B, Kuzon WM, Jr., Dennis RG, Franz MG. Mesh incisional herniorrhaphy increases abdominal wall elastic properties: a mechanism for decreased hernia recurrences in comparison with suture repair. Surgery 2006;140(1):14-24.

203. Klinge U, Klosterhalfen B, Muller M, Schumpelick V. Foreign body reaction to meshes used for the repair of abdominal wall hernias. Eur J Surg 1999;165(7):665-73.

204. Zieren J, Neuss H, Paul M, Muller J. Introduction of polyethylene terephthalate mesh (KoSa hochfest) for abdominal hernia repair: an animal experimental study. Biomed Mater Eng 2004;14(2):127-32.

205. Klosterhalfen B, Junge K, Hermanns B, Klinge U. Influence of implantation interval on the long-term biocompatibility of surgical mesh. Br J Surg 2002;89(8):1043-8.

206. Trabucchi E, Corsi F, Meinardi C, Cellerino P, Allevi R, Foschi D. Tissue response to polyester mesh for hernia repair: an ultramicroscopic study in man. Hernia 1998;2:107-12.

207. Ferrando JM, Vidal J, Armengol M, Gil J, Manero JM, Huguet P, Segarra A, Quiles MT, Schwartz S, Arbos i Via MA. Experimental evaluation of a new layered prosthesis exhibiting a low tensile modulus of elasticity: long-term integration response within the rat abdominal wall. World J Surg 2002;26(4):409-15.

208. Karamuk E, Mayer J, Raeber G. Tissue engineered composite of a woven fabric scaffold with tendon cells, response on mechanical simulation in vitro. Comp Sci Tech 2004;64:885-91.

CHAPTER TWO

EFFECT OF MESH CONSTRUCTION ON THE PHYSICOMECHANICAL PROPERTIES OF BICOMPONENT KNIT MESH USING YARNS DERIVED FROM DEGRADABLE COPOLYESTERS

Introduction

The efficacy of hernia repair has challenged surgeons for decades. The high recurrence and complication rate for hernia repair has resulted in the clinical exploration of many surgical procedures, debate over the etiology and pathology of hernia formation, and an evolution toward mesh repairs from the use of primary closure. Recently, the deficiencies of meshes and their role in hernia recurrence and patient complications have been well documented.[1-10] In part, these deficiencies are a result of a mesh/tissue complex which is less compliant than the abdominal wall due to the design of traditional meshes.[11-13] Furthermore, traditional meshes used for hernia repair are chemically inert and permanent. As a result, absorbable polymers made from degradable copolyesters are not routinely used in hernia repair, despite the fact that their use may hold significant advantages. Consequently, a focused investigation of the physicomechanical characteristics of new mesh designs, that employ different knit technologies which consider the temporal characteristics of the wound healing process, may improve the clinical outcome of hernioplasty.

When a mesh is placed *in vivo* the host produces a wound healing response simultaneously with a foreign body response against the mesh. The typical wound healing process has overlapping, temporal stages including inflammation, proliferation, and maturation/remodeling. During the early phases of inflammation and proliferation,

cellular responses clear the site of bacteria, fibroblasts migrate to the site and form extracellular matrix (ECM), and vascular structures infiltrate to facilitate the local increase in cellular metabolism. However, during the first 2-3 weeks the ECM acts as a scaffold for cellular motility but lacks significant mechanical integrity. For the next several months during the maturation/remodeling phase, deposited collagen begins to strengthen as collagen is degraded and reformed, crosslinked, and fibril diameters increase as the tissue adapts to the perceived mechanical loading conditions. Consideration for the specific needs of each stage within the wound healing process may hold the potential for improving mesh biocompatibility. Traditional and proposed additional design criteria for a hernia mesh are listed in Table 2.1.

Table 2.1

Traditional and Proposed Additional Design Criteria for a Hernia Mesh

Traditional Design Criteria	**Proposed Additional Design Criteria**
• Chemically Inert • Permanent • Low levels of inflammatory response • Compliant to the required anatomical form • Structurally stable • Adequately porous for tissue integration • Non-immunogenic • Resistant to mechanical strains • Sterilizable • Resistant to infection • Promote collagen deposition and tissue remodeling	• Absorb fully to minimize potential long-term complications • Maintain structural stiffness during the early phases of wound repair to provide stability to developing tissue • Replicate the extensional properties of the abdominal wall to provide mechanical stimulation for the remodeling extracellular matrix • Establish homeostatic conditions with endogenous tension restored within and around the mesh

The chemical biocompatibility and efficacy of linear aliphatic copolyesters, such as those produced from glycolide and lactide, is well established with decades of clinical use as sutures. For hernia repair, the use of fast-degrading absorbable meshes, as well as the absence of a slow-degrading alternative, has resulted in unacceptably high hernia recurrence rates for fully absorbable meshes. The use of a high-glycolide mesh for hernia repair does not provide adequate strength to the remodeling ECM in sufficient time to produce structurally supportive, self-sustaining collagen.[14] As a consequence, the use of these meshes has been discouraged by surgeons, with the exception of use in temporary closure of the abdominal wall.[15] Alternatively, the use of high-lactide yarns may provide the necessary healing time to facilitate the development of mature collagen, making the necessity of permanent implants limited to individuals that have a compromised wound healing response. To date, there are no commercially available high-lactide meshes, although their development has been explored for soft tissue repair.[16-18] Compared to glycolide, lactide's methyl group makes the polymer more hydrophobic and provides steric hindrance to water molecules, partially shielding the labile ester bond. Consequently, using lactide as the primary yarn chemical constituent will significantly slow the rate of hydrolysis and improve its strength retention with time. Strength retention greater than 50% at 6 months is obtainable with high-lactide yarn. In a like manner, the slow degradation rate of lactide polymers is routinely leveraged in orthopedic devices where healing times typically require strength retention for several months. Moreover, the use of a fully absorbable hernia mesh may alleviate long-term complications due to the complete absorption of the mesh following its intended function.

Subsequent surgical procedures local to the implantation of a non-absorbable mesh pose significant surgical challenges, may not even be possible, and add to patient risk. This is well documented for certain vascular and urological operations.[19-22]

Stress applied to the hernia repair site prior to the development of tissue integration and wound strength (first 2-3 weeks post insult) can result in acute wound failure. At this early stage, anchoring devices, such as sutures, absorb the majority of the applied stress.[23] Consequently, suture loops can pull through tissue, creating disruptions that later result in a hernia recurrence.[24] From an engineering perspective, a distribution of applied loads across the mesh and wound site is required to avoid a stress concentration around a small number of suture points. A stiff mesh may better distribute applied loads through its non-compliant structure to several suture points. Furthermore, wound stability within the confines of the mesh during the inflammation and proliferation phases may prevent the disruption of developing, delicate connective tissue and vascular structures.

The long-term (>3 weeks) strength and integrity development of the mesh/tissue complex requires dynamic, mechanical stimulation. To date, the majority of meshes used in hernioplasty are polypropylene meshes,[25] designed with significant strength, and constructed from stiff monofilament yarn to establish a perceived robust repair site. More recently, reduced mass and increased porosity have been investigated to improve the biocompatibility of these so-called heavy-weight meshes. Reduced mass has been reported to lessen the long-term foreign body response[26-29] to permanent meshes while increased porosity minimizes the bridging of collagen between pores[30-32], where bridged

collagen results in a continuous, rigid scar plate. However, minimal attention has been given to replicating the mechanics of the abdominal wall within the mesh/tissue complex. In part, this lack of attention can be attributed to the design limitations of single-component, non-absorbable meshes to meet the temporal needs associated with hernia repair. An extremely high level of mesh extensibility is required to match that of the abdominal wall, especially once the mesh extensibility is reduced after being encapsulated in tissue. To further complicate matters, the long-term requirement for a mesh to match the high extensibility of the abdominal wall means that it will lack initial handling stability making surgical placement difficult, and will provide minimal support to developing, fragile tissue.

The force-extension characteristics of a mesh, and the ability to match those of the abdominal wall, are predominately influenced by construction. When a mesh is stressed, the mesh filaments show minimal if any elongation, while the mesh itself produces significant extension from geometric deformation within the pores perpendicular to the applied strain. However, to establish normal tissue function in and around the implant, the mechanical properties of the mesh/tissue complex must closely match those of the abdominal wall. Mismatch in the compliance properties of the mesh/tissue complex and local tissue is clinically believed to be a significant contributing factor in mesh failures. Most of these failures are due to marginal mesh-fascial dehiscence from fatigue.[10,32-35] Cyclic stresses at the margins of the mesh which are well below maximum failure values result from differences in stiffness within, and around the mesh/tissue complex. As a

consequence, the long-term extensional properties of the mesh have significant relevance to biocompatibility and thus efficacy.

The objective of any hernia mesh repair should be to restore homeostatic conditions. Mechanical homeostasis of the abdominal wall is a dynamic, endogenous state of tension established by cellular, mostly fibroblastic, interaction with the ECM. However, stress shielding will prevail if the stiffness of the mesh is greater than that of the forces generated within the ECM and those applied by the surrounding tissue. Increasingly, the importance of tension in connective tissues is being realized, this force is paramount during the remodeling process where the mechanical environment influences cell function and ECM structure. Changes in the mechanical environment have been shown to influence cellular function during *in vitro* studies.[36-38] For example, endogenous tension is purported to inhibit collagen degradation by reducing collagenases production[39], control gene expression[40], prevent apoptosis[41], and control fibroblast phenotype[42]. Each of these cellular functions influences ECM remodeling and requires a mesh/tissue complex with sufficient compliance so as to not interfere with the development or transmission of tension through the repair site.

Presented is a study focused on the *in vitro* conditioned modulation of biocompatibility-relevant physical and mechanical mesh properties using (1) degradable yarns with different degradation profiles and (2) different mesh constructions employing warp and weft knitting technologies. Specifically, a novel bicomponent mesh was developed that modulates physicomechanical properties and that (1) possesses short-term

structural stiffness, (2) provides a gradual transition phase, and (3) possesses long-term compliance with force-extension properties similar to the abdominal wall.

Materials and Methods

Polymer Synthesis and Characterization

Polymer Synthesis

MG-9, the proposed fast-degrading yarn of the bicomponent meshes, was synthesized as a polyaxial, segmented, high-glycolide copolymer. A two-step, solid state, ring-opening reaction method was used to polymerize MG-9. The first step produced a trimethylolpropane-initiated, trimethylene carbonate (TMC) segment. Next, the TMC segment was end-grafted using 95/5 (molar) glycolide/caprolactone (G/CL). The weight ratio of the polymer initiator to the end-graft was 2/98. A more detailed explanation of the polymerization process is described in U.S. Patent No. 7,129,319 (2006).

SMC-7, the proposed slow-degrading yarn of the bicomponent meshes, was synthesized as a linear, segmented, high-lactide copolymer. The 88/12 (molar) l-lactide/TMC copolymer was prepared using a two-step, solid state, ring-opening reaction method. Propanediol was used to initiate the TMC polymeric initiator that was then end grafted by l-lactide. A more detailed explanation of the polymerization process is described in U.S. Patent No. 6,342,065 (2002).

Both polymers were isolated, ground, dried, and purified using high vacuum (< 1.5 torr) to remove traces of unreacted monomer.

Determination of Molecular Weight

The number average and weight average molecular weight of SMC-7 were assessed by gel permeation chromatography (GPC) analysis (Waters, 1515 Pump and 717 Plus Autosampler). A 4 mg/ml solution, with dichloromethane (DCM) as the mobile phase, was passed through a 0.4 micron syringe filter prior to analysis to remove any gel particles. A portion of each solution was analyzed using the Waters GPC equipped with four columns (HR6, HR4, HR2, and HR0.5) at a flow rate of 1.0 ml/min with refractive index detector (Waters, RI detector 2414). Chromatograms were compared against calibration curves for twenty poly(methyl methacrylate) (PMMA) standards to determine the relative number and weight average molecular weights. GPC measurements for MG-9 were not obtained due to its insolubility in DCM.

Solution viscosity according to ASTM D2857-95(2007) *Standard Practice for Dilute Solution Viscosity of Polymers* was used to characterize the molecular weight of SMC-7 and MG-9 by measuring inherent viscosity at the standard solution concentration of 0.1 g/dL. Measurements for SMC-7 and MG-9 were carried out in the mobile phases of chloroform and hexafluoroisopropanol (HFIP), respectively.

Determination of Thermal Characteristics

A differential scanning calorimeter (DSC; Perkin Elmer, Pyris 6) was used to evaluate each polymer's melt temperature (T_m) and corresponding endothermic heat of fusion (ΔH_m). A sample weighing between 5-10 mg was heated from room temperature

to 240°C at a rate of 10°C/min. Dry nitrogen was used as a purge gas to eliminate influences due to oxidation.

Yarn Preparation and Properties

Melt Extrusion of Multifilament Yarn

Melt-extruded yarn was produced using a 3/4″ diameter screw extruder equipped with a 43-hole die for SMC-7 yarn. MG-9 was melt-extruded using the same extruder with a 20-hole die. The extruded multifilament yarns were further oriented using a series of heated Godets at temperatures between 100-120ºC prior to their use for knitted mesh construction.

Yarn Physical and Mechanical Testing

Yarn denier, a unit measure of weight for the size of a bundle of filaments (g/9000 m), was measured on the SMC-7 and MG-9 yarns by weighing 50 m of yarn and scaling this quantity to the equivalent of 9000 m.

A universal testing machine (MTS, Synergie 200) equipped with a 500 N load cell was used to obtain mechanical properties for each yarn. Measurements were made using a gauge length of 70 mm and cross-head speed of 2.33 mm/s. The maximum force and elongation at the maximum force were obtained from each stress-strain curve. The maximum force and the denier of the yarn were used to calculate the yarn tenacity (tenacity = maximum force/denier). Mechanical properties were reported as a range

determined from measurements made during the beginning, middle, and end of the extrusion.

Mesh Knit Construction

The weft knit mesh (DM1) was constructed using a single feed circular knitting machine (LAMB, LX96) equipped with a 171 needle knitting head of 113 mm diameter. The feed was a plied, single yarn comprised of one MG-9 and two SMC-7 ends. SMC-7 yarn was dyed violet (D&C violet #2) to assist in its identification.

The warp knitted mesh (WK1) was prepared using a two step process of warping yarn onto beams and then constructing meshes using a raschel knitting machine (American LIBA, RACOP TR-6). The warping process began by preparing 90 packages of each yarn type and transferring their yarn to beams using a creel and warper (American LIBA, GE203A). In all, four beams, two wound with a two-ply SMC-7 yarn and two wound with a two-ply MG-9 yarn, were produced. The knit patterns for each yarn type were coknit into a single interpenetrating construction.

DM1 and WK1 knit mesh were heat set by stretching a tubular mesh over a stainless steel circular mandrel. The DM1 weft knit mesh was knitted in the form of a tube and used as such. However, to accommodate heat setting of the WK1 mesh on circular mandrels, the flat mesh sheet was edge sewn into a tube using a standard sewing machine (Brother International, LX3125) and high-strength polyethylene terephthalate yarn. Heat setting was completed at 110°C for 1 hour while under high vacuum (< 1 torr). Meshes were then cut from the mandrel to produce a stabilized sheet of mesh.

Images of each mesh construction were obtained using a camera (Cannon USA, EOS 20D) equipped with a macro lens and mounted to stand. In addition, images were obtained of each bicomponent mesh and their respective structurally independent MG-9 and SMC-7 mesh components. Meshes of only MG-9 and SMC-7 were obtained by accelerated *in vitro* degradation of the MG-9 yarn and solvent extraction of the SMC-7 yarn using DCM, each process is described below.

Mesh Physical Properties

Accelerated In Vitro Conditioned Degradation

Long-term mesh physical properties (only the SMC-7 yarn component of the mesh) were determined for bicomponent meshes following the degradation and removal of the MG-9 yarn under accelerated *in vitro* degradation conditions to expedite processing. A 0.1M solution of buffered sodium phosphate was pH adjusted using 5.0M sodium hydroxide to a target value of 12.0pH. Using the prepared medium, samples were incubated in 50 mL tubes at 50ºC under static conditions for 5-7 days until the MG-9 component was significantly hydrolyzed. Thereafter, samples were scoured in isopropyl alcohol under ultrasonic agitation to remove MG-9 yarn fragments followed by drying under reduced pressure (< 1.5 torr) to a constant weight.

Mesh Area Weight

The determination of mesh area weight followed option C in ASTM D3776-07 *standard test method for mass per unit area of fabric*. Specifically, the area weight for

each mesh construction was determined by first using a lever arm fabric cutter to cut 10 cm x 15 cm rectangular samples of annealed mesh. Each sample was then weighed (Mettler Toledo, AB204-S) to the nearest one thousands of a gram. The following equation was used to calculate the area weight in grams per meter squared.

$$\text{Area Weight } \left({}^{g}/_{m^2}\right) = \frac{\text{Weight of Sample } (g)}{0.015\ (m^2)}$$

Mesh Thickness

For meshes, thickness is measured as the distance between the upper and lower surfaces of two plates subjected to a specified pressure. Mesh thickness was determined using the procedure as outlined in the ASTM D1777-96 *standard test method for thickness of textile materials*. Using a lever arm fabric cutter, random 57 mm x 57 mm square samples of annealed mesh were obtained for evaluation. Each sample was measured in the center of the mesh swatch using a comparator (B.C. Ames, 05-0191) gauge. The comparator gauge was equipped with a 28.7 mm diameter foot and used a 9 ounce weight to apply the standardized pressure to the mesh.

Weight Ratio of the Bicomponent Constituents

The relative weight ratio of the fast- and slow-degrading yarns was determined from solvent extraction of SMC-7 from the composite using DCM. Three random 57 mm x 57 mm square samples of annealed mesh were obtained and weighed (Mettler Toledo, AB204-S). Next, all three samples were placed in 200 mL of DCM for 30 minutes while under constant orbital agitation at room temperature. Samples were

removed from DCM, rinsed using acetone, and dried under reduced pressure (< 1 torr) to a constant weight. The initial weight of the three composite samples (W_i) and the final weight of the MG-9 yarn component (W_f) were used in the following equation to determine the percent MG-9 in the composite.

$$\text{Weight Ratio of the MG} - 9 \text{ Yarn Component } (\%) = \left[\frac{W_i - W_f}{W_i}\right] \text{x } 100$$

Mesh Porosity

Mesh porosity was characterized as (1) a percentage of the mesh covered by pores and as (2) the mean pore size. Photographic images were obtained using a microscope equipped with a camera (Cannon USA, EOS 20D) and evaluated using NIS Elements (Nikon Instruments, Inc) software. The total pore area, or open apertures, for each mesh was calculated from an obtained image that contained at least 20 large apertures. Manipulation of the images was performed by high-contrast colorizing of the pores followed by software determination of the color covered area. Using this information, the fraction of area covered by pores compared to the total area was determined as a percentage. Using the same image, individual pores were analyzed with respect to area. Since pore shapes are highly variable, both within and among different meshes, the area of individual pores were recalculated to an equivalent average pore diameter and reported as such.

Mesh Tensile and Burst Properties

In Vitro Conditioned Degradation

Samples evaluated for mechanical testing following *in vitro* degradation were conditioned using a 0.1 M solution of buffered sodium phosphate in 50 mL tubes at a 7.2pH. Buffered sodium phosphate was prepared by adding 23.3 grams of dibasic (K_2HPO_4) potassium phosphate and 9.0 grams of monobasic (KH_2PO_4) potassium phosphate into 2 liters of deionized water and stirred until dissolution. A pH meter (Symphony, SB80PI) was used to verify a 7.2pH measurement and slight adjustments were made to using 0.5 N hydrochloric acid (HCl). Tubes containing buffer and 4 to 5 mesh samples were placed in racks and incubated at 37°C under constant orbital-agitation at a speed of 28 revolutions per minute (Innova 4300). Bicomponent mesh samples were removed at the predetermined time periods of 7, 14, 21, 28, and 35 days for mechanical properties testing.

Tensile Properties

Tensile testing of 2.5 cm wide strips of mesh was conducted using a universal testing machine (MTS, Synergie 200) and a set of wedge grips (Chatillon, GF-9). Meshes were tested using a gauge length of 25.4 mm and constant cross-head traverse of 2.33 mm/s. The maximum breaking force and extension at 16 N/cm were recorded. Force-extension data was extracted from the system software (TestWorks 4.0) and used to create force-extension profile curves. Knitted meshes typically have directional structure and properties, regardless of the knitting process or pattern. Therefore, mesh

tensile properties have been reported in the course and wale directions, which correspond to the cross-machine and machine knit direction, respectively.

Burst Properties

Burst mechanical testing was conducted using a universal testing machine (MTS, Synergie 200) equipped with a 1 kN load cell. The ball burst test fixture geometry was determined from ASTM D3787-07 *standard test method for bursting strength of textiles-constant-rate-of-traverse ball burst test*. The MTS machine was connected to a data acquisition system that recorded the force and displacement of the steel ball. Tests were performed using a 2.54 cm/min constant-rate-of-traverse for the ball. Prior to the initiation of the test, a 0.1 N preload force was placed against the mesh by the ball. For each test the maximum burst force (N) obtained during the test and the extension at 71 N load (mm) were recorded. The extension at 71 N was used to determine the elongation at 16 N/cm. The value of 71 N is derived from the diameter of the opening in the clamp plate (4.44 cm x 16 N/cm = 71 N). A detailed explanation of the mathematical expression, which relates the linear travel of the ball (mm) to the extension at 16 N/cm (%), can be found in Appendix A.

Statistical Analysis

Significant differences in physical properties between initial and *in vitro* conditioned meshes were determined using an independent, two-tailed Student t-test to compare means. Two-factor analysis of variance (ANOVA) was used to test for effects

due to time during *in vitro* conditioned degradation and mesh construction, as well as their interaction, for each mechanical property response variable. All analysis was completed using statistical analysis software (SAS, version 9.2) and p-values < 0.05 were considered to be statistically significant.

Results

Polymer Synthesis and Characterization

Before conversion to yarn, two copolyester polymers were prepared and characterized with specific polymerization conditions and analytical data summarized in Table 2.2.

Table 2.2

Polymerization Scheme and Analytical Data for MG-9 and SMC-7

	Description	MG-9	SMC-7
Polymeric Initiator	Monomers, type[a]	TMC	TMC
	Initiator, type	Trimethylolpropane	Propanediol
	Analytical Data: GPC: Mn, Mw (kDa)	>2, >5	>30, >60
Crystalline Copolyester	Polymeric Initiator/Monomer Ratio (weight)	2/98	6/94
	Monomers, type[a] (molar)	95/5 G/CL	96/4 L/TMC
	Analytical Data: GPC: M_n, M_w (kDa)	N/A	235, 436
	η_{lhv}: (dL/g)	>1.0[b]	>2.5[c]
	DSC: T_m (°C)	220	185
	ΔH_m (J/g)	94	67

a, CL = ε-caprolactone, TMC = trimethylene carbonate, G = glycolide, L = l-lactide; b, HFIP mobile phase; c, DCM mobile phase

To produce high quality yarn from the relatively high modulus lactide and glycolide polymer, copolymerization using trimethylene carbonate (TMC) was performed, as reported in Table 2.2. However, to facilitate crystallinity, each polymer was segmented. Results from DSC heat of fusion (ΔH_m) measurements for MG-9 and SMC-7 showed high levels of crystallinity at 94 J/g and 67 J/g, respectively. Polymer synthesis was completed successfully with near complete conversion of monomer, which resulted in high molecular weights (M_n, $M_{w,}$ η_{Ihv}) and melt temperatures (T_m) typical of high glycolide or lactide copolymers.

Yarn Preparation and Properties

Ground and purified polymers were converted into yarn and further orientated to optimize mechanical and physical properties. The resultant properties of both MG-9 and SMC-7 yarn are listed in Table 2.3. Yarn quality was assessed from the tenacity, a measure of strength normalized for yarn size, which exceeded 3.0 for both yarns. Furthermore, the elongation at maximum force, a measure of ductility, for both yarns was greater than 20%. Taken together, these values indicate a high level of yarn toughness.

Table 2.3

Typical Physical and Mechanical Properties of MG-9 and SMC-7 Yarn

Description	MG-9	SMC-7
Filament count	20	43
Denier (g/9000m)	55 - 60	80 - 100
Tenacity (grams-force/denier)	4.2 - 4.6	3.0 - 3.4
Elongation at maximum force (%)	25 - 35	20 - 30

Mesh Knit Construction

Figure 2.1 provides comparative images of each mesh construction following stabilization by heat setting. The construction of the DM1 and WK1 meshes was similar in that each yarn type, MG-9 and SMC-7, was coknit together to form an interdependent structure; however, the mesh produced by each individual yarn type was also capable of functioning as an autonomous, structurally stable mesh. Figure 2.2 provides comparative images of each mesh construction initially and following the removal of the MG-9 or the SMC-7 yarn using accelerated *in vitro* degradation and solvent extraction, respectively. In contrast to the DM1 mesh, the two yarn types within the WK1 mesh were knit in different patterns. The DM1 mesh possessed the same knit pattern for both yarns due to the limitations of weft knitting. Specifically, the DM1 mesh construction consisted of a pattern of interlocking loops comprised of a single, plied yarn of MG-9 and SMC-7. On the other hand, the WK1 mesh was constructed from hundreds of yarn ends that were interlocked in a series of sequenced guide bar movements around the knitting needles.

Two guidebars of each yarn were used to knit two separate patterns that were constructed simultaneously or coknit into a single structure.

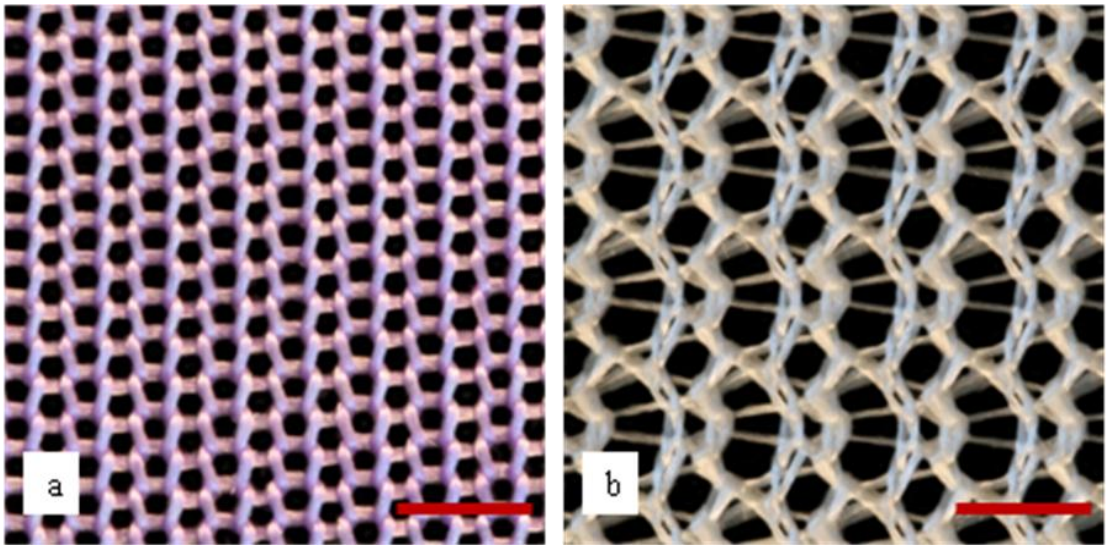

Figure 2.1

Images of the knit construction for the (a) DM1 and (b) WK1 mesh. (Red scale bars = 3 mm)

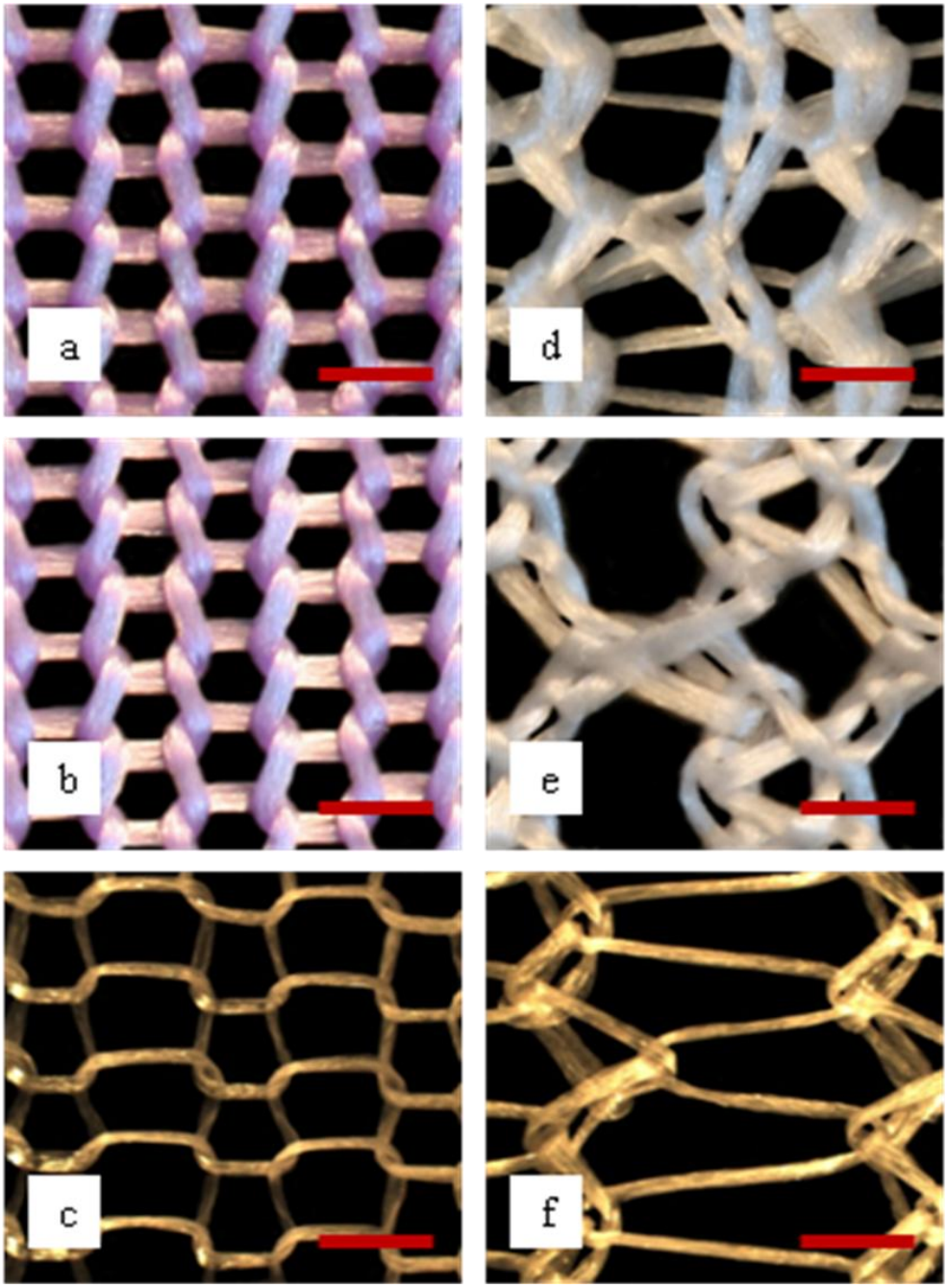

Figure 2.2

Images of the components of the DM1 and WK1 mesh. (a) DM1 mesh (b) SMC-7 yarn component of the DM1 mesh (c) MG-9 yarn component of the DM1 mesh (d) WK1 mesh (e) SMC-7 yarn component of the WK1 mesh and (f) MG-9 yarn component of the WK1 mesh (Red scale bars = 1 mm)

Mesh Physical Properties

Mesh samples of each construction were quantitatively evaluated for their biocompatibility-relevant physical properties, both initially and following accelerated *in vitro* conditioning. The results, detailed in Table 2.4 are reported with one standard deviation.

Table 2.4

Initial and *In Vitro* Conditioned Mesh Physical Properties for the DM1 and WK1 Meshes (n = 5)

Mesh Physical Property	DM1		WK1	
	Initial	*In Vitro* Conditioned	Initial	*In Vitro* Conditioned
Mesh Thickness (mm)	.421 ± .008	.316 ± .006	.536 ± .005	.346 ± .006
Ratio of Constituents (weight % of MG-9)	24 ± 1	--	33 ± 2	--
Area Weight (g/m^2)	131 ± 2	99 ± 3	126 ± 3	83 ± 2
Porosity:				
Pore Area (%)	34.2 ± .72 †	32.0 ± 2.56 †	29.6 ± .78	34.6 ± 1.28
Pore Diameter, Mean (μm)	520 ± 33 ‡	499 ± 33 ‡	698 ± 27	1045 ± 73
Pore Diameter, Range of values (μm)	495 - 585	390 - 547	320 - 1040	349 - 1548

† ‡ Indicates changes in physical properties that were not found to be significantly different between initial and *in vitro* conditioned samples ($p < .05$)

Results show that, for comparable initial area weights, the construction of the WK1 mesh possessed a greater weight fraction of MG-9 than did the DM1 mesh. As a consequence, the WK1 mesh showed a greater reduction in area weight and thickness after *in vitro* conditioning. Mean *in vitro* conditioned area weights of 99 g/m^2 and 83

g/m^2 were significantly lower than the initial values for the DM1 and WK1 meshes, respectively. The porosity measurement of total pore area increased from 29.6% to 34.6% following *in vitro* conditioning for the WK1 mesh. Additionally, the mean pore diameter increased from 698 μm to 1045 μm with a 50% increase in the maximum value of the range from 1040 μm to 1548 μm. Due to the plied construction of the DM1 mesh, the degradation of the MG-9 yarn produced no significant change in porosity. In contrast, the dramatic increase in porosity for the WK1 mesh was due to the opening of the large pores after the degradation of the MG-9 yarn. On the whole, the use of two yarns with different degradation profiles facilitated the *in vitro* modulation of the thickness and area weight; however, only the WK1 mesh produced an increase in its porosity following the removal of the MG-9 yarn.

Mesh Tensile and Burst Properties

The initial structural stiffness of each mesh was evaluated both qualitatively and quantitatively. Qualitative observations during tensile testing indicated that the edges of the WK1 mesh did not readily collapse. On the other hand, the edges of the DM1 mesh immediately collapsed as the unrestrained pores deformed perpendicular to the applied strain. These observations were reinforced by quantitative measures for the extension at 16 N/cm (Figure 2.3) and force-extension data (Figure 2.4). Using the theoretical maximum physiologic condition of 16 N/cm applied to initial samples under uniaxial tension, the WK1 mesh produced between 20% and 30% extension, which was less than half the value obtained for the DM1 mesh. More importantly, from force-extension data,

it can be seen that for typical physiologic conditions which are a fraction of maximum values, the WK1 mesh produced immediate and substantial resistance to an applied strain in both the wale and course directions. In contrast, the DM1 mesh showed significant extension before developing substantial resistance.

The different initial response of the two meshes was construction dependent. For instance, the different yarn knit patterns which comprise the bicomponent, coknit structure of the WK1 mesh restricted pore deformation. As a consequence, under uniaxial strain the structural stiffness of the MG-9 yarn knit pattern, which was coknit into the WK1 mesh, exhibited significant structural stability and resistance to an externally applied strain. In contrast, the knit pattern of the MG-9 yarn coknit into the DM1 mesh did not exhibit any significant resistance to the applied strain.

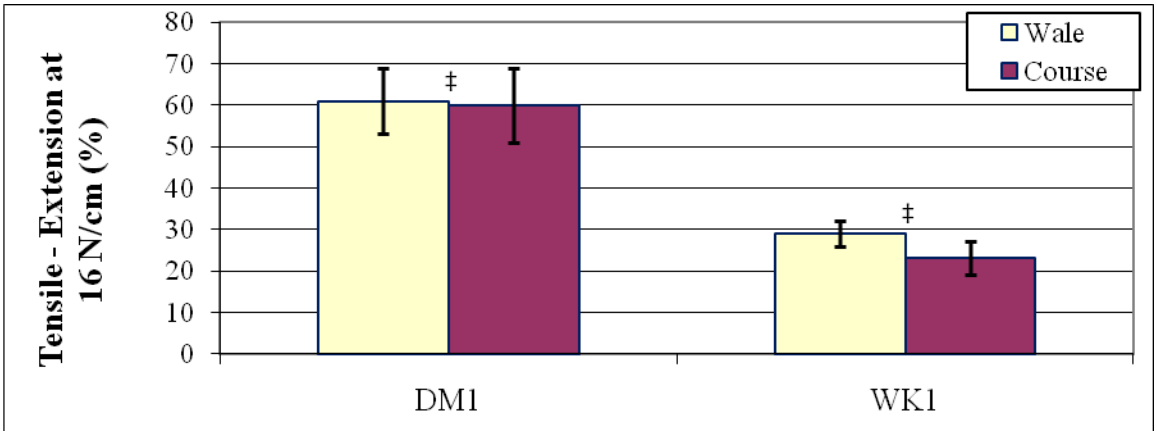

‡ Indicates a significant difference ($p < .05$) between (‡) the DM1 and WK1 meshes, No difference was found between wale and course for a given mesh

Figure 2.3

The initial extension at 16 N/cm in the wale and course directions for the DM1 and WK1 meshes during mechanical tensile testing.

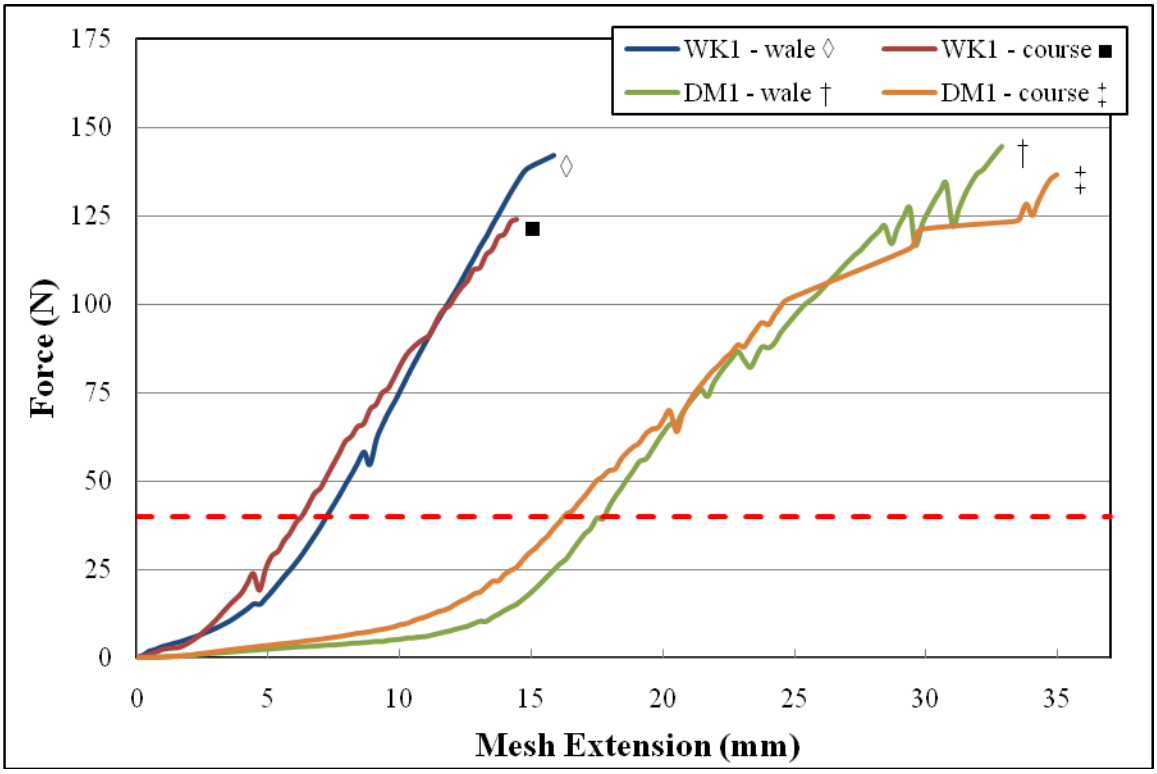

Figure 2.4

Force-extension data for initial tensile testing of the DM1 and WK1 meshes in the wale and course directions. The dotted red line represents the 16 N/cm maximum abdominal wall loading condition. (25.4mm extension represents a strain equal to 1)

The location of failure for tensile tested mesh samples was not centrally located; rather, it consistently occurred at one edge of the two grips. No slipping of the mesh within the grips was observed. The MG-9 yarn of each mesh was observable throughout the *in vitro* conditioning test period; however, fragmentation prior to testing was first observed at 14 days.

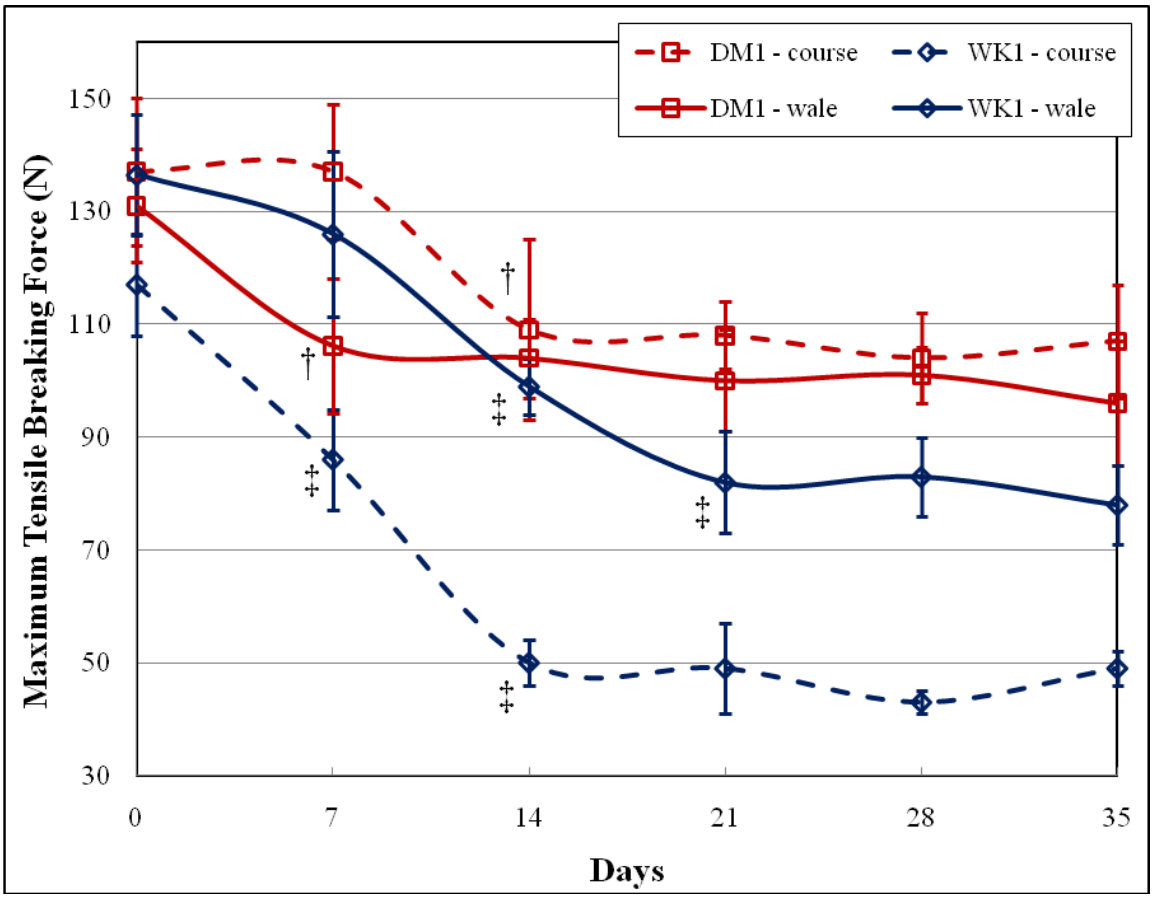

† ‡ Indicates a significant difference ($p < .05$) from the previous time point for the DM1 (†) and WK1 (‡) meshes

Figure 2.5

The temporal *in vitro* conditioned maximum breaking force in the course and wale directions for the DM1 and WK1 meshes during mechanical tensile testing. (7.2pH,37ºC)

As seen in Figure 2.5, both the DM1 and WK1 mesh constructions showed a reduction in their maximum tensile breaking force in the course and wale directions during the first 14-21 days. However, the reduction in maximum breaking force for the WK1 mesh was more dramatic, with 40-60% reductions compared to 20-25% for the DM1 mesh. Beyond 21 days, no significant change in the maximum tensile breaking force was observed for either mesh (all p-values > .193).

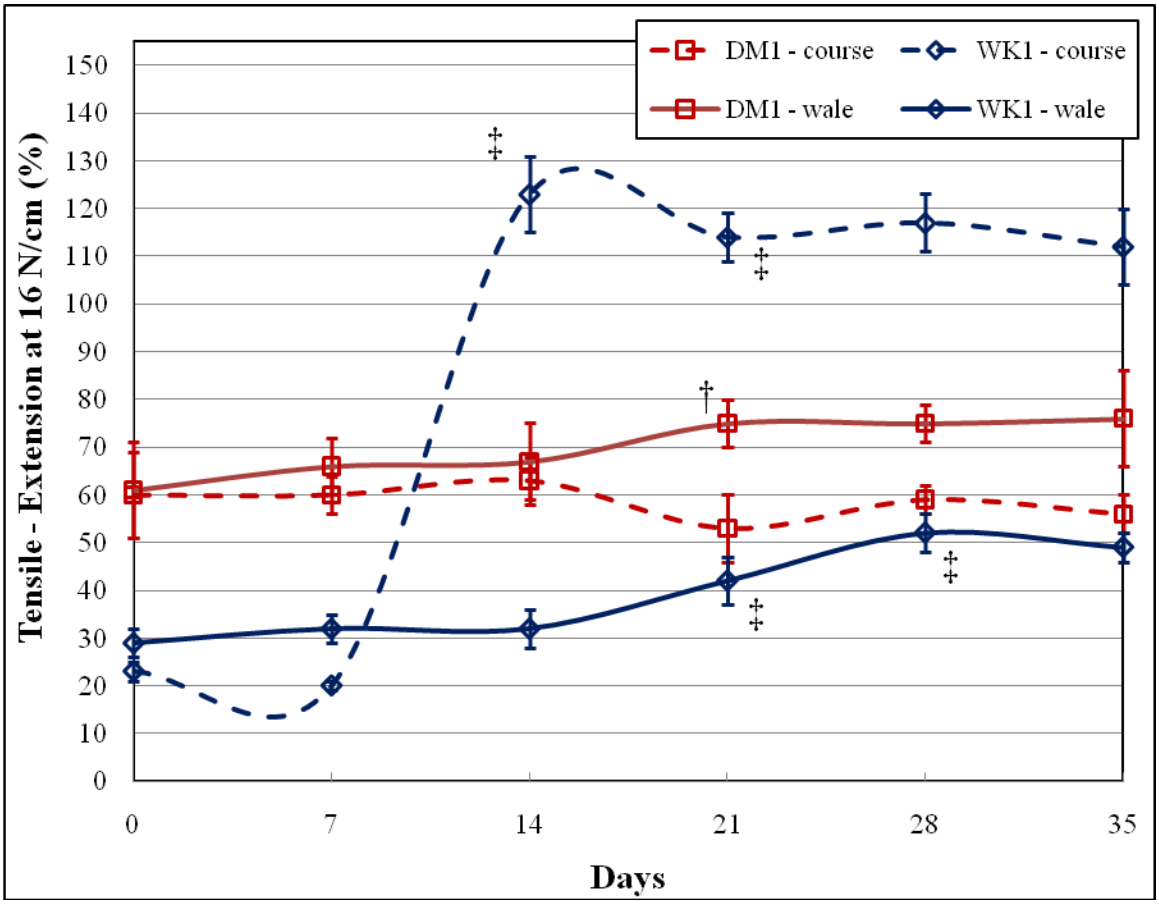

† ‡ Indicates a significant difference ($p < .05$) from the previous time point for the DM1 (†) and WK1 (‡) meshes

Figure 2.6

The temporal *in vitro* conditioned extension at 16 N/cm in the course and wale directions for the DM1 and WK1 mesh during mechanical tensile testing. (7.2pH, 37ºC)

The *in vitro* conditioned tensile extension at 16 N/cm of the DM1 mesh did not produce a pronounced change with time. On the other hand, in the course direction the WK1 mesh showed a 6-fold increase in the extension at 16 N/cm between 7 and 14 days, a marginal decrease between 14 and 21 days, and no change thereafter. These changes were paralleled in the wale direction with a significant increase, although less dramatic,

from 28% to approximately 50% between 14 and 28 days. From 28 to 35 days, no difference was observed for either mesh.

Collectively, observed changes in mechanical tensile properties were directly related to the degradation of the MG-9 yarn; however, the specific response of that change within each mesh was construction dependent. For example, both mesh constructions experienced a reduction in breaking force as the MG-9 yarn lost breaking strength with time; however, the extension at 16 N/cm for the WK1 mesh was drastically different than that of the DM1 mesh. Since the MG-9 and SMC-7 yarns were knit in different patterns, each construction contributed specific properties to the WK1 mesh. For instance, the traversing MG-9 yarn lay-in within the pores provided resistance to deformation from applied strains. Specifically, this structural stiffness was derived from a chain stitch running in the wale direction and angled lay-in yarn connections that traverse the chain stitch in the course direction. Moreover, being interlaced with the sandfly net pattern of the SMC-7 yarn further restricted the relative strain between different points within the mesh. On the other hand, once liberated following the degradation of the MG-9 yarn, the knit pattern of the SMC-7 mesh possessed significantly greater extension at 16 N/cm. The modulation in compliance resulted from the relaxed configuration of the SMC-7 yarn mesh being constrained by the marquisette pattern of the MG-9 yarn mesh, and its large, open pores that deform when strained. As a result, the knit construction of each yarn type in the WK1 mesh produced two levels of extensibility during tensile testing, early structural stiffness with restricted mobility transitioning to a high degree of extension.

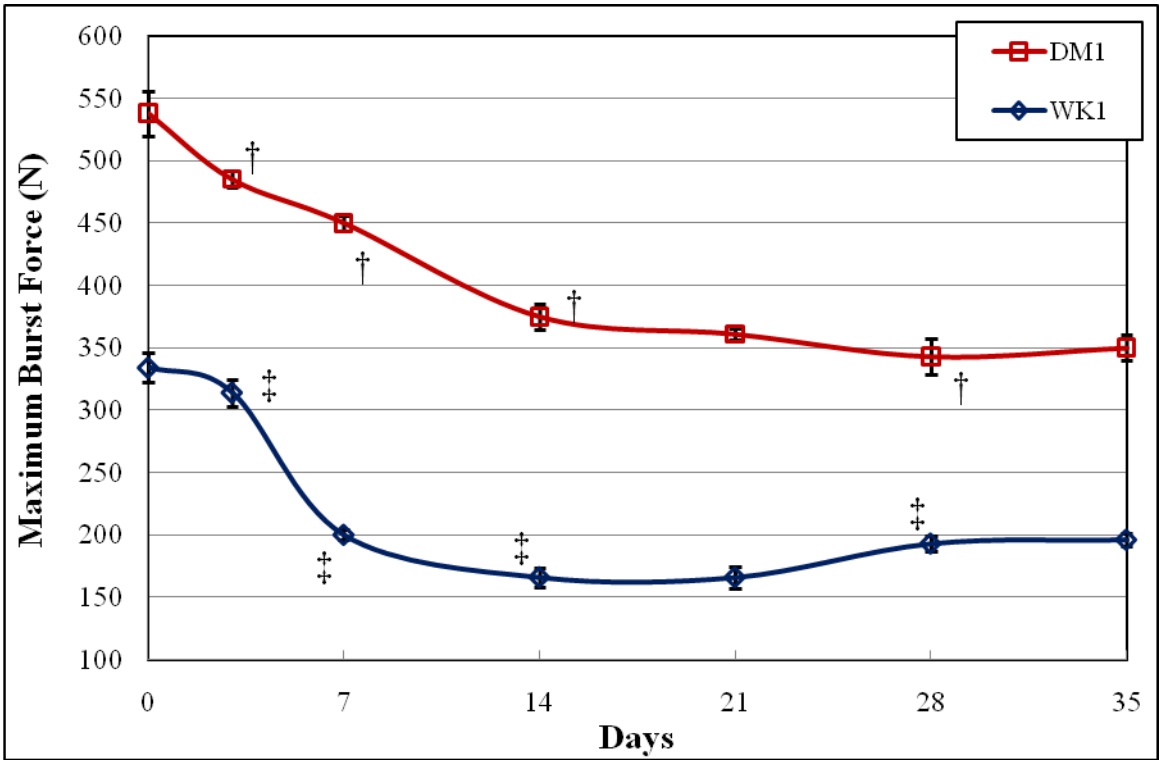

† ‡ Indicates a significant difference ($p < .05$) from the previous time point for the DM1 (†) and WK1 (‡) meshes

Figure 2.7

The temporal *in vitro* conditioned maximum burst force for the DM1 and WK1 mesh during mechanical burst testing. (7.2pH, 37ºC)

The ball-burst test determines the strength and extensional characteristics of a constrained mesh subjected to a perpendicular force. The failure mode of mesh samples was centrally located and at no time did slipping between the plates occur. For all time points, the DM1 mesh exhibited a significantly greater maximum burst force with mean values at least 150 N greater than that of the WK1 mesh. Both mesh types experienced significant reductions in maximum burst force up to 14 days with a leveling in burst force between 14 and 21 days. During the time period from 21 to 28 days, the WK1 mesh

showed an increase of approximately 30 N ($p < .001$) while the DM1 mesh produced a slight decrease ($p = .091$) of 20 N. No change for either mesh was experienced beyond 28 days.

The maximum burst force verifies the ability of a mesh to resist the expected *in vivo* mechanical loading conditions. As found in the tensile test, both the DM1 and WK1 meshes experienced a reduction in strength up to 14 days; however, both meshes exhibited the necessary strength required for clinical use. For the specified geometry of the burst test fixture, a burst force of 71 N corresponds to the theoretical maximum physiologic condition. The maximum burst force for the DM1 mesh was at least 5 times greater than the physiologic maximum.

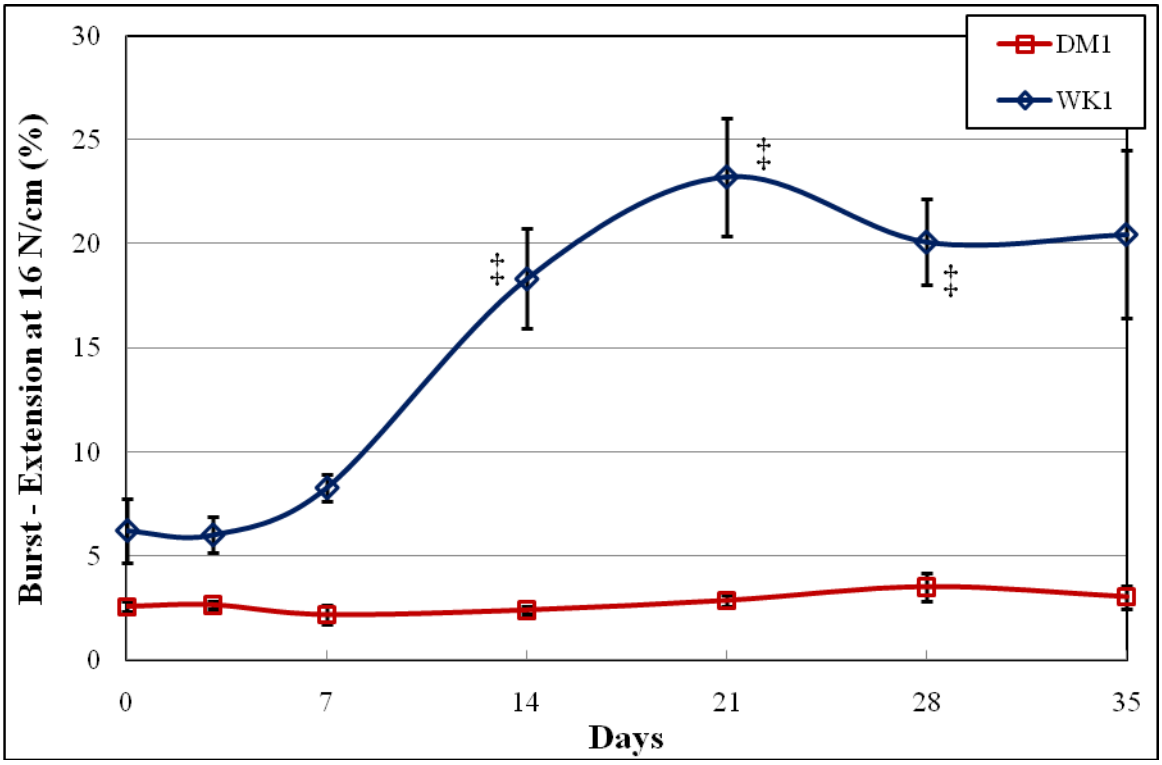

† ‡ Indicates a significant difference ($p < .05$) from the previous time point for the DM1 (†) and WK1 (‡) meshes

Figure 2.8

The temporal *in vitro* conditioned extension at 16 N/cm for the DM1 and WK1 mesh during mechanical burst testing. (7.2pH, 37ºC)

Figure 2.8 depicts the extension at 16 N/cm for the two mesh constructions during burst testing. For the first 7 days of *in vitro* conditioning, the WK1 mesh maintained a constant, low level of extension. Between 7 and 14 days and again between 14 and 21 days, a statistically significant shift in the extension at 16 N/cm for the WK1 mesh was realized. From 21 to 28 days the WK1 mesh extension reduced by 3.2% ($p = .007$). Beyond 28 days, no change for the WK1 mesh type was observed ($p > .825$). The

extension at 16 N/cm for the DM1 mesh construction did not change during the *in vitro* study (all $p > .453$).

The burst test extension at 16 N/cm of the WK1 mesh revealed two levels of mesh stiffness with approximately a 7% extension until 7 days, a transition period from 7-14 days, and a second plateau with approximately 20% extension. These results show that the coknit structure of the WK1 mesh, where different degradation profile yarns are initially interdependent, will transition to exhibit independent, functional mechanical properties for the SMC-7 yarn with extensional characteristics that match the extension of the abdominal wall under maximum conditions. The DM1 showed significant structural stiffness in the burst mode of testing, with only a slight, and not statistically significant, increase in mean extensional values at 16 N/cm.

Discussion

The ideal hernioplasty requires that the mesh provide support to the local tissue, without mechanical failure, and that it match the dynamic and multiaxial strains of the abdominal wall. The former has historically not been an issue, with central mesh ruptures being a rare occurrence.[43,44] In fact, the strength of most meshes is several orders of magnitude above clinical requirements. However, the extensional characteristics of hernia meshes, and more importantly the resultant mesh/tissue complex, may provide inadequate stability to the developing ECM and then lack long-term extensibility. For these reasons, this study has focused on developing a novel mesh for application in hernia repair using construction and absorbable polymers possessing

different degradation profiles to modulate the biocompatibility- and clinically-relevant physical and mechanical properties.

The physical properties of area weight and porosity, and to a lesser extent thickness, are important mesh design variables that influence biocompatibility and tissue integration. So called heavy-weight (HW) polypropylene meshes (>80 g/m^2) produce a persistent, profound inflammatory response and scar production which has been linked to pain and discomfort, reduced abdominal wall compliance, and mesh contraction.[9,11,12] As a result, there has been an initiative in recent years to reduce the area weight of typical polypropylene meshes in an effort to reduce the foreign body response.[31,45-48] However, the overwhelming majority of meshes used clinically are HW meshes constructed from monofilament, polypropylene yarn[25] of area weight within the range of 80 to 110 g/m^2. Inclusive in this range is the slow absorbing SMC-7 yarn of the WK1 mesh. However, as a fully absorbable mesh the overall area weight as a measure of long-term biocompatibility (> 3years) has less relevance. Ideally, the tissue reaction to an implanted mesh can be divided into two stages. Initially, a short-term, moderate reaction to the mesh is a desirable outcome and facilities the integration of the mesh into the abdominal wall; however, beyond the integration stage, a continuous inflammatory response is undesirable. Fully absorbable meshes hold the potential to provide an initial inflammatory response but their absorption after their intended function will eliminate the long-term chronic foreign body response.

Mesh porosity facilitates the infiltration of cells, ECM, and blood vessels within the mesh to (1) allow the diffusion and vascular transport of nutrients and waste and (2)

mechanically interlock the mesh into the abdominal wall, and (3) facilitate, in part, the extensibility of the mesh/tissue complex. Porosity facilitates mesh extensibility in two ways. First, as discussed previously, mesh extensibility is derived from geometric changes within the pores. Consequently, meshes with larger pores produce greater uniaxial extension. Second, porosity of adequate size minimizes the complete encapsulation of the mesh, which results in additional resistance to deformation of the mesh/tissue complex. From experience to date, pore sizes greater than 1000 μm have been suggested by Junge and coworkers[49] to avoid bridging of granulation tissue and the subsequent complete encapsulation of the mesh. Although the DM1 mesh produced adequate size pores for the infiltration of cells and neotissue, the WK1 mesh possessed mean pore sizes greater than 1000 μm. HW meshes exhibit about 50% porosity[50] with an average pore size of 460 μm reported for one commonly used prosthesis.[51] For the reasons stated, pore size is the major factor which affects *in vivo* mechanics. In essence, the WK1 mesh will likely integrate forming a mesh/tissue complex whereby yarn filaments, rather than the entire mesh, are encapsulated, better preserving the inherent biomechanics of the mesh construction.

The strength of HW meshes is several orders of magnitude higher than physiologic conditions. Using a comparable burst test to that used in this study, values as high as 1165 N have been reported in literature.[52] Therefore, a maximum physiologic burst force of 71 N produces a safety factor greater than 16. Although the DM1 mesh is significantly stronger, the WK1 mesh provided adequate clinical strength with a steady

state burst force plateau of approximately 200 N, almost 3 times the theoretical physiologic maximum, beyond 28 days.

A mesh which is structurally stiff during the inflammation and proliferation stages and transitions to become highly extensible is novel to soft tissue repair. However, stability or immobilization of healing tissue is not a new concept, with many examples in the inherent pathology of wound healing and in clinical treatment. For example, following a bone fracture the rapid formation of woven bone minimizes relative movement at the site. In addition, the primary function of a scab is the stabilization of the delicate epidermal granulation tissue.[53] These inherent processes are often augmented clinically with additional external stabilization (e.g. sutures, casting, pins, and plates). Consequently, the pathological approach to wound healing is to stabilize the delicate neotissue, which is often enhanced with clinical treatment. Likewise, during the initial healing period the WK1 mesh showed a high degree of stiffness which was measured as resistance to both uniaxial and multiaxial strain. It is novel for a mesh to resist uniaxial and multiaxial strain. The DM1 mesh's lack of variation in knitting pattern resulted in a one dimensional response with only a reduction in breaking force and little or no change in extensional characteristics with time during *in vitro* conditioning. Currently available hernia meshes do not possess a structure which opposes pore deformation. As a result, they show minimal resistance during low levels of uniaxial applied strain, producing a similar response as that of the DM1 mesh, but remain structurally stiff in a multiaxial mode of deformation. The structure of the WK1 mesh is unique in that it uses two

constructions which interpenetrate, whereby the pattern of one limits the deformation within the pores of the other. This novel characteristic may hold several advantages.

The early phases of wound healing and mesh integration are critical to the outcome of hernioplasty. The acute wound healing phase is the timeframe when inflammatory and repair cells are recruited, but during which no meaningful tissue integrity is yet established.[54] Mesh stress shielding, caused by restricted uniaxial and multiaxial extension, may better protect the neotissue from widespread micro-trauma or an isolated disruption of neotissue from a single overload event. These disruptions have the potential to slow the progression of wound healing and stimulate the production of pro-inflammatory chemical factors.

Although short-term meta-analysis studies continue to show lower recurrence rates associated with mesh use, recurrence continues to be a problem.[10] Several authors have suggested that, in part, the origin of recurrence is associated with a defect created early in the mesh wound healing and integration process caused by stressed suture points disrupting local tissue at the margins of the mesh.[23,24,55-57] For incisional hernias, these disruptions occur in the first month, starting small and asymptomatic, but increasing in size later.[58] The immediate and significant transfer of load observed in uniaxial testing may have benefit in reducing recurrence. The non-compliant nature of the WK1 mesh will allow the distribution of load applied at any single point to multiple attachment points as the mesh moves as one structure with minimal relative displacement between pores. Consequently, a reduction in the load realized by any single attachment point will reduce the likelihood of early induced trauma.

A further benefit may be found in the wound healing response to tension applied during the proliferation stage. Although tensional homeostasis exists in almost all connective tissues, under normal circumstances, loads seen by cells are minimal compared to their surrounding ECM.[59] Cells stress shield themselves from bulk external loading. Specifically, fibroblasts actively control the local mechanical environment by depositing collagen, contracting the matrix, and increasing the crosslink density of the ECM to either increase or decrease cellular reaction to local mechanical conditions.[60] The differentiation of fibroblasts to the myofibroblast phenotype is, in part, driven by high ECM stress.[61] Myofibroblasts are characterized by their ability to secrete collagen and contract the ECM, which has undesirable results when unregulated.[62] The modern study of mechanobiology has established a link between wound tension and its effect on myofibroblast activity. Within the first week of wound healing, external applied tension has been shown to promote excessive fibrosis, with effects for 6 months thereafter, due to an inhibition of myofibroblast apoptosis.[63] In a separate study by Hinz and coworkers, mechanical tension was found to be crucial for differentiation and maintenance of the myofibroblast phenotype.[64] Stress shielding of proliferating myofibroblasts, as provided by the structurally stiff WK1 mesh, may reduce myofibroblast differentiation and/or promote apoptosis, effectively reducing the likelihood of the early developed and well documented excessive scar plate and mesh contraction.[9,65-68] Unlike the initial stages of inflammation and proliferation, where cellular activity is high and ECM strength is minimal, a properly timed transition to tensional homeostasis and biomechanical stimulation provides the cues for remodeling and adaptation to develop functional tissue.

The clinical use of meshes requires that the force/extensional characteristics are evaluated against those approximated from human physiology. It is of interest to characterize the extension of a mesh at the anticipated maximum physiologic condition, determined to be 16 N for each centimeter of width or 16 N/cm.[69] At this theoretical maximum physiologic force the associated strain as determined from fresh cadavers was 25% ± 7%.[70] It is reasonable to expect that meshes *in vivo* experience multiaxial and uniaxial strain. However, it should be noted that only low to moderate (strain < 1) levels of uniaxial deformation have clinical relevance. Significant changes to the mesh length/width aspect ratio begin to negate the relevance of the test method since *in vivo* uniaxial deformation is limited by secured mesh edges and pores which are infiltrated with tissue. More appropriately, ball burst testing applies a perpendicular applied stress to a mesh where the edges are fully constrained. In addition, these conditions simulate the multiaxial expansion expected from increased abdominal pressure.

Optimized hernia repair will establish self-sustaining, functional tissue which will prevent hernia recurrence. To accomplish this objective the biomechanical environment of the abdominal wall must be replicated. Complications associated with traditional meshes are certainly a response to their lack of biomechanical compatibility, as traditional mesh materials are considered inert and do not illicit an immune response.[71] Increasingly, the importance of biomechanical stimulation for load-bearing connective tissues is being recognized as being governed by the same modern principles initially conceived as Wolffs' Law for bone. Connective tissue morphology follows function, the magnitude and frequency of repetitive loads trigger remodeling, a lack of stress produces

atrophy while excessive stress results in hypertrophy. Each of these pathological findings become circumvented when the implant stress shields the remodeling tissue, and thus prevents adaptation. For example, as the compliance of vascular grafts approaches that of the native tissue their patency linearly increases.[72] For traditional HW meshes, a significant decrease in the mobility of the abdominal wall is realized 2-3 weeks after implantation from the induction of the ECM.[73] For the WK1 mesh, the timing of this event occurs 1-2 weeks later than the observed transition to its highly compliant structure. However, it should be noted that with chemical modification and/or further annealing optimization temporal breaking strength of the MG-9 yarn can be modulated to prolong the mesh transition point. As the transition progresses, load is gradually transferred from the mesh to the ECM. At this point in the wound healing process, the ECM has established sufficient strength and the remodeling process is initiated. As a result of the coknit construction, the mesh is 'set' in a relaxed configuration and encapsulated in the ECM. This configuration is unique and only obtainable through the use of an absorbable component which degrades to realize this relaxation event. Consequently, the mesh possesses both uniaxial and multiaxial extensibility as evidenced by the tensile and burst test results. Of special interest is that the multiaxial extensibility of the WK1 mesh is within the maximum physiologic range of 25% ± 7%.[70] In contrast, traditional HW meshes in the multiaxial mode of deformation produce 16 N/cm extension values well below physiologic conditions, with observed values between 6 and 14%.[31,70] The extensibility of the mesh i*n vivo* will be reduced even further due to the formation of the composite mesh/tissue complex[73] and observed cyclic strain hardening which may occur

before ECM filtration.[74] As a consequence, hernia meshes must be highly extensible to restore the abdominal wall mechanics, rendering them possibly too extensible to be efficiently handled during the surgical procedure. Hence, a mesh which is structurally stiff and stable during the surgical procedure, but will transform to a high level of extensibility after encapsulation *in situ* may be critical to achieving both sufficient initial handling characteristics as well as physiologic extensibility. Furthermore, *in situ* placement in a relaxed configuration means that endogenous tension within and around the mesh may be established.

Conclusion

The construction of the WK1 mesh met the suggested additional design criteria of being fully-absorbable, maintaining structurally stiffness during the early phases of wound repair, and replicating the extensional properties of the abdominal wall during the remodeling/maturation phase while providing an adequate level of strength. The use of warp knitting whereby each yarn type was coknit using different knitting patterns allowed for the modulation of mesh physicomechanical properties and a configuration allowing (1) short-term structural stiffness, (2) a gradual transition of the perceived loads from the mesh to local tissue, and (3) long-term compliance with extensional elasticity similar to the abdominal wall. The initially interdependent construction provided a high level of structural stiffness and following the substantial degradation of the fast-degrading yarn, transitioned to liberate a compliant slow-degrading mesh. The use of two different degradable copolyester yarns facilitated the modulation of the physicomechanical

properties while the knit construction determined the resultant porosity, area weight, thickness, strength, and extension of the mesh, both during the initial phase when the fast-degrading yarn was load bearing, and once the structurally independent, slow-degrading yarn component was liberated. The lack of variation in the knit pattern for the DM1 mesh made it one-dimensional, producing strength loss with time but showing significant structural stiffness with minimal change in extensibility following the substantial degradation of the fast-degrading yarn. Future studies will explore the optimization of the high-glycolide yarn, the restoration of homeostatic tension within the coknit mesh, and the long-term *in vitro* response of different warp knit designs based upon the coknit construction and will compare the coknit mesh mechanics to that of traditional meshes.

References

1. Beltran MA, Cruces KS. Outcomes of Lichtenstein hernioplasty for primary and recurrent inguinal hernia. World J Surg 2006;30(12):2281-7; discussion 2288-9.

2. Mann DV, Prout J, Havranek E, Gould S, Darzi A. Late-onset deep prosthetic infection following mesh repair of inguinal hernia. Am J Surg 1998;176(1):12-4.

3. Agrawal A, Avill R. Mesh migration following repair of inguinal hernia: a case report and review of literature. Hernia 2006;10(1):79-82.

4. Kes E, Lange J, Bonjer J, Stoeckart R, Mulder P, Snijders C, Kleinrensink G. Protrusion of prosthetic meshes in repair of inguinal hernias. Surgery 2004;135(2):163-70.

5. Staal E, Nienhuijs SW, Keemers-Gels ME, Rosman C, Strobbe LJ. The impact of pain on daily activities following open mesh inguinal hernia repair. Hernia 2008;12(2):153-7.

6. Palumbo P, Minicucci A, Nasti AG, Simonelli I, Vietri F, Angelici AM. Treatment for persistent chronic neuralgia after inguinal hernioplasty. Hernia 2007;11(6):527-31.

7. Nienhuijs S, Staal E, Strobbe L, Rosman C, Groenewoud H, Bleichrodt R. Chronic pain after mesh repair of inguinal hernia: a systematic review. Am J Surg 2007;194(3):394-400.

8. Aasvang E, Kehlet H. Chronic postoperative pain: the case of inguinal herniorrhaphy. Br J Anaesth 2005;95(1):69-76.

9. Klinge U, Klosterhalfen B, Muller M, Ottinger AP, Schumpelick V. Shrinking of polypropylene mesh *in vivo*: an experimental study in dogs. Eur J Surg 1998;164(12):965-9.

10. Kockerling C, Schug-Pass C. Recurrence and mesh material. In: Schumpelick V, Fitzgibbons RJ, editors. Recurrent Hernia. Berlin, Germany: Springer-Verlag; 2007.

11. Champault G, Bernard C, Rizk N, Polliand C. Inguinal hernia repair: the choice of prosthesis outweighs that of technique. Hernia 2007;11(2):125-8.

12. Welty G, Klinge U, Klosterhalfen B, Kasperk R, Schumpelick V. Functional impairment and complaints following incisional hernia repair with different polypropylene meshes. Hernia 2001;5(3):142-7.

13. McLanahan D, King LT, Weems C, Novotney M, Gibson K. Retrorectus prosthetic mesh repair of midline abdominal hernia. Am J Surg 1997;173(5):445-9.

14. Tyrell J, Silberman H, Chandrasoma P, Niland J, Shull J. Absorbable versus permanent mesh in abdominal operations. Surg Gynecol Obstet 1989;168(3):227-32.

15. Schachtrupp A, Fackeldey V, Klinge U, Hoer J, Tittel A, Toens C, Schumpelick V. Temporary closure of the abdominal wall (laparostomy). Hernia 2002;6(4):155-62.

16. Klinge U, Schumpelick V, Klosterhalfen B. Functional assessment and tissue response of short- and long-term absorbable surgical meshes. Biomaterials 2001;22(11):1415-24.

17. de Tayrac R, Chentouf S, Garreau H, Braud C, Guiraud I, Boudeville P, Vert M. *In vitro* degradation and in vivo biocompatibility of poly(lactic acid) mesh for soft tissue reinforcement in vaginal surgery. J Biomed Mater Res B Appl Biomater 2008;85(2):529-36.

18. de Tayrac R, Oliva-Lauraire MC, Guiraud I, Henry L, Vert M, Mares P. Long-lasting bioresorbable poly(lactic acid) (PLA94) mesh: a new approach for soft tissue reinforcement based on an experimental pilot study. Int Urogynecol J Pelvic Floor Dysfunct 2007;18(9):1007-14.

19. Stoppa R, Diarra B, Verhaeghe P, Henry X. Some problems encountered at re-operation following repair of groin hernias with pre-peritoneal prosthesis. Hernia 1998;2(1):35-38.

20. Vijan SS, Wall JC, Greenlee SM, Farley DR. Consequences of endoscopic inguinal hernioplasty with mesh on subsequent open radical prostatectomy. Hernia 2008;12(4):415-9.

21. Stolzenburg JU, Anderson C, Rabenalt R, Do M, Ho K, Truss MC. Endoscopic extraperitoneal radical prostatectomy in patients with prostate cancer and previous laparoscopic inguinal mesh placement for hernia repair. World J Urol 2005;23(4):295-9.

22. Foley CL, Kirby RS. Bilateral laparoscopic inguinal hernia repair can complicate subsequent radical retropubic prostatectomy. J Urol 2003;169(4):1475.

23. Franz MG. The biology of hernias and the abdominal wall. Hernia 2006;10(6):462-71.

24. Franz MG. The biological treatment of the hernia disease. In: Schumpelick V, Fitzgibbons RJ, editors. Recurrent Hernia. Berlin, Germany: Springer-Verlag; 2007.

25. Conze J, Rosch R, Klinge U, Weiss C, Anurov M, Titkowa S, Oettinger A, Schumpelick V. Polypropylene in the intra-abdominal position: influence of pore size and surface area. Hernia 2004;8(4):365-72.

26. Bellon JM, Rodriguez M, Garcia-Honduvilla N, Pascual G, Bujan J. Partially absorbable meshes for hernia repair offer advantages over nonabsorbable meshes. Am J Surg 2007;194(1):68-74.

27. Klinge U, Junge K, Stumpf M, Ap AP, Klosterhalfen B. Functional and morphological evaluation of a low-weight, monofilament polypropylene mesh for hernia repair. J Biomed Mater Res 2002;63(2):129-36.

28. Klinge U, Klosterhalfen B, Muller M, Anurov M, Ottinger A, Schumpelick V. Influence of polyglactin-coating on functional and morphological parameters of polypropylene-mesh modifications for abdominal wall repair. Biomaterials 1999;20(7):613-23.

29. Rosch R, Junge K, Quester R, Klinge U, Klosterhalfen B, Schumpelick V. Vypro II mesh in hernia repair: impact of polyglactin on long-term incorporation in rats. Eur Surg Res 2003;35(5):445-50.

30. Schumpelick V, Klinge U. Prosthetic implants for hernia repair. Br J Surg 2003;90(12):1457-8.

31. Klosterhalfen B, Junge K, Klinge U. The lightweight and large porous mesh concept for hernia repair. Expert Rev Med Devices 2005;2(1):103-17.

32. Doctor H. Evaluation of various prosthetic materials and newer meshes for hernia repairs. J Min Access Surg 2006;2(3):110-16.

33. Junge K, Klinge U, Klosterhalfen B, Rosch R, Stumpf M, Schumpelick V. Review of wound healing with reference to an unrepairable abdominal hernia. Eur J Surg 2002;168(2):67-73.

34. Schumpelick V, Klinge U, Rosch R, Junge K. Light weight meshes in incisional hernia repair. J Min Access Surg 2006;2(3):pNA.

35. Klinge U, Marcel B, Rosch R, Peter M. Hernia recurrence as a problem of biology and collagen. J Min Access Surg 2006;2(3):151-54.

36. Brown RA, Prajapati R, McGrouther DA, Yannas IV, Eastwood M. Tensional homeostasis in dermal fibroblasts: mechanical responses to mechanical loading in three-dimensional substrates. J Cell Physiol 1998;175(3):323-32.

37. Eastwood M, McGrouther DA, Brown RA. Fibroblast responses to mechanical forces. Proc Inst Mech Eng [H] 1998;212(2):85-92.

38. Chicurel ME, Chen CS, Ingber DE. Cellular control lies in the balance of forces. Curr Opin Cell Biol 1998;10(2):232-9.

39. Nabeshima Y, Grood ES, Sakurai A, Herman JH. Uniaxial tension inhibits tendon collagen degradation by collagenase *in vitro*. J Orthop Res 1996;14(1):123-30.

40. Lavagnino M, Arnoczky SP. *In vitro* alterations in cytoskeletal tensional homeostasis control gene expression in tendon cells. J Orthop Res 2005;23(5):1211-8.

41. Grinnell F, Zhu M, Carlson MA, Abrams JM. Release of mechanical tension triggers apoptosis of human fibroblasts in a model of regressing granulation tissue. Exp Cell Res 1999;248(2):608-19.

42. Eckes B, Zweers MC, Zhang ZG, Hallinger R, Mauch C, Aumailley M, Krieg T. Mechanical tension and integrin alpha 2 beta 1 regulate fibroblast functions. J Investig Dermatol Symp Proc 2006;11(1):66-72.

43. Schippers E. Central mesh rupture - myth or real concern? In: Schumpelick V, Fitzgibbons RJ, editors. Recurrent Hernia. Berlin, Germany: Springer-Verlag; 2007.

44. Langer C, Neufang T, Kley C, Liersch T, Becker H. Central mesh recurrence after incisional hernia repair with Marlex--are the meshes strong enough? Hernia 2001;5(3):164-7.

45. Agarwal BB, Agarwal KA, Mahajan KC. Prospective double-blind randomized controlled study comparing heavy- and lightweight polypropylene mesh in totally extraperitoneal repair of inguinal hernia: early results. Surg Endosc 2009;23(2):242-7.

46. Bellon JM, Rodriguez M, Garcia-Honduvilla N, Gomez-Gil V, Pascual G, Bujan J. Comparing the behavior of different polypropylene meshes (heavy and lightweight) in an experimental model of ventral hernia repair. J Biomed Mater Res B Appl Biomater 2009;89B(2):448-55.

47. Pascual G, Rodriguez M, Gomez-Gil V, Garcia-Honduvilla N, Bujan J, Bellon JM. Early tissue incorporation and collagen deposition in lightweight polypropylene meshes: bioassay in an experimental model of ventral hernia. Surgery 2008;144(3):427-35.

48. Klosterhalfen B, Junge K, Hermanns B, Klinge U. Influence of implantation interval on the long-term biocompatibility of surgical mesh. Br J Surg 2002;89(8):1043-8.

49. Junge K, Klinge U, Rosch R, Klosterhalfen B, Schumpelick V. Functional and morphologic properties of a modified mesh for inguinal hernia repair. World J Surg 2002;26(12):1472-80.

50. Anurov MV, Titkova SM, Shchegoleva NN, Mikhaleva LM, Tsitovich IG, Galushkina NV, Oettinger AP. Experimental study of the impact of the textile structure of mesh endoprostheses for the efficiency of reconstruction of the anterior abdominal wall. Bull Exp Biol Med 2008;145(5):642-6.

51. Klinge U, Klosterhalfen B, Birkenhauer V, Junge K, Conze J, Schumpelick V. Impact of polymer pore size on the interface scar formation in a rat model. J Surg Res 2002;103(2):208-14.

52. Cobb WS, Burns JM, Peindl RD, Carbonell AM, Matthews BD, Kercher KW, Heniford BT. Textile analysis of heavy weight, mid-weight, and light weight polypropylene mesh in a porcine ventral hernia model. J Surg Res 2006;136(1):1-7.

53. Galko MJ, Krasnow MA. Cellular and genetic analysis of wound healing in Drosophila larvae. PLoS Biol 2004;2(8):E239.

54. Franz MG, Steed DL, Robson MC. Optimizing healing of the acute wound by minimizing complications. Curr Probl Surg 2007;44(11):691-763.

55. DuBay DA, Wang X, Adamson B, Kuzon WM, Jr., Dennis RG, Franz MG. Mesh incisional herniorrhaphy increases abdominal wall elastic properties: a mechanism for decreased hernia recurrences in comparison with suture repair. Surgery 2006;140(1):14-24.

56. Dubay DA, Wang X, Kirk S, Adamson B, Robson MC, Franz MG. Fascial fibroblast kinetic activity is increased during abdominal wall repair compared to dermal fibroblasts. Wound Repair Regen 2004;12(5):539-45.

57. Pollock AV, Evans M. Early prediction of late incisional hernias. Br J Surg 1989;76(9):953-4.

58. Burger JW, Lange JF, Halm JA, Kleinrensink GJ, Jeekel H. Incisional hernia: early complication of abdominal surgery. World J Surg 2005;29(12):1608-13.

59. Tomasek JJ, McRae J, Owens GK, Haaksma CJ. Regulation of alpha-smooth muscle actin expression in granulation tissue myofibroblasts is dependent on the intronic CArG element and the transforming growth factor-beta1 control element. Am J Pathol 2005;166(5):1343-51.

60. Pedersen JA, Swartz MA. Mechanobiology in the third dimension. Ann Biomed Eng 2005;33(11):1469-90.

61. Hinz B, Phan SH, Thannickal VJ, Galli A, Bochaton-Piallat ML, Gabbiani G. The myofibroblast: one function, multiple origins. Am J Pathol 2007;170(6):1807-16.

62. Hinz B. The myofibroblast: Paradigm for a mechanically active cell. J Biomech 2010;43(1):146-55.

63. Aarabi S, Bhatt KA, Shi Y, Paterno J, Chang EI, Loh SA, Holmes JW, Longaker MT, Yee H, Gurtner GC. Mechanical load initiates hypertrophic scar formation through decreased cellular apoptosis. FASEB J 2007;21(12):3250-61.

64. Hinz B, Mastrangelo D, Iselin CE, Chaponnier C, Gabbiani G. Mechanical tension controls granulation tissue contractile activity and myofibroblast differentiation. Am J Pathol 2001;159(3):1009-20.

65. Garcia-Urena MA, Vega Ruiz V, Diaz Godoy A, Baez Perea JM, Marin Gomez LM, Carnero Hernandez FJ, Velasco Garcia MA. Differences in polypropylene shrinkage depending on mesh position in an experimental study. Am J Surg 2007;193(4):538-42.

66. Gonzalez R, Fugate K, McClusky D, 3rd, Ritter EM, Lederman A, Dillehay D, Smith CD, Ramshaw BJ. Relationship between tissue ingrowth and mesh contraction. World J Surg 2005;29(8):1038-43.

67. Amid PK. Classification of biomaterials and their related complications in abdominal wall hernia surgery. Hernia 1997;1:15-21.

68. Scheidbach H, Tamme C, Tannapfel A, Lippert H, Kockerling F. *In vivo* studies comparing the biocompatibility of various polypropylene meshes and their handling properties during endoscopic total extraperitoneal (TEP) patchplasty: an experimental study in pigs. Surg Endosc 2004;18(2):211-20.

69. Klinge U, Klosterhalfen B, Conze J, Limberg W, Obolenski B, Ottinger AP, Schumpelick V. Modified mesh for hernia repair that is adapted to the physiology of the abdominal wall. Eur J Surg 1998;164(12):951-60.

70. Junge K, Klinge U, Prescher A, Giboni P, Niewiera M, Schumpelick V. Elasticity of the anterior abdominal wall and impact for reparation of incisional hernias using mesh implants. Hernia 2001;5(3):113-8.

71. Klosterhalfen B, Hermanns B, Rosch R, Junge K. Biological response to mesh. Eur Surg 2003;35:16-20.

72. Salacinski HJ, Goldner S, Giudiceandrea A, Hamilton G, Seifalian AM, Edwards A, Carson RJ. The mechanical behavior of vascular grafts: a review. J Biomater Appl 2001;15(3):241-78.

73. Karamuk E, Mayer J, Raeber G. Tissue engineered composite of a woven fabric scaffold with tendon cells, response on mechanical simulation *in vitro*. Comp Sci Tech 2004;64:885-91.

74. Velayudhan S, Martin D, Cooper-White J. Evaluation of dynamic creep properties of surgical mesh prostheses--uniaxial fatigue. J Biomed Mater Res B Appl Biomater 2009;91(1):287-96.

CHAPTER THREE

EFFECT OF CHEMICAL COMPOSITION AND THERMAL TREATMENT ON THE PROPERTIES OF MULTIFILAMENT YARNS MADE OF SEGMENTED HIGH-GLYCOLIDE COPOLYESTERS

Introduction

Lactones, primarily glycolide, lactide, and ε-caprolactone, and the cyclic carbonate, trimethylenecarbonate (TMC), represent a class of materials which are commercially copolymerized and of significant interest for biomedical applications. As a group of synthetic polymers which are degradable, bioabsorbable, and non-toxic, their use as medical devices in the form of yarns to construct sutures and surgical meshes has grown substantially over the past four decades. Due to their similar ring-opening reaction mechanism from cyclic monomers, they are often produced as copolymers to achieve application specific requirements using their diverse properties. In the synthesis process, the choice of monomer and the relative distribution of monomeric sequence, influences the properties of the resultant copolymer. Due to differences in the surrounding chemical environment of the labile ester -linkage, the rate of degradation for each monomer is variable. Since these copolymers are designed -to -degrade, the variables which control their *in vivo* degradation profile, which is often first simulated *in vitro*, are of special interest. Simply stated, the rate of hydrolysis is modulated, within limitations, and balanced against mechanical property requirements using the interdependent variables of chemical composition, structural arrangement, and molecular morphology. Chemical composition and monomer sequencing are established during the synthesis process while

molecular morphology is subsequently developed via thermomechanical treatment during processing. Of these variables, the choice of monomers is most influential in determining absorbable copolymer properties.

Polyglycolide (PG) is the simplest linear aliphatic polyester. PG is a fast-degrading polymer with substantial loss in mechanical properties within 1 month and complete mass loss within 6-12 months.[1] PG is highly crystalline[2] (46-52%) with a relatively high crystallization rate compared to other bioabsorbable polyesters, primarily due to its simple, stereoregular structure that forms crystals in a planar zig-zag conformation.[3] As such, it exhibits good mechanical properties and has excellent fiber forming ability. The glass transition temperature (T_g) of PG is typically in the range of 35-40ºC, as determined by differential scanning calorimetry (DSC).

PG is often synthesized as the major component in a copolymer, using a more hydrolytically stable monomer to temporally extend its function. Additionally, the interjection of a different monomer changes the regular, repeat sequencing of monomer units which results in a slightly lower, and/or less perfect, crystallite structure. The random copolymer of 90/10 poly(glycolide-co-lactide) (polyglactin 910) is commonly used in biomedical products. In the form of a multifilament yarn, the strength retention of polyglactin 910 has been determined to be slightly longer and absorption sooner than that of PG.[4] The slightly longer strength retention is the result of the more hydrophobic nature and lower hydrolysis rate of lactide. The increased absorption rate has been suggested to be the result of differences in morphology (lower amount of and/or less perfect crystallite structure) since amorphous domains are preferentially degraded.[5]

Consequently, polyglactin 910 degradation products are generated more quickly and are less crystalline which may increase local phagocytosis.[6] Segmented high-glycolide copolymers are also used to produce compliant, slower-degrading monofilament sutures.[7] In this case, copolymers consist of a slow-degrading 'soft' amorphous middle segment which is end grafted with a 'hard', crystalline PG. Compliance is derived from the core, while the stiff, crystalline end segments impart strength. These materials have shown to retain strength longer, degrade less rapidly, and induce less tissue reaction compared to a PG homopolymer.[8]

Poly(L-lactide) (PLL) is semi-crystalline, linear aliphatic polyester which differs distinctly from PG by the addition of a pendant methyl group. The chemical structure of PLL is such that an asymmetric carbon atom in the chain backbone can produce two atoms with the same elements and bonding pattern but with different spatial arrangement. The result is two optically active stereoisomeric forms, D(-) and L(+). However, in acid form the L(+) isomer is the physiologically natural configuration.[2] As a homopolymer, the time required for substantial degradation of PLL is greater than 24 months.[9] The significantly longer degradation time for PLL, compared to PG, can be attributed to the pendant methyl group which shields the labile ester group in two ways.[10] First, steric hindrance inhibits the physical access of water molecules to the ester group. Second, the voluminous, hydrophobic methyl group limits the diffusion of water into the polymer due to its relatively high T_g. Compared to PG, the added methyl group increases the T_g of PLL to 60-65ºC, significantly above physiologic temperature.[11]

In fiber form, ε-caprolactone and TMC are almost exclusively used as toughening, softening, and/or as slower hydrolyzing copolymers in high modulus polymers such as glycolide or lactide. Polymeric TMC (pTMC) is a tacky, amorphous, thermoplastic elastomer which has not found application as a structural biomaterial due to its poor dimensional stability and low mechanical performance.[1,2] As a high molecular weight homopolymer, pTMC possesses a T_g of -18ºC and can be crystallized only by strain induction, which results in a low melt temperature (T_m) of 36°C.[12] However, used as a segment within a copolymer, the extremely tough and compliant pTMC imparts flexibility to the device. For example, this technique has been used for suture materials.[8] Other investigated biomaterial applications of pTMC copolymers include drug delivery.[13,14] Polycaprolactone (PCL) is a semicrystalline, low-melting (T_m = 65-70°C), linear aliphatic polyester with a Tg of -60ºC. Unlike pTMC, as a homopolymer, PCL exhibits a semi-crystalline morphology. However, its slow degradation rate and moderate mechanical properties have limited its application for use in medical devices. Like TMC, ε-caprolactone has found a more significant role as a modifier in absorbable copolymers.[15]

There are five primary factors which can be considered as controlling the bulk degradation rate of absorbable polymers. They are chemical bond stability (e.g. esters, anhydrides, carbonates), hydrophobicity, steric effects (e.g. T_g, chain interlocking and entanglement), local pH or autocatalytic effects, and morphology (e.g. crystallinity, porosity). In addition, external conditions such as temperature and load[16] are important factors but, for biomedical applications, *in vitro* evaluation is conducted at physiologic

temperature and load is not typically a studied variable. For the investigated copolymers in this study, each monomer is a linear, aliphatic polyester, i.e. the cleaved bonds in the backbone of the chain are the same. Furthermore, autocatalytic effects are considered minimal for fibers, as they have a high surface to volume ratio, resulting in high diffusion rates and thus significant clearing of generated acidic byproducts. Therefore, of pertinent consideration are changes in chemistry, which result in hydrophobic and steric effects, and post processing differences, which modify morphology.

The morphology of absorbable copolymers has significant influence on their end-use performance. The fiber formation process of PG produces a two-phase system consisting of crystalline and amorphous regions along the fiber axis, with semi-oriented amorphous regions running in parallel.[17] It is well established that degradation commences in the amorphous domains.[18] As summarized by Fu and coworkers,[19] bulk degradation by hydrolysis is governed by two major stages. First, water molecules diffuse into the amorphous regions and hydrolysis results in chain scission. Primary crystalline segments, however, are largely protected due to their tightly packed, ordered structure which inhibits water penetration. The substantial degradation of the amorphous regions marks the loss of mechanical properties and initiation of the second stage of degradation. During the second stage, water molecules more slowly cleave accessible ester groups, eventually resulting in soluble fragments which are metabolized. Of specific interest to this investigation are the mechanisms of the first stage. As such, factors which affect the accessibility of water to the amorphous domains are fundamental to controlling degradation rate and the temporal preservation of mechanical properties.

The size, number, location, and perfection of polymer crystallites are governed by annealing temperature and time. In general, an increased degree of crystallinity prolongs degradation time; however, crystallite structure can heavily influence the initial and *in vivo* retention of mechanical properties for semicrystalline, absorbable copolymers. The isothermal annealing process, or heat setting, takes place as a result of a thermodynamic balance governed by enthalpic and entropic competing events. At low temperatures, molecular mobility is not adequate to allow crystallite formation, while at elevated temperatures high levels of kinetic energy prevent secondary bond formation. Measureable crystallization rates are generally accepted to occur between (T_m - 10°C) and (T_g + 30°K), a range in which the kinetic energy of the polymer chains is conducive to crystallite formation.[20] Within an optimal range, molecular mobility facilitates crystallite formation to an already formed nucleus and the resultant crystallite size is governed by the rate of chain addition and the provided time interval.[21] Consequently, the temperature and time of isothermal annealing is critically influential to the performance of absorbable yarn constructs, as is the characterization of the resultant morphology.

The primary objective of fiber annealing is to modify molecular morphology through the rearrangement of secondary bonds. As such, it is vital to quantify changes to the first-order (e.g. melting and crystallization) and second-order (e.g. relaxation events such as T_g) transitions. The analytical techniques of DSC and dynamic mechanical analysis (DMA) are complementary in their ability to identify and characterize the morphology of semicrystalline fibers. DSC is particularly proficient at quantifying latent

heat changes during first-order transitions. DMA is well suited to quantify second-order transitions which are difficult, or even impossible to characterize by DSC. It has been reported that DMA is 1000 times more sensitive than DSC at detecting glass transition temperature.[22,23] DMA measures the viscoelastic properties of storage modulus (E') and loss modulus (E'') as a function of temperature and frequency. The E' is reflective of the stiffness of the material while the E'' is a measure of damping or the ability of the material to absorb energy. Tan δ is a dependent, calculated value (E"/E') and is of significant importance. From an application perspective, tan δ is an indicator of how well a material loses energy to molecular rearrangement and internal friction (energy lost as heat) or stores elastic energy in bond stretching and rotation. For semicrystalline copolymers the amorphous and crystalline domains are intimately joined, which affects the T_g relaxation event. Typically, any increase in crystallinity results in a broadening of the tan δ curve and a shift toward higher temperatures. The maximum of the tan δ curve is used historically in literature as the T_g of the polymer. Additionally, the E'' curve also obtains a maximum during the Tg event. Consequently, E'' is an independent measure of damping and occurs at a lower temperature than the tan δ peak.

Uncontrolled free shrinkage due to heat prior to use, or *in vivo*, is undesirable for biomedical devices. The dimensional stability of fibrous constructs is of particular concern due to their natural tendency to relax. Therefore, the annealing process is a key step in conferring dimensional stability of the amorphous region through the formation and reorganization of crystallites which act as pseudo crosslinks. However, during annealing it is not desirable to lose the orientation imparted during the fiber formation

process, which gives the yarn its mechanical properties. As a result, annealing is often conducted under tension to restrict molecular relaxation. Furthermore, for absorbable polymers the temporal *in vivo* breaking strength retention is significantly affected by tension during the annealing process. Browning and Chu found that PG sutures annealed with any level of axial tension always exhibited a lower rate of hydrolytic degradation than did freely hung samples.[24,25] The authors attributed the difference to tie-chain molecules acquiring less constrained conformations, resulting in a loss of the orientation established during drawing. Consequently, logic suggests that the relaxed morphology would contain more free volume for water diffusion.

A key objective of the study described in this chapter was the development and optimization of a segmented high-glycolide copolymer yarn for use in the construction of a bicomponent mesh for hernia repair. As a medical device, the degradation profile and resultant strength loss with time are of significant interest to investigators. Functionally, the high-glycolide copolymer must provide strength retention for greater than 14 days, and optimally between 18-24 days, to facilitate the temporal modulation of the mesh properties. This temporal alteration marks the transfer from providing a structurally stiff and stable mesh during the inflammation and proliferation stages to a gradual transition of external loading to the developing extracellular matrix. To this end, two copolymers were polymerized with subsequent yarn formation and isothermal annealing. Chemical modification between the two copolymers and different annealing conditions were investigated to optimize the initial maximum breaking force, temporal *in vitro*

conditioned maximum tensile force profile, and yarn stabilization against dimensional changes.

Materials and Methods

Polymer Synthesis and Characterization

Polymer Synthesis

MG-9 and MG-17 were synthesized as polyaxial, segmented, high-glycolide copolymers. To determine the effect of polymer chemistry, two significant modifications were made to the MG-17 copolymer compared to MG-9. First, the molecular weight of the pTMC polymeric initiator was increased. Second, lactide was replaced by ε-caprolactone as a comonomer. A two-step, solid state, ring-opening polymerization was used to produce both systems. The first step produced a trimethylolpropane-initiated, trimethylene carbonate (TMC) segment. Next, the TMC polymeric initiator was end-grafted using a molar ratio of 95/5 glycolide/caprolactone (G/CL) and 95/5 glycolide/L-lactide (G/L) for MG-9 and MG-17, respectively. The weight ratio of the polymer initiator to the end-graft was 2/98 in both cases. A more detailed discussion of the polymerization process is described in U.S. Patent No. 7,129,319 (2006).

Both polymers were isolated, ground (Thomas Wiley mill), and dried and purified (Buchi, Rotovapor) using reduced pressure (< 1.5 torr) to remove traces of unreacted monomer.

Determination of Molecular Weight

Solution viscosity according to ASTM D2857-95(2007) *Standard Practice for Dilute Solution Viscosity of Polymers* was used to characterize the molecular weight using a viscometer (Cannon-Fenske) in a mobile phase of hexafluoroisopropylene (HFIP; Sigma-Aldrich, 99.8% grade) for MG-9 and MG-17 by measuring inherent viscosity at the standard solution concentration of 0.1 g/dL.

Determination of Thermal Characteristics

A differential scanning calorimeter analyzer (DSC; Perkin Elmer, Pyris 6) was used to evaluate each polymer's melt temperature (T_m) and degree of crystallinity characterized in terms of heat of fusion (ΔH_m). A sample weighing between 5-10 mg was heated from room temperature to 240°C at a rate of 10°C/min. Dry nitrogen was used as a purge gas to eliminate influences due to oxidation.

Yarn Preparation and Properties

Melt Extrusion of Multifilament Yarn

Melt-extruded yarn of MG-9 and MG-17 was processed using similar extrusion and in-line drawing conditions. Each copolymer was processed using a 3/4″ diameter screw extruder equipped with a metering gear pump and a 10-hole die. The processing conditions of extruder output, spin head draw-ratio, and in-line orientation were similar between the MG-9 and MG-17 extrusions which resulted in nearly identically yarn

denier. In-line orientation was completed using a series of heated Godets at temperatures between 25ºC and 90ºC.

Yarn Physical Testing

Yarn denier, a unit measure of weight for the size of a bundle of filaments (g/9000 m), was measured on both yarns by weighing (Mettler-Toledo, MS analytical balance) 50 m of yarn and scaling this quantity to the equivalent of 9000 m.

Yarn Stabilization by Annealing

Annealing, or heat setting, was completed by wrapping yarn around an expandable rack which had two parallel bars of stainless steel. Yarn was wrapped in a continuous fashion, secured, and a strain of 0.02 was applied by expanding the rack prior to annealing. The annealing time periods of 30, 60, and 180 minutes were used to condition yarn at the temperatures of 100ºC, 120ºC, and 140ºC while under a high vacuum (< 1.5 torr). To improve the handling of the yarn during subsequent testing, the yarn was plied (2x) together prior to annealing.

To simplify the description of different yarn annealing conditions the following coding was used. The first letter of the yarn designation is either "C" for MG-9 or "L" for MG-17. Next the annealing temperature is described by A, B, or C for 100°C, 120°C, or 140°C, respectively. Finally, the time associated with the annealing step, either 30, 60, or 180 minutes is determined by subsequent identification as 3, 6, or 18. For example, LB18 is MG-17 yarn annealed at 120°C for 180 minutes.

Yarn Tensile Mechanical Properties

A universal testing machine (MTS, Synergie 200) equipped with a 500 N load cell and a set of fiber testing grips were used to measure tensile mechanical properties for each yarn. Measurements were made according to ASTM D2256-09 *Standard Test Method for Tensile Properties of Yarns by the Single-Strand Method* using a gauge length of 70 mm and cross-head speed of 2.33 mm/s. The maximum tensile force (MTF) and elongation at that maximum force were obtained from each stress-strain curve.

Yarn Shrinkage Measurement

Percent shrinkage and shrinkage onset temperature measurements were conducted on annealed yarn using a dynamic mechanical analyzer (DMA; Perkin Elmer Pyris Diamond DMA) operated in a thermomechanical analysis (TMA) mode. Using an 8-ply yarn (8 ends of yarn total of 10-filaments each), samples were analyzed in a nitrogen atmosphere using a tensile mode, 3°C/min heating rate, and a temperature sweep from room temperature to 130°C. The onset temperature and percent yarn shrinkage at 80ºC and 120ºC were determined using a constant force of 3 mN.

Yarn Thermomechanical Properties

A DMA (Perkin Elmer Pyris Diamond DMA) equipped with a liquid nitrogen cooler was used to determine the viscoelastic properties of loss modulus (E’’), storage modulus (E’), and tan delta (tan δ) as a function of temperature for each yarn type, and for each time and temperature annealing condition. A temperature sweep was conducted

in a nitrogen atmosphere at a heating rate of 2ºC/min from -20ºC to 200ºC. A minimum 200 mN force was applied to yarn samples which were strained with a 10 micron cyclic amplitude in a tensile mode. Reported values for the T_g were taken at the peak of the tan δ curve for the frequency of 1 Hz. Tan δ onset temperatures were determined at the temperature where the baseline increased to produce a 0.02 shift.

Additionally, the frequency dependent T_g values for each annealing condition were used to calculate the apparent activation energy (E_a) using the Arrhenius method. The multiplexed frequencies of 1, 5, 10, and 20 Hz were used to determine the frequency dependent Tg value for each yarn sample using the same conditions described previously. The Arrhenius equation was used in the following form:

$$\mathbf{F = Ae^{-\frac{E_a}{RT}}} \quad \rightarrow \quad \mathbf{ln}(F) = \mathbf{ln}(A) - \frac{E_a}{RT}$$

where F is frequency, A is the pre-exponential factor, E_a is the activation energy, R is the gas constant (8.314 J/K mol), and T is the temperature in degrees Kelvin. As such, the natural log of frequency plotted against the reciprocal of the corresponding T_g results in a line which has a slope equal to the negative of the activation energy divided by the gas constant. The correlation coefficient for each annealing condition was determined to measure the strength of a linear relationship between the independent (1/RT) and dependent (ln(F)) variables.

In Vitro Conditioned Degradation

Samples evaluated for mechanical tensile testing following *in vitro* degradation were conditioned using a 0.1 M solution of buffered sodium phosphate in 50 mL tubes

(Simport, C571-2) at a 7.2pH. Buffered sodium phosphate was prepared by adding 23.3 grams of dibasic (K_2HPO_4; Sigma-Aldrich, ACS ≥ 98%) potassium phosphate and 9.0 grams of monobasic (KH_2PO_4; Sigma-Aldrich, ACS ≥ 98%) potassium phosphate into 2 liters of deionized water and stirred until dissolution. A pH meter (Symphony, SB80PI) was used to verify a 7.2pH measurement and slight adjustments were made to using 0.5 N hydrochloric acid (HCl; Sigma-Aldrich, ACS reagent). Tubes containing a 400 mm long piece of yarn were placed in racks and incubated (Innova 4300) in the prepared buffer at 37°C under constant orbital-agitation at a speed of 28 revolutions per minute. Samples were removed at the predetermined time periods of 7, 10, 14, and 21 days for mechanical tensile testing.

Statistical Analysis

Significant differences in physical properties between the two yarn types were completed using an independent, two-tailed Student's t-test to compare means. Two-factor analysis of variance (ANOVA) was used to test for effects due to annealing conditions and yarn type, as well as their interaction, for the mechanical property response variables of MTF and elongation at maximum force. All analysis was completed using statistical analysis software (SAS, version 9.2) and p-values < 0.05 were considered to be statistically significant.

Results

Polymer Synthesis and Characterization

Polymerization conditions and analytical data are summarized in Table 3.1. Analytically, the results of the changes made to the MG-17 copolymer were evidenced in each DSC thermogram, i.e. the peak of the melting endotherm (T_m) and the heat of fusion. MG-17 had a lower melt temperature than MG-9 by approximately 8°C and lower degree of crystallinity, with a corresponding drop in ΔH_m of 6 J/g.

Near complete conversion of monomer was realized, as evidenced by the high molecular weights (η_{lhv}) and melt temperatures (T_m) typical of high-glycolide copolymers.[26] Copolymers of equivalent molecular weight, as determined by inherent viscosity, were polymerized for this study.

Table 3.1

Polymerization Scheme and Analytical Data for MG-9 and MG-17

Description		MG-9	MG-17
Polymeric Macroinitiator	Monomers, type[a]	TMC	TMC
	Initiator, type	Trimethylolpropane	Trimethylolpropane
	Analytical Data: GPC: Mn, Mw (kDa)	> 2, > 6	> 6, > 20
Crystalline Copolyester	Polymeric Macroinitiator/Monomer Ratio (weight)	2/98	8/92
	Monomers, type[a] (molar)	95/5 G/CL	95/5 G/L
	Analytical Data:		
	η_{lhv}: (dL/g)[b]	1.0	1.0
	DSC: T_m (°C)	223	215
	ΔH_m (J/g)	94	88

a, CL = ε-caprolactone, TMC = trimethylene carbonate, G = glycolide, L = l-lactide; b, HFIP mobile phase

The denier for the two copolymer yarns, MG-9 and MG-17, were identical. However, the MTF was greater and elongation at that maximum force was lower for the MG-17 yarn (Table 3.2).

Table 3.2

Physical and Initial Mechanical Properties of MG-9 and MG-17 Yarn

Description	**MG-9**	**MG-17**
Filament count	10	10
Denier (g/9000m)	142 ± 2	144 ± 2
Maximum tensile force (N)	11.7 ± 0.4†	14.8 ± 0.5†
Elongation at maximum force (%)	70 ± 13‡	47 ± 4‡

† ‡ Indicates significant differences in physical or mechanical properties between yarn types ($p < .05$)

Table 3.3 lists the thermal and initial mechanical properties of melt-extruded and annealed yarn. It should be noted that no cold crystallization exotherms were observed in any of the first heat thermograms indicating a high level of initial crystallinity. There was an increase in the heat of fusion measurements for both annealed yarn types. Yarn crystallinity for both yarn types increased as a result of all annealing conditions, except for MG-9 samples annealed at 140ºC which had minimal change. Annealing of the MG-9 yarn had no observable effect on melt temperature; however, the melting temperature of the MG-17 yarn increased by 3-4ºC which was independent of annealing condition.

Table 3.3

Initial Thermal and Mechanical Properties "As Extruded" and Annealed MG-9 and MG-17 Yarn

Sample ID	Melt Temperature (°C)	Heat of Fusion (J/g)	Maximum Tensile Force (N)	Elongation at Maximum Force (%)
MG-9	216	70	11.7 ± 0.4 †	70 ± 13 †
MG-17	203	60	14.8 ± 0.6 ‡	47 ± 4 ‡
CA3	216	78	12.9 ± 0.3 †	53 ± 3 †
CA6	217	81	12.6 ± 0.4 †	49 ± 4 † *
CA18	216	83	12.8 ± 0.3 †	51 ± 7 † *
CB3	217	74	13.5 ± 0.2 †	59 ± 4 †◊
CB6	217	75	13.5 ± 0.3 †	53 ± 7 †
CB18	216	75	13.2 ± 0.1 †	49 ± 1 †◊
CC3	216	68	12.7 ± 0.5 †◊	49 ± 3 †◊
CC6	216	71	11.9 ± 0.6 ◊¤	42 ± 4 †◊¤
CC18	216	72	8.7 ± 0.7 †◊¤	31 ± 6 †◊¤*
LA3	206	67	15.5 ± 0.6	43 ± 5
LA6	207	65	15.2 ± 0.7	44 ± 3 *
LA18	206	64	15.8 ± 1.0 ‡	44 ± 2 *
LB3	206	66	17.1 ± 0.6 ‡◊	41 ± 4
LB6	207	65	15.2 ± 0.6 ◊	35 ± 5 ‡
LB18	207	66	14.6 ± 1.1 ◊	35 ± 10 ‡
LC3	206	66	14.3 ± 1.2	33 ± 11 ‡
LC6	206	65	13.7 ± 1.2 ‡◊	33 ± 6 ‡
LC18	207	65	14.6 ± 0.2 ◊	34 ± 4 ‡ *

†‡ Indicates a significant difference between the 'as extruded' and annealed sample for each yarn type ($p < .05$)
◊ ¤Indicates a significant differences between different annealing times for a given annealing temperature ($p < .05$)
*Indicates no significant difference found between yarn types for the same annealing condition ($p < .05$)

The mechanical behavior of yarn is highly dependent on morphology changes during annealing. The primary observation from the data in Table 3.3 is that annealing generally decreased elongation and increased the MTF compared to the 'as extruded' yarn value. Each MG-9 yarn sample annealed at the temperatures of 100°C and 120°C showed a significant increase in MTF and decrease in elongation. At these temperatures, minimal effect due to time was observed. However, when the annealing temperature was

increased to 140ºC the effect of each step increase in time produced a reduction in MTF and elongation. For the extreme condition of sample CC18, MG-9 yarn produced the lowest MTF and elongation values observed in the study. The MTF for MG-17 was greater than that of MG-9 for the 'as extruded' and for each annealing condition. However, for MG-17 an increase in MTF due to annealing was less pronounced. For example, the LA18 and LB3 were the only samples which had a significant increase in MTF after annealing. Of the two samples, the LB3 sample produced the greatest MTF value in the study ($p < .003$) at 17.1 N.

Figure 3.1 presents DMA curves for each 'as extruded' yarn and a typical response of each yarn type to annealing. Figures 3.2 and 3.3 isolate the tan δ response to depict the effect of annealing time and temperature, respectively. A complete set of DMA results which includes all annealing conditions for both yarn types is tabulated in Table 3.4.

In Figure 3.1 it can be seen that, for both yarn types, the glass transition region encompasses a peak for both the tan δ and E'' curves as well as a significant decrease in E'. Annealing increased the peak position of the tan δ curve (T_g), increased the breadth and reduced the height of the tan δ peak, increased the storage modulus onset temperature, and modified the rubbery plateau (region between T_g and T_m) such that stiffness was increased. Comparing the two yarn types, MG-17 and MG-9, it can be seen that MG-9 has a lower T_g, peak of the E'' curve, and E' reduction onset temperature. It is interesting to note that the storage modulus was greater for the MG-9 yarn during the rubbery plateau.

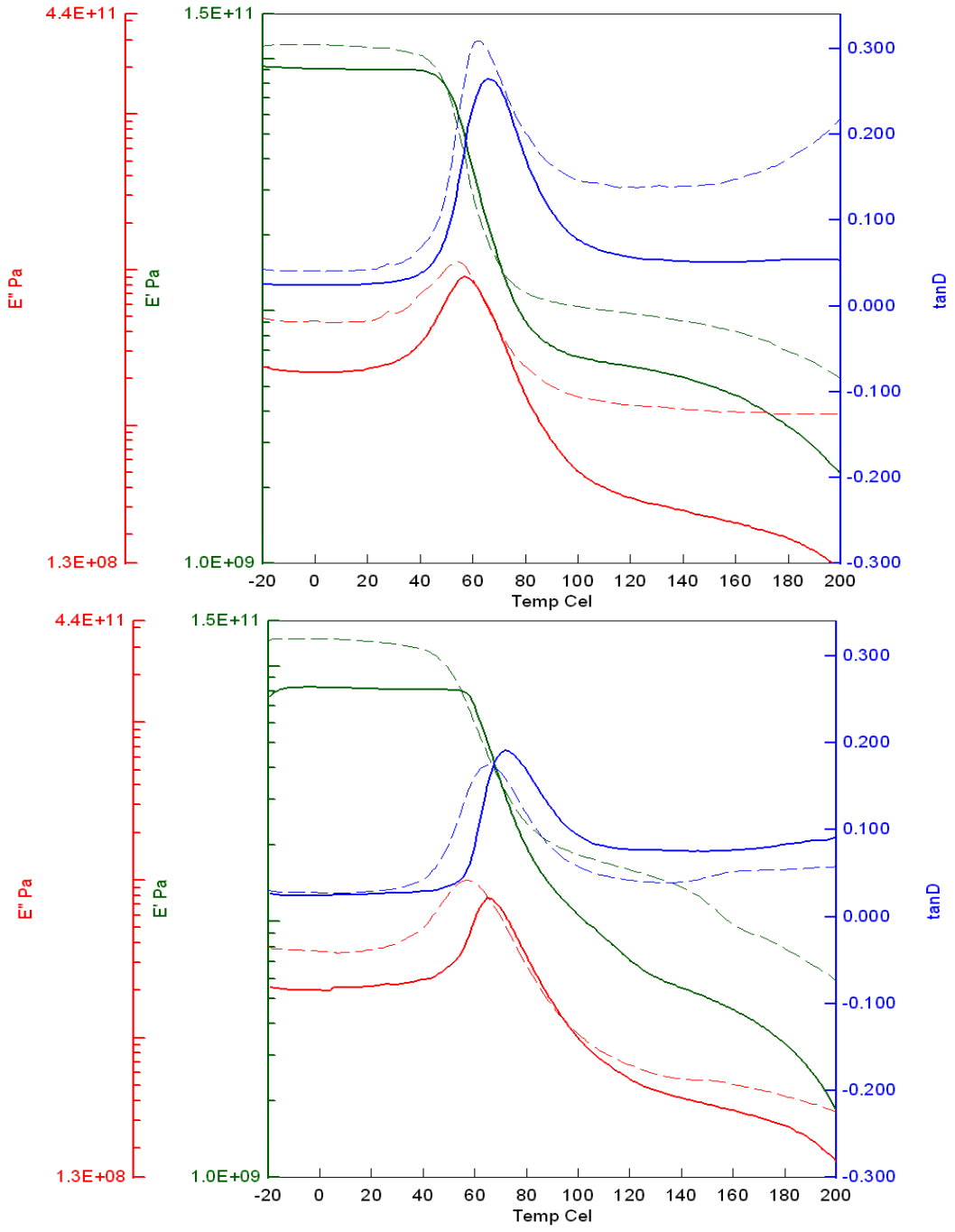

Figure 3.1

The storage modulus (E'), loss modulus (E''), and tan δ response for the "as extruded" (top) and annealed (bottom, 120°C for 60 minutes) MG-9 (dashed) and MG-17 (solid) yarn. Depicted data presented as a comparative typical effect of annealing on the thermomechanical properties.

A direct comparison of the tan δ responses for annealed yarn depicting the effect of annealing time and temperature is displayed in Figures 3.2 and 3.3, respectively. For MG-9 yarn, differences in the tan δ curve between annealing times or temperatures was minimal. However, the height, breadth, and peak position of tan δ for MG-17 yarn was sensitive to changes in annealing conditions with step increases in temperature showing the most significant shifts. Most notable was the tan δ peak shift toward a lower temperature for MG-17 at the temperature of 140°C.

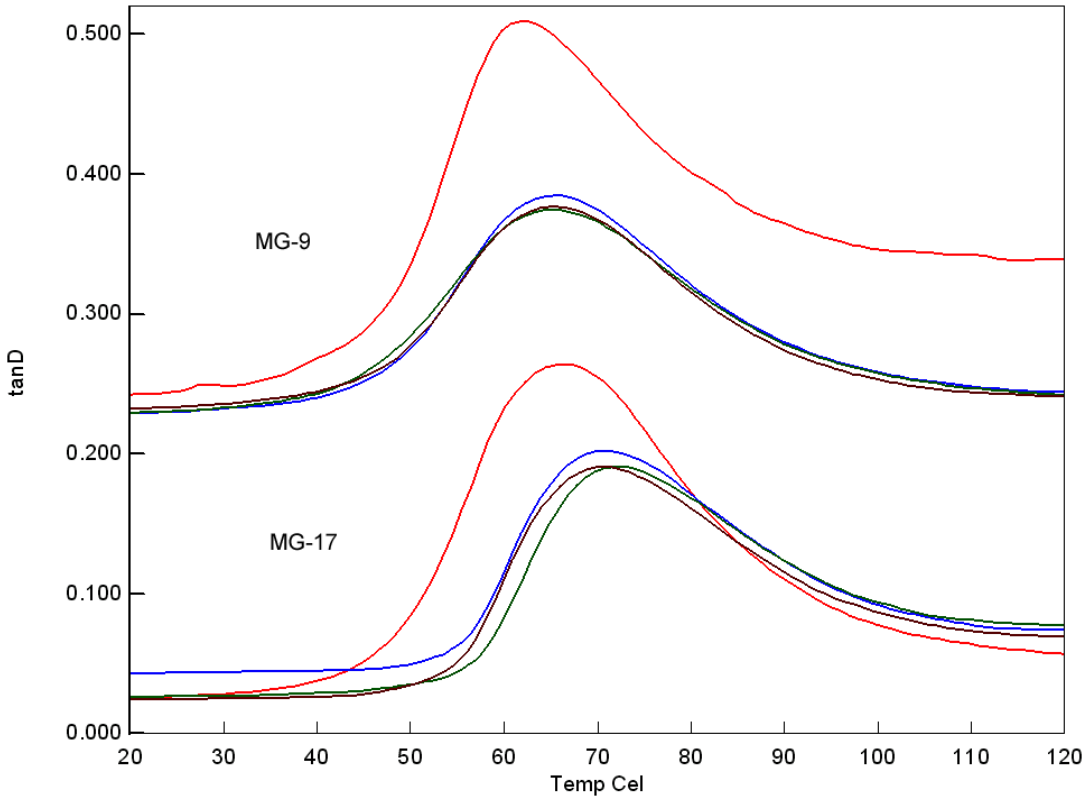

Figure 3.2

The typical tan δ response of annealed MG-9 and MG-17 yarn depicted for the annealing temperature of 120ºC conditioned for the times of 30 (blue), 60 (green), and 180 (maroon) minutes. "As extruded" (red) data has been included for comparison.

Of significant interest is the proximity of the onset or shift in the baseline of the tan δ curve with reference to physiologic temperature (37°C). The onset of the T_g transition for MG-9 is significantly lower than that of MG-17. As such, at 37°C the MG-9 tan δ curve shows changes in the slope of the curve indicating the initiation of molecular mobility and increased free volume. At 37°C, nearly all of the tan δ curves for the depicted MG-17 yarn samples have minimal, or no slope, indicating the relaxation event of T_g has not initiated. Exceptions to this finding for MG-17 yarn include the 'as extruded' and samples annealed at 140°C for 30 minutes.

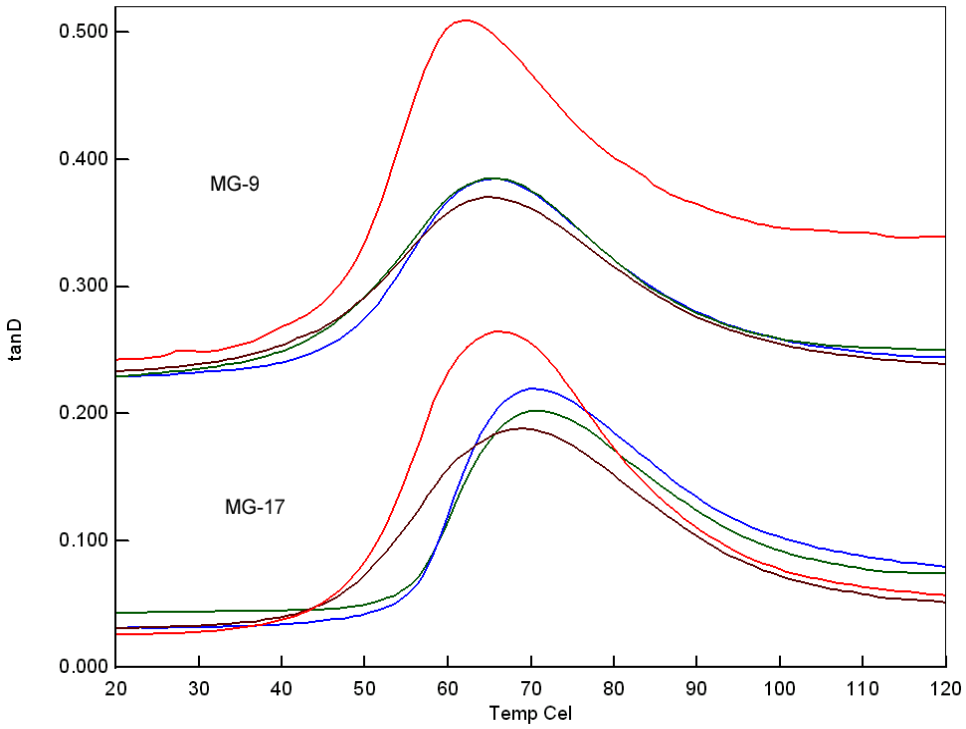

Figure 3.3

The typical tan δ response of annealed MG-9 and MG-17 yarn depicted for the annealing time of 30 minutes conditioned at the temperatures of 100°C (blue), 120°C (green), and 140°C (maroon). "As extruded" (red) data has been included for comparison.

The principal observation from the DMA data presented in Table 3.4 is that in all cases, initial and annealed, the T_g of MG-17 yarn was greater by 4-6°C than that of MG-9 yarn. In addition to changes in peak position of tan δ, changes to the onset temperature of tan δ were dramatic following annealing. The annealing conditions of 100°C for 180 minutes and 120°C for 30 and 60 minutes produced the greatest onset temperatures for both yarn types. But at the same time, MG-17 produced onset values about 16°C greater than that of MG-9. When the annealing temperature was increased from 120°C to 140°C, the tan δ onset temperature initiated earlier for both yarn types. The peak height of tan δ for annealed MG-9 yarn was generally lower than that of MG-17.

Table 3.4

Thermomechanical Properties of "As Extruded" and Annealed MG-9 and MG-17 Yarn Determined by DMA

Sample ID	T_g (°C)	Tan δ half-width (°C)	Onset of Tan δ (°C)	Peak Height of Tan δ	Onset of Storage Modulus (°C)	Peak of Loss Modulus, E'' (°C)
MG-9	62	27	28	0.309	47	54
MG-17	67	27	34	0.265	49	57
CA3	65	27	29	0.185	51	57
CA6	66	28	28	0.185	50	57
CA18	67	29	35	0.178	50	59
CB3	66	26	37	0.185	49	58
CB6	66	27	37	0.174	46	57
CB18	66	28	34	0.177	49	58
CC3	65	31	29	0.170	51	57
CC6	62	25	33	0.175	45	54
CC18	65	24	33	0.176	47	57
LA3	71	21	49	0.219	56	62
LA6	70	23	46	0.218	56	62
LA18	72	18	53	0.204	60	64
LB3	72	18	53	0.203	59	63
LB6	72	20	53	0.191	58	65
LB18	71	20	50	0.192	56	62
LC3	69	27	40	0.188	51	58
LC6	69	31	38	0.188	54	61
LC18	69	36	30	0.179	51	58

Annealing increased yarn dimensional stability as shown by the data listed in Table 3.5. Initially, MG-17 shrank approximately twice the amount as MG-9 yarn. For both yarn types all post-annealed shrinkage measurements were lower than the 'as extruded' initial value ($p < .04$). In spite of the dramatic reductions observed for MG-17, post-annealed shrinkage measurements for MG-9 yarn remained lower.

Table 3.5

Percent Shrinkage and Shrinkage Onset Temperature of "As Extruded" and Annealed MG-9 and MG-17 Yarn

Sample ID	Shrinkage at 80°C (%)	Shrinkage at 120°C (%)	Shrinkage Onset Temperature (°C)
MG-9	5.6 ± 0.5	7.1 ± 0.9	43.0 ± 0.9 *
MG-17	10.2 ± 2.2	14.1 ± 1.3	44.1 ± 1.0 *
CA3	2.9 ± 0.6 †	5.0 ± 1.0 †	46.7 ± 1.4 †
CA6	2.2 ± 0.1	4.6 ± 0.3 ‡	46.4 ± 1.0 ‡
CA18	1.7 ± 0.2 †	3.5 ± 0.3 †‡	49.9 ± 0.3 †‡
CB3	1.6 ± 0.2	2.3 ± 0.2	52.7 ± 0.3
CB6	1.8 ± 0.4	2.9 ± 0.5	51.3 ± 1.7 *
CB18	1.6 ± 0.2	2.2 ± 0.3	51.9 ± 0.8
CC3	2.0 ± 0.3	2.5 ± 0.3	44.8 ± 1.0 † *
CC6	1.9 ± 0.1 *	2.5 ± 0.3	47.1 ± 1.6 †‡
CC18	1.6 ± 0.2	1.9 ± 0.1	42.2 ± 0.7 †‡
LA3	6.5 ± 0.5 †	12.7 ± 0.5 †	49.0 ± 1.0 †
LA6	5.1 ± 1.1 †	11.6 ± 2.0	51.3 ± 0.9 †
LA18	4.3 ± 0.5 †	11.3 ± 1.3 †	52.4 ± 1.1 †
LB3	3.5 ± 0.3 †	7.8 ± 0.8 †	50.3 ± 1.6
LB6	3.6 ± 0.4	7.7 ± 0.8 ‡	50.6 ± 1.0 *
LB18	2.6 ± 0.4 †	5.9 ± 0.8 †‡	49.4 ± 0.3
LC3	4.0 ± 0.5 †	7.7 ± 1.2 †	44.8 ± 0.6 † *
LC6	2.1 ± 0.1 †*	4.0 ± 0.4 †	48.8 ± 1.4 †‡
LC18	2.8 ± 0.4 †	4.4 ± 0.7 †	46.3 ± 0.7 ‡

†‡ Indicates a significant difference within each yarn type between different annealing times for the indicated annealing temperature ($p < .05$)
*Indicates no significant difference found between yarn types for the same treatment conditions ($p < .05$)

At the annealing temperature of 100°C, increased annealing time significantly reduced yarn shrinkage for both yarn types. However, varying the annealing time did not produce any differences in shrinkage values for MG-9 at the annealing temperatures of 120°C and 140°C. On the contrary, the shrinkage of MG-17 yarn continued to be reduced as annealing time increased at the annealing temperatures of 120°C and 140°C.

On the whole, MG-17 yarn required greater temperatures and times to influence shrinkage measurements, whereas MG-9 yarn was mostly unresponsive to annealing conditions beyond a temperature of 100°C for 60 minutes.

All temperature onset measurements for annealed samples were greater than the 'as extruded' values ($p < .01$), with the exception of samples CC18 and LC3. In these two cases, no difference was observed. In addition, it is interesting to note that for the onset temperature there was no difference between the MG-9 and MG-17 'as extruded' yarn samples. For MG-9 yarn, annealing at 100°C increased the onset temperature with a continuation of this trend as annealing time increased. Further improvements were obtained at the annealing temperature of 120°C; however, at this temperature no difference was determined due to time. MG-17 showed a similar trend, but rather than an increase, a slight decrease was observed for each step change in time at the annealing temperature of 120°C. Annealing at 140°C had a negative effect on the shrinkage onset temperature for MG-9 and MG-17. All in all, similar initial and maximum shrinkage onset temperatures were observed between the two yarn types of approximately 44°C to 52°C, respectively.

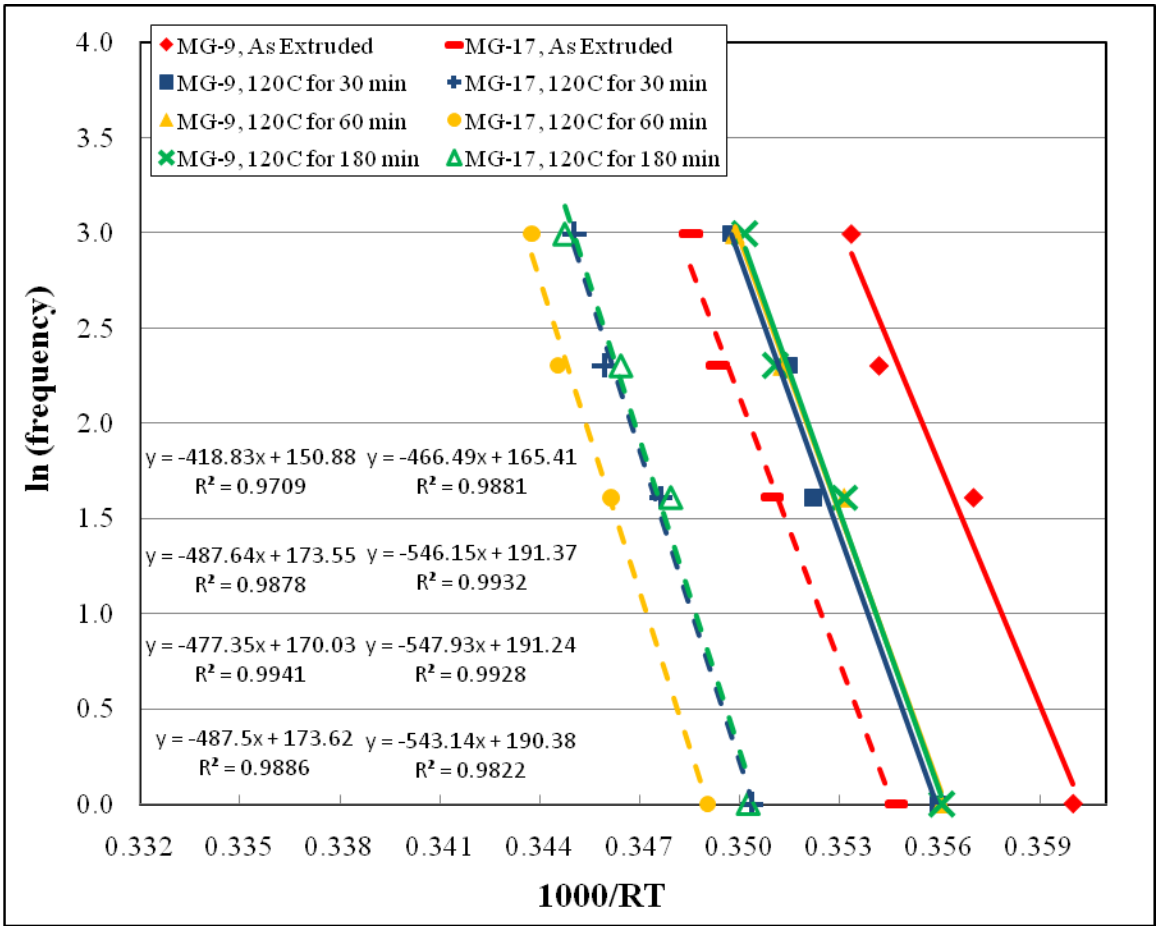

Figure 3.4

A typical Arrhenius plot demonstrating the relationship between logarithmic frequency and reciprocal peak temperature for the Tg transition. Depicted data is for the annealing condition of 120ºC. Reported linear slope and correlation coefficient data is organized in the same configuration as presented in the legend.

Figure 3.4 depicts the relationship used to determine the activation energy associated with each annealing condition determined by the associated slope (E_a) (data for the other annealing temperatures not shown). In addition, the correlation coefficient (R^2) has been reported to assess linear fit. A strong linear response was found (R^2 >

0.970) which validates the Arrhenius relationship. Figure 3.5 depicts the resulting E_a data as a function of annealing temperature for different annealing times.

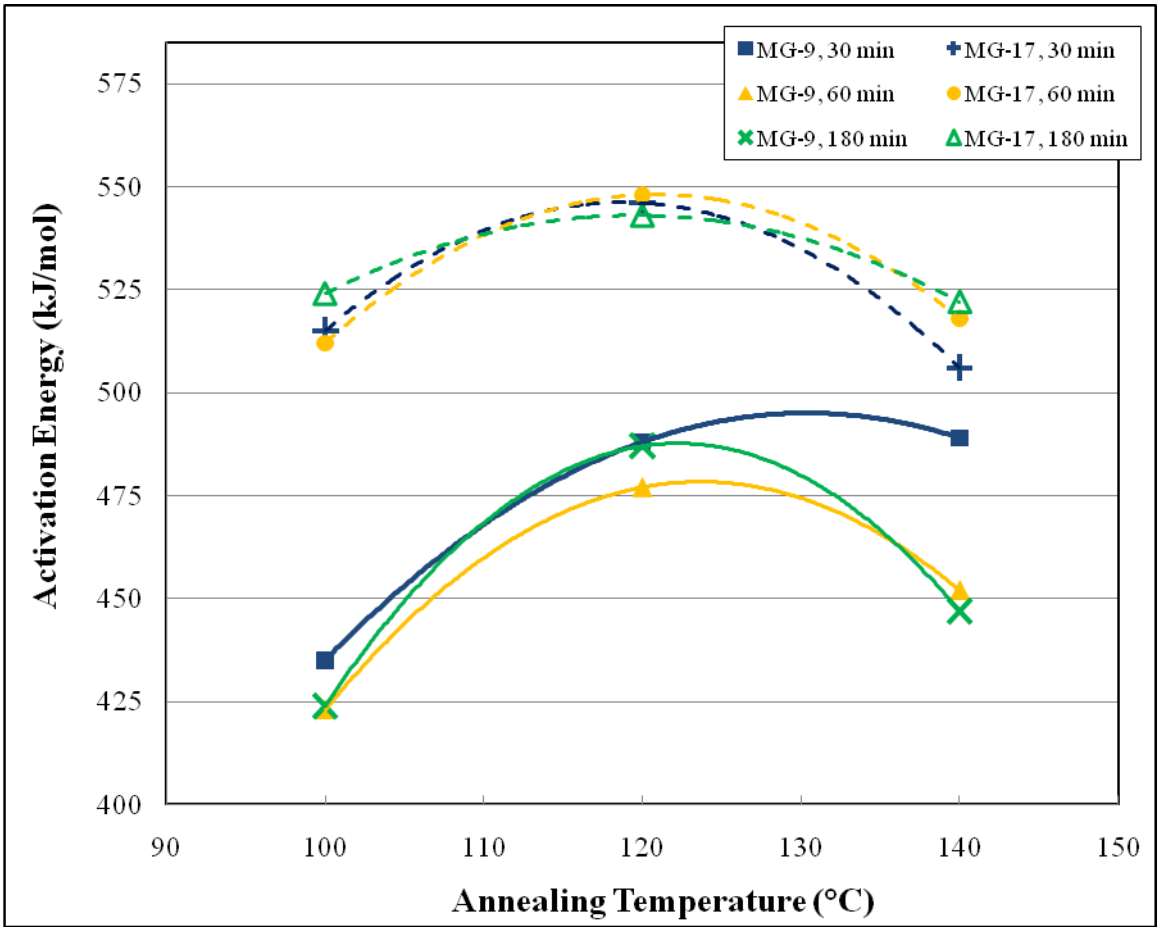

Figure 3.5

The apparent activation energies of the Tg transition calculated from the slope of the Arrhenius plot. The activation energies for the "as-extruded" samples were 419 kJ/mol and 466 kJ/mol for the MG-9 and MG-17, respectively.

Several interesting observations can be made from the data in Figure 3.6. First, minimal differences in E_a were observed for data within each yarn type at the three

annealing temperatures. Second, a maximum occurred for both yarn types at the temperature of 120°, regardless of annealing time. Lastly, a clear separation existed between the two yarn types with the E_a of the Tg transition for MG-17 substantially greater than that of MG-9.

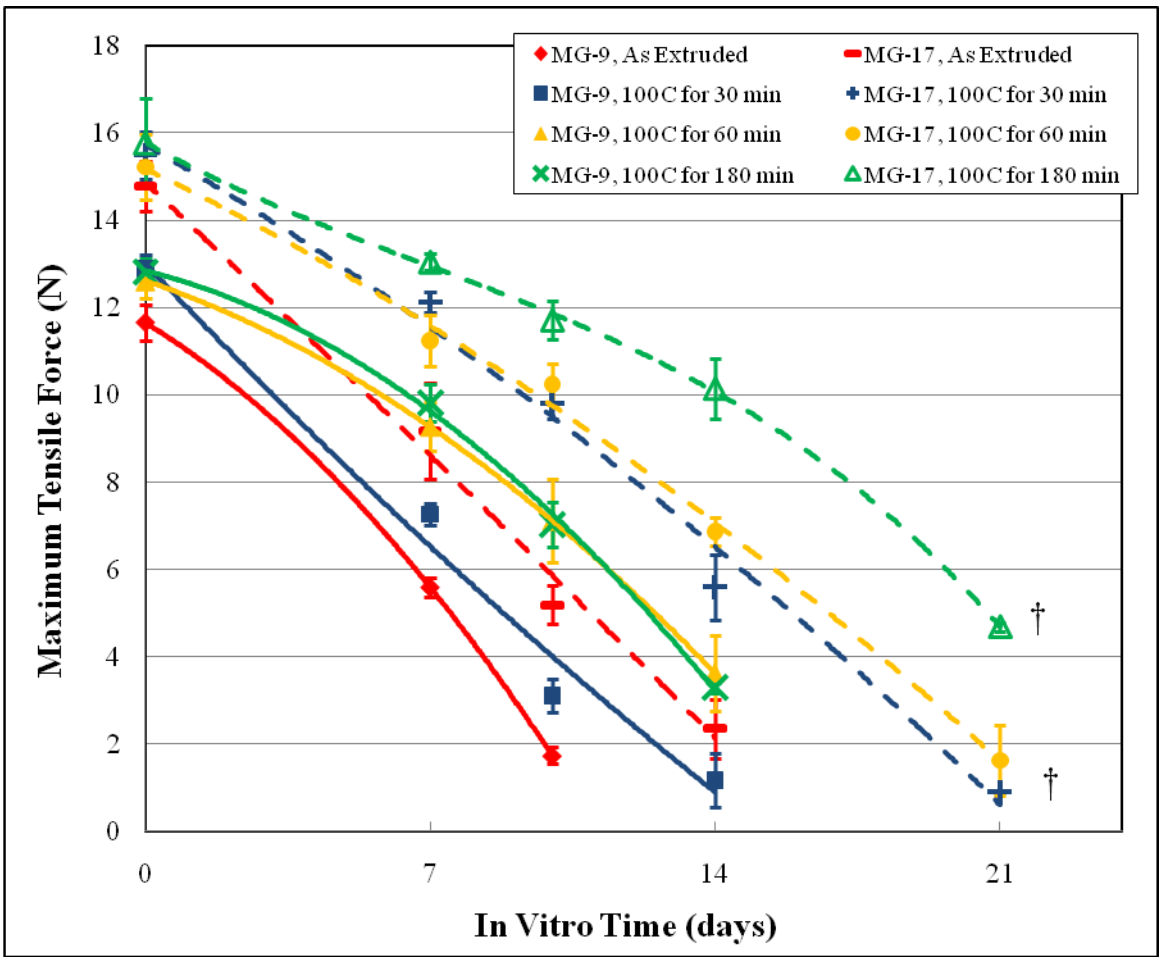

† Indicates a significant differences between 21 day *in vitro* samples ($p < .05$)

Figure 3.6

The temporal *in vitro* conditioned maximum tensile force for MG-9 and MG-17 samples annealed at 100ºC for 30, 60, and 180 minutes.

From inspection of the data in Figures 3.6, 3.7, and 3.8, clearly the annealing process increased the temporal *in vitro* conditioned MTF for both yarn types. The only exception to this observation is the MG-9 sample annealed at 140°C for 180 minutes which produced lower MTF values than that of the 'as extruded' sample. In all cases, MG-9 and MG-17 produced a reduction in strength that was immediate, continuous, and almost linear. However, the rate of that change or slope of the resultant profile was variable. Of specific importance is that MG-17 showed greater MTF values for all annealing temperatures and annealing times through 14 days. MG-9 showed a steeper slope that resulted in low MTF values by 14 days and no measurable results by 21 days. In contrast, all annealed MG-17 samples produced measurable MTF values at 21 days.

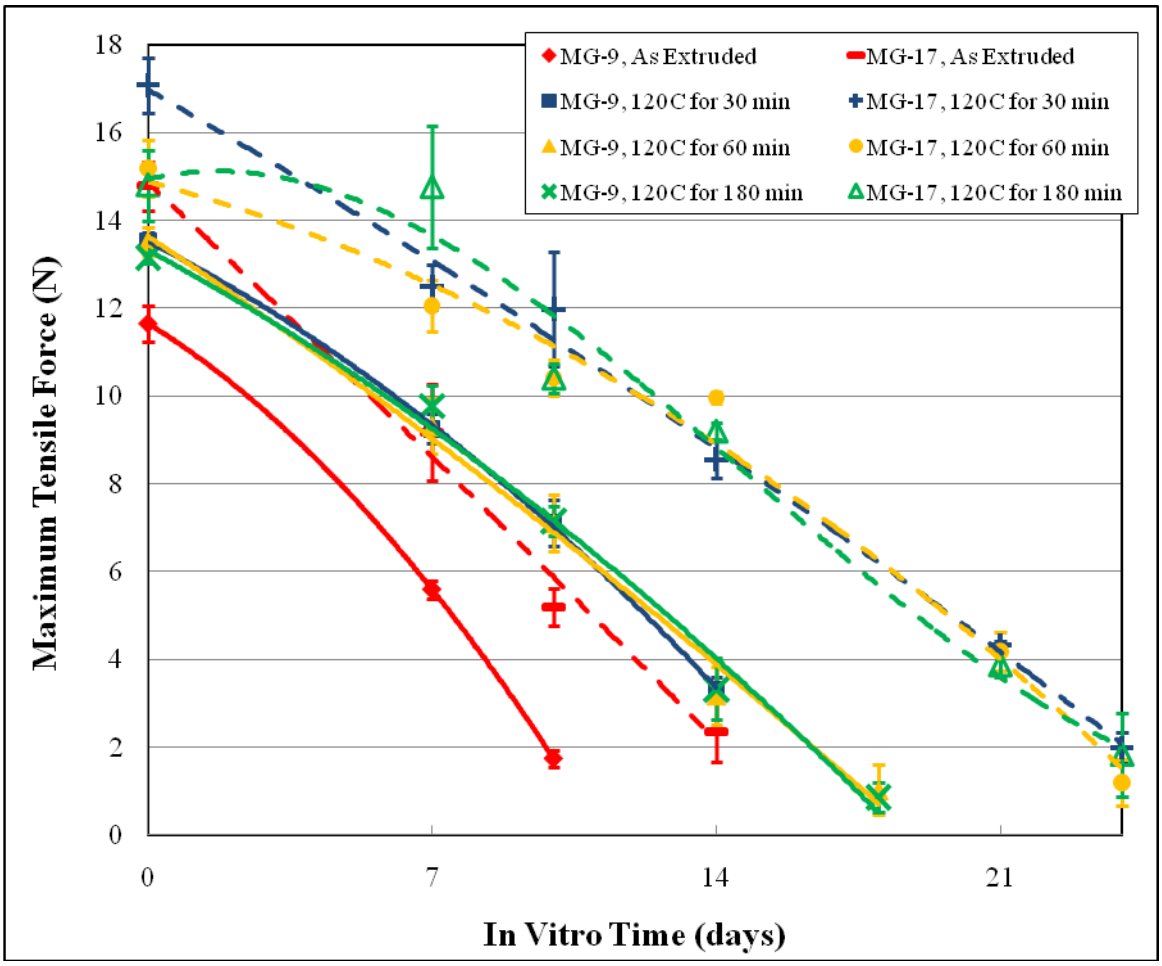

Figure 3.7

The temporal *in vitro* conditioned maximum tensile force for MG-9 and MG-17 samples annealed at 120ºC for 30, 60, and 180 minutes. (No significant differences found between MG-17 samples at 21 days of *in vitro* conditioning ($p < .05$))

At the *in vitro* time point of 21 days, annealing at 100°C for 180 minutes was not significantly different than each of the samples annealed at 120°C ($p > .06$) Samples annealed at 140°C were significantly lower than any of those annealed at 120°C ($p < .01$). In brief, the longest time period of 180 minutes for the lowest annealing temperature, as well as, all of the annealing times at 120°C produced similar, and the highest temporal

MTF values for MG-17 yarn. The temporal *in vitro* conditioned MTF values for MG-9 were significantly lower and marginally met the 14 day strength retention objective.

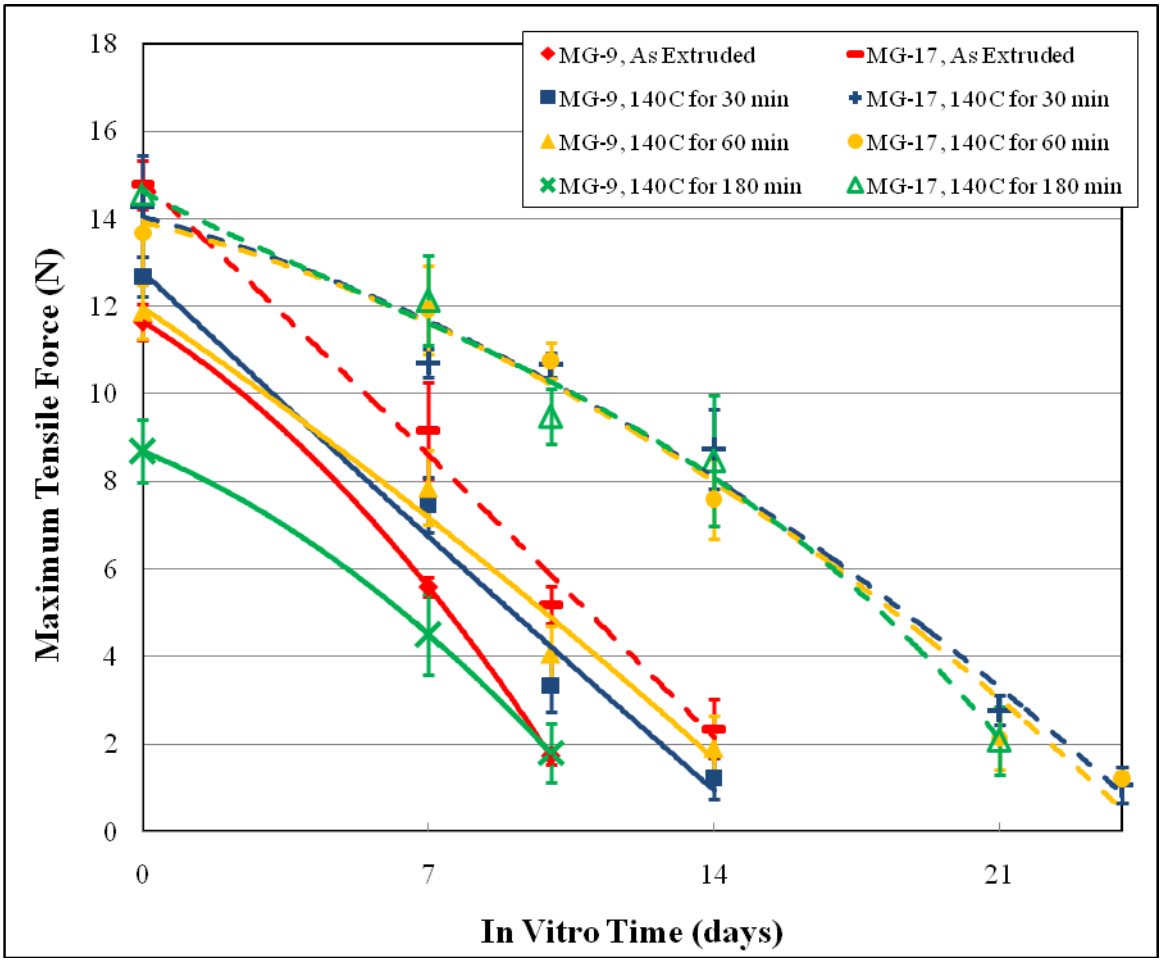

Figure 3.8

The temporal *in vitro* conditioned maximum tensile force for MG-9 and MG-17 samples annealed at 140ºC for 30, 60, and 180 minutes. (No significant differences found between MG-17 samples at 21 days of *in vitro* conditioning ($p < .05$))

Discussion

Three distinct variables were investigated to develop a high-glycolide copolymer for use in the construction of a bicomponent mesh. Specifically, comonomer composition, annealing time, and annealing temperature were investigated to determine their effect on the initial maximum breaking force, temporal *in vitro* conditioned maximum breaking force profile, and yarn stabilization against dimension changes. In addition to the direct measurement of these study objectives, several analytical techniques were employed to better understand morphological differences including thermal properties by DSC and viscoelastic properties by DMA. Significant results related to each copolymer and for each investigated annealing time and temperature will be discussed.

As polymerized, MG-17 revealed a clear reduction in T_m and crystallinity compared to MG-9. The peak temperature of the melting event is driven by crystallite perfection and thickness. Chu described that when a PLL comonomer is dispersed in PG, the sheet crystalline structure (also described as planar zig-zag) is disturbed because the methyl group affects chain packing.[27] The steric effect from the pendant methyl group of PLL protruding outward along the main chain of MG-17 likely interrupts the regular, repeat structure between adjacent chains, resulting in a less perfect crystalline structure. For comparison, the T_m for a homopolymer of PG is about 225°C. A commonly used and widely investigated copolymer for suture and meshes is polyglactin 910, a random copolymer of 90/10 poly(glycolide-co-lactide) which, compared to PG, displays (1) a lower T_m of about 205°C and less crystallinity and (2) a slower crystallization rate.[28]

These reported findings are similar to the reduction observed for MG-17. Following melt-extrusion, greater differences in T_m and degree of crystallinity were observed between MG-9 and MG-17.

During processing, each polymer was melted, extruded, and in-line oriented into fibers to produce a 10-filament yarn. As a result, crystallinity is developed which is detectable by DSC. In effect, during the extrusion process molten polymer is cooled rapidly, or quenched, which does not allow sufficient time for complete crystallization leaving a substantial amorphous fraction that upon reheating will partially crystallize. An inherent characteristic of absorbable polyesters is that their crystallization kinetics are relatively slow. As such, the effect of different molecular structures becomes magnified as a result of the rapid quenching during the melt-extrusion process. This difference was evident between MG-17 and MG-9. MG-17 showed a greater difference in T_m between the synthesized copolymer and "as extruded" yarn compared to that of MG-9. Furthermore, during annealing appreciable increases were observed for MG-17. As such, it is likely that the added kinetic energy facilitated a reorganization of the crystallite structure for MG-17 that was initially hindered by the dispersed lactide moiety. Some disturbance was also realized as a result of using PCL as a comonomer in MG-9. However, the reduction in T_m and degree of crystallinity was less pronounced due to the lack of a bulky side group in the monomers. It is interesting to note that for MG-9 yarn, minimal differences in T_m were observed following annealing. This was likely the result of faster crystallization kinetics which initially produced greater crystallite perfection that

did not significantly change during annealing. Instead only an increase in the degree of crystallinity was observed.

The mechanical tensile properties of MTF and elongation have significant influence on the maximum burst force of meshes. For the investigated yarns, one might have hypothesized that MG-17 would elongate more than MG-9 due to the greater weight percent of the low T_g and low modulus pTMC macroinitiator in the MG-17. Results indicated the contrary, however; mechanical tensile testing showed that MG-9 yarn produced significantly greater elongation. The interlocking effect of the added lactide monomer units between adjacent chains dominated the extensional behavior and negated any effect from the greater molecular weight of the pTMC segment. Likewise, steric hindrance and molecular interlocking prevented rotational and translational mobility between adjacent chains in the amorphous domain, resulting in greater chain entanglement and thus greater MTF for MG-17. A similar response was observed when tercopolymer of PCL, TMC, and PLL with different molar ratios were synthesized.[29] The authors noted that as the content of PLL increased, chain slippage decreased, which increased the tensile strength and decreased elongation.

The temperature position, height, onset temperature, and temperature range of tan δ provide quantitative measures which are related to the degree of crystallinity and morphology of semicrystalline polymers. The amorphous and crystalline domains of fibers are intimately connected which has an effect on the T_g relaxation. The temperature of the T_g relaxation is a measure of chain rigidity and resistance to segmental molecular mobility. As such, segmental movement must overcome chain friction and steric barriers.

This interaction is detectable in the breadth, peak, and onset of the Tg transition as segmental motion in the amorphous region is constrained or unrestrained due to different annealing conditions. Furthermore, the onset temperature for the reduction in storage modulus is also an indicator of how well the amorphous region is constrained by annealing to long-range segmental motion. It should be noted that the values determined for T_g using DMA are higher than those determined using the more commonly used DSC method. Other authors have reported the same observation.[19] This difference lies in the fact that each technique measures a different property. DSC measures differences in specific heat while DMA measures thermally induced molecular mobility.

The Tg transition represents a major physical change to the polymer as it goes from a 'glassy' structure with limited molecular mobility to the 'rubbery' state with increased free volume and chain mobility within the amorphous domain. A significant finding, which has substantial influence on degradation rate, was that the Tg of MG-17 yarn (69-72°C) was greater by 4-6°C than that of MG-9 (65-66°C). Again, adding PLL increased the barrier to molecular rotation and translation leading to a higher T_g. Values of T_g determined using DMA for a homopolymer of PLG and polyglactin 910 yarn in suture form have been reported as 72°C and 74°C, respectively.[30] Similar to results of the present study, the addition of PLL as a comonomer to PG increased the temperature of the T_g relaxation event. Moreover, in a study by Penning and coworkers,[31] PLL was polymerized with a 0.10 and 0.05 molar fraction of PCL or D-lactide, respectively. Of interest was the response of T_g, T_m, and heat of fusion to the addition of each comonomer unit. In the case of PCL, a reduction in all three thermal properties was observed.

However, the addition of D-lactide maintained the value of T_g but depressed, even more dramatically than PCL, the T_m and heat of fusion values. Although the major component was PLL and not PG as used in the current study, the response was similar to that of MG-17 and MG-9. Steric effects from lactide heavily influenced crystallite formation and perfection, which significantly lowered the T_m and heat of fusion values. PCL had the same effect but to a lesser degree. The dramatic reduction in T_g when PCL was introduced was explained as being the result of the extremely low T_g of PCL (T_g = -60°C) which shifted the T_g a proportional amount to its molar content. Again, this was similar to the T_g response of MG-9. Since the T_g of D-lactide is the same as L-lactide no difference was observed. Therefore, for the monomers used in the present study, the reduction in MG-9 was likely the result of the low T_g of PCL, while the increase in MG-17 was from the greater T_g of PLL.

Differences in the amount of soft segment were most noticeable in the DMA storage modulus curves. The finding that the storage modulus was greater for the MG-9 yarn within the rubbery plateau is related to the amount of soft segment within each copolymer and differences in the degree of crystallinity. Below T_g the stiffness of the chain backbone is highly influential on the stiffness of the polymer. As such, the greater proportion of the soft polymeric initiator in MG-17 is a likely cause for the lower E' response below T_g. In addition, the height of the rubbery plateau is related to a polymers degrees of crystallinity. Crystallites resist chain slippage which results in a greater elastic response. Compared to MG-9, MG-17 was less crystalline which was concluded from DSC measurements.

There is a well documented link between degradation rate and crystallinity.[3,32] Higher degrees of crystallinity prolong the strength retention profile by inhibiting the access of water to molecular chains which are protected within tightly packed crystallites. However, crystallinity alone does not dictate degradation rate. Rather it is the accessibility of water to the amorphous domain which is also influenced by molecular orientation, T_g, and the hydrophobicity of the constituent monomers.[33] This study illustrates this point; MG-9 was more crystalline yet it showed an increased rate of degradation. The explanation for this finding can be found in differences in T_g.

Of particular interest to this study is the *in vitro* conditioned retention of mechanical strength as it has the greatest impact on the function of the device. The greater T_g of MG-17 influenced the temporal *in vitro* conditioned strength retention profile. The affect of T_g on degradation rate is evidenced in the DMA tan δ curve for each yarn type and at each annealing condition. With overall lower T_g values for MG-9, the tan δ curve begins to increase sooner than that of MG-17. From the tan δ onset temperature it is clear that MG-9 began to show evidence of the initiation of the T_g relaxation event at or below physiologic temperature. The increase in tan δ marks a physical increase in free volume for the copolymer, induced by molecular movement. A consequence of this increased free volume, it would be expected that larger gaps between chains would increase the diffusion of water. This is a significant finding since porosity is a major factor which affects degradation rate. For the majority of the investigated annealing conditions, MG-17 does not show any increase in tan δ until 10°C, or more, above physiologic temperature. This finding correlates well with the *in vitro* conditioned

MTF data which indicated that MG-17 in all cases has better *in vitro* conditioned strength retention.

Changes to the size and shape of a fibrous medical device due to elevated temperature during sterilization or shipment is often detrimental to its intended function. In addition to undesirable dimensional changes, a relaxed yarn will have modified initial and temporal *in vivo* mechanical properties. These changes result from the thermal relaxation of orientation within the amorphous region which is triggered by entropic molecular changes to acquire a lower energy conformation. In this study, the annealing process was found to substantially decrease the amount of shrinkage and increase the shrinkage onset temperature. Although the annealing process imparts resistance to deformation from the relaxation of some chains and the crystallization of others, for fibers this process is never absolute. MG-17 exhibited about two times more free shrinkage than MG-9. It is reasonable to expect that steric effects induce stressed chain configurations, which were frozen in as the yarn transitioned into the glassy state during fiber orientation. Consequently, MG-17 experienced substantially more thermally induced free shrinkage as the stressed chains were allowed to relax into lower energy conformations. In the case of MG-9, the PCL comonomer unit would have imparted increased chain flexibility that facilitated chains to assume lower stress levels. Furthermore, the greater crystallinity of MG-9 would have better constrained the microstructure against relaxation. Regardless, for annealed samples equal to or greater than 120°C, the absolute amount of shrinkage at 80°C is low. For comparison, using a similar technique, Fu and coworkers[19] determined that polyglactin 910 sutures processed

and annealed at different conditions produced shrinkage values from 3.3 to 5.1% at 80°C. These values are comparable to those obtained for MG-17 and slightly greater than MG-9. The temperature at which the shrinkage initiates, i.e. the shrinkage onset temperature, is equally important to the dimensional stability of yarn as is the absolute amount of shrinkage. The amount of shrinkage at the onset of shrinkage temperature would be expected to be essentially zero at typical end-use (37°C) and sterilization temperatures (< 42°C); both yarn types met this criterion when annealing was conducted at temperatures greater than 120°C.

Since the rearrangement of polymer chains into crystallites is time dependent, it was important to determine the effect of different annealing times on each yarn type. Longer annealing times allow more chains to diffuse into suitable orientations for crystalline arrangement; thus, the perfection, size, and degree of crystallinity increase with increased annealing time.[34] In this study minimal differences in degrees of crystallinity were observed between the annealing times of 30, 60, and 180 minutes, indicating that the percent of crystallite formation within both copolymers was achieved prior to the lowest time point of 30 minutes. This result has been observed for the slower crystallizing PLL homopolymer. Molded articles of PLL have been shown to reach equilibrium with regard to percent crystallinity by 30 minutes for the same investigated annealing temperatures.[35] However, although differences in amount of crystallinity were not observed between each annealing time, changes in morphology were apparent.

At the studied annealing temperatures and given adequate time, polymer chains have sufficient mobility that, below a critical size, small crystallites melt and create larger

crystallites that grow at their expense.[36] Additionally, when annealing conditions in which nucleation dominates (lower temperatures), smaller crystals are formed. When few nucleation sites exist and conditions favor crystallite growth, then larger crystallites form.[37] The extent of each condition is time dependent. Different crystallite sizes were evidenced in the mechanical, viscoelastic, and dimensional stability results. First, mechanical tensile testing data showed significant reductions in MTF and elongation as annealing time increased, especially at the annealing temperature of 140°C. Reductions in elongation are characteristic of the formation of large crystallites that result in a loss in toughness and more brittle mechanical failure. Similar results were found for PLL films annealed at different temperatures and times.[38] Furthermore, at the lower annealing temperature of 100°C, the amount of free shrinkage decreased with annealing time due to greater restriction from the reorganization of small crystallites into larger crystallites that span greater distances and include more tie chains. As a result, less dimensional change is allowed during free shrinkage. In addition, for both yarn types the peak of tan δ was reduced with time, as larger crystallites result in less viscous flow. Observations related to the annealing time were most notable for the tan δ onset temperature at the extreme annealing temperatures of 100°C and 140°C. For example, longer annealing times at 100°C showed an increase in onset, while at 140°C a marked reduction was realized. Similar results were observed by Loo and coworkers.[21] In a study using films of poly(lactide-co-glycolide) (PLG) where T_g was observed to decrease significantly with increased annealing time. The authors attributed the reduction to a loss in the amorphous fraction and the formation of voids as chains were redistributed into local crystallites.

Several other authors have noted that for poly(ethylene terephthalate), increased crystallinity increases T_g, to a point, and then a further increase to crystallinity results in a reduction in T_g.[39-41] In this study, shifts in T_g were apparent but less dramatic, likely due to the highly oriented and crystalline nature of the yarn. Rather, more dramatic changes were noted in the onset of the tan δ event with reductions as annealing temperature and time increased. The effect of this phenomenon was also witnessed in the temporal *in vitro* conditioned strength retention.

Differences in annealing time had a clear impact on the temporal *in vitro* conditioned MTF profile. For MG-17 yarn, at the temperature of 100°C the strength profile benefited significantly when the time point was increased from 60 to 180 minutes. Reductions in the *in vitro* conditioned strength profile for both yarn types were consistently lower when the annealing temperature was increased from 120°C to 140°C. These findings were similar to those found for the previously mentioned PLG films.[21] In that study, the degradation rate was reported to decrease for annealing times less than 30 minutes and increase when annealing time was greater than 30 minutes. As before, the authors attributed the initial decrease in degradation rate to crystallites retarding water penetration, followed by a loss in the amorphous fraction which created voids that allowed greater water uptake and faster hydrolysis. Another explanation for the increased degradation rate and loss of mechanical strength due to increased crystallinity of absorbable polymers has been suggested by Tsuji.[42,43] Studies showed that for PLL films a higher initial crystallinity was found to result in enhanced hydrolysis. The authors suggested that an increased density of hydrophilic terminal carboxyl and

hydroxyl groups, which are excluded from crystalline domains, causes loose chain packing and an increase in the diffusion rate of water into amorphous domains. The increased degradation rate associated with advanced crystallite formation determined in these studies parallel the results of both yarn types in this study, specifically the annealing conditions which produced enhanced crystallization. Namely, annealing at 140°C produced diminishing *in vitro* conditioned strength retention with each step increase in time.

As demonstrated, the three annealing temperatures were all influential on the properties of both yarn types. However, the temperature of 120°C increased the mechanical properties, T_g, onset temperature for tan δ, onset temperature of E', peak of the E'' curve, and produced the greatest temporal *in vitro* strength retention for both MG-9 and MG-17 yarn. This data was further supported by the calculated E_a for each yarn type and each annealing condition. The activation energy provides a quantitative measurement of the energy required to transition through the thermomechanical relaxation event of T_g. As such, it provides information about how well the amorphous region was constrained. In other words, it is effectively the energy barrier that the material has to overcome in order to generate segmental molecular motion on a long-range scale. The obtained E_a values were clearly greater for MG-17 and produced a maximum at 120°C which corresponded with the copolymer and annealing temperature that resulted in the greatest initial strength, highest tan δ onset temperature, and greatest *in vitro* conditioned strength retention. On the other hand, a reduction in E_a was observed at the annealing temperature of 140°C. Overall, annealing at 140°C resulted in a

reduction in properties. This was most notable in the reduced mechanical properties, lower T_g values, and faster degradation rate. When annealing was conducted at 100°C morphology development required the longer time point of 180 minutes to achieve marked increases in the onset of tan δ, shrinkage, and a greater strength retention *in vitro* profile.

For copolymers, two or more inherently incompatible polymer sequences are forced to co-exist in a single phase. The coupling of their properties results in a single T_g relaxation which is between each individual segments homopolymer. The properties of the investigated copolymers in this study were largely influenced by the temperature of the T_g relaxation. Steric effects from the addition of the PLL in MG-17 increased T_g, and more importantly, the onset temperature of the tan δ transition. It is difficult to predict the *in vivo* performance of an absorbable yarn based on only a single characteristics as there are many interactions; however, in this study the most influential factor on the initial and temporal *in vitro* conditioned strength profile was the replacement of PCL with PLL for MG-17.

Conclusion

A high-glycolide yarn was developed for use in a bicomponent mesh for hernia repair whereby its function requires strength retention during the inflammatory and proliferation period of healing with subsequent gradual transfer of the load to remodeling tissue. Chemical modification resulted in two triaxial, segmented high-glycolide copolymers for evaluation, namely MG-9 and MG-17. Experimental results indicated that the addition of L-lactide as a comonomer in MG-17, compared to ε-caprolactone for

MG-9, increased T_g, the onset of the tan δ transition, the E_a of the T_g transition, the maximum tensile force, and decreased the tensile elongation. A further aim of this work was to determine the isothermal annealing time and temperature which optimized the temporal *in vitro* conditioned strength profile. In summary, it can be concluded that MG-17 annealed at a temperature of 120°C for 30 minutes met the desired functional requirements and provided the greatest initial maximum tensile force, longest temporal *in vitro* conditioned strength retention, and yarn stabilization against dimensional changes induced by unrestrained thermal relaxation.

References

1. Nair L, Laurencin C. Biodegradable polymers as biomaterials. Progress in Polymer Science 2007;32:762-798.

2. Engelberg I, Kohn J. Physico-mechanical properties of degradable polymers used in medical applications: a comparative study. Biomaterials 1991;12(3):292-304.

3. Chu CC. Hydrolytic degradation of polyglycolic acid: tensile strength and crystallinity study. Journal of Applied Polymer Science 1981;26:1727-1734.

4. Craig P, Williams J, David K. A biological comparison of polyglactin 910 and polyglycolic acid synthetic absorbable sutures. Surg Gynecol Obstet 1975;141:1-10.

5. Barrows T. Degradable implant materials: a review of synthetic absorbable polymers and their applications. Clin Mat 1986;1:233-257.

6. Bergsma JE, Rozema FR, Bos RR, Boering G, de Bruijn WC, Pennings AJ. Biocompatibility study of as-polymerized poly(L-lactide) in rats using a cage implant system. J Biomed Mater Res 1995;29(2):173-9.

7. Lee S, Kim K, Kang SW, Kim C. Microstructural analysis and structure-property relationship of poly(glycolide-co-1,3-trimethylene carbonate). Polymer 2005;46:7953-7960.

8. Metz SA, Chegini N, Masterson BJ. In vivo and in vitro degradation of monofilament absorbable sutures, PDS and Maxon. Biomaterials 1990;11(1):41-5.

9. Middleton JC, Tipton AJ. Synthetic biodegradable polymers as orthopedic devices. Biomaterials 2000;21(23):2335-46.

10. Gopferich A. Mechanisms of polymer degradation and erosion. Biomaterials 1996;17(2):103-14.

11. Wang Y, Ribelles J, Sanchez M, Mano J. Morphological contributions to glass transition in poly(L-lactic acid). Macromolecules 2005;38:4712-18.

12. Pego A, Feijen G. Enhanced mechanical properties of 1,3-trimethylene carbonate polymers and networks. Polymer 2003;44:6495-6504.

13. Jie C, Zhu K, Shilin Y. Preparation, characterization and biodegradation characteristics of poly(1,3-trimethylene carbonate-co-glycolide). Polym Int 1996;41:369-375.

14. Noorsal K, Mantle M, Gladden L, Cameron R. Degradation and drug-release studies of a poly(glycolide-co-trimethylene carbonate) copolymer (Maxon). J Appl Polym Sci 2005;95:475-786.

15. Bezwada RS, Jamiolkowski DD, Lee IY, Agarwal V, Persivale J, Trenka-Benthin S, Erneta M, Suryadevara J, Yang A, Liu S. Monocryl suture, a new ultra-pliable absorbable monofilament suture. Biomaterials 1995;16(15):1141-8.

16. Deng M, Zhou J, Chen G, Burkley D, Xu Y, Jamiolkowski D, Barbolt T. Effect of load and temperature on in vitro degradation of poly(glycolide-co-L-lactide) multifilament braids. Biomaterials 2005;26(20):4327-36.

17. Montes de Oca H, Ward IM. Structure and mechanical properties of PGA crystals and fibres. Polymer 2006;47:7070-77.

18. Fredericks R, Melveger A, Dolegiewitz L. Morphological and structural changes in a copolymer of glycolide and lactide occurring as a result of hydrolysis. J Poly Sci (Poly Phys Ed) 1984;22:57-66.

19. Fu B, Hsiao, B., Chen, G., Zhou, J., Koyfman, I., Jamiolkowski, D., Dormier, E. Structure and property studies of bioabsorbable poly(glycolide-co-lactide) fiber during processing and in vitro degradation. Polymer 2002;43:5527-5534.

20. Cowie J. Polymers: chemistry and physics of modern materials. New York: Chapman and Hall; 1991.

21. Loo SC, Ooi CP, Wee SH, Boey YC. Effect of isothermal annealing on the hydrolytic degradation rate of poly(lactide-co-glycolide) (PLGA). Biomaterials 2005;26(16):2827-33.

22. Wetton R. Dynamic mechanical thermal analysis of polymers and related systems. In: Dawkins J, editor. Development in polymer characterization. Barking: Elsevier; 1986.

23. Wetton R. Dynamic mechanical method in the characterization of solid polymers. Polymer Testing 1984;4:117-129.

24. Chu CC, Browning A. The study of thermal and gross morphologic properties of polyglycolic acid upon annealing and degradation treatments. J Biomed Mater Res 1988;22(8):699-712.

25. Browning A, Chu CC. The effect of annealing treatments on the tensile properties and hydrolytic degradative properties of polyglycolic acid sutures. J Biomed Mater Res 1986;20(5):613-32.

26. Cohn D, Younes H, Marom G. Amorphous and crystalline morphologies in glycolic acid and lactic acid polymers. Polymer 1987;28(12):2018-22.

27. Chu CC. Classification and general characteristics of suture materials. In: Chu CC, editor. Wound Closure Biomaterials and Devices: CRC Press; 1996. p 39-64.

28. Shalaby SW, Johnson RA. Synthetic absorbable polyesters. In: Shalaby SW, editor. Biomedical Polymers, Designed-to-Degrade. Cincinnati, OH: Hanser/Gardner Publications; 1994. p 8-10.

29. Jia Y, Shen X, Gu X, Dong J, Mu C, Zhang Y. Synthesis and characterization of tercopolymers derived from e-caprolactone, trimethylene carbonate, and lactide. Polym. Adv. Technol 2008;19:159-166.

30. Von Fraunhofer J, Chu CC. Mechanical Properties. In: Chu CC, editor. Wound Closure Biomaterials and Devices: CRC Press; 1997. p 118-19.

31. Penning JP, Dijkstra H, Pennings AJ. Preparation and properties of absorbable fibres from L-lactide copolymers. Polymer 1993;34(5):942-951.

32. Williams DF. Biodegradation of surgical polymers. J Mater Sci 1982;17(5):1233-46.

33. Reed AM, Gilding DK. Biodegradable polymers for use in surgery - poly(glycolic)/poly(lactic acid) homo and copolymers: 2. In vitro degradation. Polymer 1981;22:494-498.

34. Zhoa N, Wang L, Huang D, Zhang T, Zhang L, Xiong C. Effect of isothermal annealing on degree of crystallinity and mechanical properties of poly(l-lactide-co-glycolide). Cryst Res Technol 2010;45(3):275-280.

35. Migliaresi C, Cohn D, De Lollis A, Fambri L. Dynamic mechanical and calorimetric analysis of compression-molded PLLA of different molecular weights: Effect of thermal treatment. J Appl Polym Sci 1991;43:83-95.

36. Hurrell S, Cameron RE. The effect of initial polymer morphology on the degradation and drug release from polyglycolide. Biomaterials 2002;23(11):2401-9.

37. Andjelic S, Fitz B, Jamiolkowski D. Advances in morphological development to tailor the performance of absorbable medical devices. In: Shalaby SW, Burg K, editors. Absorbable and biodegradable polymers. Boca Raton: CRC Press; 2004.

38. Tsuji H, Ikada Y. Properties and morphologies of poly(L-lactide): 1. Annealing condition effects on properties and morphologies of poly(L-lactide). Polymer 1995;36(14):2709-2716.

39. Illers K, Breuer H. Molecular motions in polyethylene terephthalate. J Colloid Sci 1963;18(1):1-31.

40. Dumbleton J, Murayama T. Temperature dependence of the dynamic mechanical behavior of poly(ethylene terephthalate). Colloid Polym Sci 1967;220(1):41-48.

41. Dumbleton J, Murayama T. On the dynamic mechanical behavior of drawn poly(ethylene terephthalate) fibers. Colloid Polym Sci 1968;228(1-2):54-58.

42. Tsuji H, Mizuno A, Ikada Y. Properties and morphology of poly(L-lactide). III. Effect of initial crystallinity on long-term in vitro hydrolysis of high molecular weight poly(L-lactide) film in phoshate-buffered solution. J Appl Polym Sci 2000;77(7):1452-1464.

43. Saha S, Tsuji H. Effects of rapid crystallization on hydrolytic degradation and mechanical properties of poly(L-lactide-co-E-caprolactone). React Funct Polym 2006;66:1362-1372.

CHAPTER FOUR

AN INVESTIGATION OF THE TISSUE RESPONSE AND INTEGRATION OF AN ABSORBABLE BICOMPONENT CONSTRUCT IN A RAT MODEL

Introduction

When implanted in living tissues, mesh materials elicit a cellular response which triggers a tissue reaction that results in the encapsulation of the implant. The characteristics of the tissue encapsulation are variable and largely dependent on the mesh design variables of yarn chemistry, yarn form (monofilament or multifilament), yarn size, and the physical configuration or knit construction. Previously, an absorbable bicomponent mesh (ABM) comprised of a fast-degrading and slow-degrading yarn was shown to modulate mesh temporal physical and biomechanical properties for application in hernia repair (Chapters 2 and 5). As such, the ABM goes through a transition phase whereby the structural stiffness of the mesh changes from low extensibility to high extensibility given the same force. This transition is timed to take place between the inflammation/proliferation phase and the maturation/remodeling phase of the wound healing process. During the former, the ABM mesh shields the neotissue from biomechanical stimulation resulting in an integration process primarily influenced by yarn chemistry, yarn form, and knit construction. In this investigation, a simulated ABM knit construct was evaluated to determine the cellular and tissue integration response during the transition phase using a rat model.

Mesh hernia repair efficacy is dependent upon strengthening weak native abdominal wall tissue by a strong mesh/tissue complex. A significant factor in achieving

this objective is the integration of the mesh at the host tissue interface. The acute foreign body cellular response to the mesh is initially responsible for the mesh-tissue integration process. For the proposed ABM, the temporal transition period associated with the substantial degradation of the fast-degrading yarn is a critical timeframe. The development and optimization of a fast-degrading yarn was shown (Chapter 3) to retain strength for greater than 18 days. As a result, the ABM possesses a transition period between 18 and 28 days (Chapter 5). Efficacy of the ABM is dependent on its integration with the host tissue before the mesh transitions to a state of high extensibility. Significant integration of the extracellular matrix (ECM) into polypropylene (PP) and polyethyleneterephthalate (PET) meshes has been observed in animal studies, reducing abdominal wall compliance 2-3 weeks post implantation.[1] This temporal change in the bending stiffness of the abdominal wall of rats correlated with the histological finding of activated fibroblasts and the accumulation of collagen. In the same study, grades of collagen content within the PET mesh steadily increased from 3 days to a maximum at 21 days, with no subsequent change up to 90 days. High-glycolide coated meshes are associated with vigorous collagen deposition.[2,3] Partially-absorbable (PA) meshes which incorporate a fast-degrading absorbable yarn into a light-weight (LW) PP mesh have been shown to induce greater cellular activity and fibrosis within the first 28 days post-implant compared to the LW PP mesh alone.[4] Furthermore, the introduction of high-glycolide filaments into a PA mesh increases the quantity of collagen at 21 days compared to PP and PET meshes.[5] Overall, the use of a fast-degrading absorbable polymer results in an

intense cellular reaction followed by greater collagen deposition compared with non-absorbable yarns.

The tissue response to a new mesh design is often first evaluated in animal models. *In vivo* evaluations for absorption and tissue response using the gluteal muscle of rats as an implantation site has been reported frequently for sutures[6,7] and tissue adhesive analyses.[8] This animal model provides two implantation sites to facilitate paired experimental designs, allowing within animal variability to be minimized when comparing the effect of two different implant types. As a result, the rat gluteal muscle model provides a simple method to compare the tissue reaction of different mesh materials. To evaluate the integration of a mesh into the surrounding tissue it is important to quantify the extent of encapsulation. To quantitatively characterize changes in the foreign body response with time, a measure of the inner ring of granuloma (i.e. the zone of high cellular activity) and the outer ring (i.e. the fibrotic capsule) has been suggested by several authors.[4,7,9] To determine the total amount of collagen deposition surrounding an implant, Junge and coworkers used a quantitative method based on the selective binding of histological stains to collagen and noncollagenous protein.[5,10] Evaluated with histological qualitative observations, quantitative measurements of cellular activity and tissue integration provide a mechanism to evaluate device performance *in vivo*.

In this investigation, a simulated ABM knit construct was implanted *in vivo* and evaluated at 3 and 6 weeks. As a result, the biological reaction to the simulated ABM construct during the early stability phase was closely simulated. These evaluation time

points bracket the transition phase of the proposed ABM to evaluate (1) the extent of foreign body response measured as the thickness of the granuloma or zone of high inflammatory cell density, (2) the degree of collagen encapsulation measured as capsule thickness, and (3) the amount of deposited collagen measured as the collagen/total protein ratio. Additionally, qualitative histological observations coupled with the quantitative results provided insight into the anticipated device efficacy. For comparison, a similar construct comprised of PET yarn served as a clinically-relevant control.

Materials and Methods

Materials

The polymer synthesis and production of yarn for the investigated polymers of MG-17 (Chapter 3) and SMC-7 (Chapter 2) were described previously. In summary, MG-17 is a triaxial, segmented, high-glycolide copolymer that is melt-extruded into a 10-filament yarn. SMC-7 is a linear, segmented, high-lactide copolymer that is melt-xtruded into a 43-filament yarn. The denier (g/9000m) of the MG-17 and SMC-7 yarn was 150 and 86, respectively. Additionally, a non-absorbable yarn of polyethylene terephthalate (PET) was procured for use as a control (Unifi, Dacron, 115 denier, 56-filament).

Implant Construction

Using MG-17 and SMC-7 yarns, a warp knitted absorbable bicomponent construct (ABC) was knit using an 18-gauge raschel knitting machine (American LIBA, RACOP TR-6). To produce the ABC, a single end of MG-17 was plied with two ends of

SMC-7 yarn (S1) prior to knitting and wound onto a spool. Additionally, a three-ply of SMC-7 yarn (S2) was wound onto a spool in the same manner. Prepared spools of yarn, S1 and S2, were fed through a tensioning device and then directly into guidebars (GB) one and two, respectively. Knitting was completed by threading S1 and S2 yarn through a single guide of each GB such that the construct was produced by knitting around only a single needle within the needle bar. Using the same knitting process, PET yarn was plied to closely match the denier of the yarns used to construct the ABC and was knit (knit PET termed PETC) using the same knit pattern. As such, GB 1 was fed with a two-ply and GB2 was fed with a three-ply PET yarn.

The knit ABC and PETC were annealed or heat set by wrapping the knit construct around an expandable rack which had two parallel bars of stainless steel. Yarn was wrapped in a continuous fashion, secured, and a strain of 0.02 was applied prior to annealing. Annealing was completed at 120°C for 1/2 hour while under high vacuum (< 1 torr). Following annealing, implants were cleaned using ultrasonic agitation (Branson, 5510) in isopropyl alcohol (Sigma-Aldrich, ACS Plus, A416) for 6 minutes. An image of each mesh construct was obtained using a digital camera (Moticam 2300) attached to a microscope (40x, Leica, DME).

Implant Sterilization

Sterilization of the ABC and PETC implants was completed using a low-temperature (40°C) ethylene oxide (EtO) cycle (Anderson Scientific Inc., EOGas™ Series 3 Plus Sterilization Chamber). Constructs were sealed (FUJI, Impulse OPL-300-

10) in Tyvek pouches (Oliver-Tolas, 1073B) to facilitate EtO gas diffusion and preserve sterility of the device until implantation. To complete the removal of EtO residuals, pouches containing the implants were placed under reduced pressure (< 1.0 torr) for 12 hours following sterilization. To protect against ambient exposure and premature degradation of the ABC implants, all pouched implants were sealed in foil pouches (Oliver-Tolas, TPC-0764B)

Study Design and Surgical Procedure

Four adult female Sprague-Dawley rats (approximately 250 grams) were used for the cellular and tissue response study. The study design included two rats for each time period (3 and 6 weeks) with one knit construct (ABC and PETC) implanted in each gluteal muscle. This design resulted in two implant sites for each construct at each time period.

All animals were acclimated for a minimum of one week before the surgical procedure. Each rat was pre-medicated with 0.5 mg/kg acepromazine and 0.5 mg/kg buprenorphine subcutaneously 15 minutes prior to induction of general anesthesia, which was isoflurane in oxygen. Each rat was shaved and prepped with iodine at the incision sites for both gluteal muscles. Subsequently, each animal was placed in a sterile surgical environment, draped, and positioned so that the dorsal area was exposed. Using a #11 scalpel blade, a cutaneous stab incision was made at the proximal end of each gluteal muscle. A sterile ABC and PETC implant was drawn through the left and right gluteal muscles (one implant in each muscle) using the proximal incision as the entry point. A

segment of approximately 2 cm length of each implant was left *in situ*. The cutaneous stab incisions were closed with one autoclip (staple) at each of the incision locations. Staples were removed 7-10 days post-surgery. No antibiotic treatment was given before or during the treatment.

At the predetermined time periods of 3 and 6 weeks, two animals were administered ½ cc of heparin 15 minutes before being euthanized by carbon dioxide asphyxiation. Immediately following euthanasia, the abdominal aorta was cannulated and vascular perfusion was administered by first using saline and then 10% neutral buffered formalin (NBF). Subsequently, the surgical sites were opened and each gluteal muscle was excised leaving the implant *in situ* and undisturbed. Each gluteal muscle/implant was preserved in a sterile, labeled container filled with 10% NBF.

Histological Evaluation

A transverse section of each NBF fixed tissue sample was trimmed, placed in a cassette, labeled, dehydrated, cleared, and embedded in paraffin. Paraffin-embedded tissue samples were sectioned (6 μm), placed on a slide, deparaffinized, and stained (Goode Histology Lab, New Brunswick, NJ). Histological investigations of granuloma and fibrotic capsule thickness were performed after staining with hematoxylin (Polysciences, #02749) & eosin Y (Polysciences, #09859) (H&E) and Masson's trichrome (Polysciences, #25088), respectively. Using a digital camera (National Optical, Moticam 2300) attached to a brightfield microscope (400x, Leica Microsystems, DME), five pictures of random sites around the irregular tissue/implant interface were

captured from five slides per implant site. Measurements of the granuloma from H&E stained sections and fibrotic capsule thickness from Masson's trichrome stained sections were made using digital image-analysis software (Motic Image Plus, 2.0 ML). Measurements (5 slides x 5 locations = 25 measurements) were pooled, resulting in a single representative average value for each implant type at each implantation time period.

Collagen/Total Protein Ratio

The procedure for determining the collagen/protein ratio is described in detail elsewhere.[11,12] In brief, 10% NBF fixed samples were embedded in paraffin and 15 µm thick sections were obtained. Four sections for each sample were deparaffinized and maintained in distilled water at 4°C until staining. Four individual sections were first stained with 0.04% Fast Green FCF (Polysciences Inc., C.I. 42053) in saturated picric acid (Fisher-Scientific, Aqueous, SP9200) for 15 minutes in a small test tube (10x45 mm). The sections were then washed with distilled water and stained with 0.1% Sirius red F3B (Polysciences Inc., C.I. 35780) and 0.1% Fast Green FCF at room temperature for 30 minutes in a rotary shaker. Fluids were carefully withdrawn with a disposable pipette and the sections were rinsed several times with distilled water until the supernatant was colorless. Subsequently, the dyes were eluted from the sections using 0.1 N sodium hydroxide (NaOH) in absolute methanol. The fluid was read using a spectrophotometer (PerkinElmer, LAMBDA 35) at the wavelengths corresponding to the maximum absorbance of Sirius red (538 nm) and Fast Green (605 nm). The absorbance

of each stain was used to calculate the amount of collagen and noncollagenous protein in the samples. Results were expressed as the ratio of collagen (μg) to total protein (mg). Collagen contained within the implant capsule, within and between the muscle cells, and surrounding the muscle tissue was included in the measurement. To limit the influence of collagen within and between the muscle cells and surrounding the muscle tissue, sections were first stained with Fast Green to maximize the attachment of the dye to noncollagenous tissues and limit the Sirius Red dye uptake to highly concentrated collagen regions.

Statistical Analysis

To study differences in tissue reaction and integration a split plot design analyzed by two-factor analysis of variance (ANOVA) to compare means was completed. Two-factor ANOVA was used to test for effects due to implant type (ABC or PETC) and *in vivo* time period (3 or 6 weeks), as well as their interaction, for the response variables of granuloma thickness, fibrotic capsule thickness, and collagen/total protein ratio. The analysis of collagen data based on a split-plot design limited errors by introducing the same background signal into paired measurements for each implant type such that differences could be distinguished. The data for each implant type from each rat at each *in vivo* implantation time period was pooled. All analysis was completed using statistical analyses software (Statistical Analyses Software, v9.2) and a p-value less than 0.05 was considered to be significant.

Results

Figure 4.1 provides comparative images of the ABC and PETC samples following stabilization by heat setting. The same knit pattern and the similar denier of the yarn resulted in the nearly identical size and shape of the ABC and PETC.

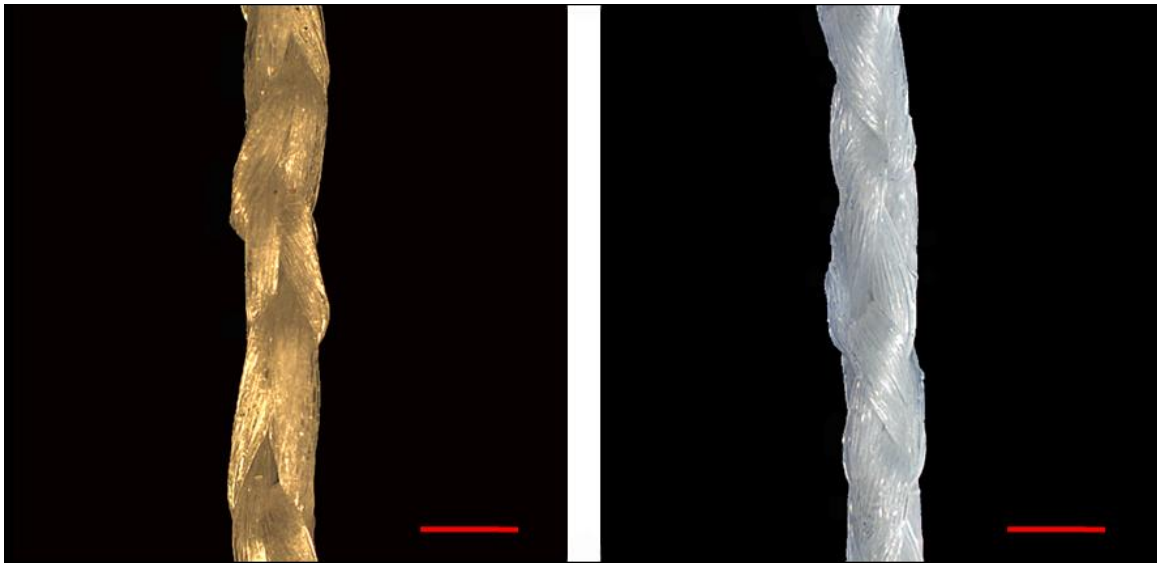

Figure 4.1

Images of the ABC (left) and PETC (right) showing the knit construction and high aspect ratio. (Red scale bar = 0.5 mm)

The cellular response of each implant was measured quantitatively using the granuloma thickness at the tissue/implant interface. Figure 4.2 depicts the cellular response measurements for the 3 and 6 week post-implantation periods.

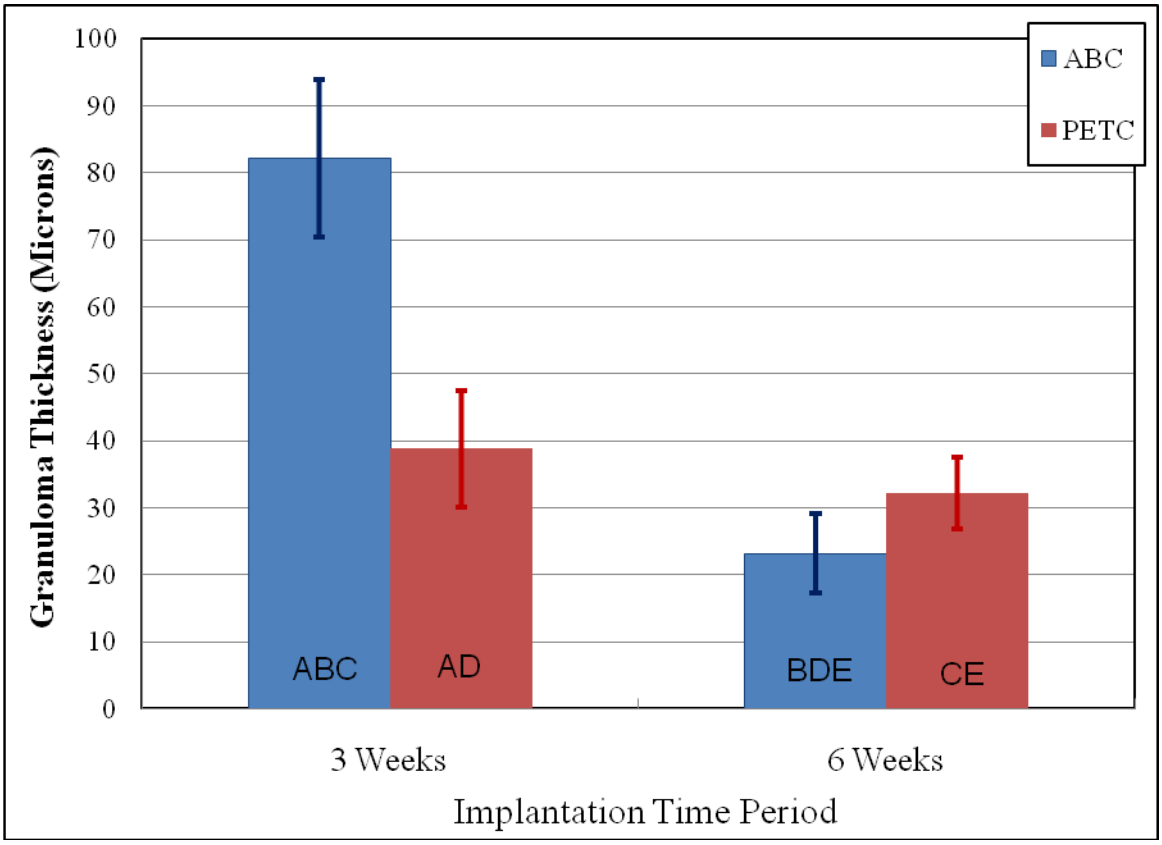

Corresponding letters indicate a significant difference ($p < .05$) between samples.

Figure 4.2

The granuloma thickness for the ABC and PETC implants at the implantation periods of 3 and 6 weeks.

The PETC produced a small and nonsignificant effect on granuloma thickness ($p = 0.17$) between 3 and 6 weeks *in vivo*. On the other hand, the ABC produced a significant reduction between 3 and 6 weeks. At 3 weeks, the thickness of the granuloma for the ABC was approximately twice that of the PETC. However, at 6 weeks the average thickness of the cellular response around the ABC had decreased almost four-fold from 3 weeks to a level which was lower than that of the PETC ($p = 0.02$).

As seen in Figure 4.3, the ABC capsule thickness at 3 weeks was significantly greater ($p = 0.02$) than that surrounding the PETC. At 6 weeks, the ABC was statistically unchanged ($p = 0.13$) while the average capsule thickness of PETC was greater than that produced by the ABC.

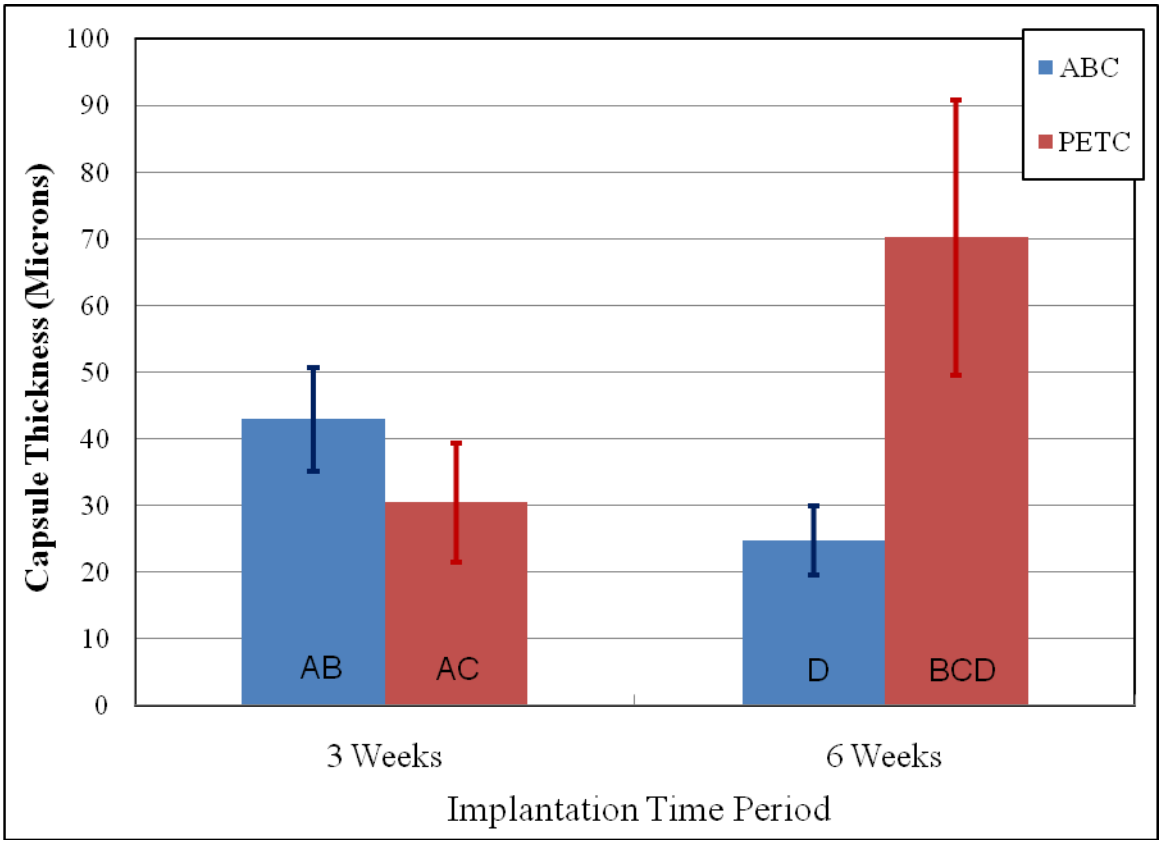

Corresponding letters indicate a significant difference ($p < .05$) between samples.

Figure 4.3

The capsule thickness for the ABC and PETC implants at the implantation periods of 3 and 6 weeks.

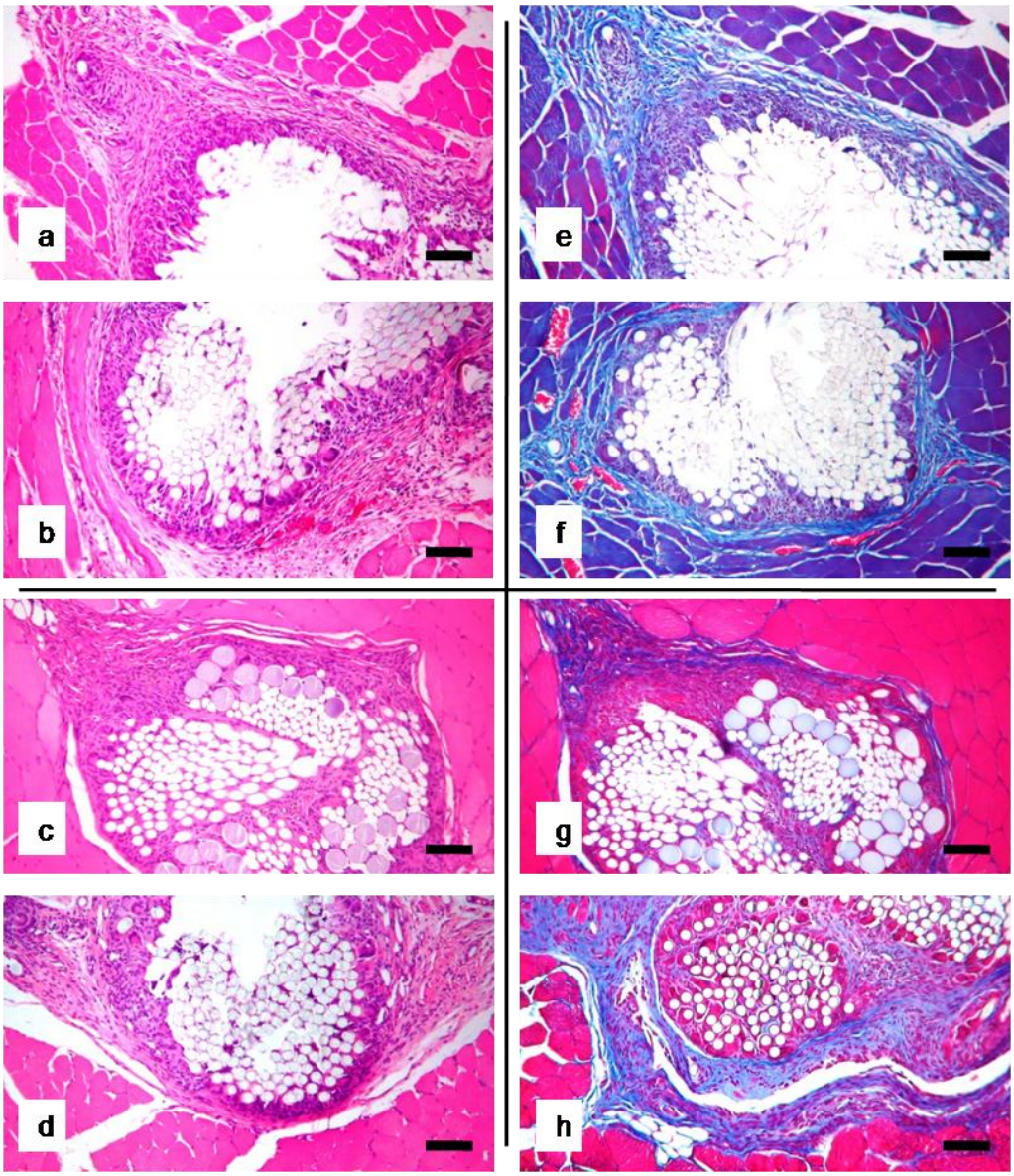

Figure 4.4

Histological sections of the tissue/implant interface in rat gluteal muscle for the ABC and PETC at 3 (top) and 6 (bottom) weeks post-implantation. a, e – ABC at 3 weeks showing the high cellular activity adjacent to the implant and the formation of collagen surrounding the granuloma. b, f – PETC at 3 weeks surrounded by fewer cells than that of the ABC and several capillaries. c, g – ABC at 6 weeks surrounded by fewer inflammatory cells than at 3 weeks and a dense and homogenous collagen capsule. d, h – PETC at 6 weeks showing significantly more collagen formation than that of the ABC. (a - d → H&E / e - h → Masson's trichrome / original magnification 100x, Black scale bars = 100 microns)

Histological analysis (Figure 4.4) showed that the ABC and PETC were markedly colonized with cells in a zone near the implant filaments and the knit yarn was well encapsulated. Observed effects due to implant type included less cellular activity for the PETC at 3 weeks compared to the greater granuloma thickness induced by the ABC. However, the PETC produced several capillaries around the implant while new vascular constructs were non-existent for the ABC. At 6 weeks, the major difference between the ABC and PETC was the characteristics of the respective collagen capsules. The ABC capsule was highly oriented and dense as highlighted by the dark purple/blue color in Masson's trichrome stained sections; the capsule was devoid of inflammatory cells. In contrast, the PETC capsule was thick and permeated with cells. Significant numbers of spindle shaped, fibroblasts appeared to infiltrate a less compacted fibrous capsule compared to that of the ABC. From 3 to 6 weeks, the ABC was surrounded by fewer inflammatory cells and the capsule was compacted. The change in time from 3 to 6 weeks for the PETC resulted in a dramatic increase in the effected zone around the implant. During the studied implantation time period, there was minimal evidence of collagen fibers infiltrating the individual filaments for either implant type. There were no signs of substantial mass loss for the fast-degrading yarn of the ABC. The larger MG-17 yarn filaments were well dispersed within the much smaller SMC-7 filaments and did not change in size or shape by the later time point of 6 weeks.

The selective binding of Sirius red and Fast Green was used to determine the ratio of collagen to total protein within sections of the implant/muscle (Figure 4.5). No difference in the collagen/total protein ratio was determined between 3 and 6 weeks for

each implant type. The amount of collagen around the PETC was found to be on average greater at 6 weeks than at 3 weeks, but not significantly different ($p = 0.09$). However, the amount of detected collagen was different between each implant type at 3 weeks, and again at 6 weeks. At 3 weeks, the collagen/total protein ratio was greater for the ABC tissue specimens, while at 6 weeks the PETC tissue specimens contained a greater amount of collagen.

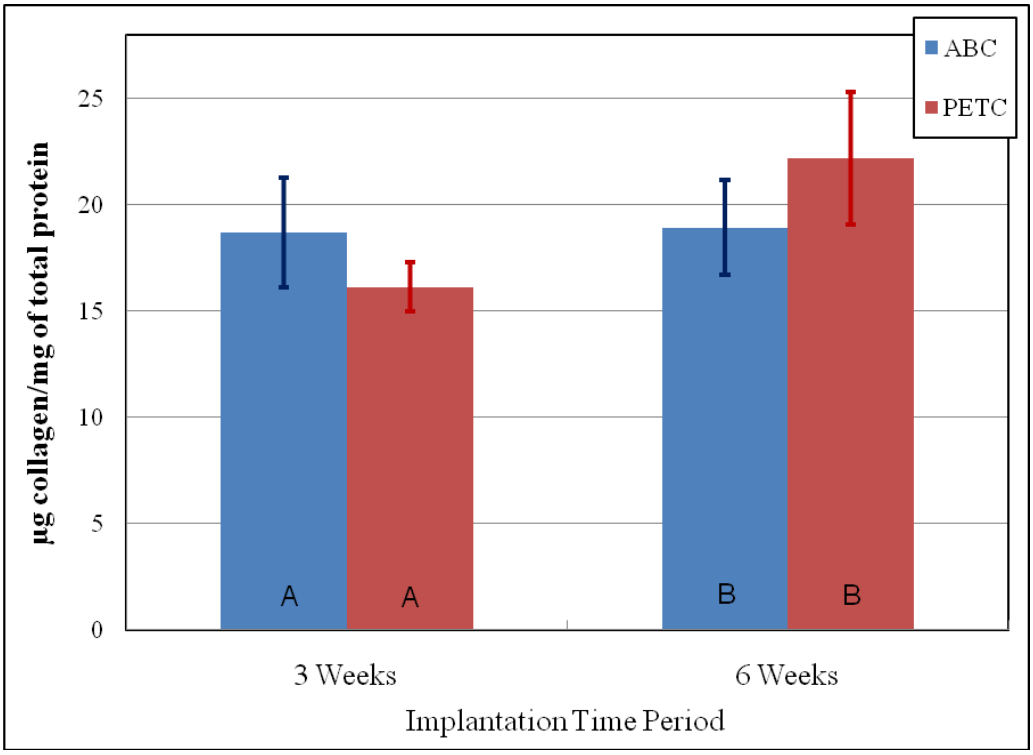

Corresponding letters indicate a significant difference ($p < .05$) between samples.

Figure 4.5

The collagen/total protein ratio for the ABC and PETC implants at the implantation periods of 3 and 6 weeks.

Discussion

The initial stability and transition phases of the mesh biomechanics are critical time periods in evaluating the efficacy of the WK6 absorbable bicomponent mesh (ABM) (Chapter 5). For meshes, the cellular response is initially responsible for the mesh-tissue integration process. However, the level and duration of the inflammatory response can delay the quantity and quality of collagen deposition. In this study, a strong initial (< 3 weeks) foreign body granuloma representing the accumulation of inflammatory cells was observed for the ABC which at 6 weeks was significantly reduced. Approximately 30% of the ABC mass is a high-glycolide yarn; hence, a substantial initial cellular response was expected. Klinge and coworkers investigated the tissue response to fast- and slow-degrading absorbable surgical meshes.[13] A fast-degrading mesh revealed an intense macrophage response at the mesh/tissue interface that peaked at 14 days, was reduced by about four-fold at 21 days, and was reduced to a low level by 90 days. The inflammatory response reported by Klinge was similar to that triggered by the ABC; however, the ABC response was shifted approximately one week earlier. This shift in the ABC response may be the result of the additional cellular response to the slow-degrading yarn. In the same article, Klinge reported a lower, but slowly increasing response to the slow-degrading absorbable mesh. The simultaneous cellular response against both the absorbable components of the ABC may have been additive and contributed to the overall observed reaction. Nevertheless, the cellular response for the ABC was significantly diminished, although still present, at the 6 week implantation time period. This result is significant. Although the use of degradable yarns incite an initially strong

cellular response, by 6 weeks the inflammatory cell response had subsided to a level below that of the non-absorbable PET implant.

The PETC showed no change in cellular response between 3 and 6 weeks. Similarly, an investigation reported in literature, detailing implantation of PET mesh in rats showed that the number of macrophages at the mesh/tissue interface did not change between 7 and 90 days.[14] In another study using PET mesh, the total percentage of macrophages and giant cells were scored and both were found to peak at 14 days with a steady reduction in macrophages, but little change to the number of giant cells through 90 days.[1] Overall, the results from the granuloma thickness measurements indicate that within the 3 to 6 week time period the ABC elicited an intense initial cellular response which was substantially reduced by 6 weeks; whereas, the PETC cellular response was initially lower, likely reached steady-state prior to 3 weeks, and was maintained through 6 weeks.

Mesh biocompatibility has been reported to be improved when angiogenesis accompanies the integration process.[15] Angiogenesis provides the wound site with a conduit for the delivery of inflammatory cells, fluid, and nutrients, while at the same time removing metabolic waste. In this investigation the PETC implants stimulated neovascularization at 3 weeks which was sustained at 6 weeks. On the contrary, the ABC implant sites showed no signs of neovascularization. Neovascularization local to PET mesh implants has been reported to be substaintial.[1] For other mesh-like constructions such as vascular grafts, investigations have found that a strong up-regulation of inflammatory cytokines is an inhibitor to angiogenesis.[16] This may explain the lack of

neovascularization for the ABC. The strong inflammatory response observed at 3 weeks would likely have produced a strong cytokine response. If true, the lack of observed vascular structures local to the ABC would be consistent with the finding that strong inflammatory responses prevent angiogenesis. For this investigation, the lack of new vascular structures for the ABC may be perceived as a positive outcome as the greater access of inflammatory cells to the wound site may have increased and prolonged the initial strong cellular response.

A successful hernioplasty requires effective encapsulation of the individual bundles of yarn which comprise the mesh to prevent migration and support the local tissue. This event is particularly important for the ABM, which after 6 weeks has modulated biomechanical features such that it becomes highly extensible. The amount of collagen between 3 and 6 weeks around the ABC was not found to be different. Consequently, the collagen deposition process for the ABC occurs quickly with no significant change from 3 to 6 weeks. However, qualitative changes to the newly deposited collagen were apparent from 3 to 6 weeks. Differences in the collagen capsule from 3 to 6 weeks included a reduction in the average capsule thickness (nonsignificant change, $p = 0.13$) surrounding the implant. As such, the collagen deposition upon entering the transition phase (3 weeks) was already established, but the density and orientation increased, which was likely the result of the decreased cellular reaction and cytokine production. This observation is important since the collagen capsule must possess high mechanical strength, which would be facilitated by a dense and oriented structure. In other words, collagen of high mechanical quality rather than high quantity is

optimal. In contrast, the deposition of collagen increased for the PETC during the studied implantation time period. Unlike the ABC, the capsule formation of the PETC consisted of significant amount of low density connective tissue containing many apparent spindle shaped fibroblasts. Consequently, the tissue response was characteristic of a wound healing process that results in excessive fibrosis.

Excessive fibrosis surrounding non-absorbable hernia meshes is well documented[17-20] and is associated with many complications.[14,21-26] Although collagen formation is critical to mesh efficacy, the amount of collagen present at the wound site is not a good indicator of mechanical integrity. For example, it has been demonstrated that large amounts of collagen encapsulating a mesh does not prevent recurrence.[1,27] Loose, disorganized collagen which is delayed from reorganization by inflammation lacks strength facilitated by the reorganization and crosslinking process. The ABC appeared to down-regulate cellular activity and collagen synthesis which are characteristic markers for the initiation of the next wound healing phase of collagen remodeling. In contrast, the high number of proliferating fibroblasts, lack of change in the number of inflammatory cells, and intensifying collagen production are consistent with features describing a chronic foreign body response against the PETC. Although fast-degrading absorbable polymers have been shown to result in an intense cellular reaction followed by greater collagen deposition compared with non-absorbable yarns,[2-5] the segmented, copolyester yarns used in this study evaluated from 3 to 6 weeks did not show greater collagen deposition than the PET control. The observed difference in tissue reaction between MG-17 and the typical random structured, high-glycolide yarn (e.g. Vicryl) may be in the rate

of acidic byproduct production or differences in the temporal fragmentation of the yarn, which may shift or reduce fibroblast chemotaxis and/or modify fibroblast phenotype. The exact mechanism requires investigation and may hold promise in improving the biocompatibility of absorbable meshes.

Conclusion

Using the ABC as a model of the ABM, the results of this study suggest that during the transition phase of the ABM a moderate, but decreasing cellular response and the mesh will be well encapsulated without excessive fibrosis. ABC granuloma thickness values representing the accumulation of inflammatory cells were lower at 6 weeks compared to that of the non-absorbable PETC control. Capsule thickness and collagen/total protein ratio measurements indicated that the ABC was well integrated with a dense, compacted, concentrically oriented capsule. In contrast, the PETC tissue samples had evidence of excessive fibrosis, including a thicker, less dense capsule which was with infiltrated fibroblasts. Although the results must be interpreted with caution due to the limited number of animals and observation time points, the ABC showed a down-regulation of the inflammatory process and good integration. Additionally, it must be stated that results obtained from small animal models have limited translation to clinical outcomes; however, the developed knit construct implanted in a gluteal muscle rat model does provide a baseline to evaluate relative differences in tissue reaction and implant integration for future mesh designs.

References

1. Klinge U, Klosterhalfen B, Conze J, Limberg W, Obolenski B, Ottinger AP, Schumpelick V. Modified mesh for hernia repair that is adapted to the physiology of the abdominal wall. Eur J Surg 1998;164(12):951-60.

2. Klinge U, Klosterhalfen B, Muller M, Anurov M, Ottinger A, Schumpelick V. Influence of polyglactin-coating on functional and morphological parameters of polypropylene-mesh modifications for abdominal wall repair. Biomaterials 1999;20(7):613-23.

3. Pans A, Pierard GE. A comparison of intraperitoneal prostheses for the repair of abdominal muscular wall defects in rats. Eur Surg Res 1992;24(1):54-60.

4. Rosch R, Junge K, Quester R, Klinge U, Klosterhalfen B, Schumpelick V. Vypro II mesh in hernia repair: impact of polyglactin on long-term incorporation in rats. Eur Surg Res 2003;35(5):445-50.

5. Junge K, Klinge U, Klosterhalfen B, Mertens PR, Rosch R, Schachtrupp A, Ulmer F, Schumpelick V. Influence of mesh materials on collagen deposition in a rat model. J Invest Surg 2002;15(6):319-28.

6. Bezwada RS, Jamiolkowski DD, Lee IY, Agarwal V, Persivale J, Trenka-Benthin S, Erneta M, Suryadevara J, Yang A, Liu S. Monocryl suture, a new ultra-pliable absorbable monofilament suture. Biomaterials 1995;16(15):1141-8.

7. Im JN, Kim JK, Kim HK, Chang HI, Lee YL, Park WH. *In vitro* and *in vivo* degradation behaviors of synthetic absorbable bicomponent monofilament suture prepared with poly(p-dioxanone) and its copolymers. Poly Degr Stab 2007;92:667-674.

8. Henderson AM, Stephenson M. 3-Methoxybutylcyanoacrylate: evaluation of biocompatibility and bioresorption. Biomaterials 1992;13(15):1077-84.

9. Jansen JA, Dhert WJ, van der Waerden JP, von Recum AF. Semi-quantitative and qualitative histologic analysis method for the evaluation of implant biocompatibility. J Invest Surg 1994;7(2):123-34.

10. Junge K, Rosch R, Anurov M, Titkova S, Ottinger A, Klinge U, Schumpelick V. Modification of collagen formation using supplemented mesh materials. Hernia 2006;10(6):492-7.

11. Lopez-De Leon A, Rojkind M. A simple micromethod for collagen and total protein determination in formalin-fixed paraffin-embedded sections. J Histochem Cytochem 1985;33(8):737-43.

12. Gascon-Barre M, Huet PM, Belgiorno J, Plourde V, Coulombe PA. Estimation of collagen content of liver specimens. Variation among animals and among hepatic lobes in cirrhotic rats. J Histochem Cytochem 1989;37(3):377-81.

13. Klinge U, Schumpelick V, Klosterhalfen B. Functional assessment and tissue response of short- and long-term absorbable surgical meshes. Biomaterials 2001;22(11):1415-24.

14. Rosch R, Junge K, Schachtrupp A, Klinge U, Klosterhalfen B, Schumpelick V. Mesh implants in hernia repair. Inflammatory cell response in a rat model. Eur Surg Res 2003;35(3):161-6.

15. Arbos MA, Ferrando JM, Quiles MT, Vidal J, Lopez-Cano M, Gil J, Manero JM, Pena J, Huguet P, Schwartz-Riera S and others. Improved surgical mesh integration into the rat abdominal wall with arginine administration. Biomaterials 2006;27(5):758-68.

16. Salzmann DL, Kleinert LB, Berman SS, Williams SK. Inflammation and neovascularization associated with clinically used vascular prosthetic materials. Cardiovasc Pathol 1999;8(2):63-71.

17. Klinge U, Klosterhalfen B, Muller M, Ottinger AP, Schumpelick V. Shrinking of polypropylene mesh in vivo: an experimental study in dogs. Eur J Surg 1998;164(12):965-9.

18. Kockerling C, Schug-Pass C. Recurrence and mesh material. In: Schumpelick V, Fitzgibbons RJ, editors. Recurrent Hernia. Berlin, Germany: Springer-Verlag; 2007.

19. Welty G, Klinge U, Klosterhalfen B, Kasperk R, Schumpelick V. Functional impairment and complaints following incisional hernia repair with different polypropylene meshes. Hernia 2001;5(3):142-7.

20. Champault G, Bernard C, Rizk N, Polliand C. Inguinal hernia repair: the choice of prosthesis outweighs that of technique. Hernia 2007;11(2):125-8.

21. Leber GE, Garb JL, Alexander AI, Reed WP. Long-term complications associated with prosthetic repair of incisional hernias. Arch Surg 1998;133(4):378-82.

22. Cobb WS, Kercher KW, Heniford BT. The argument for lightweight polypropylene mesh in hernia repair. Surg Innov 2005;12(1):63-9.

23. Paajanen H. A single-surgeon randomized trial comparing three composite meshes on chronic pain after Lichtenstein hernia repair in local anesthesia. Hernia 2007;11(4):335-9.

24. Palumbo P, Minicucci A, Nasti AG, Simonelli I, Vietri F, Angelici AM. Treatment for persistent chronic neuralgia after inguinal hernioplasty. Hernia 2007;11(6):527-31.

25. Aasvang E, Kehlet H. Chronic postoperative pain: the case of inguinal herniorrhaphy. Br J Anaesth 2005;95(1):69-76.

26. Aasvang E, Kehlet H. Surgical management of chronic pain after inguinal hernia repair. Br J Surg 2005;92(7):795-801.

27. Klinge U, Si ZY, Zheng H, Schumpelick V, Bhardwaj RS, Klosterhalfen B. Abnormal collagen I to III distribution in the skin of patients with incisional hernia. Eur Surg Res 2000;32(1):43-8.

CHAPTER FIVE

A COMPARISON OF THE CLINICALLY RELEVANT BIOMECHANICAL PROPERTIES OF WARP KNIT, FULLY ABSORBABLE BICOMPONENT MESHES WITH TRADITIONAL MESHES FOR HERNIA REPAIR

Introduction

Mesh hernioplasty is the most common general surgical procedure with more than 1 million procedures performed annually worldwide.[1-3] For the last two decades, a so-called "tension-free" mesh surgical procedure has been considered the gold standard for any sizable hernia defect.[4] The majority of the hernia repairs are completed using meshes constructed from non-absorbable polymers, primarily polypropylene (PP), and to a lesser extent polyethylene terephthalate (PET). Although the tension-free, non-absorbable mesh approach to hernia repair has been reported to reduce the incidence of recurrence compared to primary repair,[5-7] traditional mesh physicomechanical properties and their presence in a permanent biomaterial that alters the biomechanics of the abdominal wall has produced several well documented long-term clinical complications.[8-18] Moreover, recent data suggests that while the percentage of inguinal hernia repairs completed with meshes has increased dramatically, the percentage of recurrence has only slightly decreased.[19,20] In fact, questions still remain if current meshes are properly designed[21] and if recurrence rates are actually reduced or simply delayed as a result of the use of traditional meshes.[19,22-24] Consequently, there still exists an unmet need for a mesh which exhibits improved biocompatibility for the repair of abdominal wall defects.

A novel hernia mesh design concept which uses a bicomponent, fully absorbable mesh that temporally modulates biomechanical properties to meet the expected needs of the wound healing process has been suggested (Figure 5.1).[25] To this end, a bicomponent fully absorbable mesh has been developed which provides (1) short-term structural stiffness, (2) a gradual transition phase, and (3) long-term force-extensional properties similar to the abdominal wall (Chapter 2). As a critical component of the device, a fast-degrading, segmented, high-glycolide yarn was developed which has a temporal degradation profile that overlaps the expected commencement of the wound strength profile (Chapter 3).

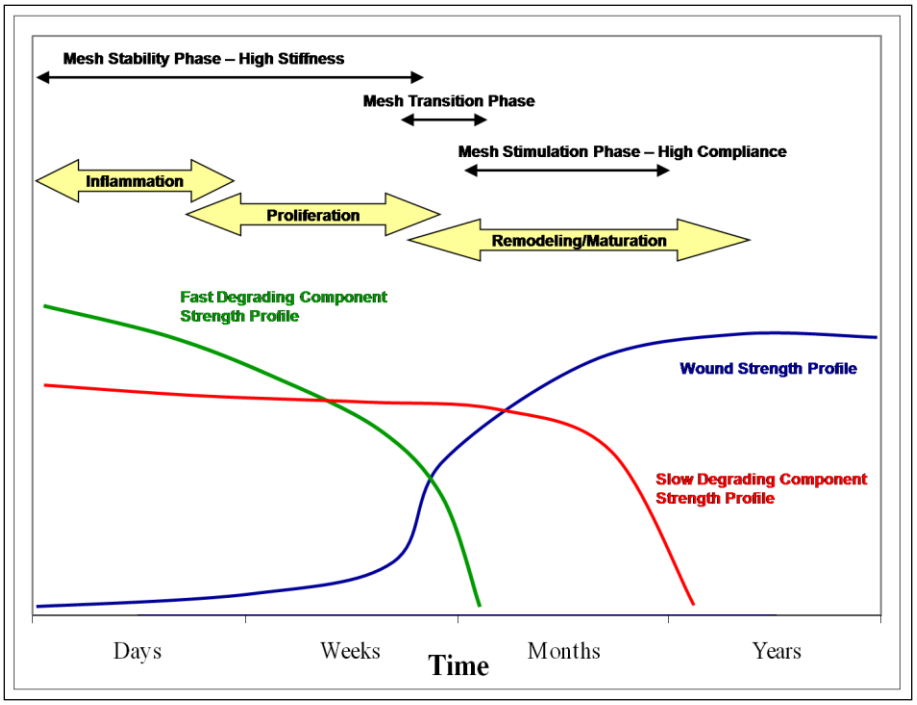

Figure 5.1

The modulated mechanical characteristics of a bicomponent mesh superimposed with the temporal wound healing response.[25]

The wound healing process is dynamic with overlapping phases, each of which has different biomechanical needs. A mesh which considers the temporal phases of the wound healing process by providing structural stability to the developing extracellular matrix and facilitating mechanical stimulation to remodeling collagen may be required to improve mesh biocompatibility. To accomplish this objective a mesh must modulate properties with a load transition period (LTP) that is timed to coincide with the commencement of wound strength. Following the transition phase, a compliant mesh must prevent stress shielding and allow local tissue to adapt to the perceived external loading conditions during the remodeling/maturing process. After a sufficient time period (> 9 months), the slow-degrading mesh should lose integrity and gradually transition the load completely to the repair site. As such, this temporal progression of the wound healing process may produce self-sustaining, functional tissue that resists recurrence.

Abdominal wall biomechanics are complex and largely unknown. Theoretical calculations suggest that a maximum load of 16 N/cm is developed within the abdominal wall.[26] Cobb and coworkers, using bladder pressure to approximate intra-abdominal pressure found that the activities of coughing and jumping may result in a maximum load of 27 N/cm.[27] Using the value of 16 N/cm, measurements of harvested abdominal wall tissue from male cadavers produced an extension in the sagittal plane of 25% ± 7% and transverse plane of 15% ± 7%.[28] Song and coworkers, using carbon dioxide insufflation within the peritoneal cavity, measured a 15 % increase in area with approximately twice the strain in the sagittal plane compared to the transverse plane (10.5% vs. 5%).[29] Other

studies have confirmed that the abdominal wall is twice as stiff in the transverse direction as in the sagittal direction.[30] The investigated shutter mechanism at the inguinal canal suggests the mesh must be able to accommodate uniaxial deformation.[31] Investigations by Peiper and coworkers suggests that the transversalis fascia is predominately loaded by intra-abdominal pressure.[32] As such, the mesh must distend in multiaxial directions to a distributed perpendicular load. Nevertheless, it is well accepted that the abdominal wall is a composite laminate structure of connective tissue which allows expansion or contraction in multiple planes simultaneously.[33] Logic suggests that a mesh placed on the abdominal wall will be required to accommodate uniaxial distension (lateral forces from muscle/aponeurotic structures) and non-isotropic, multiaxial distension (intra-abdominal pressure). Consequently, the evaluation of mesh biomechanics should include uniaxial (tensile) and multiaxial (burst) modes of deformation. Furthermore, since the mesh does not act alone but rather as a mesh/tissue complex, it is clinically pertinent to measure mesh biomechanics as a composite structure.

Mesh biomechanics are determined by the design variables of yarn chemistry and the textile characteristics of knit construction (knit pattern, stitch density, secondary processing), yarn type (monofilament or multifilament), and yarn size (diameter/denier). Collectively, these design variables control the clinically-relevant mesh properties of area weight, porosity, suture pullout force, tear resistance, flexural rigidity, maximum burst force, and the force-extension profile (FEP) response. Each mesh property is regulated by at least one, but generally two or more design variables. As a consequence of the number of design variables and the significant interaction between variables on each

mesh property, a countless number of mesh designs are possible. As a result, hernia meshes differ widely in physical and biomechanical properties. For example, reported data for several commercially available hernia meshes showed that extension at 16 N/cm values varied from 3.5% to 31.0%.[28] This extreme variation in functional characteristics highlights the importance of careful consideration for the impact of each design variable on biomechanics. For a given yarn chemistry and knit construction, the biomechanical properties will be drastically different when the fiber type is changed from monofilament to multifilament. The same is true for yarn size; however, knit construction is the most influential variable on mesh biomechanical properties.

Usher introduced the first knitted, monofilament, PP mesh into clinical practice in 1963.[34] It was estimated in 2000 that 80% of the 750,000 inguinal procedures performed in the United States use the same material and basic mesh design invented by Usher almost four decades earlier.[35-37] Today the overwhelming major of meshes used worldwide are still monofilament PP meshes. Recently, the use of light-weight (LW) meshes has received significant attention in literature[37,38] as a replacement to the so called "heavy-weight" (HW) traditional monofilament PP mesh. The LW mesh concept focuses on lowering area weight and changing the knit construction to an open structure (larger pore sizes). Additionally, some LW mesh constructions incorporate absorbable yarn to produce a partially absorbable (PA) mesh which loses 50%, or more, of original mass *in vivo*. The primary objective for the addition of absorbable yarn is to augment the strength and bending stiffness of the mesh to improve handling characteristics and reduce the long-term foreign body reaction and fibrosis.[39-42] However, this concept has been

challenged and it has been suggested that mesh area weight alone is not a good metric for biocompatibility.[43,44] Nonetheless, large pore sizes from 1 - 5 mm and area weights that are 25-40% of HW meshes are typical of LW meshes. Most LW mesh designs use monofilament PP yarn and some match the extension of the abdominal wall at the maximum physiologic condition (16 N/cm).[26,28] As a result, LW meshes restrict abdominal wall mobility less than HW meshes[45] and there is evidence that their use results in less chronic groin pain.[46-51] LW mesh explants from animal studies have demonstrated good tissue incorporation and mechanical strength.[52] In one study, explants from a canine animal model using LW and HW mesh produced comparable mesh/tissue strength after 90 days even though the LW mesh possessed 3.6 times lower initial strength.[53] However, randomized clinical trial results using LW mesh have not been encouraging. Several clinical studies using LW meshes have shown no reduction in patient complications,[2,54-57] and others have noted an increase in recurrence rates.[58-60] In essence, data from animal studies indicate that LW meshes may improve the quality of collagen within the mesh and clinical data suggest patients experience less chronic pain; though this may be, there is no clear clinical advantage with regard to minimizing long-term complications and recurrence.

Key objectives of the presented study are (1) to characterize the temporal modulation of the clinically-relevant physical and biomechanical mesh properties of two different absorbable bicomponent mesh (ABM), and (2) to compare the physical and biomechanical properties of the investigated ABM with traditional meshes used for hernia repair.

Materials and Methods

Mesh Materials and Construction

Traditional Meshes

Meshes of two types were procured for this investigation, namely Prolene® (PP) and Mersilene® (PET). Both meshes are manufactured by Ethicon, Inc. Prolene® is a high-strength, monofilament, polypropylene mesh which is commonly used for hernia repair. Mersilene® is knit from multifilament PET yarn using a knit pattern that produces a light-weight, open pore construction which contrasts that of Prolene®. Each mesh approximates the upper and lower bounds for the physical and mechanical properties associated with traditional meshes.

Absorbable Yarns

The polymer synthesis and production of yarn for the polymers of MG-17 (Chapter 3) and SMC-7 were previously described (Chapter 2). In summary, MG-17 is a triaxial, segmented, high-glycolide polymer that is melted extruded into a 10-filament yarn. SMC-7 is a linear, segmented, high-lactide polymer that is melt-extruded into a 43-filament yarn. The denier (g/9000 m) of the MG-17 and SMC-7 yarn is 150 and 86, respectively.

Absorbable Bicomponent Mesh

Warp knitting was completed by co-knitting two different knit patterns, then setting with heat to stabilize each mesh construction. Using MG-17 and SMC-7 yarns,

warp knitted absorbable bicomponent meshes (ABM), WK6 and WK7, were prepared using a two-step process of warping yarn onto beams and knitting meshes using a raschel knitting machine (American LIBA, RACOP TR-6). The warping process began with preparing packages of each yarn type which were loaded into a creel and wound onto beams using a warper (American LIBA, GE203A). A total of 90 ends of yarn were wound onto four beams, two holding a two-ply SMC-7 yarn and two holding a single-ply MG-17 yarn. Meshes were constructed using different knit patterns for the SMC-7 yarn between the two constructions of WK6 and WK7.

To accommodate heat setting on circular mandrels, flat mesh sheets were edge sewn into a tube using a standard sewing machine (Brother International, LX3125) and high-strength polyethylene terephthalate yarn. Knit mesh of both types was heat set by stretching the tubular mesh over a stainless steel circular mandrel. Heat setting was completed at 120°C for 1/2 hour while under high vacuum (< 1 torr). Meshes were then cut from the mandrel to produce a stabilized sheet of mesh which was 210 mm wide. Digital images of the PP, PET, and ABM were obtained using a digital camera (Cannon USA, EOS 20D) equipped with a macro lens and mounted on a stand. In addition, images were obtained of each ABM following the removal of the MG-17 yarn. Meshes of the SMC-7 yarn only were obtained by removing the MG-17 yarn from each ABM by accelerated *in vitro* degradation as described below.

Simulated Mesh/Tissue Complex Construction and Properties

Simulated mesh/tissue complex (SMTC) samples of each investigated mesh were prepared by constructing a silicone/mesh composite structure. Part A and B of the silicone elastomer (NuSil Technology, Med 4950) were mixed in equal parts using a 1 liter stainless steel kettle and mechanical paddle wheel stirring apparatus. To facilitate the diffusion of water into the silicone, 10% by weight of polyethylene glycol (PEG; Sigma-Aldrich, M_n = 4,600) was added and evenly dispersed during the mixing process. Silicone/mesh composites were molded using four stacked stainless steel plates (20 x 20 cm) of 1.5 mm thickness. The centers of the middle two plates were cut out (10 x 10 cm) which created the cavity of the mold. Mesh was placed between the middle two mold plates, filled with the uncured silicone/PEG elastomer, compressed for 10 minutes under a pressure of 2.4 MPa (Carver Press, Model 3895), placed under reduced pressure (< 2.5 torr) for 1/2 hour to remove trapped air pockets, and cured at 45°C for 7 days. Cured SMTC samples were 3.5 ± 0.2 mm thick, with the mesh centrally located with respect to the thickness.

Mesh Physical Properties

Accelerated In Vitro Conditioned Degradation

Long-term mesh physical properties, simulated by using only the SMC-7 yarn component of the mesh, were determined for WK6 and WK7 meshes following the degradation and removal of the MG-17 yarn under accelerated *in vitro* degradation conditions. A 0.1 M solution of buffered sodium phosphate was pH adjusted using 5.0 M

sodium hydroxide (Sigma-Aldrich, cat#221465) to a target value of 12.0pH. Using the prepared medium, samples were incubated in 50 mL tubes (VWR International, cat#14231-880) at 50ºC under static conditions for 7-9 days until the MG-17 component was significantly hydrolyzed. Thereafter, samples were scoured in isopropyl alcohol under ultrasonic agitation (Branson, 5510) to remove MG-17 yarn fragments followed by drying under reduced pressure (< 1.5 torr) to a constant weight.

Mesh Area Weight

The determination of mesh area weight followed option C in ASTM D3776-07 *standard test method for mass per unit area of fabric*. Specifically, the area weight for each mesh construction was determined by first using a lever arm fabric cutter to cut 10 cm x 15 cm rectangular samples of annealed mesh. Each sample was then weighed (Mettler Toledo, AB204-S) to the nearest one thousands of a gram. The following equation was used to calculate the area weight in grams per meter squared.

$$\text{Area Weight } \left(\mathrm{g}/\mathrm{m}^2\right) = \frac{\text{Weight of Sample } (\mathrm{g})}{0.015\ (\mathrm{m}^2)}$$

Mesh Thickness

For meshes, thickness is measured as the distance between the upper and lower surfaces of two plates compressed against the mesh and subjected to a specified pressure. Mesh thickness was determined using the procedure as outlined in the ASTM D1777-96 *standard test method for thickness of textile materials*. Using a lever arm fabric cutter, random 57 mm x 57 mm square samples of the annealed mesh were obtained for

evaluation. Each sample was measured in the center of the mesh swatch using a comparator (B.C. Ames, 05-0191) gauge. The comparator gauge was equipped with a 28.7 mm diameter foot and used a 9 ounce weight to apply the standardized pressure to the mesh.

Weight Ratio of the Bicomponent Constituents

The relative weight ratio of the fast and slow degrading component was determined by solvent extraction of SMC-7 from the composite using dichloromethane (DCM). Three random 57 mm x 57 mm square samples of annealed mesh were obtained and weighed (Mettler Toledo, AB204-S). Next, all three samples were placed in 200 mL of DCM for 30 minutes while under constant orbital agitation at room temperature. Samples were removed from DCM, rinsed using acetone, and dried under reduced pressure (< 1 torr) to a constant weight. The initial weight of the three composite samples (W_i) and the final weight of the MG-17 yarn component (W_f) were used in the following equation to determine the percent MG-17 in the composite.

$$\textbf{Weight Ratio of the MG} - \textbf{17 Yarn Component (\%)} = \left[\frac{W_i - W_f}{W_i}\right] \textbf{x 100}$$

Mesh Porosity

Mesh porosity was characterized as (1) a percentage of the mesh covered by pores and as (2) the mean pore size. Photographic images were obtained using a microscope equipped with a camera (Cannon USA, EOS 20D) and evaluated using NIS Elements (Nikon Instruments, Inc) software. The total pore area, or open apertures, for each mesh

was calculated from an obtained image that contained at least 20 large apertures. Manipulation of the images was performed by high-contrast colorizing of the pores followed by software determination of the color covered area. Using this information, the fraction of area covered by pores compared to the total area was determined as a percentage. Using the same image, individual pores were analyzed with respect to area. Since pore shapes are highly variable, both within and among different meshes, the area of individual pores were recalculated to an equivalent average pore diameter and reported as such.

Mesh Mechanical Properties

In Vitro Conditioned Degradation

Samples evaluated for mechanical testing following *in vitro* degradation were conditioned using a 0.1 M solution of buffered sodium phosphate in 50 mL tubes at a 7.2pH. Buffered sodium phosphate was prepared by adding 23.3 grams of dibasic (K_2HPO_4; Sigma-Aldrich, ACS ≥ 98%) potassium phosphate and 9.0 grams of monobasic (KH_2PO_4; Sigma-Aldrich, ACS ≥ 98%)) potassium phosphate into 2 liters of deionized water and stirred until dissolution. A pH meter (Symphony, SB80PI) was used to verify a 7.2pH measurement and slight adjustments were made to using 0.5 M hydrochloric acid (HCl; Sigma-Aldrich, ACS reagent). Tubes (VWR International, cat#14231-880) containing buffer and 4 to 5 mesh samples were placed in racks and incubated at 37°C under constant orbital-agitation (Innova 4300) at a speed of 28 revolutions per minute. Mesh samples were removed at predetermined time periods of 1,

2, 3, 4, 8, 12, 16, 20, 28, 34, and 39 weeks for mechanical properties testing. For SMTC samples, *in vitro* conditioning was conducted for one day (initial) to hydrate the silicone and at the predetermined time period of 8 weeks.

Tensile Properties

Tensile testing of 2.5 cm wide strips of mesh and SMTC samples was conducted using a universal testing machine (MTS, Synergie 100) equipped with a 500 N load cell and a set of wedge grips (Chatillon, GF-9). Each sample was tested using a gauge length of 25.4 mm and constant cross-head traverse of 2.33 mm/s. FEP data was extracted from the system software (TestWorks 4.0) to construct FEP curves.

Burst Properties

Burst mechanical testing of mesh and SMTC samples was conducted using a universal testing machine (MTS, Synergie 200) equipped with a 1 kN load cell. The ball burst test fixture geometry was determined from ASTM D3787-07 *standard test method for bursting strength of textiles-constant-rate-of-traverse ball burst test*. The MTS machine was connected to a data acquisition computer and software (TestWorks 4.0) that recorded the force and displacement of the steel ball. Tests were performed using a 2.54 cm/min constant-rate-of-traverse for the ball. Prior to the initiation of the test, a 0.1 N preload force was placed against the mesh by the ball. For each test the maximum burst force obtained during the test (N) and the extension at 71N load (mm) were recorded. The extension at 71 N was used to determine the elongation at 16 N/cm. The value of 71

N is derived from the diameter of the opening in the clamp plate (4.44 cm x 16 N/cm = 71 N). A detailed explanation of the mathematical expression which relates the linear travel of the ball (mm) to the extension at 16 N/cm (%), can be found in Appendix A. FEP data for each investigated mesh and SMTC was exported from the data acquisition software to construct FEP curves.

Mesh Flexural Stiffness

Mesh flexural stiffness was measured according to the cantilever test method as described in option A of ASTM D1388 *standard test method for stiffness of fabrics*. Test samples were cut to the dimension of 20 mm x 150 mm in the course and wale directions. Test specimens were slid at a constant speed of 120 mm/min until the edge of the specimen deflected under its own mass and touched the knife edge, which was set to a 41.5° angle. The length of the overhang, to the nearest 0.1 cm, was measured on the knife edge scale at the point of contact and recorded as the overhang length (OL). The mass per unit area (w) was expressed in mg/cm^2. The following formulas were used to calculate the bending length and flexural stiffness:

Bending length $c = OL / 2$ (cm)

Flexural stiffness $G = w \times c^3$ (mg•cm)

Suture Pullout Force

The suture pullout force test was completed using a universal testing machine (MTS, Synergie 200) and a set of wedge grips (Chatillon, GF-9). Using a lever arm fabric cutter, fourteen 20mm x 50mm samples were cut from each mesh type, seven

samples with the 50mm length direction corresponding to the course direction and the other seven in the wale direction. In the course direction, half of each sample was clamped in the lower wedge jaw and a 2/0 monofilament polypropylene suture was threaded through the mesh at a distance of 6-9 mm from the upper edge. The ends of the suture were secured in the upper wedge grip and the test was completed at a speed of 75 mm/min. The maximum force obtained during the test was recorded for each sample.

Tear Resistance

Tear resistance testing was conducted using a universal testing machine (MTS, Synergie 200) and a set of wedge grips (Chatillon, GF-9). Samples measuring 30 mm x 80 mm were cut in the wale and course directions for each mesh type. To initiate the location of the tear, a 10 mm deep defect was created from one edge at the midpoint of the 80 mm long side. Each mesh was secured in the grips with the 10-mm slit centered between a 20 mm gauge length. Testing was conducted at 50 mm/min and the maximum force obtained during the test was recorded.

Statistical Analysis

Significant differences in physical properties between initial and *in vitro* conditioned ABM and the traditional meshes were completed using a student's t-test to compare means. For temporal *in vitro* conditioned ABM, a two-factor analysis of variance (ANOVA) was used to test for effects due to time and mesh construction for the response variables of maximum burst force (MBF) and extension at 16 N/cm. All

analysis was completed using statistical analysis software (SAS, version 9.2) and a p-value less than 0.05 was considered to be significant.

Results

Mesh Materials and Construction

Figure 5.2 provides comparative images of each mesh construction. Figure 5.3 provides comparative images of each traditional mesh, PP and PET, and each ABM construction, both initially and following the accelerated *in vitro* conditioned degradation of the MG-17 yarn.

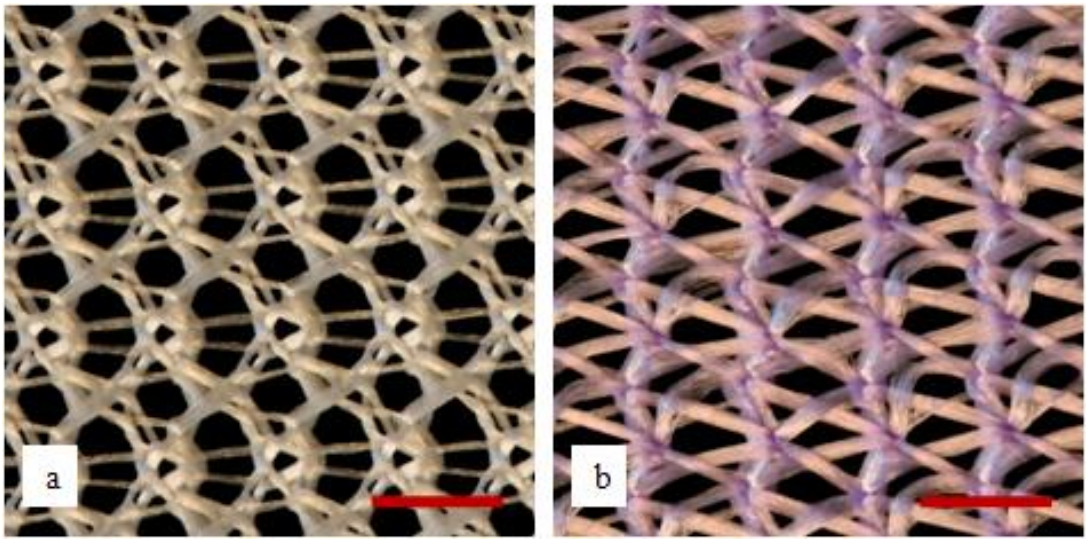

Figure 5.2

Images of the knit construction for the (a) WK6 and (b) WK7 meshes. (Red scale bars = 3 mm)

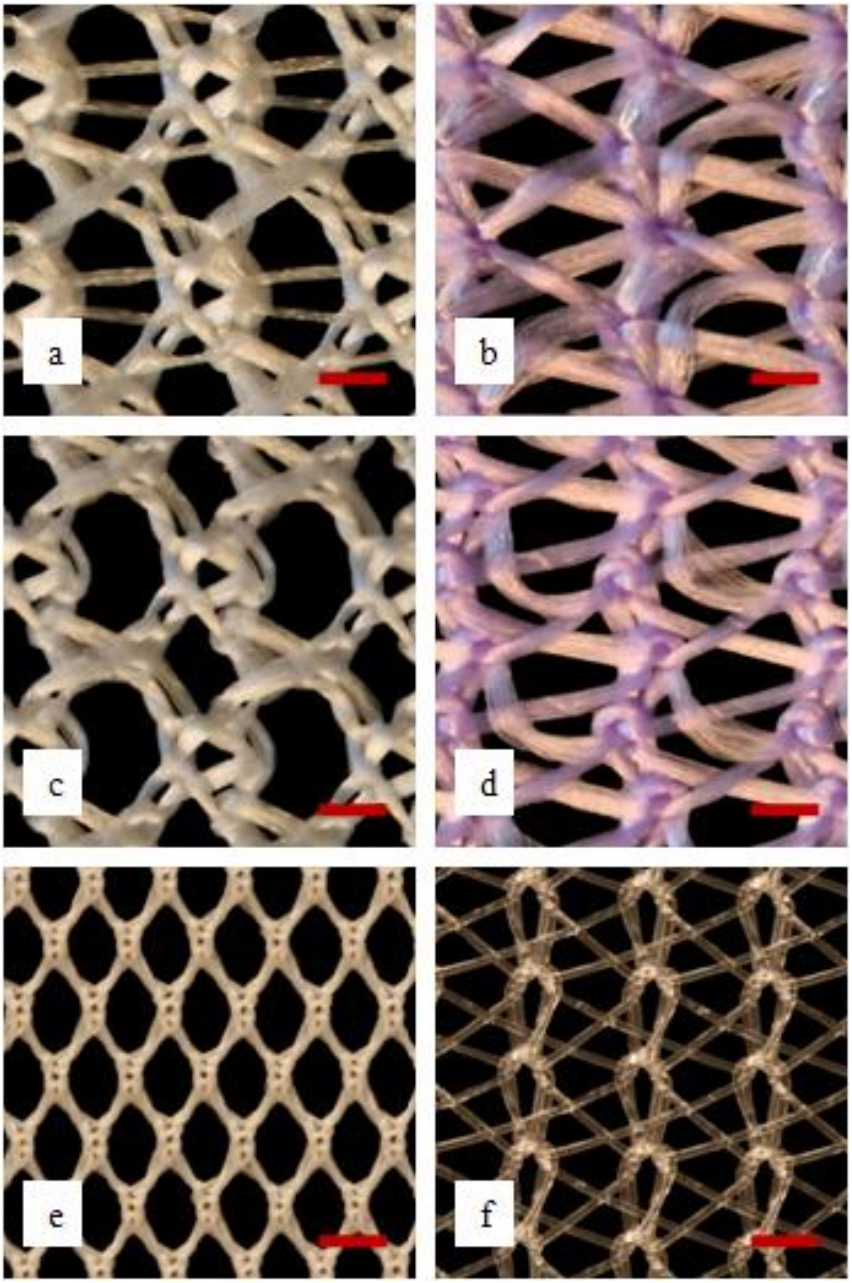

Figure 5.3

Images of the knit construction for the WK6, WK7, PP, and PET meshes. (a) WK6 mesh (b) WK7 mesh (c) SMC-7 yarn component of the WK6 mesh (d) SMC-7 yarn component of the WK7 mesh (e) PET mesh (f) PP mesh (Red scale bars = 1 mm)

Mesh Physical Properties

Table 5.1 lists the clinically-relevant physical properties of each evaluated mesh. The WK6 and WK7 meshes were also evaluated following accelerated *in vitro* conditioning to assess the long-term physical properties following the substantial degradation of the MG-17 component.

Table 5.1

Initial and *In Vitro* Conditioned Mesh Physical Properties for the ABM, PET, and PP (n = minimum of 5)

Mesh Description		Thickness (µm)	Area Weight* (g/m^2)	Porosity		
				Pore Area (%)	Mean Pore Diameter (µm)	Pore Diameter Range (µm)
WK6	Initial	530 ± 30	138 ± 3	34.4 ± 1.7	698 ± 27	281 - 1068
	In Vitro Conditioned	362 ± 12†	82 ± 4†	37.7 ± 1.4	1180 ± 64	368 - 1568
WK7	Initial	626 ± 15	146 ± 2	21.8 ± 0.6	543 ± 20†	230 - 1063
	In Vitro Conditioned	351 ± 10†	102 ± 2	24.7 ± 1.9	601 ± 43†	252 - 1173
PET		266 ± 13	41 ± 2	59.8 ± 2.0	930 ± 43	827 - 983
PP		514 ± 10	83 ± 6†	44.9 ± 1.7	555 ± 21†	445 - 752

*Ratio of constituents determined by solvent extraction of SMC-7 for the ABM: WK6 = 41 ± 1%; WK7 = 31 ± 1%
† Indicates corresponding samples that were not found to be significantly different ($p > .05$)

The mesh thickness was significantly reduced following *in vitro* conditioning for both ABM. The thickness of the ABM were initially thicker than PP (514 µm) but after *in vitro* conditioning the WK6 and WK7 meshes were thinner with values of 362 µm and

351 µm, respectively. The *in vitro* conditioned area weight measurement for the WK6 was significantly lower than that of WK7 and not different than PP. The thickness and area weight of PET was substantially lower than any other evaluated mesh.

Following the *in vitro* conditioned degradation of MG-17, the mean pore diameter for the WK6 mesh increased from 698 µm to 1180 µm ($p<.001$) which increased the maximum value of the range by 47%, from 1068 µm to 1568 µm. To a lesser degree, the WK7 mesh showed a significant increase in pore area ($p = 0.022$) with a marginally significant change in mean pore diameter ($p = 0.053$). In addition, for the WK7 mesh the maximum value of the range slightly increased by 11% from 1063 µm to 1173 µm. The pore area for the traditional meshes was significantly greater than either ABM. However, the mean pore diameter for the *in vitro* conditioned WK6 was greater than all of the other evaluated meshes at 1180 µm. The pore diameter for WK7 and PP were not different ($p > .102$) and were significantly smaller than those of the WK6 and PET. Overall, the *in vitro* conditioned WK6 had the largest pore diameter with the largest pores being 37% and 52% greater than PET and PP, respectively.

Mesh Mechanical Properties

Mesh mechanical properties listed in Tables 5.2 and 5.3 were evaluated to determine differences in initial strength, stiffness, and extensibility for each mesh using clinically-relevant test methods. PET produced the lowest and most isotropic suture pullout force, tear resistance, and flexural stiffness of the investigated meshes. The ABM and PP mesh were at least twice the value of PET for each of the tested mechanical

properties. The ABM and PP produced significant resistance to tearing. Of the three meshes, a mean range of 78.4 N to 146.9 N was observed. Flexural stiffness measurements indicated that PP mesh was significantly stiffer than all of the other meshes. The ABM produced moderate levels of stiffness.

Table 5.2

Suture Pullout Force, Tear Resistance, and Flexural Stiffness Data for the ABM and Traditional Meshes (n = 7)

Property		**WK6**		**WK7**		**PP**		**PET**	
		Wale	**Course**	**Wale**	**Course**	**Wale**	**Course**	**Wale**	**Course**
Suture Pullout Force (N)	Mean	54.0•	37.0‡	48.3•	37.2‡	49.5•	67.5	14.7†	14.1†
	SD	3.8	3.2	2.6	4.0	9.4	7.6	1.1	1.9
	Min	46.7	34.1	45.1	30.8	39.0	55.7	12.8	11.0
	Max	58.6	41.6	52.6	44.1	63.4	80.8	16.2	16.4
Tear Resistance (N)	Mean	78.4	132.1‡	95.4	146.9‡	137.2‡	112.1	47.4†	34.8†
	SD	8.2	13.9	8.8	8.8	22.9	14.4	5.2	4.1
	Min	68.7	107.9	81.7	132.6	118.5	90.3	37.5	30.1
	Max	90.5	149.3	108.7	156.9	167.4	127.0	54.2	41.2
Flexural Stiffness (mg•cm)	Mean	234.2‡	299.0‡	177.3	272.2‡	645.4	454.8	22.5†	8.5†
	SD	31.7	85.1	44.1	48.4	31.2	89.2	3.4	0.8
	Min	195.2	199.4	111.2	192.6	605.4	342.1	17.4	7.4
	Max	301.1	450.5	257.1	340.4	700.5	580.5	26.0	9.6

† ‡ • Indicates corresponding samples that were not found to be significantly different ($p > .05$)

Table 5.3

Burst Test Data for the ABM and Traditional Meshes (n=7)

		WK6	WK7	PP	PET
Maximum Burst Force (N)	Mean	421	602	839	184
	SD	23	26	61	4
	Min	393	582	774	179
	Max	443	631	911	189
Extension at 16 N/cm (%)	Mean	5.5†	6.1† ‡	6.4‡	11.6
	SD	0.3	0.2	0.9	0.4
	Min	5.2	5.9	5.8	11.3
	Max	5.8	6.4	7.6	12.1

† ‡ Indicates corresponding samples that are not significantly different ($p > .05$)

From the burst test data it is obvious that the maximum burst force between each evaluated mesh varied considerably. PP mesh was the strongest, producing about 4.5 times the resistance to central burst as that of PET mesh. The ABM were markedly different as well with 421 N and 602 N burst force values for the WK6 and WK7 meshes, respectively. However, the WK6, WK7, and PP meshes all exhibited similar extensibility at 16 N/cm. In addition to being the weakest, PET mesh was the most extensible producing nearly twice the extension at 16 N/cm as each of the other meshes.

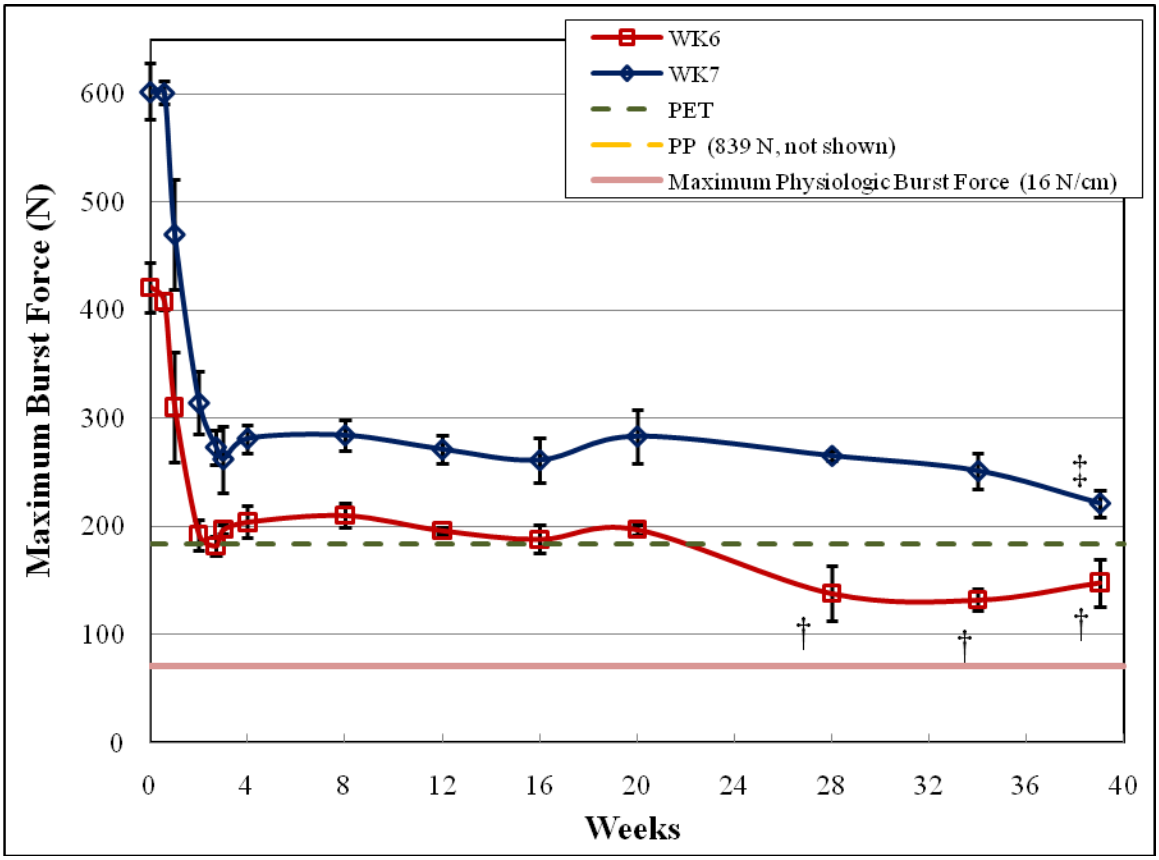

† ‡ Indicates samples from 8 to 39 weeks that have significantly different burst force than those recorded at the 4 week time period ($p < .05$)

Figure 5.4

The temporal *in vitro* conditioned maximum burst force for the ABM during mechanical burst testing (7.2pH, 37ºC). Initial burst test data obtained for PET and PP, as well as the maximum physiologic burst force at 16 N/cm, has been included for comparison (n = minimum of 4).

Figures 5.4 and 5.5 depict the effect of *in vitro* conditioned degradation on temporal changes in maximum burst force and extension at 16 N/cm. The failure of mesh burst test samples was centrally located and at no time did the mesh slip between the plates. At each time period, the WK7 mesh exhibited a significantly greater maximum burst force (all $p < .001$) with mean values at least 62 N greater than that of the WK6

mesh. Both ABM experienced a significant reduction in maximum burst force during the first 2 weeks (all $p < .005$) which was followed by an inflection and slight increase in maximum burst force from 2 to 4 weeks. Beyond 4 weeks, the WK6 mesh produced a reduction in burst force at 28 weeks which was unchanged through 39 weeks (9 months). Beyond 4 weeks, the WK7 mesh first realized a significant reduction at 39 weeks ($p = .011$). Both ABM types showed maximum burst force values at 39 weeks which were at least twice that of the maximum physiologic burst force.

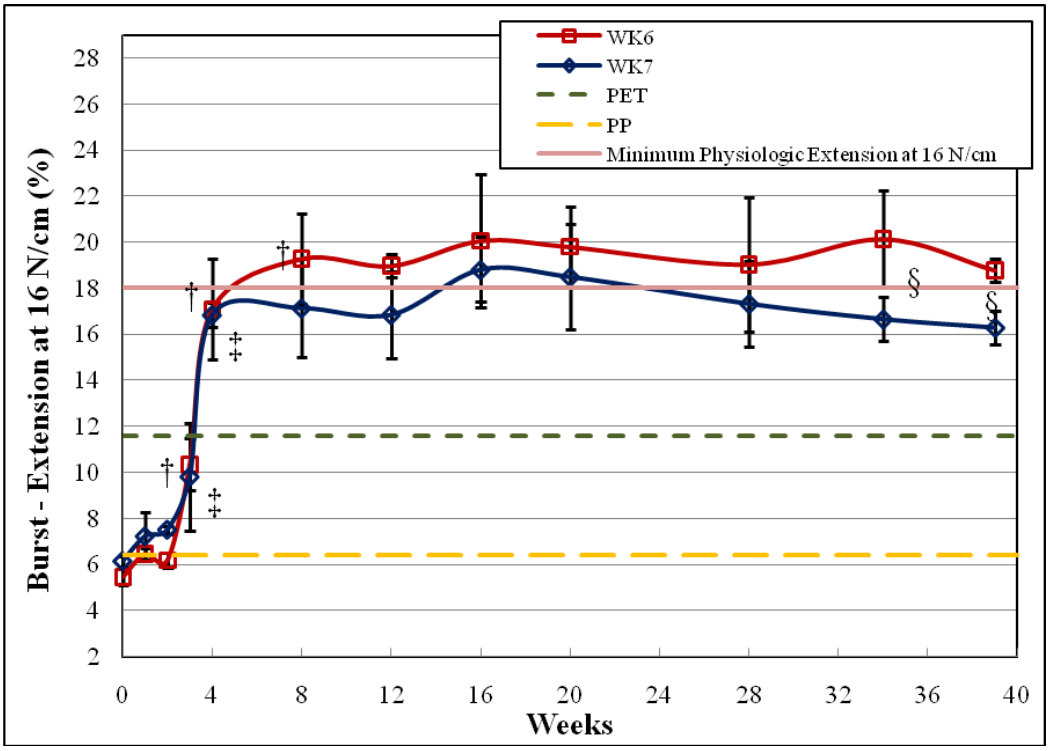

† ‡ Indicates a significant difference from the previous time period for the WK6 (†) and WK7 (‡) meshes ($p < .05$)
§ Indicates a significant difference between WK6 and WK7 samples at the indicated time period ($p < .05$)

Figure 5.5

The temporal *in vitro* conditioned extension at 16 N/cm for the ABM during mechanical burst testing (7.2pH, 37ºC). Burst extension at 16 N/cm test data obtained for PET and PP have been included for comparison. In addition, the minimum physiologic extension at 16 N/cm (25% ± 7%) has been shown as a reference (n = minimum of 4).

Figure 5.5 depicts the extension at 16 N/cm for the ABM during burst testing. For the first 14 days of *in vitro* conditioning, the ABM possessed an unchanged, low level of extension (all $p > .266$) that was similar to that of the PP mesh. In the subsequent days, a transition in the extension at 16 N/cm for the ABM was realized between the time periods of 2 and 8 weeks and 2 and 4 weeks for the WK6 and WK7 meshes, respectively. Beyond 8 weeks, no change for either ABM was observed (all $p > .123$). No difference in extension at 16 N/cm was observed between the ABM from 8 to 34 weeks. Furthermore, both ABM approximated the minimum physiologic extension at 16 N/cm (18%) of the abdominal wall after 4 weeks and maintained this degree of extensibility through 39 weeks. Although not statistically significant until after 34 weeks, the mean extension was greater for the WK6 mesh.

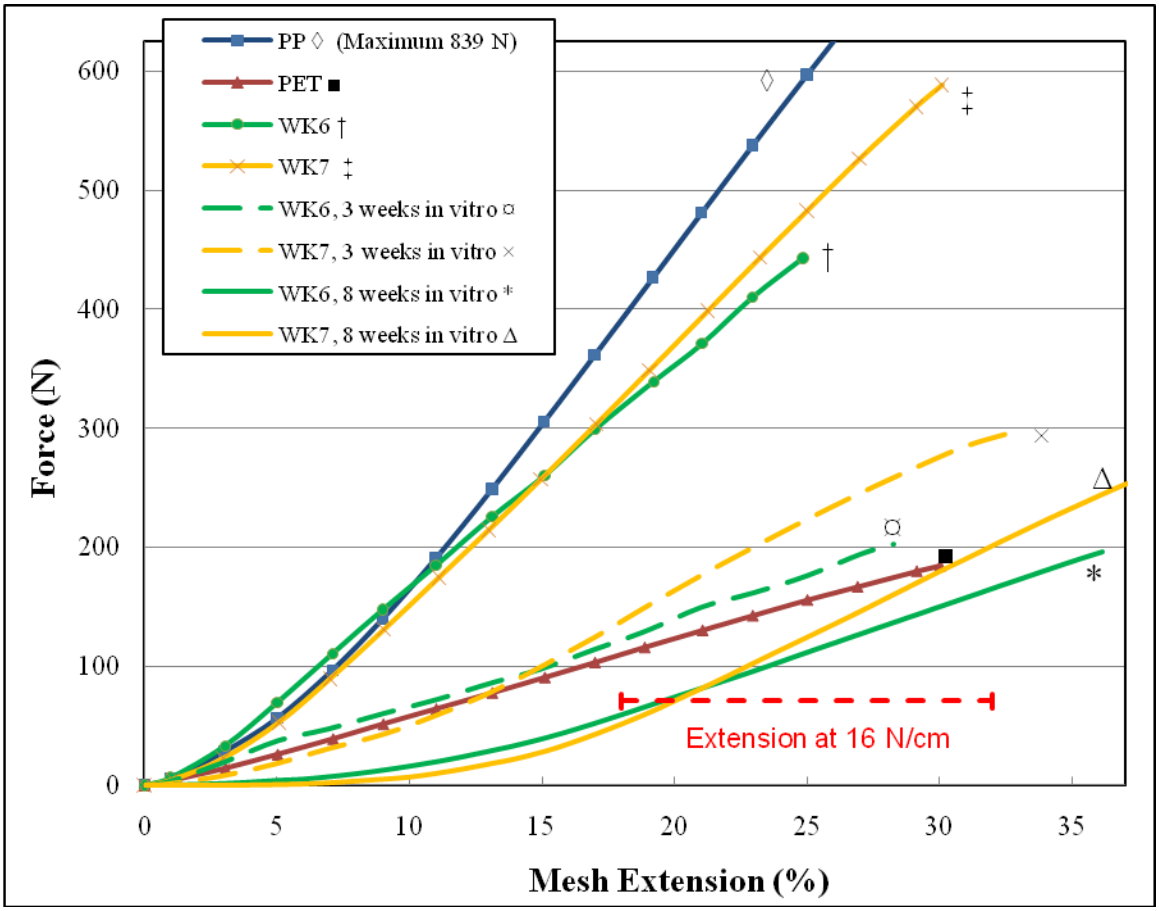

Figure 5.6

FEP data for burst testing of ABM, PET, and PP meshes. ABM results are shown of initial phase (stability phase), at 3 weeks (transition phase), and at 8 weeks (remodeling phase) of *in vitro* conditioning (7.2pH, 37ºC). The dotted red line represents the range associated with the maximum physiologic loading condition of the abdominal wall (16 N/cm).

In Figure 5.6, FEP data in the burst test mode is depicted for the resistive mechanical force of different meshes over the entire range of applied strain until failure. With the exception of the 3 week *in vitro* data for the ABM, each set of data exhibited a curved profile which transitioned to a linear response until failure. However, the

curvature, transition point, and slope of the linear portion of each profile were drastically different among the meshes and within the different *in vitro* time periods of the ABM. In general, the different profiles can be segregated into three groups of high, moderate, and low structural stiffness. The first group contains the initial ABM (stability phase) and PP mesh. Each of these meshes produced profiles that exhibited an initial curvature with a transition by 5% extension into a high stiffness, linear response until failure at a force significantly above the physiologic maximum value. The moderate group contained the 3 week *in vitro* conditioned ABM (transition phase) and PET mesh. PET was slightly less resistant up to about 12% extension where its stiffness increased at a greater rate than the ABM. The ABM showed an almost linear response with a level of structural stiffness that divided its initial and long-term FEP response. Finally, the third group consisted of only the 8 week *in vitro* conditioned ABM. Each ABM started with a low level of stiffness that gradually transitioned into a linear response. The 8 week *in vitro* conditioned ABM were the only samples which passed through the range of force-extension values which represented the maximum physiologic loading condition of the abdominal wall.

Simulated Mesh/Tissue Complex Properties

Figures 5.7 through 5.10 depict the burst and tensile FEP response of mesh and SMTC samples using ABM and traditional meshes. Results showed that the resistive force to an applied strain increased for SMTC samples. However, for meshes that showed high structural stiffness, the relative difference between the mesh and

corresponding SMTC sample was negligible. For example, the high degree of mesh structural stiffness dominated the resultant FEP for SMTC samples during the burst testing of PP, WK6, and WK7, as well as, during tensile testing of WK6 and WK7.

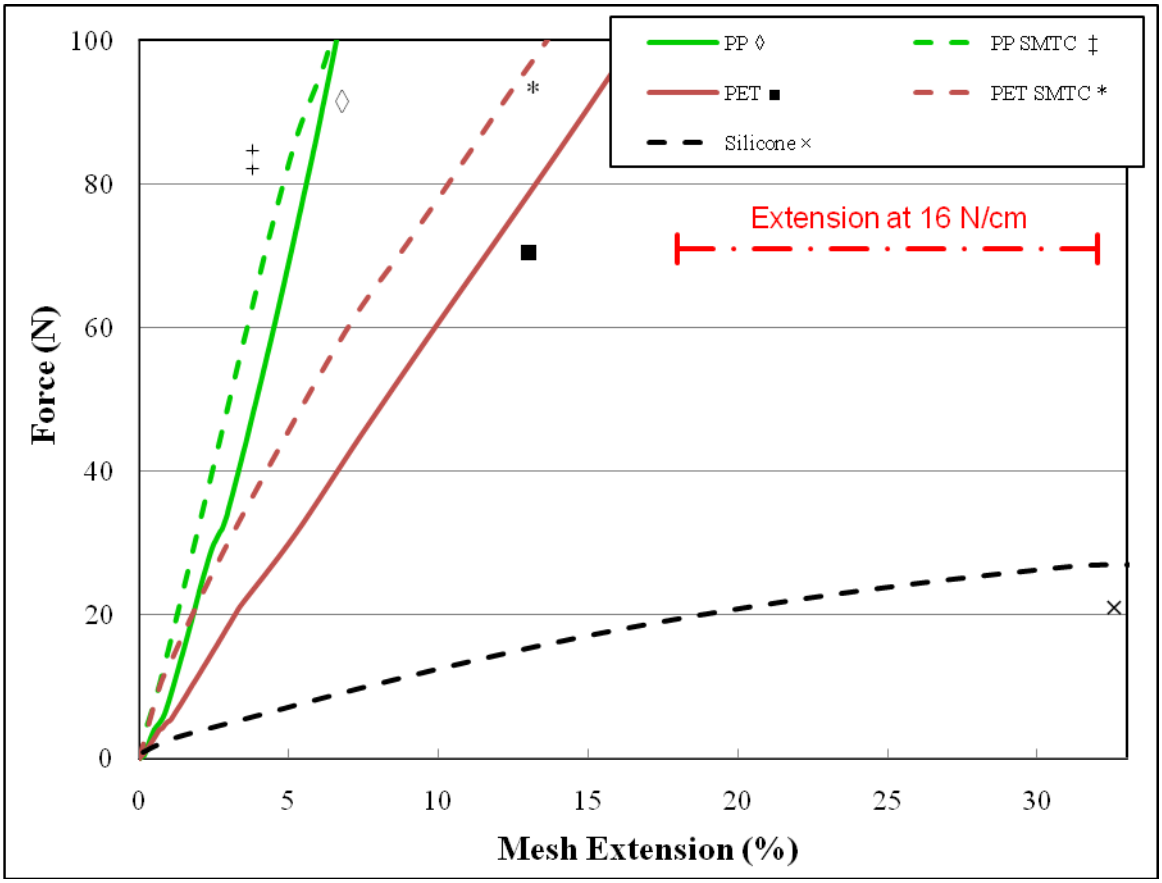

Figure 5.7

FEP data for multiaxial burst testing of SMTC using traditional meshes. The dotted red line represents the force-extension range associated with the maximum physiologic loading condition of the abdominal wall (16 N/cm).

In Figures 5.7 and 5.8, only the 8 week *in vitro* conditioned ABM produced a FEP which exhibited lower stiffness than the simulated matrix (silicone) up to approximately 10-12% of mesh extension. Burst tested 8 week *in vitro* conditioned ABM samples passed through the range of force-extension values which represented the maximum physiologic loading condition of the abdominal wall. However, the WK6 SMTC produced a FEP profile that was almost linear with an extension at 16 N/cm and was slightly below the maximum physiologic range (~ 15%). In comparison, the WK7 SMTC produced approximately half the extension at 16 N/cm as did the WK6 SMTC.

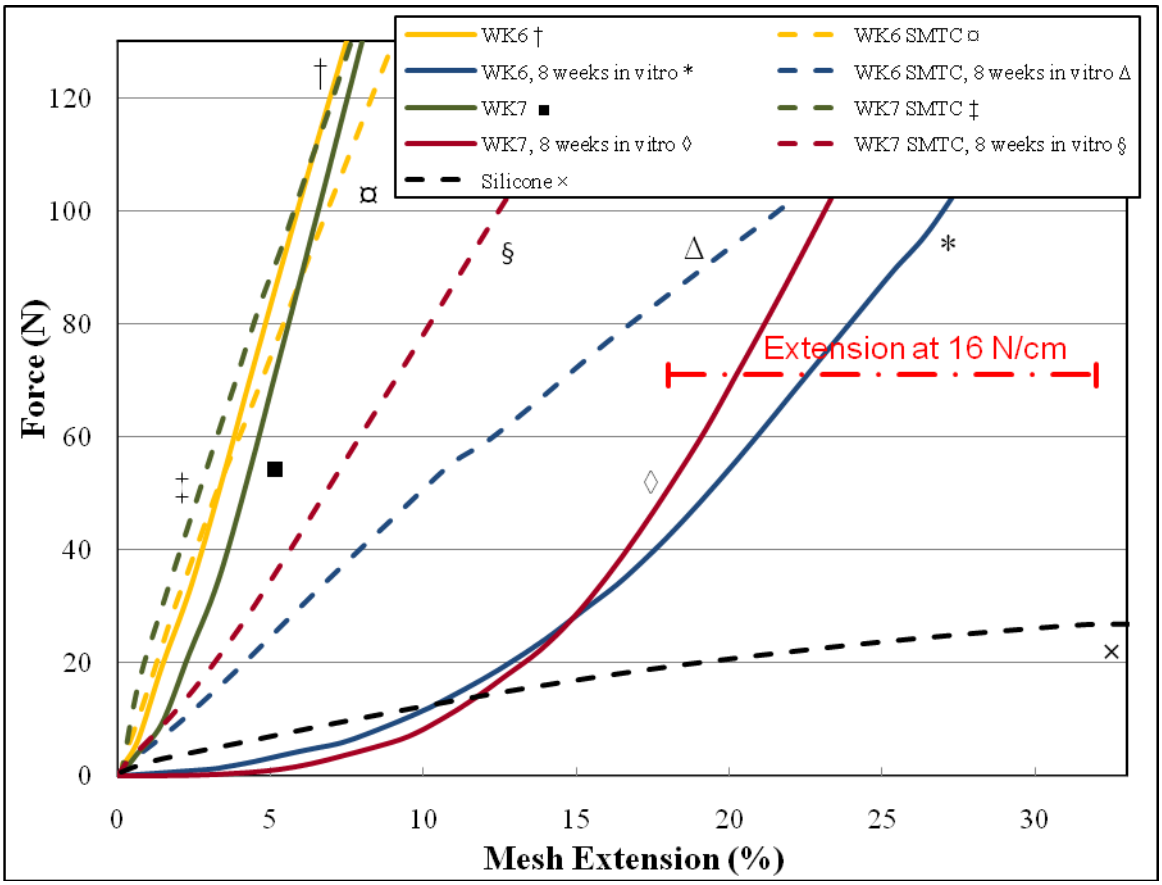

Figure 5.8

FEP data for multiaxial burst testing of SMTC using ABM. Data are from the initial (stability phase) and the 8 week (remodeling phase) *in vitro* conditioned samples (7.2pH, 37ºC). The dotted red line represents the force-extension range associated with the maximum physiologic loading condition of the abdominal wall (16 N/cm).

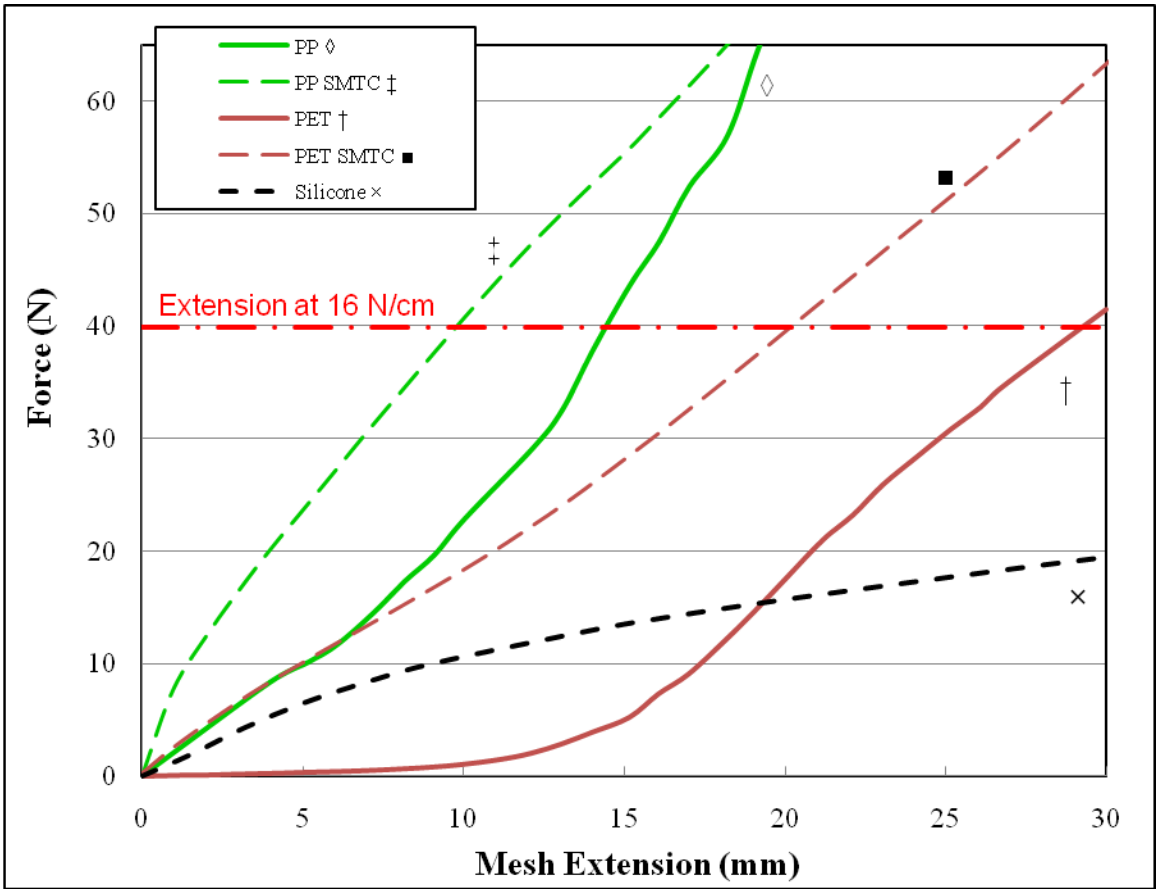

Figure 5.9

FEP data for uniaxial tensile testing of SMTC using PET and PP mesh in the course direction. The dotted red line represents the maximum abdominal wall loading condition (16 N/cm). (25.4 mm extension represents a strain equal to 1)

FEP data for uniaxial tensile testing depicted in Figures 5.9 and 5.10 showed that, for low strain values, the 8 week *in vitro* conditioned ABM exhibited lower stiffness than the simulated matrix. Similar to the result observed during burst testing, the WK6 SMTC possessed a greater degree of extension at 16 N/cm than did the WK7 SMTC. Unlike the response for burst testing, PET mesh produced an initial low stiffness FEP response for uniaxial testing which was below the simulated matrix. In the form of a SMTC, the PET

mesh possessed increased stiffness, but did maintain a level of extensibility similar to the WK6 SMTC. The PP mesh was stiffer than the simulated matrix for all strain values in tensile and burst testing.

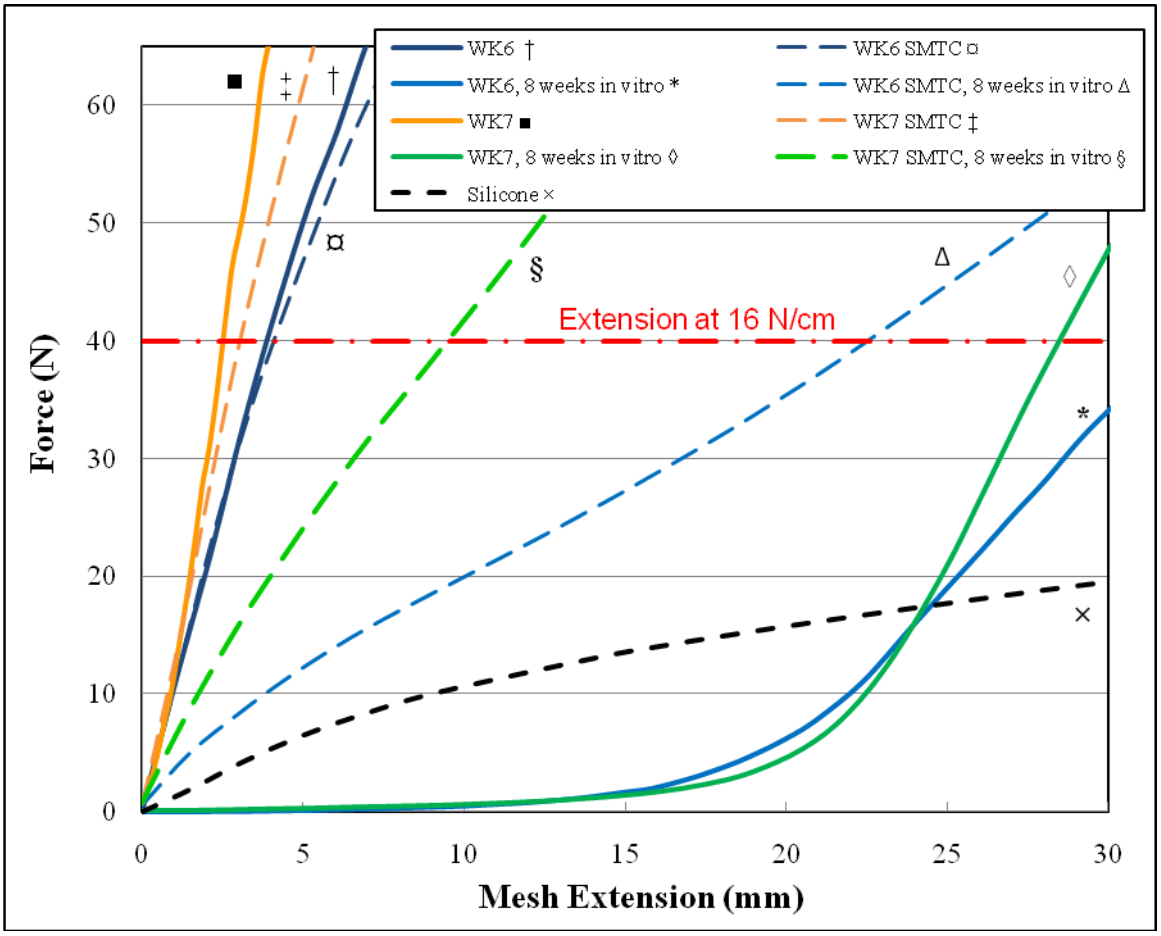

Figure 5.10

FEP data for uniaxial tensile testing of SMTC using ABM in the course direction. Depicted data for the initial (stability phase) and the 8 week (remodeling phase) *in vitro* conditioned samples (7.2pH, 37ºC). The dotted red line represents the maximum abdominal wall loading condition (16 N/cm). (25.4 mm extension represents a strain equal to 1)

Discussion

Biocompatibility is a complex concept that continues to evolve as research uncovers the cause and effect relationship of biochemical and biomechanical influences on the pathology of disease and wound healing. The active stimulation or suppression/allowance of biological responses, consideration for cellular signaling through biochemical and biomechanical pathways, and recognition that the inertness of the biomaterial is not the only mediator of biocompatibility have increasingly been recognized as important design considerations. Historically, HW meshes have been designed to produce a perceived mechanically robust repair site, due to their significant strength, and to have minimal interaction with the biological environment due to the use of inert PP monofilament yarn. However, these meshes have not taken into account the concepts of establishing early wound site stability and restoring physiologic abdominal wall biomechanics in the long-term. The influence of mesh biomechanics on the cellular and extracellular matrix (ECM) responses of the wound healing process may be critical to improving mesh biocompatibility.

As a primary design objective, a surgical mesh must exhibit mechanical properties that prevent acute catastrophic failure of the device. In particular, the mesh should have mechanical integrity such that the mesh does not centrally burst, tear from an edge, or allow the suture to pull through an edge. ABM exceeded mean suture retention values reported for fascia (16.9 N).[61] Furthermore, suture pullout force and tear resistance values for the ABM were significantly greater than PET, comparable to that of PP, and similar to values reported elsewhere.[38,62] All and all, reports of the mechanical failure of

traditional meshes are uncommon; the mechanical strength properties of the ABM mesh were greater than PET and similar to PP. Hence, the mechanical integrity of the ABM is expected to resist acute failure. In spite of the rare reports of traditional mesh acute mechanical failure, mesh complications due to planar migration and tissue erosion is a documented complication.

Logic suggests that a mismatch between the implant flexural stiffness and the surrounding tissue will cause erosion in the latter. Results of this study were consistent with other findings that HW PP monofilament meshes possess high flexural stiffness.[63] As a result, HW meshes have significant structural memory with a limited ability to conform to anatomical structures.[64] As a consequence, the use of HW meshes has been implicated in tissue erosion with potentially severe complications.[65] For example, the mesh can erode into the abdominal cavity causing visceral adhesions and/or fistula formation.[19] Yarn form, type, and construction are mesh design factors which affect flexural stiffness. Multifilament yarn morphology provides flexibility and drapability which is essential to the conformation of the mesh to anatomical structures. Despite the potential clinical advantages, the use of multifilament yarn for meshes has been limited due to reports of increased infection rates.[66-70] Therefore, stiff monofilament meshes have gained favor but with the unintended consequence of increased flexural stiffness and reduced extensibility. The very fine filament and open pore construction of the PET mesh produced substantially lower flexural stiffness values than all of the other tested meshes. Flexural stiffness measurements show that the ABM provides a high level of conformity even during the initial noncompliant stability phase. Although flexural

stiffness measurements were not made on *in vitro* conditioned samples of the ABM, stiffness values close to those determined for PET would be expected due to the similar multifilament, open pore construction. As a result, the likelihood of the mesh to erode through adjacent tissue layers would be reduced. With respect to infection, the absorbable multifilament yarn used to construct the ABM may have less susceptibility to infection than meshes constructed from nonabsorbable multifilament yarn. For instance, the fast-degrading yarn creates a dynamically changing mesh surface with the substantial loss of approximately one-third of the meshes mass within 3 months. Moreover, the median interval for late-term infection has been reported to be 2 years;[71] at this time period the slow-degrading mesh component will be substantially degraded and macrophages will have access to any harbored bacteria. In a similar manner, absorbable suture (Vicryl®) has been documented to be more effective at preventing surgical site infection than a nonabsorbable suture.[72]

Although the design of meshes to resist maximum physiologic conditions is critical to preventing acute device failure, improved biocompatibility will likely be achieved from evaluating and optimizing sub-failure mesh biomechanics. It is common to characterize the extension of hernia meshes using a single data point (extension at 16 N/cm) representing the maximum physiologic loading condition; however, to date the FEP response of meshes has been given minimal attention. The evaluation of FEP data illustrates mesh biomechanics at sub-failure or normal physiologic conditions. Unfortunately the exact FEP of the abdominal wall is not well established. However, current knowledge indicates that the profile passes through a range of extension values

associated with the maximum physiologic condition. For burst testing, the strength and force-extension response of each mesh has relevance within an evaluation window bounded by the maximum physiologic force[26] (< 71 N for 16 N/cm) and the maximum expected physiologic extension at that force (< 32%).[28] For uniaxial tensile testing it should be noted that only low to moderate (strain < 1) levels of uniaxial deformation are clinically -relevant. Significant changes to the mesh length/width aspect ratio are limited clinically by secured mesh edges and pores, which are infiltrated with tissue.

To better simulate the *in vivo* environment, sub-failure biomechanical FEP data for each mesh was investigated in a simulated mesh/tissue complex (SMTC) model at physiologic loading conditions. The silicone simulated matrix does not precisely replicate ECM biomechanics; rather, it provides a synthetic analog which is reproducible and homogenous to evaluate the effect of ECM infiltration on different mesh designs. As such, the SMTC can illustrate mesh stress shielding of the matrix and alterations in mesh biomechanics due to the wound healing process.

Early wound stability facilitated by the mesh may be an important factor in the timely resolution of the wound healing process. The healing processes for soft tissue where significant amounts of granulation tissue are formed, as is the case for secondary intention dermal wounds, require early wound stability. A scab functions to provide stability to a dermal wound site and to temporarily shield the fragile soft tissue from external insults.[73] Also, the importance of initial implant stability during bone healing is increasingly being recognized. Primary stability of the implant for the first 2-3 weeks, which facilitates secondary stability created by the deposition of bone, expedites the

wound healing process for endosseous implants.[74] In a similar manner, the ABM will provide stability until the ECM is anchored into the surrounding tissue. The initial healing response to a foreign body, such as a mesh, includes high cellular activity with abundant deposition of fragile, immature collagen as the body attempts to isolate the implant. During the inflammation and early in the proliferation phase, the developing collagen has practically no strength and an externally applied strain can disrupt the developing ECM and vascular constructs. Therefore, stabilization of the neotissue will minimize disruptions that slow the wound healing process and stimulate the production of pro-inflammatory cytokines.

Compared to traditional meshes, the observed significant resistance to uniaxial and multiaxial induced strain by the ABM will improve early stability of neotissue. The FEP response for multiaxial burst testing of the ABM, PET, and PP meshes using the SMTC model showed a high degree of stress and strain shielding. Additionally, the ABM SMTC also significantly resisted deformation during uniaxial tensile testing. This unique biomechanical response is the result of the knit pattern of the interpenetrating fast-degrading yarn which constrained pore deformation. Consequently, the ABM shielded an externally applied strain by resisting the relative displacement of mesh pores in multiple axes. As such, during the initial phases of wound healing the ABM more closely emulated the stiffness of a woven, rather than a knitted structure. This novel biomechanical stability may have clinically -relevant advantages such as reduced recurrence rates and less mesh contraction (Chapter 2). In addition, the structural stability of such a knitted structure improves surgical handling and placement. Following

the early stability phase for the ABM, the substantial degradation of the fast-degrading yarn temporally modulates biomechanical properties such that load is partially, and eventually fully, transferred to the ECM.

The ABM concept results in two load transfer periods (LTP) to the local tissue with a gradual transition of the perceived load at 2-3 weeks and again at greater than 9 months. The importance of fracture stability with properly timed subsequent mechanical stimulation in the bone healing process has been realized for decades. More recently, research in tissue engineering, and more specifically mechanobiology, has reinforced the importance of mechanical stimulation in soft tissue, and to a lesser extent the importance of early stability. An intermediate LTP is required to achieve the modulation of biomechanical properties from a single implant. The use of a fast-degrading yarn facilitated the ability of the ABM to temporally alter biomechanical properties of the mesh at a LTP which coincides with the expected development of collagen integrity. *In vivo* this phenomenon has been reported in a rat model to initiate at 2-3 weeks following the surgical procedure and is associated with significant collagen infiltration.[26] Abdominal wall fascial defects have a rapid healing capacity that results in fast strength recovery;[75,76] for example, fascial wounds in rabbits were observed to rapidly increase in strength from 1 to 6 weeks. At 6 weeks the wound strength was 40-70% the strength of unwounded tissue.[77] Douglas investigated the strength recovery for an incision in the lumbar aponeurosis of a rabbit model and found that the strength increased 20% after 2 weeks, 50% after 1 month, and after 6 months the strength reached a plateau at 60 – 80% compared to the unwounded control.[78] Furthermore, in this study the *in vitro*

investigation of the second LTP determined that the high-lactide yarn mesh provided better than 9 months of strength retention, with meaningful strength retention expected for greater than 12 months. Under mechanically stimulated, aseptic wound healing conditions after 9 months the wound site will achieve significant and near maximum strength. In a previous canine study the use of a LW mesh was able to produce a mesh/tissue complex that resulted in a burst strength several fold greater than the mesh itself after 90 days.[53] The significant increase in strength was attributed to collagen quality. The quality and strength of the resultant tissue will be heavily influenced by the biomechanical cues provided during the collagen maturation process.

Although the understanding of how fibroblasts respond to mechanical signals is incomplete, it is clear that mechanical stimulation is required and is responsible for hard and soft tissue adaptation. Tissue adaptation results routinely following wound healing, just as physiological changes in morphology follow tissue functional requirements. Collagenous connective tissue remodeling is influenced by a complex combination of crosslinking degree and collagen type, which alter structure, composition, and mechanical properties.[79] Fibroblasts sense mechanical changes in their ECM environment, transducer mechanical signals into chemical information, and integrate these signals with growth factor derived stimuli to achieve specific changes in gene expression.[80] For fibroblasts in connective tissue, the production and modification of the ECM is a primary response to changes in the mechanical environment. For biological systems this is a continuous evolutionary process so as to attain, and maintain, a steady state or homeostatic condition. Conversely, abnormal mechanical loading conditions

alter cellular function that changes ECM function, eventually leading to a diseased state.[81,82] As such, for meshes the ECM regulation pathway requires endogenous tension or tensional homeostasis within the mesh/tissue complex.

Homeostatic conditions for collagenous structures include endogenous tension with continuous dynamic cycling. The 8 week *in vitro* conditioned ABM produced low mechanical resistance at low strain levels. It is interesting to note that the profile of the ABM is similar to that reported for collagenous structures, with a low-resistance, highly extensible "toe" region, curved transition region, and a steep, linear region characteristic of high stiffness. A similar response, with a shorter "toe" region, has been reported to be also exhibited by scar tissue.[83] A similar mesh biomechanical response was observed for the 8 week *in vitro* conditioned ABM and is required to establish endogenous tension within the interpenetrating extracellular matrix (ECM). Furthermore, the 8 week *in vitro* conditioned response for the ABM possessed less resistance than the simulated matrix for strain values less than 10%. Therefore, at low physiologic strain levels the ECM will share in resisting the applied stress and perceive the applied strain such that homeostatic, endogenous tension will be established. This characteristic is novel and derived from the unique co-knit construction. Following the substantial degradation of the fast-degrading yarn, the resultant slow-degrading mesh became highly extensible, likely due to (1) the removal of the constraint on pore deformation, (2) the space once occupied by the fast-degrading yarn creating voids between knit loops, resulting in a loose knit structure, and (3) the mesh constructed from the slow-degrading yarn being liberated in a relaxed and constrained state. Furthermore, theses mesh structural changes take place subsequent to

the mesh being "set" within a load bearing ECM. This temporal change in biomechanics results in the preservation of the mesh configuration and may resist early changes in mesh stiffness due to cyclic strain hardening.[84] Collectively, these mesh structural changes facilitate biomechanical stimulation of the ECM due to the unique observed multiaxial mesh extension.

To achieve biomechanical stimulation the mesh must not stress shield the ECM. When a mesh is several orders of magnitude stiffer than the surrounding ECM, the mesh bears most of the stress and dictates the strain response. As a result, under these conditions minimal strain is perceived by the ECM. Using the SMTC model, stress shielding was determined to result when (1) the mesh produced a stiffer FEP than that of the simulated matrix, and (2) the FEP for the mesh and corresponding SMTC were nearly identical. Stress shielding was observed in the FEP response of the traditional meshes with the exception of PET tensile tested samples. The most commonly used HW meshes produce 16 N/cm extension values less than 14%, with several equal to or below 7%.[26,28,85] This inherent mesh stiffness, combined with increased stiffness following tissue integration, is purported to be responsible for substantial abdominal wall restriction and subsequent complications.[86] In contrast, 8 week *in vitro* conditioned ABM produced the only FEP to pass through the range of physiologic extension values associated with 16 N/cm. Traditional hernia meshes do not possess the ability to accommodate multiaxial deformation, as suggested by the high degree of stiffness observed during burst testing. For example, if the abdominal wall were subjected to a strain of 5% the PP and PET meshes would resist with a force of 70 N and 30 N, respectively. On the other

hand, the WK6 and WK7 meshes resisted with less than a 5 N force, resulting in a 14-fold and 6-fold reduction compared to the PP and PET meshes. When the WK6 and WK7 meshes were evaluated in the SMTC model, the resistive forces were 24 N and 34 N, respectively. The observed difference in force values between the mesh and SMTC is the load transferred or perceived by the matrix. For the same conditions, the traditional meshes resisted with a force of 46 N and 83 N for the PET and PP, respectively. Again, the traditional meshes were significantly stiffer than the ABM.

Synthetic materials and biologic tissues more often fail by repetitive sub-failure loading than by a single maximal loading event. A mesh attached to the abdominal wall must be able to replicate multiaxial strains to avoid stress concentrations at the margins of the mesh in response to abdominal wall distention. Mismatch in the FEP of the mesh/tissue complex and local tissue is clinically believed to be a significant contributing factor in mesh failures. Due to the stiffness of traditional meshes, recurrent hernias develop 99% of the time at the margins of the mesh/tissue complex.[38,87-89] It is likely that a fatigue mechanism is a contributing factor in late-term marginal mesh-fascial dehiscence. Fatigue failure occurs as a result of cyclical loading, where the level of stress is well below ultimate failure loads. However, the number of cycles to failure is a function of the level of stress. As previously discussed, for a given strain value the resistive force for a stiff mesh will be greater by several orders of magnitude. As a result, differences in the FEP of the mesh/tissue complex and surrounding tissue at physiologic cyclic loading will create high shear stresses at the marginal interface. Consequently, the low extensibility of the PP mesh could develop high shear stresses which may induce

marginal dehiscence.[90] In contrast, the observed compliance, especially at low strain values, of the ABM would minimize the gradient in stiffness between the local tissue and the mesh/tissue complex and reduce the likelihood of recurrence.

The 8 week *in vitro* conditioned ABM and traditional meshes produced greater resistance to strain when evaluated in a SMTC. Although constructed with different co-knit patterns, the FEP for each ABM was remarkably similar at both the initial and 8 week *in vitro* conditioned time periods. However, a significant difference was observed between the 8 week *in vitro* conditioned WK6 SMTC and WK7 SMTC samples. The WK6 SMTC produced less resistance to an applied strain in uniaxial and multiaxial testing than did the WK7 mesh. The observed difference is likely the result of the larger pores of the WK6 mesh. When a mesh is stressed, the mesh filaments show minimal if any elongation, while the mesh itself produces significant extension from geometric deformation of the pores. The infiltration of each pore resists pore deformation, but for larger pores the effect was less pronounced as less resistance was likely realized by the more extensible silicone matrix.

In part, the inability of nonabsorbable meshes to modulate their biomechanical properties during integration with the surrounding tissue in a temporal manner that coincides with the functional needs of the wound healing process and approximates physiologic biomechanical conditions has limited the efficacy of nonabsorbable meshes. The use of the SMTC model illustrates the need for highly compliant meshes to obtain mesh biomechanics that do not stress shield the ECM. The observed lack of long-term compliance will continue to hinder the biocompatibility of traditional meshes.

Consequently, advances in hernia mesh technology will likely come from the use of highly compliant meshes that approximate abdominal wall biomechanics and establish some level of tensional homeostasis. However, nonabsorbable LW meshes, which have improved compliance over HW meshes, have inferior surgical handling characteristics[91,92] and lack the ability to facilitate early wound stability.

Conclusion

The ideal hernioplasty requires, in part, that the mesh provides support to the wound site without mechanical failure, conforms to anatomical structures, and that it facilitates a wound healing response which prevents recurrence. The latter is primarily influenced by mesh biomechanics and is a primary determinant of biocompatibility. In this study, a focused comparison of the sub-failure biomechanical properties for two ABM employing different constructions and traditional meshes was completed. The *in vitro* conditioned biomechanics of the ABM indicated each mesh provided (1) improved stability compared to traditional meshes during the inflammation and proliferation phases, and (2) approximated the biomechanics of the abdominal wall and established tensional homeostasis within the mesh/tissue complex during the remodeling/maturation phase. These ABM properties were derived from the unique co-knit construction and facilitated by the use of two copolyester yarns possessing different degradation profiles. Using a simulated mesh/tissue complex (SMTC) model, quantitative changes in mesh biomechanics were determined which demonstrated mesh stress shielding and significant resistive forces at low strain values for traditional meshes. Consequently, a highly

extensible mesh was shown to be required to closely replicate abdominal wall biomechanics following simulated tissue integration. However, the two evaluated ABM constructs differed in extensibility using the SMTC model with an apparent dependence on pore size. Following encapsulation using the SMTC model, the ABM with larger pores was found to produce less resistance to an applied strain in uniaxial and multiaxial distention. Overall, the results of the present study suggest that the ABM concept will temporally augment the wound healing process by establishing stability to the developing neotissue during the inflammation and proliferation phase and restoration of abdominal wall biomechanics and tensional homeostasis during the remodeling and maturation phase. The temporal modulation of biomechanics observed for the ABM may augment the natural healing process and improve the clinical outcome of mesh hernioplasty.

References

1. Bhattacharjee P. Surgical options in inguinal hernia: Which is the best. Ind J Surg 2006;68(4):191-200.

2. Paajanen H. A single-surgeon randomized trial comparing three composite meshes on chronic pain after Lichtenstein hernia repair in local anesthesia. Hernia 2007;11(4):335-9.

3. Schwab R, Klinge U. Principle actions for re-currences. In: Schumpelick V, Fitzgibbons RJ, editors. Recurrent Hernia. Berlin, Germany: Springer-Verlag; 2007.

4. Park AE, Roth JS, Kavic SM. Abdominal wall hernia. Curr Probl Surg 2006;43(5):326-75.

5. Luijendijk RW, Hop WC, van den Tol MP, de Lange DC, Braaksma MM, JN IJ, Boelhouwer RU, de Vries BC, Salu MK, Wereldsma JC. A comparison of suture repair with mesh repair for incisional hernia. N Engl J Med 2000;343(6):392-8.

6. Bisgaard T, Bay-Nielsen M, Kehlet H. Groin hernia repair in young males: mesh or sutured repair? Hernia 2010;14(5):467-9.

7. Grant AM. Open mesh versus non-mesh repair of groin hernia: meta-analysis of randomised trials based on individual patient data [corrected]. Hernia 2002;6(3):130-6.

8. Ferzli GS, Edwards ED, Khoury GE. Chronic pain after inguinal herniorrhaphy. J Am Coll Surg 2007;205(2):333-41.

9. Beltran MA, Cruces KS. Outcomes of Lichtenstein hernioplasty for primary and recurrent inguinal hernia. World J Surg 2006;30(12):2281-7; discussion 2288-9.

10. Mann DV, Prout J, Havranek E, Gould S, Darzi A. Late-onset deep prosthetic infection following mesh repair of inguinal hernia. Am J Surg 1998;176(1):12-4.

11. Agrawal A, Avill R. Mesh migration following repair of inguinal hernia: a case report and review of literature. Hernia 2006;10(1):79-82.

12. Kes E, Lange J, Bonjer J, Stoeckart R, Mulder P, Snijders C, Kleinrensink G. Protrusion of prosthetic meshes in repair of inguinal hernias. Surgery 2004;135(2):163-70.

13. Staal E, Nienhuijs SW, Keemers-Gels ME, Rosman C, Strobbe LJ. The impact of pain on daily activities following open mesh inguinal hernia repair. Hernia 2008;12(2):153-7.

14. Palumbo P, Minicucci A, Nasti AG, Simonelli I, Vietri F, Angelici AM. Treatment for persistent chronic neuralgia after inguinal hernioplasty. Hernia 2007;11(6):527-31.

15. Nienhuijs S, Staal E, Strobbe L, Rosman C, Groenewoud H, Bleichrodt R. Chronic pain after mesh repair of inguinal hernia: a systematic review. Am J Surg 2007;194(3):394-400.

16. Aasvang E, Kehlet H. Chronic postoperative pain: the case of inguinal herniorrhaphy. Br J Anaesth 2005;95(1):69-76.

17. Aasvang E, Kehlet H. Surgical management of chronic pain after inguinal hernia repair. Br J Surg 2005;92(7):795-801.

18. van Hanswijck de Jonge P, Lloyd A, Horsfall L, Tan R, O'Dwyer PJ. The measurement of chronic pain and health-related quality of life following inguinal hernia repair: a review of the literature. Hernia 2008;12(6):561-9.

19. Klinge U, Krones CJ. Can we be sure that the meshes do improve the recurrence rates? Hernia 2005;9:1-2.

20. Nixon SJ, Jawaid H. Recurrence after inguinal hernia repair at ten years by open darn, open mesh and TEP--no advantage with mesh. Surgeon 2009;7(2):71-4.

21. Bringman S, Conze J, Cuccurullo D, Deprest J, Junge K, Klosterhalfen B, Parra-Davila E, Ramshaw B, Schumpelick V. Hernia repair: the search for ideal meshes. Hernia;14(1):81-7.

22. Klinge U, Conze J, Krones CJ, Schumpelick V. Incisional hernia: open techniques. World J Surg 2005;29(8):1066-72.

23. Flum DR, Horvath K, Koepsell T. Have outcomes of incisional hernia repair improved with time? A population-based analysis. Ann Surg 2003;237(1):129-35.

24. Burger JW, Luijendijk RW, Hop WC, Halm JA, Verdaasdonk EG, Jeekel J. Long-term follow-up of a randomized controlled trial of suture versus mesh repair of incisional hernia. Ann Surg 2004;240(4):578-83; discussion 583-5.

25. Peniston SJ, Shalaby SW, Burg KJ. Design of Abdominal Wall Hernioplasty Meshes Guided by Mechanobiology and the Wound Healing Response. In: Nagatomi J, editor. Mechanobiology Handbook: CRC Press; 2011. *In Press*.

26. Klinge U, Klosterhalfen B, Conze J, Limberg W, Obolenski B, Ottinger AP, Schumpelick V. Modified mesh for hernia repair that is adapted to the physiology of the abdominal wall. Eur J Surg 1998;164(12):951-60.

27. Cobb WS, Burns JM, Kercher KW, Matthews BD, James Norton H, Todd Heniford B. Normal intraabdominal pressure in healthy adults. J Surg Res 2005;129(2):231-5.

28. Junge K, Klinge U, Prescher A, Giboni P, Niewiera M, Schumpelick V. Elasticity of the anterior abdominal wall and impact for reparation of incisional hernias using mesh implants. Hernia 2001;5(3):113-8.

29. Song C, Alijani A, Frank T, Hanna GB, Cuschieri A. Mechanical properties of the human abdominal wall measured in vivo during insufflation for laparoscopic surgery. Surg Endosc 2006;20(6):987-90.

30. Kureshi A, Vaiude P, Nazhat SN, Petrie A, Brown RA. Matrix mechanical properties of transversalis fascia in inguinal herniation as a model for tissue expansion. J Biomech 2008;41(16):3462-8.

31. Fortuny G, Rodriguez-Navarro J, Susin A, Lopez-Cano M. Simulation and study of the behaviour of the transversalis fascia in protecting against the genesis of inguinal hernias. J Biomech 2009;42(14):2263-7.

32. Peiper C, Junge K, Prescher A, Stumpf M, Schumpelick V. Abdominal musculature and the transversalis fascia: an anatomical viewpoint. Hernia 2004;8(4):376-80.

33. Brown SH, McGill SM. An ultrasound investigation into the morphology of the human abdominal wall uncovers complex deformation patterns during contraction. Eur J Appl Physiol 2008;104(6):1021-30.

34. Usher FC. Hernia repair with knitted polypropylene mesh. Surg Gynecol Obstet 1963;117:239-40.

35. Di Vita G, Milano S, Frazzetta M, Patti R, Palazzolo V, Barbera C, Ferlazzo V, Leo P, Cillari E. Tension-free hernia repair is associated with an increase in inflammatory response markers against the mesh. Am J Surg 2000;180(3):203-7.

36. Shin D, Lipshultz LI, Goldstein M, Barme GA, Fuchs EF, Nagler HM, McCallum SW, Niederberger CS, Schoor RA, Brugh VM, 3rd and others. Herniorrhaphy with polypropylene mesh causing inguinal vasal obstruction: a preventable cause of obstructive azoospermia. Ann Surg 2005;241(4):553-8.

37. Cobb WS, Kercher KW, Heniford BT. The argument for lightweight polypropylene mesh in hernia repair. Surg Innov 2005;12(1):63-9.

38. Klosterhalfen B, Junge K, Klinge U. The lightweight and large porous mesh concept for hernia repair. Expert Rev Med Devices 2005;2(1):103-17.

39. Bellon JM, Rodriguez M, Garcia-Honduvilla N, Pascual G, Bujan J. Partially absorbable meshes for hernia repair offer advantages over nonabsorbable meshes. Am J Surg 2007;194(1):68-74.

40. Rosch R, Junge K, Quester R, Klinge U, Klosterhalfen B, Schumpelick V. Vypro II mesh in hernia repair: impact of polyglactin on long-term incorporation in rats. Eur Surg Res 2003;35(5):445-50.

41. Junge K, Klinge U, Rosch R, Klosterhalfen B, Schumpelick V. Functional and morphologic properties of a modified mesh for inguinal hernia repair. World J Surg 2002;26(12):1472-80.

42. Barbolt TA. Biology of polypropylene/polyglactin 910 grafts. Int Urogynecol J Pelvic Floor Dysfunct 2006;17 Suppl 1:S26-30.

43. Weyhe D, Belyaev O, Buettner G, Mros K, Mueller C, Meurer K, Papapostolou G, Uhl W. In vitro comparison of three different mesh constructions. ANZ J Surg 2008;78(1-2):55-60.

44. Weyhe D, Schmitz I, Belyaev O, Grabs R, Muller KM, Uhl W, Zumtobel V. Experimental comparison of monofile light and heavy polypropylene meshes: less weight does not mean less biological response. World J Surg 2006;30(8):1586-91.

45. Welty G, Klinge U, Klosterhalfen B, Kasperk R, Schumpelick V. Functional impairment and complaints following incisional hernia repair with different polypropylene meshes. Hernia 2001;5(3):142-7.

46. Nikkolo C, Lepner U, Murruste M, Vaasna T, Seepter H, Tikk T. Randomised clinical trial comparing lightweight mesh with heavyweight mesh for inguinal hernioplasty. Hernia;14(3):253-8.

47. O'Dwyer PJ, Kingsnorth AN, Molloy RG, Small PK, Lammers B, Horeyseck G. Randomized clinical trial assessing impact of a lightweight or heavyweight mesh on chronic pain after inguinal hernia repair. Br J Surg 2005;92(2):166-70.

48. Post S, Weiss B, Willer M, Neufang T, Lorenz D. Randomized clinical trial of lightweight composite mesh for Lichtenstein inguinal hernia repair. Br J Surg 2004;91(1):44-8.

49. Langenbach MR, Schmidt J, Zirngibl H. Comparison of biomaterials in the early postoperative period. Surg Endosc 2003;17(7):1105-9.

50. Bringman S, Wollert S, Osterberg J, Smedberg S, Granlund H, Heikkinen TJ. Three-year results of a randomized clinical trial of lightweight or standard polypropylene mesh in Lichtenstein repair of primary inguinal hernia. Br J Surg 2006;93(9):1056-9.

51. Khan LR, Liong S, de Beaux AC, Kumar S, Nixon SJ. Lightweight mesh improves functional outcome in laparoscopic totally extra-peritoneal inguinal hernia repair. Hernia;14(1):39-45.

52. Pascual G, Rodriguez M, Gomez-Gil V, Garcia-Honduvilla N, Bujan J, Bellon JM. Early tissue incorporation and collagen deposition in lightweight polypropylene meshes: bioassay in an experimental model of ventral hernia. Surgery 2008;144(3):427-35.

53. Greca FH, Souza-Filho ZA, Giovanini A, Rubin MR, Kuenzer RF, Reese FB, Araujo LM. The influence of porosity on the integration histology of two polypropylene meshes for the treatment of abdominal wall defects in dogs. Hernia 2008;12(1):45-9.

54. Bringman S, Wollert S, Osterberg J, Smedberg S, Granlund H, Fellander G, Heikkinen T. One year results of a randomised controlled multi-centre study comparing Prolene and Vypro II-mesh in Lichtenstein hernioplasty. Hernia 2005;9(3):223-7.

55. Lauscher JC, Yafaei K, Buhr HJ, Ritz JP. Total extraperitoneal hernioplasty: does the long-term clinical course depend on the type of mesh? J Laparoendosc Adv Surg Tech A 2008;18(6):803-8.

56. Smietanski M. Randomized clinical trial comparing a polypropylene with a poliglecaprone and polypropylene composite mesh for inguinal hernioplasty. Br J Surg 2008;95(12):1462-8.

57. Heikkinen T, Wollert S, Osterberg J, Smedberg S, Bringman S. Early results of a randomised trial comparing Prolene and VyproII-mesh in endoscopic extraperitoneal inguinal hernia repair (TEP) of recurrent unilateral hernias. Hernia 2006;10(1):34-40.

58. Conze J, Kingsnorth AN, Flament JB, Simmermacher R, Arlt G, Langer C, Schippers E, Hartley M, Schumpelick V. Randomized clinical trial comparing lightweight composite mesh with polyester or polypropylene mesh for incisional hernia repair. Br J Surg 2005;92(12):1488-93.

59. Chowbey PK, Garg N, Sharma A, Khullar R, Soni V, Baijal M, Mittal T. Prospective randomized clinical trial comparing lightweight mesh and heavyweight polypropylene mesh in endoscopic totally extraperitoneal groin hernia repair. Surg Endosc.

60. Akolekar D, Kumar S, Khan LR, de Beaux AC, Nixon SJ. Comparison of recurrence with lightweight composite polypropylene mesh and heavyweight mesh in laparoscopic totally extraperitoneal inguinal hernia repair: an audit of 1,232 repairs. Hernia 2008;12(1):39-43.

61. Boguszewski D, Dyment N, Bailey D, Shearn J, Butler D. Biomechanical comparison of abdominal wall hernia repair materials. ASME 2008 summer bioengineering conference. June 25-29, Marriott Resort, Marco Island, Florida, USA; 2008.

62. Klinge U, Junge K, Stumpf M, Ap AP, Klosterhalfen B. Functional and morphological evaluation of a low-weight, monofilament polypropylene mesh for hernia repair. J Biomed Mater Res 2002;63(2):129-36.

63. Goldstein HS. Selecting the right mesh. Hernia 1999;3:155-162.

64. Soares BM, King MW, Marois Y, Guidoin RG, Laroche G, Charara J, Girard JF. In vitro characterization of a fluoropassivated gelatin-impregnated polyester mesh for hernia repair. J Biomed Mater Res 1996;32(2):259-70.

65. Hamouda A, Kennedy J, Grant N, Nigam A, Karanjia N. Mesh erosion into the urinary bladder following laparoscopic inguinal hernia repair; is this the tip of the iceberg? Hernia;14(3):317-9.

66. Leber GE, Garb JL, Alexander AI, Reed WP. Long-term complications associated with prosthetic repair of incisional hernias. Arch Surg 1998;133(4):378-82.

67. Klinge U, Junge K, Spellerberg B, Piroth C, Klosterhalfen B, Schumpelick V. Do multifilament alloplastic meshes increase the infection rate? Analysis of the polymeric surface, the bacteria adherence, and the in vivo consequences in a rat model. J Biomed Mater Res 2002;63(6):765-71.

68. Engelsman AF, van der Mei HC, Busscher HJ, Ploeg RJ. Morphological aspects of surgical meshes as a risk factor for bacterial colonization. Br J Surg 2008;95(8):1051-9.

69. Engelsman AF, van der Mei HC, Ploeg RJ, Busscher HJ. The phenomenon of infection with abdominal wall reconstruction. Biomaterials 2007;28(14):2314-27.

70. Tolino MJ, Tripoloni DE, Ratto R, Garcia MI. Infections associated with prosthetic repairs of abdominal wall hernias: pathology, management and results. Hernia 2009.

71. Klosterhalfen B, Junge K, Hermanns B, Klinge U. Influence of implantation interval on the long-term biocompatibility of surgical mesh. Br J Surg 2002;89(8):1043-8.

72. Togo S, Kubota T, Takahashi T, Yoshida K, Matsuo K, Morioka D, Tanaka K, Shimada H. Usefulness of absorbable sutures in preventing surgical site infection in hepatectomy. J Gastrointest Surg 2008;12(6):1041-6.

73. Galko MJ, Krasnow MA. Cellular and genetic analysis of wound healing in Drosophila larvae. PLoS Biol 2004;2(8):E239.

74. Raghavendra S, Wood MC, Taylor TD. Early wound healing around endosseous implants: a review of the literature. Int J Oral Maxillofac Implants 2005;20(3):425-31.

75. Dubay DA, Wang X, Kirk S, Adamson B, Robson MC, Franz MG. Fascial fibroblast kinetic activity is increased during abdominal wall repair compared to dermal fibroblasts. Wound Repair Regen 2004;12(5):539-45.

76. Franz MG, Smith PD, Wachtel TL, Wright TE, Kuhn MA, Ko F, Robson MC. Fascial incisions heal faster than skin: a new model of abdominal wall repair. Surgery 2001;129(2):203-8.

77. Carlson MA. Acute wound failure. Surg Clin North Am 1997;77(3):607-36.

78. Douglas DM. The healing of aponeurotic incisions. Br J Surg 1952;40(159):79-84.

79. Wang JH. Mechanobiology of tendon. J Biomech 2006;39(9):1563-82.

80. Chiquet M, Gelman L, Lutz R, Maier S. From mechanotransduction to extracellular matrix gene expression in fibroblasts. Biochim Biophys Acta 2009;1793(5):911-20.

81. Wang JH, Thampatty BP. An introductory review of cell mechanobiology. Biomech Model Mechanobiol 2006;5(1):1-16.

82. Paszek MJ, Zahir N, Johnson KR, Lakins JN, Rozenberg GI, Gefen A, Reinhart-King CA, Margulies SS, Dembo M, Boettiger D and others. Tensional homeostasis and the malignant phenotype. Cancer Cell 2005;8(3):241-54.

83. Corr DT, Gallant-Behm CL, Shrive NG, Hart DA. Biomechanical behavior of scar tissue and uninjured skin in a porcine model. Wound Repair Regen 2009;17(2):250-9.

84. Velayudhan S, Martin D, Cooper-White J. Evaluation of dynamic creep properties of surgical mesh prostheses--uniaxial fatigue. J Biomed Mater Res B Appl Biomater 2009;91(1):287-96.

85. Klosterhalfen B, Klinge U, Schumpelick V, Tietze L. Polymers in hernia repair - common polyester vs. polypropylene surgical meshes. J Mat Sci 2000;35:4769-76.

86. Bellon JM, Bujan J, Contreras L, Hernando A. Integration of biomaterials implanted into abdominal wall: process of scar formation and macrophage response. Biomaterials 1995;16(5):381-7.

87. Kockerling C, Schug-Pass C. Recurrence and mesh material. In: Schumpelick V, Fitzgibbons RJ, editors. Recurrent Hernia. Berlin, Germany: Springer-Verlag; 2007.

88. Junge K, Klinge U, Klosterhalfen B, Rosch R, Stumpf M, Schumpelick V. Review of wound healing with reference to an unrepairable abdominal hernia. Eur J Surg 2002;168(2):67-73.

89. Schumpelick V, Klinge U, Rosch R, Junge K. Light weight meshes in incisional hernia repair. J Min Access Surg 2006;2(3):pNA.

90. Doctor H. Evaluation of various prosthetic materials and newer meshes for hernia repairs. J Min Access Surg 2006;2(3):110-16.

91. Agarwal BB, Agarwal KA, Sahu T, Mahajan KC. Traditional polypropylene and lightweight meshes in totally extraperitoneal inguinal herniorrhaphy. Int J Surg;8(1):44-7.

92. Scheidbach H, Tamme C, Tannapfel A, Lippert H, Kockerling F. In vivo studies comparing the biocompatibility of various polypropylene meshes and their handling properties during endoscopic total extraperitoneal (TEP) patchplasty: an experimental study in pigs. Surg Endosc 2004;18(2):211-20.

CONCLUSIONS

In these dissertation studies a warp knit mesh was developed for application in hernia repair using (1) absorbable yarns with fast- and slow-degradation profiles and (2) a novel knit construction such that the knit pattern for each degradable yarn is interdependent. These preliminary studies suggest that the developed mesh temporally modulated physicomechanical properties such that the mesh (1) possessed short-term structural stiffness, (2) provided a gradual transition phase, and (3) possessed long-term compliance with force-extension properties similar to the abdominal wall. In the development of the degradable copolyester yarns, the use of dynamic mechanical analysis to characterize the glass transition temperature, and the associated activation energy, was shown to predict *in vitro* strength retention and used to optimize the strength profile of the fast-degrading yarn. Furthermore, an *in vitro* model was developed to prototype the mesh/tissue complex which illustrated the importance of a highly-extensible mesh construction to match physiologic abdominal wall biomechanics. Finally, a simple model for evaluating tissue reaction was developed which showed that the cellular response was reduced and collagen integration was compact and concentrically oriented around an absorbable bicomponent construct which simulated the subject mesh during an evaluation period associated with the mesh transition phase.

RECOMMENDATIONS

Completion of this hernia mesh research provides direction for future studies. To further this research, future work could be conducted to:

- Remove the external fibrous tissue from the gluteal muscle prior to tissue processing to reduce the noise associated with collagen/total protein measurements in the rat gluteal muscle model for future studies.
- Develop an animal model that can reproduce hernia recurrence to evaluate the efficacy of the absorbable bicomponent mesh.
- Investigate the effect of mesh structural stability on the wound contraction process.
- Develop an *in vitro* model to characterize the distribution of load to multiple suture attachment points for an externally applied force during the stability phase of the absorbable bicomponent mesh.
- Conduct *in vivo* studies to determine the long-term relative contribution of facilitating endogenous tension and mechanical stimulation on collagen type, density, orientation, and crosslinking surrounding the absorbable bicomponent mesh.